



Державний вищий навчальний заклад
„Національний гірничий університет“

НАУКОВИЙ ВІСНИК

Національного
гірничого
університету

Науково-технічний журнал

№ 6 (156) • 2016

Виходить 6 разів на рік • Заснований у вересні 1998 р.

Геологія
Розробка родовищ корисних копалин
Фізика твердого тіла, збагачення корисних копалин
Геотехнічна і гірнича механіка, машинобудування
Електротехнічні комплекси та системи
Технології енергозабезпечення
Екологічна безпека, охорона праці
Інформаційні технології, системний аналіз та керування
Економіка та управління

Дніпро
2016

Головний редактор	Г. Г. Півняк
Заступники головного редактора	О. С. Бешта, П. І. Пілов, О. М. Шашенко
Відповідальний редактор	Т. В. Барна
РЕДАКЦІЙНА КОЛЕГІЯ: (Україна)	М. О. Алексеєв, В. І. Бондаренко, В. І. Бузило, А. Ф. Булат, В. І. Голінько, С. С. Гребьонкін, Б. А. Грядущий, М. М. Довбніч, Р. О. Дичковський, А. О. Задоя, М. О. Ільяшов, Г. О. Козлакова, В. В. Лукінов, В. Ф. Приходченко, В. В. Проців, Ю. Т. Разумний, Т. Б. Решетілова, Д. В. Рудаков, В. С. Савчук, І. О. Садовенко, О. В. Садовий, В. І. Самуся, О. О. Сдвижкова, К. Ф. Тяпкін, В. П. Франчук, Ю. М. Халімендик, Ю. Т. Хоменко, В. Я. Швець, Ф. П. Шкрабець
ЗАКОРДОННІ ЧЛЕНИ РЕДАКЦІЙНОЇ КОЛЕГІЇ:	М. Д. Венедиктов (<i>Московський технічний університет зв'язку та інформатики, РФ</i>); Р. Вюрцлін (<i>Есслінгенський університет прикладних наук, ФРН</i>); Г. Грулер (<i>Ройтлінгенський університет, ФРН</i>); А. Дичко (<i>Інститут мінеральної сировини та енергетики Польської академії наук, Республіка Польща</i>); К. Дребенштедт (<i>Технічний університет „Фрайберзька гірнична академія“, ФРН</i>); Ю. Дубінські (<i>Головний інститут гірничої справи, Республіка Польща</i>); В. В. Кармазин (<i>Московський державний гірничий університет, РФ</i>); Є. Кіцкі (<i>Інститут мінеральної сировини та енергетики Польської академії наук, Гірничо-металургійна академія ім. Станіслава Сташиця, Республіка Польща</i>); Т. Майхерчик (<i>Гірничо-металургійна академія ім. Станіслава Сташиця, Республіка Польща</i>); Н. Нойбергер (<i>Есслінгенський університет прикладних наук, ФРН</i>); С. Прусек (<i>Головний інститут гірничої справи, Республіка Польща</i>); Л. О. Пучков (<i>Московський державний гірничий університет, РФ</i>); Б. Ракішев (<i>Казахський національний технічний університет, Республіка Казахстан</i>); Р. Сінгхал (<i>Університет Калгарі, Канада</i>); О. Стовас (<i>Норвезький університет природничих наук та технології, Королівство Норвегія</i>); С. Г. Страданченко (<i>Донський державний технічний університет, РФ</i>); Д. Стургул (<i>Університет Аделаїди, Австралійський Союз</i>); А. Тайдусь (<i>Гірничо-металургійна академія ім. Станіслава Сташиця, Республіка Польща</i>); Я. Таліандер (<i>Університет Заходу, Королівство Швеція</i>); С. Форліч (<i>Вроцлавська вища банківська школа, Республіка Польща</i>); В. Чарнецкі (<i>Есслінгенський університет прикладних наук, ФРН</i>); М. Шмідт (<i>Бранденбурзький технічний університет, ФРН</i>), Г. Шмідт (<i>Есслінгенський університет прикладних наук, ФРН</i>)
	Журнал включено до міжнародних наукометричних баз Scopus, Index Copernicus Journal Master List, тематичної бази Compendex у складі Engineering Village та баз EBSCOhost і ProQuest, каталогів періодичних видань Ulrichsweb Global Serials Directory та ResearchBib, реферується у журналі ВІНІТІ РАН, РФ.
	Передплата здійснюється в поштових відділеннях України за „Каталогом періодичних видань“ (передплатний індекс: 89166) і в передплатних агентствах „Укрінформнаука“ (індекс: 10107) та „Ідея“ (індекс: 17736).
	Комп'ютерна верстка Т. О. Клименко. Коректор М. Т. Сисун. Журнал підписано до друку за рекомендацією вченої ради Державного вищого навчального закладу „Національний гірничий університет“ (протокол № 18 від 20.12.2016 року)
Журнал зареєстровано	у Міністерстві юстиції України. Реєстраційний номер КВ № 17742-6592ПР від 27.04.2011. Наклад 200 прим. Зам. №2. Підписано до друку 23.12.2016. Формат 60 × 90/8. Ум. друк. арк. 20. Папір офсетний.
Засновник та видавець	Державний вищий навчальний заклад „Національний гірничий університет“, м. Дніпро. „Свідоцтво суб'єкта видавничої справи“ ДК №1842 від 11.06.2004
Адреса видавця та редакції:	49005, м. Дніпро, просп. Д. Яворницького, 19, корпус 3, к. 24а Тел.: (0562) 47 45 24, e-mail: nv.ngu@ukr.net; www.nvngu.in.ua; nv.nmu.org.ua
Виготовлення:	ПП КФ „Герда“. 49000, м. Дніпро, просп. Д. Яворницького, 60. „Свідоцтво суб'єкта видавничої справи“ ДК №397 від 03.04.2001



State Higher Educational Institution
“National Mining University”

**SCIENTIFIC
BULLETIN**
of National
Mining University

Scientific and technical journal

No 6 (156) • 2016

Bi-Monthly statement • Founded in September 1998

Geology
Mining
Solid-State Physics, Mineral Processing
Geotechnical and Mining Mechanical Engineering,
Machine Building
Electrical Complexes and Systems
Power Supply Technologies
Environmental Safety, Labour Protection
Information Technologies,
Systems Analysis and Administration
Economy and Management

Dnipro
2016

<i>Editor-in-chief</i>	G. G. Pivnyak
<i>Deputy editors-in-chief</i>	O. S. Beshta, P. I. Pilov, O. M. Shashenko
<i>Editor in chief</i>	T. V. Barna
EDITORIAL BOARD: (Ukraine)	M. A. Alekseev, V. I. Bondarenko, V. I. Buzylo, A. F. Bulat, V. I. Golinko, S. S. Grebonkin, B. A. Griadushyi, M. M. Dovbnich, R. O. Dychkovskiy, A. O. Zadoia, M. O. Iliashov, G. O. Kozlakova, V. V. Lukinov, V. F. Prykhodchenko, V. V. Protsiv, Yu. T. Razumnyi, T. B. Reshetilova, D. V. Rudakov, V. S. Savchuk, I. O. Sadovenko, A. V. Sadovoy, V. I. Samusia, Ye. A. Sdvizhkova, K. F. Tiapkin, V. P. Franchuk, Yu. M. Khalimendyk, Yu. T. Khomenko, V. Ya. Shvets, F. P. Shkrabets
FOREIGN MEMBERS OF EDITORIAL BOARD:	M. D. Venedyktov (<i>Moscow Technical University of Communications and Informatics, Russian Federation</i>); R. Würslin (<i>The Esslingen University of Applied Sciences, Federal Republic of Germany</i>); G. Gruhler (<i>Reutlingen University, Federal Republic of Germany</i>); A. Dyczko (<i>The Mineral and Energy Economy Research Institute of the Polish Academy of Sciences, Republic of Poland</i>), C. Drebenstedt (<i>Freiberg University of Mining and Technology, Federal Republic of Germany</i>); J. Dubinski (<i>Central Mining Institute, Republic of Poland</i>); V. V. Karmazin (<i>Moscow State Mining University, Russian Federation</i>); J. Kicki (<i>AGH University of Science and Technology, The Mineral and Energy Economy Research Institute of the Polish Academy of Sciences, Republic of Poland</i>), T. Majcherczyk (<i>AGH University of Science and Technology, Republic of Poland</i>); N. Neuberger (<i>The Esslingen University of Applied Sciences, Federal Republic of Germany</i>); S. Prusek (<i>Main Mining Institute, Republic of Poland</i>); L. A. Puchkov (<i>Moscow State Mining University, Russian Federation</i>); B. R. Rakishev (<i>Kazakh National Technical University after K. I. Satpaev, Republic of Kazakhstan</i>); R. Singhal (<i>The University of Calgary, Canada</i>); A. Stovas (<i>The Norwegian University of Science and Technology, Kingdom of Norway</i>); S. G. Stradanchenko (<i>Don State Technical University, Russian Federation</i>); J. Sturgul (<i>The University of Adelaide, Commonwealth of Australia</i>); A. Tajdu (<i>AGH University of Science and Technology, Republic of Poland</i>); J. Theliander (<i>University West, Kingdom of Sweden</i>); S. Forlicz (<i>Wroc aw Higher Bank School, Republic of Poland</i>); W. T. Czarnetzki (<i>The Esslingen University of Applied Sciences, Federal Republic of Germany</i>); M. Schmidt (<i>The Brandenburg Technical University, Federal Republic of Germany</i>), G. Schmidt (<i>The Esslingen University of Applied Sciences, Federal Republic of Germany</i>)

The journal has been included in Scopus, Index Copernicus Journal Master List, Compendex, ProQuest, EBSCOhost, Ulrichsweb Global Serials Directory, Research-Bib, abstract journal VINITI RAS (Russia).

Subscription for the journal can be done in post offices of the Ukraine (subscription index in Subscription Publication Catalogue is 89166) and in the subscription agencies Ukrinformnauka (index in Subscription Publication Catalogue is 10107) and Ideia (index is 17736)

Makeup T. A. Klimenko. Proofreading M. T. Sysun.

Passed for printing under recommendation of Academic Council of State Higher Educational Institution "National Mining University" (transaction No. 18 dated December 20, 2016).

Journal was registered	by Ministry of Justice of Ukraine. Registration number KB No.17742-6592PR dated April 27, 2011. Passed for printing December 23, 2016. Sheet size 60 × 90/8. Presswork 20. Offset paper. Number of copies printed 200. Order No.2.
Founder and editor	State Higher Educational Institution "National Mining University", Dnipro Certificate of Publisher ДК No.1842 dated June 11, 2004
Address of editor and editorial office:	19, D. Yavornytskoho Ave., building 3, room 24a, Dnipro, 49005 Tel.: (0562) 47 45 24, e-mail: nv.ngu@ukr.net, www.nvngu.in.ua; nv.nmu.org.ua
Production	PP KF "Gerda". 60, D. Yavornytskoho Ave., Dnipro, 49000. Certificate of Publisher ДК No.397 dated April 3, 2001

UDC [551.242.1.03+622.831.3](477.6)

**T. P. Volkova¹, Dr. Sc. (Geol.), Prof.,
O. V. Nikitenko¹,
O. G. Chernysh², Cand. Sc. (Geol.), Assoc. Prof.**

1 – State Higher Educational Institution “Donetsk National Technical University”, Pokrovsk, Ukraine,
e-mail: voltep@rambler.ru; paleontologist@yandex.ua
2 – Federal State Autonomous Educational Institution of Vocational Education “Far Eastern Federal University”, School of Engineering, Vladivostok, Russia, e-mail: xanfia@yandex.ua

TECTONOPHYSICAL ASPECTS OF THE DEVELOPMENT OF GEOLOGICAL STRUCTURE OF THE WESTERN CLOSURE OF THE HORLIVKA ANTICLINE OF THE DONBAS

**Т. П. Волкова¹, д-р геол. наук, проф.,
О. В. Нікітенко¹,
О. Г. Черниш², канд. геол. наук, доц.**

1 – Державний вищий навчальний заклад „Донецький національний технічний університет“, м. Покровськ, Україна, e-mail: voltep@rambler.ru; paleontologist@yandex.ua
2 – Федеральний державний автономний навчальний заклад професійної освіти „Далекосхідний федеральний університет“, Інженерна школа, м. Владивосток, РФ, e-mail: xanfia@yandex.ua

ТЕКТОНОФІЗИЧНІ АСПЕКТИ РОЗВИТКУ ГЕОЛОГІЧНОЇ СТРУКТУРИ ЗАХІДНОГО ЗМИКАННЯ ГОРЛІВСЬКОЇ АНТИКЛІНАЛІ ДОНБАСУ

Purpose. The present study focuses on the analysis of the geological structure, stress and strain fields of the western closure of the Horlivka anticline to present a general development mechanism with regard to tectonophysical features, and to determine whether the structural complexity of the study area is consistent with a single regional stress field or not.

Methodology. The kinematic and structural data available for the study zone have been studied. Further, fault data, including both the fault plane and slickenline orientations, and the sense of movement have been studied by the kinematic analysis method of O. Gushchenko to estimate characteristics of the mesoregional stress field and the total strain field. Local stress data have been processed by the method for determination of general stress fields to provide for reconstruction of principal normal stresses which are arbitrarily considered as regional stresses. Relative age chronology and staging of tectonic stresses have been processed by the stress monitoring method.

Findings. NW-trending dextral and NE and N–S-trending sinistral strike-slip faults prevail among other faults. Mesoregional stress field characterized by subhorizontal NW–SE maximum (σ_3) and NE–SW minimum (σ_1) principal axes, and apparently originated in Laramide time of Alpine orogeny is strike-slip faulting type and the youngest for the Donets Basin. Extension axis (ϵ_1) of the strain ellipsoid is NW and N–S oriented, and shortening axis (ϵ_3) is NE oriented nearly orthogonal to the anticline axis. Strike-slip faulting type of total strain field was determined for the most part of the western closure of the Horlivka anticline area, and according to the Lode–Nadai coefficient ($\mu_e = \pm 1$), deformations on the study area had been going mainly under shear conditions. The pattern of a single structural paragenesis of deformation elements of the study area, including a conjugate strike-slip fault system, dome-shaped fold and longitudinal thrusts in its limbs, was developed due to the right-lateral displacements along the longitudinal strike-slip fault system within the Main anticline paraxial part.

Originality. Strike-slip faults and large shear zone are revealed in the geological structure of the study area, and their morphology, development, and interaction of structural elements are characterized. The primary characteristics of the stress fields of local and mesoregional level, including its relative age chronology and staging, and of the total strain field are reconstructed.

Practical value. Taking importance of the results obtained by the kinematic method into account, applying of new forecasting methods based on reconstruction of primary tectonophysical characteristics and reconstruction of deformation mechanisms appears to be needed.

Keywords: *kinematic method, stress and strain fields, Lode–Nadai coefficient, slickenlines, strike-slip fault, shear zone, structural paragenesis*

Introduction. Understanding the regularities, development mechanisms, and spatial distribution of tectonic dislocations plays an important role in both academia and industry, where it may be used for both elaborating the physical theory of the development of deformation processes in the Earth's crust, and in forecasting, prospecting, and exploration of mineral deposits, mining at deeper levels in more difficult geological conditions.

Any kinds of geological forecast on various stages of mining sequence should be based on explanation of deformation mechanisms and history of the crust part development. Key issues concerning its reconstruction are: 1) what were the main directions of active tectonic forces under which the geological structure at different stages over geological time was formed; 2) which stress fields were active while the geological structure was forming; 3) what deformation and dislocation distributions within the structure are?

Tectonophysical study is one of the effective ways to objectively estimate it by determination of regularities of the stress distribution and development of tectonic deformation, appearing within the crust. In spite of having various kinds of modeling to solve tectonophysical problems now, field tectonophysics data may make an essential addition to the final results. Furthermore, the surface and underground mining used in layered sedimentary deposits creates very favorable conditions for that. For instance, application of the longwall mining method in thick coal seams, along with geological mapping and documentation of underground workings in detail, allows studying geological structures on a true scale, and to record morphology changes both all over the planar surface and cross section.

Analysis of the recent research. The Main anticline of the Donets Basin is of great interest as a subject of tectonophysical study not only because of its structural complexity and development mechanism, but also due to their effect on the safe high-efficient exploitation of coal.

As one of the major segments of the Main anticline, the Horlivka anticline is known, first and foremost, for Nikitovka ore field occurred in the crest part of the fold. Structures of Nikitovka ore field have been investigated and mapped in detail for a long time. Various massif deformation elements were geometrized there, its morphology and kinematics were determined, and stress fields for many localities, mine fields, deposits and the region as a whole were reconstructed.

The stress field reconstructed for Nikitovka ore field is characterized by a subhorizontal NW-plunging (330°) maximum principal stress axis σ_3 (maximum compression) and a subhorizontal SW-plunging (245°) minimum principal stress axis σ_1 (maximum tension) [1–3]. The stress field axes are oriented in directions diagonal to the Horlivka anticline, a major ore-controlling structure, and symmetric to second-order dome-shaped folds complicating the crest of the Horlivka anticline. Moreover, a σ_3 axis is invariably perpendicular to the dome-shaped fold axes. The ore field structure was developed under conditions of a special pulsating type of the massif stress state, changing from uniaxial compression to uniaxial tension and vice versa. This stress field that apparently originated in Laramide time of Alpine orogeny is the youngest for the Donets Basin.

According to the reconstructed stress field characteristics, fault kinematics and orientation of structural deformation elements, Korchemagin interprets the Main anticline as over-fault fold, developed in the Carboniferous ductile sedimentary series due to the right-lateral displacements along the zone of the Central Donets deep-seated fault, that also resulted in the development of the structure of the crest of the Horlivka anticline and Nikitovka ore field [1]. Reflection of the Central Donets fault in present geological structure of the study area is the Osevoy thrust, traced along the whole length of the Main anticline axis. Those studies have shown that all known deformation elements of the ore field, such as morphology and kinematics of the faults, position and orientation of the dome-shaped folds, systems of transverse fissured veins, straightness of segments of the longitudinal Sekuschaya fault, are parts of the structural paragenesis for right-lateral faulting, and are consistent with a single regional stress field.

Objectives of the article. Although the problems of deformation element structural paragenesis, stress fields of local and regional level, and also the mechanism of the development of the Main anticline western part were well studied, it should be pointed out that area of the western periclinal closure of the Horlivka anticline is not studied as well as Nikitovka ore field. Now it seems to be possible to do because of new facts of the regional geological structure, fault kinematics and stress field characteristics, obtained through the structural and tectonophysical works within Novodzerzhynska coal mine field.

The present study focuses on the analysis of geological structure and stress and strain fields of the

western closure of the Horlivka anticline to present a general development mechanism, and to determine whether the structural complexity of the study area is consistent with a single regional stress field or not.

The tasks necessary to reach these objectives are: 1) to study kinematics, morphology, and age relations of the faults; 2) to define structural pattern of the massif deformation elements, and determine a mechanism of its development; 3) to reconstruct main characteristics of stress and strain fields of local and mesoregional level; 4) to analyse an interaction between geological factors and various tectonic structures, and basic characteristics of stress-and-strain fields.

Methodology. Tectonic stresses have been studied by the kinematic method [4]. The method used principles of plasticity mechanics, in particular, the Batorf-Budiansky's plasticity theory, and postulated the coincidence of the fault side slip direction with the shear stress direction on the fracture plane. Graphic algorithm for calculating the principal stresses and evaluating the Lode-Nadai coefficient (or ratio coefficient), determining the shape of the stress ellipsoid and the ratio of deviatoric components of principal stresses were developed on this assumption. The input for the study was field-measured orientation data for faults and slickenlines from mine workings within the Novodzerzhynska mine field (more over than 900 measurements), consisting of the orientations of the fault planes and slickenlines, including the sense of movement. Mesoregional level stress field characteristics have been reconstructed by statistical processing of local stereographical solutions. Local stress data processed by the method for determination of general stress fields provide for reconstruction of main normal stresses which are arbitrarily considered as regional stresses [5]. Relative age chronology and staging of tectonic stresses have been studied by the stress monitoring method devised by O. Gushchenko and A. Mostrukov on the base of the kinematic method. It insures a possibility of space-time monitoring of tectonic fields of stresses and strains on the base of geological data, which allows us to solve the problem of age chronology of paleostresses [4]. Characteristics of the principal axes of the total strain field have been processed by means of specialized software GEOS developed by O. Gushchenko and upgraded by V. Korchemagin.

Presentation of the main research. Geological structure. The Main anticline, a major WNW-ESE-trending (290–305°) symmetrical fold, extends 300 km throughout the Donets Basin. Towards the west of the Nagolny Ridge, it divides into three right-stepping echelon fold segments: Olkhovatka-Volyntsevo and Horlivka anticlines, Druzhkivka-Konstantinovka brachyanticline. Both limbs of the fold dip generally steeply (60–65°), and the crest of the fold, wide in the west and narrow in the east, is faulted by reverse and strike-slip faults, trend parallel to the fold axis. The Horlivka anticline is the most studied segment of the Main anticline where lots of coal mines and Nikitovka ore field are situated. Nikitovka ore field is related to five similar dome-shaped folds, 1 km length and

0.4 km width, exposed in roughly equal intervals (1.4 km) within the crest of the anticline. The fold axes appear rotated at an acute angle, typically 15–30° anticlockwise towards the Horlivka anticline axis. Longitudinal faults of the Osevoy thrust system separate these folds to the north and south of the anticline crest part. Four larger dome-shaped folds expose in roughly equal intervals (3–3.5 km) to the east and to the west of fold set of Nikitovka ore field.

As the object of the field tectonophysical studies, the Novodzerzhynska coal mine is the westernmost one in the area of the western periclinal closure of the Horlivka anticline. The Middle Carboniferous (suites *K* to *M*) seams over the mine field have been basically mined. In the study area, the beds dip away from the crest of the anticline at an angle of 30–35° on the periphery, which decreases to 10–15° near the crest. In strike, they vary from a little west through a little north to south of east. The whole region is traversed by an immense number of small-scale faults. Their strikes have such varying directions, but the great number appears to follow the three trends of sublatitudinal, submeridional, and northwest. Two major faults divide mine field from the anticline limbs: Almazny fault, NW-trending high-angle fault with dip to the north, in the north, and Glavny thrust, latitudinal fault with moderate southward dip, in the south. Both of the faults show displacements with a strong component of right-lateral strike-slip.

In view of the observed structural complexity, the study area was divided into two domains along the Osevoy thrust: the first (D_1), to the north, and the second (D_2), to the southwest (Fig. 1). The geological structure of D_2 domain is relatively simple. Beds dip to the southwest, and the amount of the displacement or deformation is comparatively insignificant. In strike, the beds are bounded by the Osevoy and Glavny thrust planes in the west-northwest and south, respectively.

On the contrary, the structural pattern of D_1 domain is more complex, characterized by the plicative dislocation structure severely complicated by the faults. In their orientation, faults follow the three trends of the northwest, west-northwest, and longitudinal (N-S). NW- and N-S-trending high-angle (75–80°) faults with dip to the northeast and west, respectively, while the dip of WNW-trending faults is about 40° to the south-southwest (Fig. 2, a).

To form a better view of the structural pattern of D_1 domain it was also subdivided into two subdomains: the eastern (D_{1E}), and western (D_{1W}). The most important fault system in the D_{1E} subdomain is the large shear zone 300 m width, a NW-trending set of faults consisting of several parallel high-angle (70–80°) fault planes with dip to the northeast that can be followed for 500–800 m over the domain area (Fig. 3). It is traced to the east into the crest of the Horlivka anticline where it merges into the Osevoy thrust. The echelon NW faults are composed of right-stepping segments that imply a right sense of movement. The segment set has regular spacing of 100–150 m. The

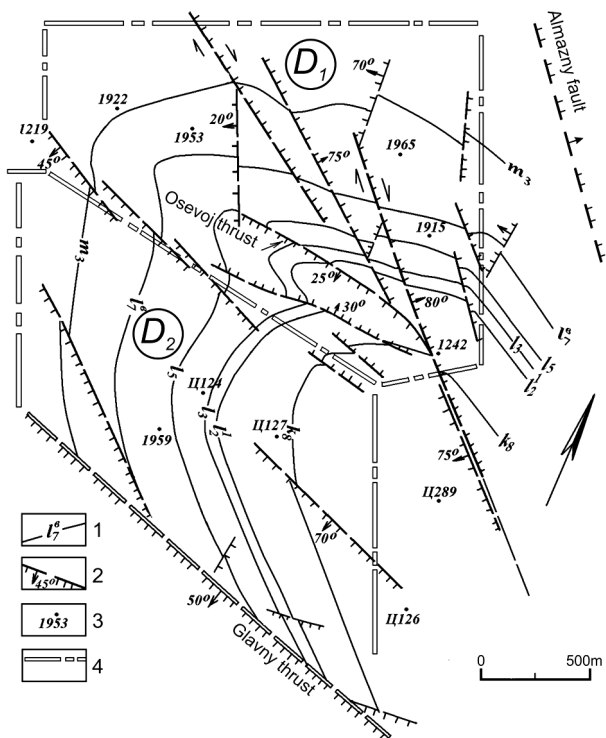


Fig. 1. Simplified geological and structural map of Novodzerzhynska mine field (plan of level -502 m):

1 – major coal seams; 2 – faults with attitude of dip; 3 – prospecting drills; 4 – structural domain boundaries

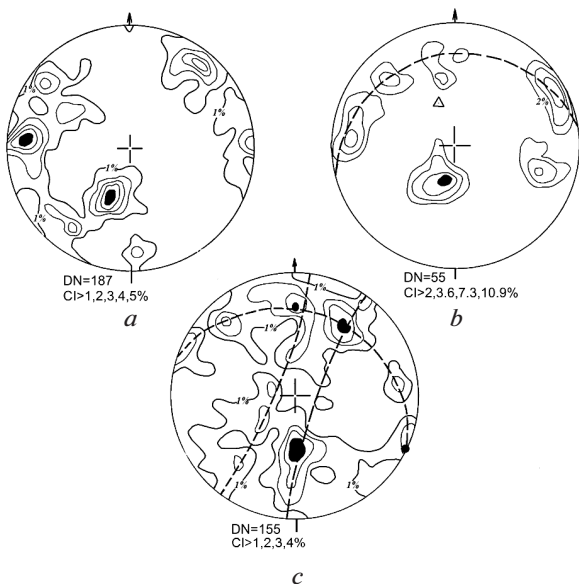


Fig. 2. A structural pattern of D_1 domain (all stereographic plots in this paper are upper-hemisphere projections):

a – contouring of poles to faults. Osevoj thrust zone; b – contouring of poles to faults; c – contouring of poles to slickenlines and grooves. Arcs of great and small circles are shown by dashed lines. Poles to those circles are shown by solid circles. DN, data number; C_1 , contouring interval

slickenlines plunge gently to the southeast, giving predominantly dextral-normal oblique-slip faults.

The area between the NW-trending faults is traversed by the NNE-trending set of sinistral-normal oblique-slip faults consisting of several parallel high-angle fault planes with 5–7 m of stratigraphic throw. In strike, they can be followed for 400 m, and are commonly bounded by the former fault planes.

From kinematic and structural standpoints, these two fault sets, NW (dextral normal-oblique) and NE (sinistral-normal oblique), may be inferred as a conjugate strike-slip fault system.

Dome-shaped fold is an important point in the context of geological structure of the D_{1W} domain which is not observed on the present topography and becomes readily apparent at more than 450 m depth below the surface. Periclinal closure and the north limb of the fold are best exposed on the current mining level and its south limb is cut by set of low-angle faults of the Osevoj thrust system (Fig. 4). The fold has gently plunging (20°) hinge-line which plunges to the west and south-dipping nearly upright (82°) axial plane. The south limb of the fold dips 18° to the west, and the

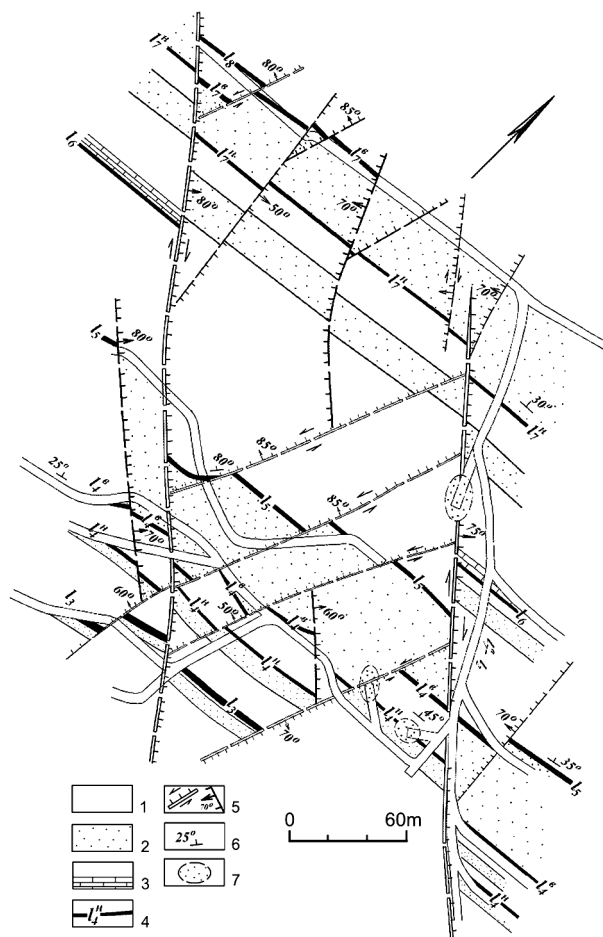


Fig. 3. A structural pattern of the D_1 domain shear zone (copy from a plan of level -502 m):

1 – argillites and aleurolites; 2 – sandstones; 3 – limestones; 4 – coal seams; 5 – faults with sense of slip, dip direction and dip angle of the fault; 6 – attitude of bedding; 7 – inrushes

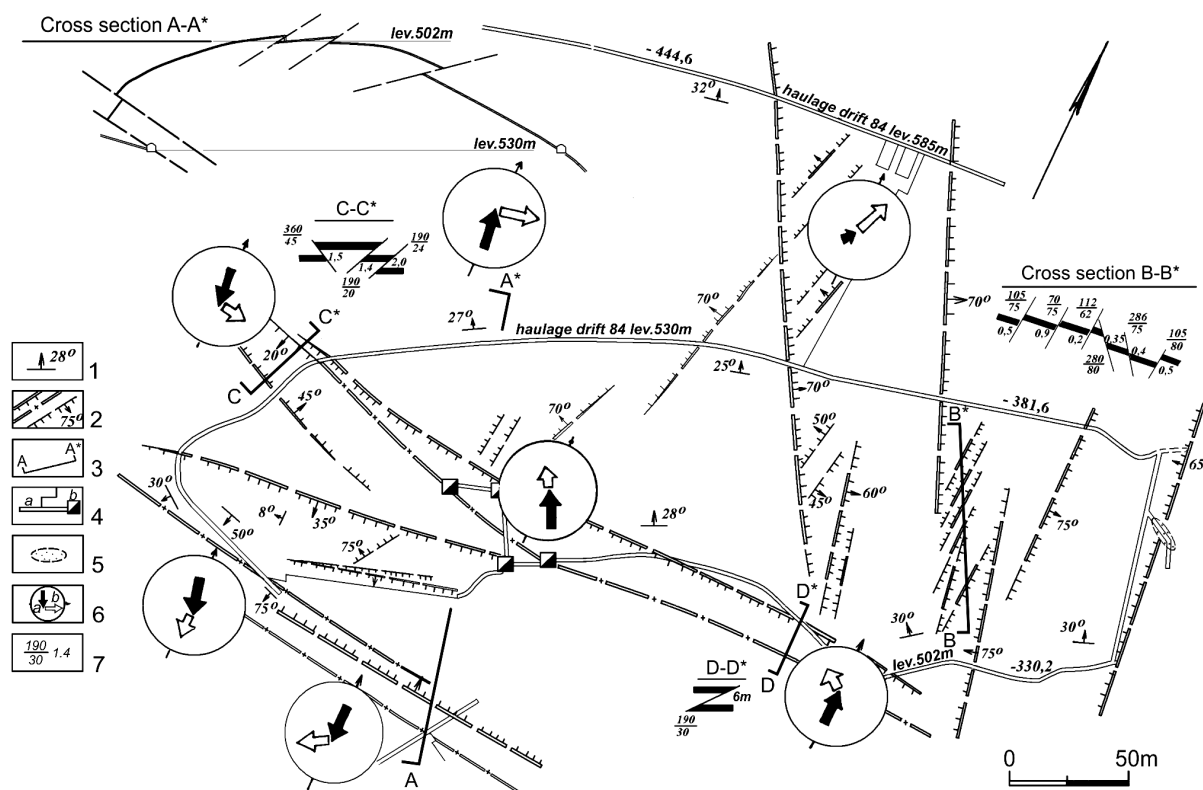


Fig. 4. Geological structure and stress fields of the Osevoy thrust zone (a copy of $1/2$ coal seam mining plan):
 1 – attitude of bedding; 2 – faults with dip direction and dip angle of the fault plane (for low-angle faults – layer crop lines in the hanging and footwalls); 3 – cross section lines; 4 – mining workings: (a) horizontal (drift), (b) vertical (rise); 5 – intrushes; 6 – points of stress fields reconstruction: (a) σ_3 upper-hemisphere projection, (b) σ_1 upper-hemisphere projection; 7 – fault attitude: dip direction (numerator), dip angle (denominator), and stratigraphic throw

north limb dips steeper (35°) than the south one to the north–northwest. According to dimensions, geometry and spatial orientation, the observed fold is similar to those of Nikitovka ore field.

In contrast to the shear zone, the faulting style of D_{1E} domain is mainly defined by WNW-trending faults of the Osevoy thrust system, parallel to the dome-shaped fold axis. Two sets of WNW-trending, N- and SSW-dipping, low-angle ($20\text{--}30^\circ$) thrust faults with the stratigraphic throw of up to 20 m on some of them have been observed there. Slickenlines are elongated parallel to the dip direction. In addition to the low-angle thrusts, network of numerous secondary high-angle faults is developed on both the hanging and footwalls of the thrusts. Relatively large and extensive ones of those are: NW-trending high-angle (75°) faults with 3–4 m of stratigraphic throw. Two sets of small high-angle ($55\text{--}70^\circ$) faults with the stratigraphic throws of a few decimeters to a couple of meters are mainly developed within the footwalls of the main NW-trending faults. In strike, they appear to follow the two trends of N–S and NE. These faults of comparatively small extent in strike, developing as fractures a few decimeters to a couple of meters away from the plane of the main fault, reach maximum stratigraphic throw in some meters, and then attenuate completely in 20–30 m in strike. Although these thrust-related faults have different kinematics, one with normal

movement and the other with a strike–slip movement, along NW- and NE-trending faults, lateral displacement prevails, and right-lateral slip along the former faults and left-lateral slip along the latter is the rule.

On equal-area plot, as shown in Fig. 2, b, poles to the fault planes, clustering around several distinct maxima, distribute along a great circle which corresponds to the Osevoy thrust plane. A slickenline analysis also shows the symmetry of the linear elements relatively to the Osevoy thrust plane (Fig. 2, c). There are three circles on equal-area plot, where one, a great circle, corresponds to the trace of the main fault plane, and two other, small circles, have a common axis, lying in the thrust plane.

According to the foregoing data, movements on all of these faults at the D_{1E} domain most likely have appeared due to general displacement of the massif along the main fault plane.

Stress fields. Tectonic stresses in the massif localities have been studied by the kinematic method [4]. The input for the study was field-measured orientation data for faults and slickenlines from mine workings within Novodzerzhynska mine field consisting of the orientations of the fault planes and slickenlines, including the sense of movement. Mesoregional level stress field characteristics have been reconstructed by statistical processing of local stereographical solutions. Local stress data processed by the method for determi-

nation of general stress fields provide for reconstruction of principal normal stresses which are arbitrarily considered as regional stresses [5].

It has been determined that maximum stress axes are concentrated in the upper left (NW) and in the diagonally opposite (SE) sector of the stereogram, while minimum stress axes, on the contrary, are concentrated in the upper right (NE) and lower left (SW) sectors (Fig. 5). At mesoregional level, the reconstructed stress field is strike-slip faulting type and characterized by a NW–SE, 320–330° and 140–150°, subhorizontal principal compression axis and subhorizontal NE–SW, 50–60 and 230°–240°, principal extension axis.

However, despite the persistent general orientation of the principal stress axes, some differences in its orientation within the domains have been revealed. For example, in the D_2 domain, as shown in Fig. 5, c , σ_1 plunges at a low angle southwestward (232°/30°) and σ_3 is southeast and horizontal (140°/5°), lying at average bedding plane of this domain. In the D_{1W} subdomain, σ_1 and σ_3 plunge moderately to the northeast (65°/24°) and northwest (330°/20°), respectively, also lying at nearly average bedding plane of this subdomain (Fig. 5, a). In the D_{1E} subdomain, σ_1 and σ_3 plunge moderately to the southwest (230°/28° SW) and northwest (330°/18° NW), respectively, but the σ_3 axis is located near to bedding plane and σ_1 is lying at the plane of the Osevoy thrust fault (Fig. 5, b).

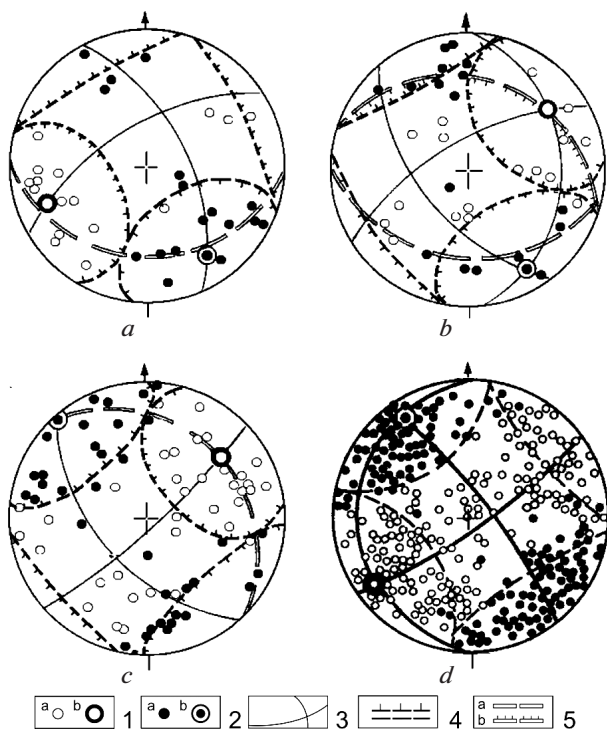


Fig. 5. Stress fields of Novodzerzhynska mine (a to c) and Nikitovka ore field (d):

1 – minimum principal stress axis of local (a) and mesoregional (b) level; 2 – maximum principal stress axis of local (a) and mesoregional (b) level; 3 – planes of principal stress axes; 4 – boundaries of compression and extension cones; 5 – planes of bedding (a) and Osevoy thrust (b)

There is such a feature of the structure of the reconstructed stress field in distribution of local stress fields as regular bending of trajectories of the principal stress axes near the large faults, where the axes tend to be oriented either perpendicularly or parallel to the fault plane. These parts interchange each other along the fault plane (Fig. 4).

The close agreement of the stress field reconstructed for the study area and Nikitovka ore field strongly suggests one origin and one stress field that resulted in present-day structural pattern, as can be seen in Fig. 5, d . This stress field that apparently originated in Laramide time of Alpine orogeny is the youngest for the Donets Basin.

Series of six stress fields (F to A) resulting in the development of the geological structure of the western closure of the Horlivka anticline has been defined and reconstructed [6]. Directed and inherited character of changing of the tectonic loading conditions of the geological structure of the study area is characterized by consecutive change of the stress field type from the oldest (F), normal faulting type, to the youngest (A), strike-slip faulting one. The main characteristics of the stress fields are given in Table 1. There is no possibility to define absolute time lags of the action of the stress fields exactly, nevertheless the youngest stress field A is synchronized with the youngest one reconstructed for the Donbas and Priazovie.

Strain fields. Strain field is heterogeneous for the western closure of the Horlivka anticline area. Orientation of axes of total strain field and type of strain field are changing both all over the study area and within the large geological structures.

Maximum extension axis ϵ_1 is the most invariable and characterized by mainly gently plunging to the southwest nearly all study area. However, as it is apparent from Fig. 6, a , some divergence of ϵ_1 axis orientation is observed within the large faults, for instance,

Table 1

Characteristics of the principal axes of the stress fields

Phase	Type	σ_1	σ_2	σ_3	μ_σ
		Dir./Pl.	Dir./Pl.	Dir./Pl.	
A	S	257/3	154/77	348/13	0.9
B	R	219/67	79/18	344/14	0.95
C	R	187/75	347/14	78/5	0.95
D	S	336/13	178/76	68/5	-0.95
E	N	350/15	260/1	166/75	-0.95
F	N	259/2	350/15	162/75	-0.9

Notes: Types of the stress field: N – normal; R – reverse; S – strike-slip; Dir. and Pl. – trends and plunges of principal stress axes in degrees; σ_1 , σ_2 , σ_3 – minimum, intermediate, and maximum principal axes of the stress field; μ_σ – Lode–Nadai coefficient: uniaxial tension (-1), uniaxial compression (+1)

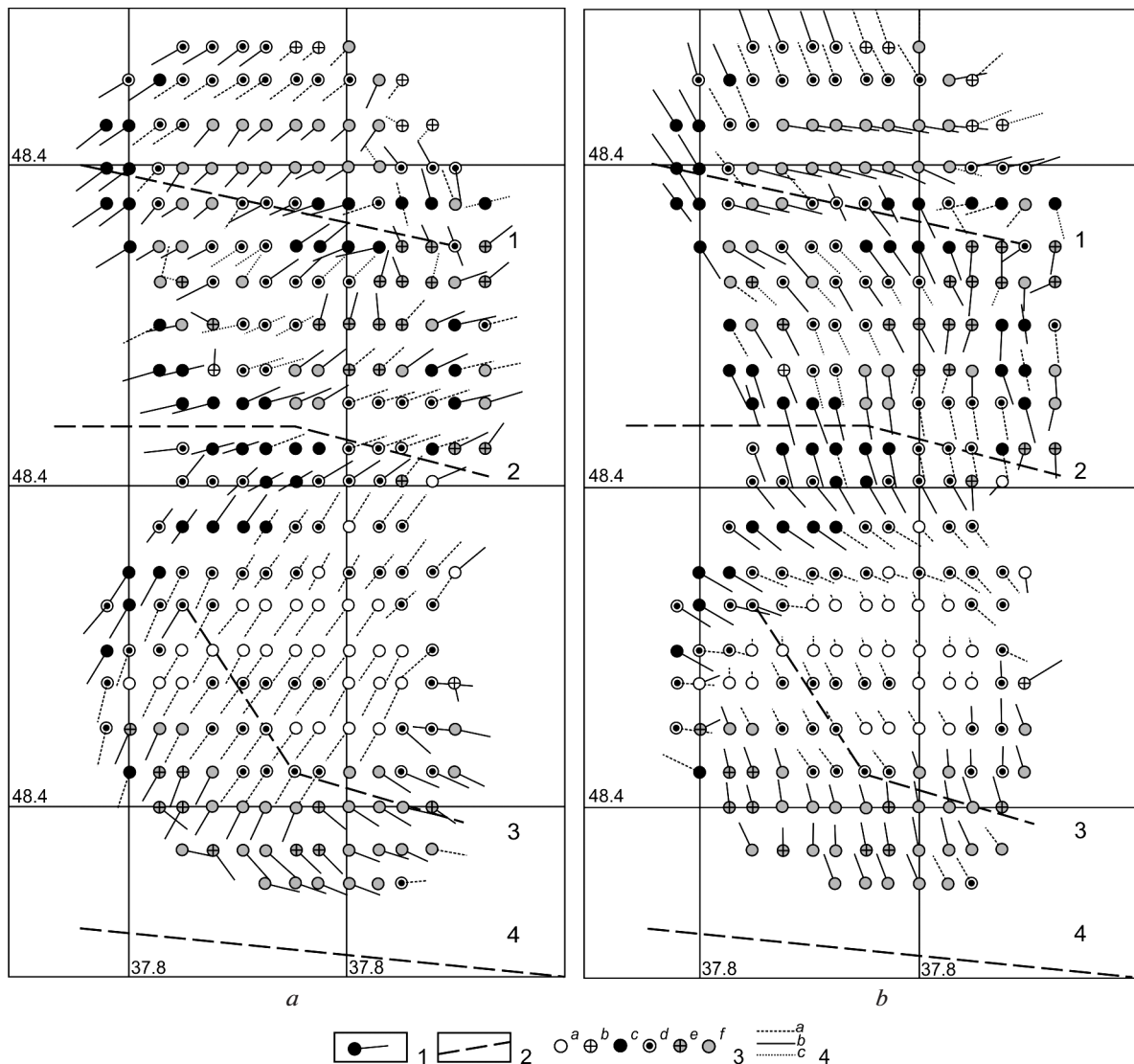


Fig. 6. Projections to a horizontal plane of the principal strain axes and distribution of the Lode–Nadai coefficient values for the western closure of the Horlivka anticline:

a – extension axis ε_1 ; *b* – shortening axis ε_3 ; 1 – horizontal projections of the strain axes (plunging is out from the circle; the length of the projection corresponds to the angle of plunge of the axis: shorter axis – steeply plunging, longer axis – gently plunging, centered point axis – (sub)horizontal); 2 – faults (shown sketched): 1 – Severny thrust, 2 – Osevoy thrust, 3 – Toretzky thrust, 4 – Glavny thrust; 3 – type of strain field (corresponding to the values of the Lode–Nadai coefficient): (a) normal, (b) reverse, (c) strike-slip, (d–e) transitional (oblique-slip), (f) octahedral; 4 – Lode–Nadai coefficient: (a) uniaxial extension ($\mu = -1$); (b) pure shear ($\mu = 0$); (c) uniaxial shortening ($\mu = +1$)

within the Osevoy thrust and transition zone between Toretzky and Hlavny thrusts, where ε_1 axis tends to be oriented sublatitudinally (Table 2).

Maximum shortening axis ε_3 is less invariable both in strike – from meridional to sublatitudinal – and in an angle of plunging – from subhorizontal to subvertical (Fig. 6, *b*). Intermediate strain axis ε_2 is the least invariable, often in irregularly standing position from gently to steeply (or vertical) plunging, especially within the large faults.

Strike-slip faulting type of total strain field was determined for most part of the western closure of the Horlivka anticline area (Fig. 6). According to the

Lode–Nadai coefficient (μ_c) which is nearly equal to ± 1 or varied in range from $+0.5$ to -0.5 , deformations on the study area had been going under shear conditions. Axial part of the anticline within Osevoy thrust and paraxial part of the anticline southern limb within Toretzky thrust are characterized by normal faulting type of the total strain field, where deformations had been going under uniaxial extension conditions ($\mu_c = -1$).

In the whole, it can be asserted that strike-slip faulting strain field type is characterized by NW and N–S-plunging maximum shortening axis and strain conditions which are similar to pure shear prevailing in

Table 2

Variability of orientation of the principal strain axes within the large faults of the study area

	ε_1	
	Dir.	Pl.
	227–238	27–60
Severny thrust	221–248; 335–346	11–55
	234–265; 51–79	11–29; 17–42
Osevoy thrust	255–257; 56–79	9–30; 11–19
	33–63; 207–217	0–20
Toretzky thrust	207–217; 95–125	16–30
	97–135; 198–215	22–43
	ε_3	
	334–342	11–18
Severny thrust	73–104; 138–189	11–55; 13–31
	136–173	34–46
Osevoy thrust	157–174	12–31
	115–144; 333–350	21–33; 57–74
Toretzky thrust	324–342	48–53
	338–359	33–47

Notes: ε_1 and ε_2 – extension and shortening axes of local strain fields; Dir. and Pl. – trends and plunges of principal strain axes in degrees

the western closure of the Horlivka anticline area of the Donets Basin. Extension axis ε_1 of the strain ellipsoid is oriented NW and N–S within the western closure of the Horlivka anticline, and shortening axis ε_3 is oriented NE nearly orthogonal to the anticline axis. Summing up the results, it can be concluded that the strain tensor forms an ellipsoid similar to the stress ellipsoid.

Thus, the western closure of the Horlivka anticline can be considered as the area of the extension in back part of right-lateral strike-slip fault.

The data above allow us to suggest the shear zone revealed in the D_{1W} subdomain is the direct extension of the regional right-lateral displacement within the Main anticline paraxial part. Conjugated strike-slip fault system was formed due to the right-lateral displacements that originated in final stages of Alpine orogeny. Horizontal displacements of the sediment masses to the west at the south limb of the anticline were accompanied by a compression in near-horizontal plane. It resulted in the longitudinal bending of the sediment masses accompanied by formation of the dome-shaped fold and sublatitudinal thrust faults developed at the limbs of the fold. Horizontal displace-

ments at the walls of thrust faults resulted in formation of normal oblique-slip faults which might have developed as normal faults subsequently.

The findings of our research are quite convincing, and thus the following conclusion can be drawn: a structural pattern of the deformation elements of the Main anticline western closure may be interpreted as a single pattern of structural paragenesis developed due to the right-lateral displacements along the longitudinal strike-slip fault system within the Main anticline paraxial part.

Conclusions. NW-trending dextral and NE and N–S-trending sinistral strike-slip faults prevail among the other faults within the study area. Mesoregional stress field, characterized by subhorizontal position of NW–SE-oriented maximum principal stress axis (σ_3) and NE–SW-oriented minimum principal axis (σ_1) is shear type. This one that apparently originated in Laramide time of Alpine orogeny is the youngest for the Donets Basin. Extension axis (ε_1) of the strain ellipsoid is NW and N–S oriented within the western closure of the Horlivka anticline, and shortening axis (ε_3) is NE oriented nearly orthogonal to the anticline axis. Strike-slip faulting type of total strain field was determined for most part of the western closure of the Horlivka anticline area, and according to the Lode–Nadai coefficient ($\mu_e = \pm 1$), deformations on the study area had been going mainly under shear conditions. The pattern of a single structural paragenesis of deformation elements of the study area, including a conjugate strike-slip fault system, dome-shaped fold and longitudinal thrusts in its limbs, was developed due to the right-lateral displacements along the longitudinal strike-slip fault system within the Main anticline paraxial part.

The present results which have just been explained briefly, may allow forecasting to be made of structural patterns of deformation structures that forms in right-lateral shear zones at deeper mine levels.

References / Список літератури

1. Gintov, O. B., 2005. *Polevaia tektonofizika i ee primenenie pri izuchenii deformatsiy zemnoy kory Ukrainy* [Field tectonophysics and its application to the studies of deformations of the Earth's crust of Ukraine]. Kyiv: Phoenix.
2. Гинтов О. Б. Полевая тектонофизика и ее применение при изучении деформаций земной коры Украины / Гинтов О. Б. — К.: Феникс, 2005. — 572 с.
3. Kopp, M. L., Korchemagin, V. A. and Kolesnichenko, A. A., 2010. Alpine deformations in Donbass: Periodicity, character of stresses, and their probable sources. *Geotectonics*, Vol. 44, No. 5, pp. 405–423.
4. Kopp, M. L., Verzhbitsky, V. E., Kolesnichenko, A. A., Tveritina, T. Yu., Vasil'ev, N. Yu., Korchemagin, V. A., Mostryukov, A. O. and Ioffe, A. I., 2014. Recent stress field in the east of the Russian Plate and the Urals from macro- and mesostructural evidence. *Geotectonics*, Vol. 48, No. 4, pp. 273–291.
5. Sim, L. A., 2013. Overview of the state of knowledge on paleotectonic stresses and their implications

for solution of geological problems. *Geodynamics & Tectonophysics*, Vol. 4, No. 3, pp. 341–361.

Сим Л. А. Краткий обзор состояния изученности палеотектонических напряжений и их значение для решения геологических задач / Л. А. Сим // Тектонофизика и геодинамика. — 2013. — Т. 4(3). — С. 341–361.

5. Sim, L. A., Zhirov, D. V. and Marinin, A. V., 2011. Stress-and-strain reconstruction for the eastern segment of the Baltic shield. *Geodynamics & Tectonophysics*. Vol. 2, No. 3, pp. 219–243.

Сим Л. А. Реконструкция напряженно-деформированного состояния восточной части Балтийского щита / Л. А. Сим, Д. В. Жиров, А. В. Маринин // Тектонофизика и геодинамика. — 2011. — Т. 2(3). — С. 219–243.

6. Nikitenko, A. V., 2014. Stress fields of the Horlivka anticline western closure of the Donbas and its progress staging. *Naukovi pratsi Donetskooho natsionalnoho tekhnichnoho universitetu. Seriya: Hirnychoheolohichna*. Issue 1(20), pp. 113–121.

Никитенко А. В. Поля напряжений западного замыкания Горловской антиклинали и стадийность их развития / А. В. Никитенко // Наукові праці Донецького національного технічного університету. Серія: Гірничо-геологічна. — 2014. — Вип. 1(20). — С. 113–121.

Мета. Визначення умов та механізму розвитку геологічної структури західного змикання Горлівської антиклиналі.

Методика. Детальне картування з елементами структурно-морфологічного аналізу всіх відомих тектонічних елементів району та тектонофізичні методи аналізу тріщинно-розривних структур.

Результати. Встановлено, що серед розривів різного структурного рівня домінують зсуви: північно-західні — праві, північно-східні та субмеридіональні — ліві. Виділено правозсувовий структурний парагенезис деформаційних елементів структури західного змикання Горлівської антиклиналі, що містить у собі комплекс спряжених північно-західних та меридіональних розривів, брахіантиклинальну складку другого порядку, крила якої ускладнені насувами, що орієнтовані повздовж осі головної складчастої структури першого порядку. Встановлено, що за просторовою орієнтацією осі головних нормальних напружень, відновлене поле напружень є зсувовим та наймолодшим для Донецького басейну, датованим ларамійською фазою альпійського тектогенезу. Зсувовий тип поля сумарних деформацій є домінуючим на більшій частині зони західного змикання Горлівської антиклиналі.

Наукова новизна. Виявлені зсуви та зсувові зони, охарактеризована їх морфологія, супутні деформації та механізми формування. Відновлені головні характеристики полів напружень та деформацій локального й мезорегіонального рівня.

Практична значимість. Впровадження у практику геологорозвідувальних та геолого-експлуата-

ційних робіт нових наукових методів прогнозу гірничо-геологічних умов, що засновані на реконструкції головних тектонофізичних параметрів і відтворенні механізмів деформаційного процесу.

Ключові слова: кінематичний метод, поля напружень та деформацій, коефіцієнт Лодє–Надаї, штрихи ковзання, зсувна зона, зсув, структурний парагенезис

Цель. Определение условий и механизма развития геологической структуры западного замыкания Горловской антиклинали.

Методика. Детальное картирование с элементами структурно-морфологического анализа всех известных тектонических элементов района и тектонофизические методы анализа трещинно-разрывных структур.

Результаты. Установлено, что среди разрывов различного структурного уровня здесь доминируют сдвиги: северо-западные — правые сдвиги, северо-восточные и субмеридиональные — левые. Выделен правозсувовый структурный парагенезис деформационных элементов структуры западного периклинального замыкания Горловской антиклинали, включающий в себя комплекс сопряженных северо-западных и меридиональных разрывов, брахиантиклинальную структуру второго порядка, крылья которой осложнены надвиговыми структурами, ориентированными продольно оси главной складчатой структуры первого порядка. Установлено, что по пространственной ориентировке осей главных нормальных напряжений, восстановленное поле напряжений является сдвиговым и самым молодым для Донецкого бассейна, датированным ларамийской фазой альпийского тектогенеза. Сдвиговый тип поля суммарных деформаций является доминирующим на большей части площади западного замыкания Горловской антиклинали.

Научная новизна. Выделены в геологической структуре изучаемого района сдвиги и сдвиговые зоны, описана их морфология, сопутствующие деформации и механизм образования. Восстановлены основные характеристики полей напряжений и деформаций локального и мезорегионального уровня.

Практическая значимость. Внедрение в практику геологоразведочных и горно-эксплуатационных работ новых научных методов прогноза горно-геологических условий, основанных на реконструкции основных тектонофизических параметров и восстановлении механизмов деформационного процесса.

Ключевые слова: кинематический метод, поля напряжений и деформаций, коэффициент Лодє–Надаи, зеркала скольжения, сдвиговая зона, сдвиг, структурный парагенезис

Рекомендовано до публікації докт. геол. наук В. І. Альохінім. Дата надходження рукопису 05.01.16.

UDC 552.4.051.6(477.63)

I. S. Paranko, Dr. Sc. (Geol.), Prof.,
O. A. MatishchukKryvyi Rih State Pedagogical University, Kryvyi Rih,
Ukraine, e-mail: matischuk@gmail.com**THE INTERRELATION BETWEEN THE NOVOKRYVORIZKA
AND SKELIUVATSKA SUITES OF THE KRYVYI RIH SERIES****I. С. Паранько**, д-р геол. наук, проф.,
О. А. МатишукКриворізький державний педагогічний університет,
м. Кривий Ріг, Україна, e-mail: matischuk@gmail.com**ДО ПИТАННЯ ПРО ВЗАЄМВІДНОШЕННЯ
НОВОКРИВОРІЗЬКОЇ ТА СКЕЛЮВАТСЬКОЇ СВІТ
КРИВОРІЗЬКОЇ СЕРІЇ****Purpose.** Explore features of the structure and the relationship between the nature of occurrence of Novokryvorizka and Skeliuvatska Suites.**Methodology.** The authors used analysis of suite sections and field research. The results of geochemical analyses were used to determine the ratio of the contents of indicator elements and facial conditions of sedimentation of rocks, quantitative assessments of weathering intensity and the extent of sedimentary differentiation of metasedimentary deposits of various paleotectonic modes for the purpose of paleotectonic reconstruction.**Findings.** The results of geological investigations of conglomerate bearing strata of Kryvbas indicate that the lower part of the section of Kryvyi Rih series there are two different of formation types of metaconglomerate – schistic and oligomictic ones – according to composition and conditions. The former are part of the metaconglomerate-schist formation, which corresponds to the volume of Novokryvorizka suite in its modern interpretation, and the latter are part of the metaconglomerate-sandstone-schist, which combines metaterrigene part of Skeliuvatska suite section. The section of the upper part of Novokryvorizka suite is represented by the association of different chlorite schists and quartz metasandstone with subordinate spread of slate metaconglomerates according to the composition. The number of layers of metasandstones and their capacity increase upsection. The lower part of the Skeliuvatska suite section is presented by rhythms, composed by paragenesis metasandstone + metagritstone. Moreover, metasandstones are deposited at the base of rhythms and are similar to the metasandstones of the upper part of the section of Novokryvorizka suite according to the mineral composition and structural-textural features. This indicates a gradual transition between these suites and refutes the assumption regarding the basal character of quartz metaconglomerates of Skeliuvatska suite, as they are inherent to its central section, where they are involved in forming rhythms made of metasandstone ± metagritstone + metaconglomerate association. That is, the section of Skeliuvatska suite bottom has regressive character rather than transgressive character, as it is believed to be.**Originality.** The nature of the contact between Novokryvorizka and Skeliuvatska suites was studied, the peculiarities of their material composition that paleotectonic features of their formation were compared.**Practical value.** The research results can be used for stratigraphic subdivision of the sections; techniques used in the article can be used for paleotectonic reconstructions.**Keywords:** *suite Novokryvorizka, Skeliuvatska, Kryvyi Rih series***Introduction.** It is considered that Skeliuvatska suite with its angular unconformity and stratigraphic break is deposited on Novokryvorizka suite rocks [1]. The reason for such understanding of interrelation between these stratigraphic units of Kryvyi Rih series is based on an assumption that the metamorphosed weathering zones are developed in the metabasites of the Novokryvorizka suite [2], transgressive character of the Skeliuvatska suite profile and occurrence of quartz metaconglomerates, which are the main diagnostic features for the Skeliuvatska suite. However, the results of the geological formation analysis of the conglomerate-bearing beds of the Kryvbas reveals that in the lower part of the section of Kryvyi Rih series there are two types of metaconglomerates which differ in compositions and the formation conditions: schistic and oligomictic. The former belong to the metacon-

glomerate-schist formation, which corresponds to the volume of the Novokryvorizka suite according to a new interpretation [3], and the latter – to metaconglomerate-sandstone-schist formation, which is the metaterrigeneous part of the Skeliuvatska suite [4, 5].

Objectives of the article. Based on the analysis of suite sections and application of methods for paleotectonic reconstructions, the work aims at researching structural features and the relationship of the bedding character of Novokryvorizka and Skeliuvatska suites.**Presentation of the main research and results.** Novokryvorizka suite is well exposed in the eastern part of the Kryvyi Rih structure, to the south of the Devladvivka fault zone, as well as in the region of the Main Synclinorium closure, in the Tarapakovskyi-Lykhmanivskyi section and in the area of the Tarapakovskyi-Lykhmanivskyi structure closure (Fig. 1). This Suite is generally composed of chlorite-bearing (quartz-chlorite, quartz-sericite-chlorite, chlorite-biotite, amphi-

bole-chlorite), biotite-amphibole and biotite-quartz schists. Quartz-amphibole-biotite, garnet-amphibole-biotite schists, metasandstones cemented with chloritic matrix and schist metaconglomerates are subordinate. The characteristic feature of the Novokryvorizka suite is lateral compositional variability and a constant presence of chlorite-bearing schists in its section.

In the western part of the Main structure closure the section of the suite is composed of alternating biotite-amphibole, quartz-biotite and chlorite-biotite schists with minor quartz-sericite and quartz-sericite-chlorite varieties (Fig. 2). Amphibole-bearing schists constitute up to 40–50 % of the suite volume, forming the beds of thickness between 4 and 7 m with a gradual decrease

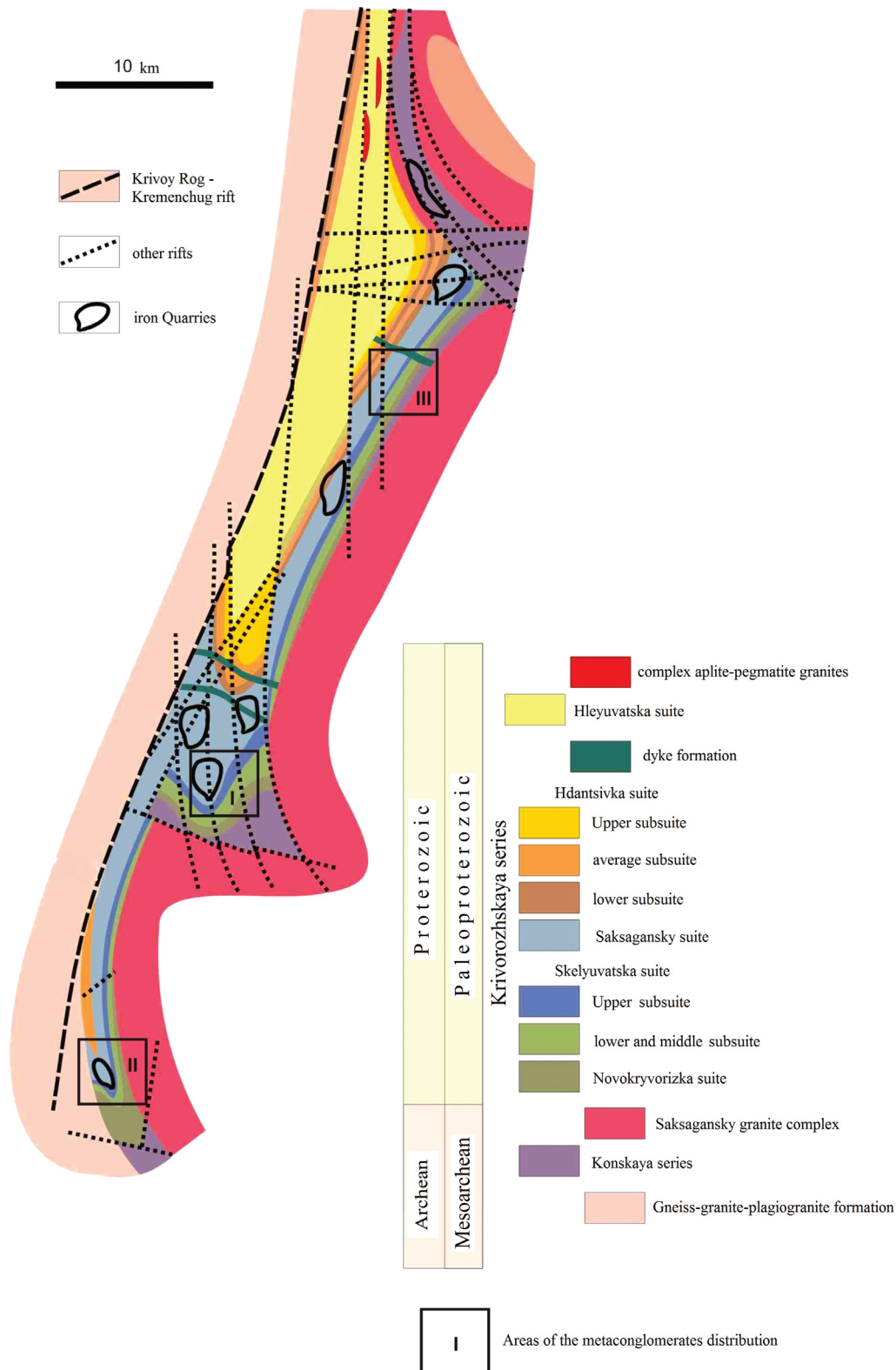


Fig. 1. Dissemination of metaconglomerate on the territory of Kryvyi Rih structure

towards the upper part of the section. These are fine-grained rocks composed of 70 % of bluish-green hornblende with many inclusions of quartz, plagioclase and biotite. The rock texture is banded, whereas the structure is poikiloblastic. Quartz-biotite varities forming beds of thickness between 2 and 5 m are strictly associated with these rocks. They are represented by fine-grained dark grey and black rocks of lepidogranoblastic structure. In general, biotite undergoes chloritization and occupies 40–50 % of the rock volume. Quartz and plagioclase occur in the same quantities: 25–30 %. Plagioclase is sericitised and contains small quartz inclu-

sions which are of spherical or sometimes needle-like shapes. Quartz is anhedral and sometimes shows rounded grain edges. There also occur single crystals of hornblende, which are petrographically similar to the hornblende form of the above mentioned schists.

Biotite-chlorite schists are distributed in all levels of the suite section in form of 1–4 m beds; however, they are more characteristic of the upper part, where they occur in association with quartz-sericite schists and quartz metasandstones. Their main rock-forming minerals are quartz and biotite, which occupy up to 75–80 % of the rock volume; however, chlorite prevails quantitatively.

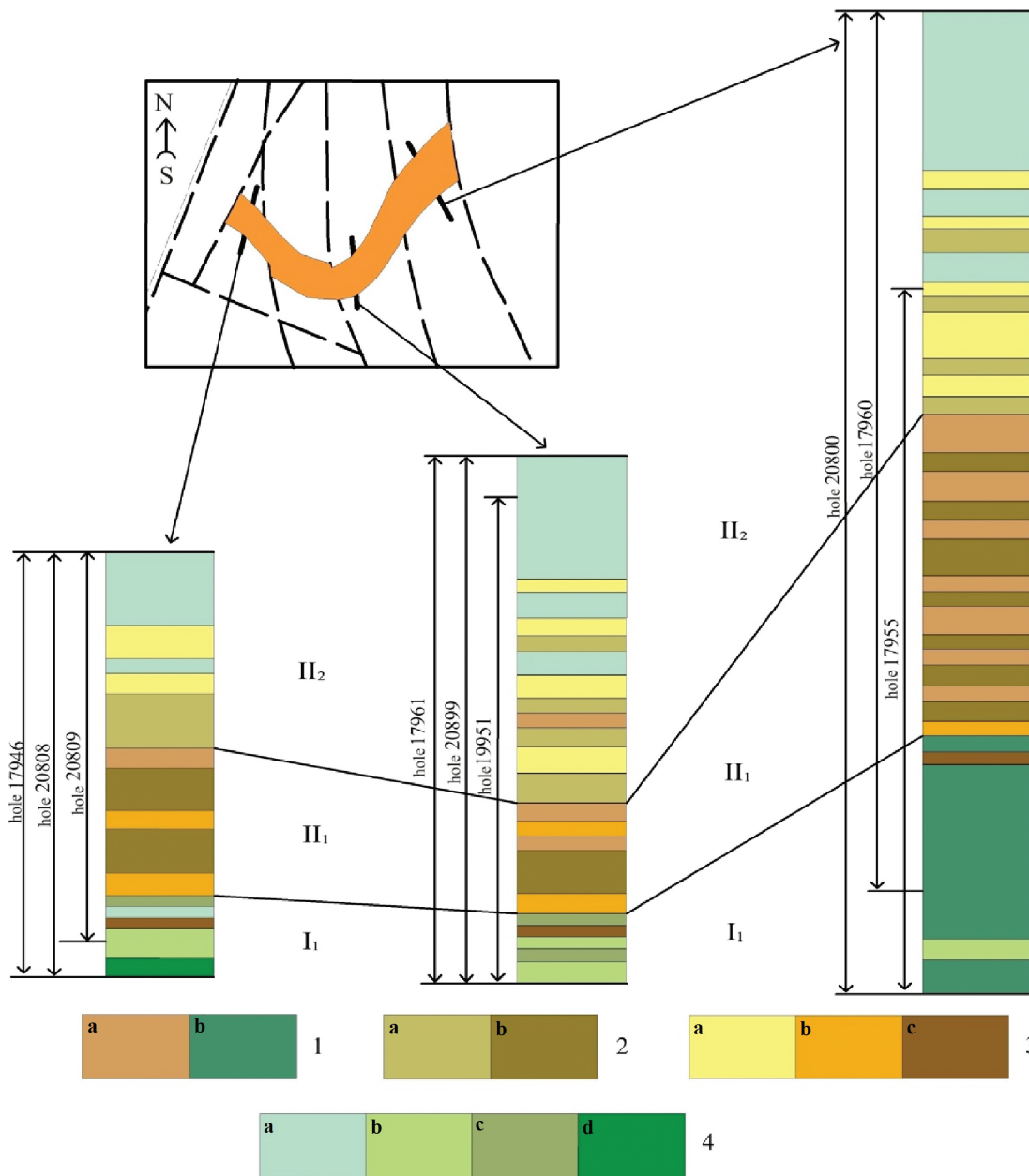


Fig. 2. Correlation of the sections of the western part of the Main closure of the Kryvyi Rih structure:

1 – metaconglomerates: a – oligomictic, b – schistic; 2 – metagravelites: a – quartz, b – feldspar-quartz; 3 – metasandstones: a – feldspar-quartz, b – quartz c – polymictic cemented with chlorite; 4 – schists: a – quartz-sericite, b – quartz-biotite-chlorite, c – garnet-chlorite-biotite, d – quartz-hornblende-biotite; Geological formations: I – metaconglomerate-schist (Novokryvorizka suite); II – metaconglomerate-sandstone-schist (Skeliuwatska suite): II₁ – metaconglomerate-gravelite-sandstone subformation, II₂ – metagravelite-sandstone-schist subformation

Quartz-sericite schists, which occupy up to 5–7 % of the section volume, occur in minority within the Suite.

In the upper part of the Suite section, 10–20 cm thick beds of fine-grained metasandstones are found in the association with schists. Their quantity and thickness increase towards the top of the Suite section.

Depending on the spatial distribution of the above mentioned rock varieties, the Suite section in the western limb of the Main Synclinorium, where its thickness does not exceed 50 m, is divided into three parts: lower, middle and upper. The lower part is characterized by amphibole-bearing, quartz-biotite and chlorite biotite schists association. The middle part is composed of paragenesis: chlorite-biotite and quartz-biotite schists. The latter, upper part comprises alternating quartz-sericite-biotite, chlorite-biotite sometimes with garnet, schists and oligomictic metasandstones.

The section in the central region of the Main Structure closure is composed mostly of biotite-amphibole schists, which unlike the schists of the western region, contain actinolite. However, regarding other mineralogical and petrographical features, they are similar to the schists from the western region. These schists in the suite section form beds of thickness ranging between 5 and 10 m and are separated by layers of quartz-biotite and biotite-chlorite varieties. Their thickness increases towards the top of the section from 0.5 up to 1.5–2.0 m. This association is overlain by a 30 m bed composed of biotite-quartz schists with intercalations of chlorite-biotite and chlorite-biotite-quartz varieties 0.1–1.5 m thick. The association of chlorite-biotite, chlorite-biotite-quartz schists and oligomictic metasandstones terminates the suite section. These mentioned rocks are similar to those mentioned above in terms of mineralogical and petrographical features. The thickness of the Suite in the given part of the Main Structure closure reaches 130–150 m.

Similar compositional features are typical of the Suite section in the Saksahanskyi interval (eastern limb of the Kryvyi Rih Structure) and Tarapakovskiy-Likhmanovskiy interval, and also in the region of Inguletskiy iron quartzite deposit (Lykhmanivskiy Synclinorium). The exception is the section of the eastern part of the Main Structure closure, due to presence of schistic metaconglomerates, which form 130–140 m thick bed in the lower part of the Suite section. The clastic material of the metaconglomerates comprises, in 80–90 %, poorly or medium sorted fragments of chlorite-quartz, chlorite-amphibole, chlorite-sericite-quartz, sericite-quartz schists, which are similar to those from the above described profiles in terms of mineralogical and petrographical features. In the composition of the metaconglomerates there also occur single clasts of vein quartz, quartzites, mafic effusive rocks and amphibole schists. The matrix cementing these clasts is sandstone of variably-sized grains, which are composed of quartz, feldspar, garnet and carbonates. These clasts are cemented with chlorite-sericite material. Regular change in the proportion of chlorite to sericite content is typical for the section. In the lower part of the bed, chlorite prevails within the matrix,

whereas in the upper part sericite dominates. This trend is also reflected in the composition in the metaconglomerates. The metaconglomerate beds from the lower part of the section are medium and coarse-grained with clasts of diameters from 2–3 to 5 cm. Towards the top of the section the diameter of the clasts decreases, simultaneously the quantity of the vein quartz and quartzite clasts increases and the amount of clastic material in the rock volume decreases from 80–85 % in the lower part of the bed to 60–70 % in the upper part.

The metaconglomerates are underlain by fine-grained, weakly banded chlorite-quartz, chlorite-amphibole and amphibole-chlorite schists. Similar schists with scarce inclusions of coarse clastic material are also found in the middle of the lower part of the metaconglomerate series, in which they form layers of thickness varying between 0.5 to 1.0 m. This indicates rhythmic internal composition of the profile. According to mineralogical and petrographical features, the schists are similar to those which contain clastic material and, as mentioned before, to the schists which were described above.

The suite section at Lenin mine (Saksahanskyi interval) features a similar composition; it also contains schist conglomerates. The only difference is that here the suite thickness reaches a few dozens of meters, whereas in the eastern part of the closure it ranges between 300 and 350 m.

Rocks of the suite have been metamorphosed in greenschists facies (Saksahanskyi region of the Kryvyi Rih structure) and epidote-amphibolite facies (Southern region) [4, 6].

Skeliuvatska suite outcrops in the eastern part of the Kryvyi Rih structure, to the south of the Devladvivka fault zone. It includes oligomictic metaconglomerates, quartz and feldspar-quartz metasandstones, quartz-biotite, quartz-sericite-biotite, sericite-biotite schists, which are conventionally known as phyllites [6].

Depending on the relative proportions of the major and minor rock types, the profile of the metaterrigenous suite is divided into two subsuites: the lower and the upper.

The lower subsuite is represented by rocks showing the regressive transition within the profile. They are quartz metasandstones, metagravelites and metaconglomerates, which reflect two- or three-component rhythms of higher orders. The former include metasandstones and metagravelites typical of the lower part of the subsuite, whereas the rhythms composed dominantly of metasandstones, metagravelites and metaconglomerates are typical of its middle and upper parts. The most complete section of the subsuite has been opened up in many boreholes in the Main Structure closure in the Kryvbass, and also in many outcrops along the banks of the Inhulets River in the region of workers' settlement of the Pivdennyi Ore-Dressing Integrated Plant.

In the region of the Main Structure closure, two types of subsuite profiles are observed. They differ in the quantitative, relative proportions of the rock types. The sections of the western and central parts of the closure include metagravelites, which form 1–40 m thick bed and are separated by layers of metasandstones and

metaconglomerates. The metagavelit + metasandstone association is more characteristic of the lower part of the subsuite section, in which metasandstones are present in form of layers of thickness increasing towards the top from 1 to 3 m. In the same direction the thickness of the metagavelite layers increases; they are quantitatively enriched in gravel-sized clastic material from its base (50 % of the rock volume) to the top (70–80 %). At the same time, inclusions of pebbles are observed in metagavelites and their amount also increases towards the top of the section. The metagavelites are gradually replaced by metaconglomerates.

The metaconglomerates form beds and lenses of thickness ranging from 1 to 7 m in the upper part of the subsuite section. The contacts between them and the metagavelites, as already mentioned, are gradual. In most cases the metaconglomerates are interbedded with thin layers (from 0.1–0.2 to 1 m) of fine- to medium-grained metasandstones. Contacts between them are sharp and clear.

The gradual transition from the base to the top of the section of the metagavelite-metasandstone association reflected in metaconglomerat+metagavelit±metasandstone paragenesis is indicative of the regressive character of the deposition.

The subsuite thickness in the western and central parts of the Main Structure closure is alternating from 25 up to 50 m.

The characteristic feature of the eastern part of the closure is increase in the thickness up to 120–140 m and the quantity of metaconglomerates, which here comprise around 50–70 % of the section volume, compared to 10–15 % in the central and western parts of the structure. The subsuite includes association of metagavelites and metaconglomerates, which form a bed of thickness from 2–10 (metaconglomerates) up to 20 m (metagavelites). Metasandstones occur as minority and form thin (tens of cm) layers and lenses. In the lower part of the section, the metagavelites prevail quantitatively over the metaconglomerates, whereas in the upper part conversely the metaconglomerates prevail. This fact emphasizes the regressive character of the deposition.

The similar compositional features are typical of the subsuite sections in other regions. However, the metaconglomerates are present only in the sections of the Lykhmanivska Structure closure (Inhuletske iron quartzite deposit) and in the region of the deposits mined by Lenin and R. Liukseburg mines. Within the Tarapakivsko-Lykhmanivskiy region and in the Saksahanskyi region (between the Ilich and Libknekh-ta mines and to the south of Lenin mine) the subsuite is composed of metagavelite-sandstone association and this suggests local distribution of metaconglomerates and their facial replacement along the strike by metagavelites and metasandstones.

The upper subsuite differs from the lower subsuite and is characterized by the transgressive type of the section. Its base consists of paragenesis of metagavelites + metasandstones ± metaconglomerates, whereas its top includes metasandstone + phyllite schist + metagavelite association. The lower part of its profile is composed of

alternating beds of metagavelites and metasandstones with minor fine-grained metaconglomerates, which form thin (from tens of cm to 2 m) layers and lenses.

Upwards the section, the quantity of metasandstones increases, the thickness of metagavelites decreases and they are gradually replaced by phyllitic schists, whereas the metasandstone + metagavelite association is replaced by metasandstone + phyllite schist paragenesis. Moreover, the quantity of metasandstones gradually decreases upwards the section and its upper part is represented by a bed of phyllitic schists.

The subsuites differ not only regarding their profile types (regressive or transgressive) but also in respect of the mineralogical and petrographical features of the rocks.

The upper subsuite is composed of fine-grained feldspar-quartz metasandstones. They contain 80 % quartz clasts, 10–15 % microcline and albite clasts and around 5–10 % clasts are microquartzites and mica quartzites. The clasts are cemented with quartz-sericite matrix.

The major part of the profile of the upper subsuite consists of dark grey phyllitic schists. The major rock-forming minerals are sericite, quartz and biotite. Depending on proportions of the constituents, their compositional varieties are divided into: quartz-sericite, quartz-biotite, quartz-sericite-biotite, biotite, and biotite-quartzite. These rocks also contain chlorite, tourmaline, opaque minerals (pyrite and pyrrhotite). According to the petrochemical analyses, the schists correspond to metamorphosed aleurite-argillite and clay rocks [6].

One of the diagnostic features of the suite is metaconglomerates. They are classified as fine-, medium-, coarse-grained depending on the size of the clasts. Fine- and medium-grained metaconglomerates are characteristic of the lower part of the sections of the lower and upper subsuites. The clast size varies between 0.5 and 2.0 cm. Their shapes are isometric, elongated and they are medium or well rounded. The content of the clastic material does not exceed 40–60 % of the rock volume. Generally, the fine-grained varieties are gradually replaced by medium-grained of sizes 2.0–3.5 cm. In these varieties clasts are very well rounded and of elongated and spindle-shaped forms. In the coarse-grained metaconglomerates medium size of the clasts along the elongated axis varies between 5 and 7 cm, but also boulders of 10–20 cm are encountered. Shape of these clasts is exclusively fusiform. Within medium- and coarse-grained varieties quantity of the clastic material reaches 70–80 % of the rock volume. The elongated axes of these clasts are oriented in the dipping direction of the rocks with sharp ending oriented towards one direction, which looks like a tile in a planar view.

The metaconglomerates are very similar in composition and contain quartz, quartzites, metasandstone, metagavelite and schist clasts. Clasts of quartz and quartzite dominate and occupy up to 70–80 % of the clast volume. It is worth mentioning that the quantitative ratios in fine- and medium-grained metaconglomerates are roughly the same with minor (10 %) deviations in one direction or another, whereas in the

coarse-grained metaconglomerates the quartzite clasts prevail and occupy up to 50–80 % of the clasts volume.

Quartz from the clasts comes mostly from veins. Light grey, grey, white and dark grey quartz clasts occur. All these color quartz clast varieties are rather randomly scattered; however, poor regularity is observed in the distribution of the dark grey quartz clasts. Lower parts of medium- and fine-grained metaconglomerate beds are enriched in the dark grey quartz clasts.

Clasts of quartz-sericite and sericite-quartz schists occupy around 10–25 % of the clastic material volume.

The metaconglomerates contain rounded clasts of metagrelites in minor quantities (2–3 % of the clasts volume). The grit within them consists of monomineral quartz cemented with a quartz-sericite matrix.

The least abundant in the metaconglomerates are clasts of metamorphosed mafic effusive rocks, which were observed only in a few cases.

The matrix of the metaconglomerates is metasandstone, which is similar to metasandstones forming beds and lenses within the Suite according to mineralogical, petrographical and petrochemical features. The major rock-forming minerals of the matrix are quartz and sericite with subordinate biotite and chlorite. The exceptions are these areas where the metaconglomerates overlie directly the schist conglomerates of Novokryvorizka suite (eastern part of the Main Structure closure and region of the deposit mined by Lenin mine).

Conventionally, the chlorite-bearing schists are known as the weathering products of the metabasites [1]. However, the above analysis of Novokryvorizka suite profile shows an alteration of the several chlorite-bearing schist varieties and metasandstones to be an integral unit, in which the chlorite is dominating in the matrix. This fact is not in an agreement with the hypothesis that these rocks are the weathering products but it favors the marine deposition environment. Analysis of the elements, which are indicative for the depositional environments [6, 7], shows that the sedimentation took place in a marine basin (Table 1). The source of the psammite-pelitic material for the formation of schists and metasandstone suite were weathered metabasites of Kryvyi Rih region. The process of re-deposition of the metabasite weathering products was triggered by the initiation of tectonic activity of the Kryvyi Rih stage, which took place after the formation of the metavolcanic-sedimentary greenstone Middle Dniprean Complex [4] and it was manifested within Kryvyi Rih region by sharp and short subsidence of the paleobasins seafloor. This point of view is supported by low thicknesses of the sections of Novokryvorizka suite and a very low maturity of the primary sedimentary material comprising the chlorite-bearing schists. The latter is favored by the ratios $Al_2O_3 : Na_2O$ and $K_2O : Na_2O$, which are, respectively, 22.04 and 2.96, and are related to areas with relatively active tectonic regimes [6].

Schist metaconglomerates, which are strictly associated with the chlorite-bearing schists and metasandstones cemented with the chloritic matrix, were formed in similar graben-like structures due to disintegration of the schists by density currents and gravitational pro-

Table 1

Ratios of element-indicators and facial conditions for deposition environments of rocks of Novokryvorizka suite

Rock and the element indicators	The value of the ratio of contents of elements	Conditions of deposition
Quartz-biotite-chlorite, quartz-sericite-chlorite schists		
Al : Ti	12.8	marine
Zr : Cu	2.76	marine
V : Cu	4.00	marine
V : Zr	1.81	marine
Chlorite-amphibole, amphibole-chlorite schists		
Zr : Cu	1.65	marine
V : Cu	4.29	marine
V : Zr	2.60	marine

cesses, which are indicated by angular and poorly rounded shapes of the schist clasts.

The dominance of high maturity quartzite metasandstones in the upper part of the suite and gradual increase in their thickness upwards the profile with simultaneous decrease of the chlorite content within their matrix, suggest relative tectonic stabilization of the region at the end of the suite deposition. Mineralogical and petrographical investigation of the mentioned metasandstones showed that they are similar in composition and structure to the metasandstones of the lower part of Skeliuvatska suite profile. This fact is evidence of continuous deposition of metaterrigenous sediments of two stratigraphical units. In areas where schist metaconglomerates are developed the content of the schist clasts gradually decreases upwards the section, whereas the content of the quartz vein clasts increases. Simultaneously, the content of chlorite within the matrix decreases in the same direction. The chlorite is displaced by quartz, which together with sericite is the major rock-forming component of the matrix of the metaconglomerates from the lower part of the subsuite, which belongs to Skeliuvatska suite [8]; this fact also infers a gradual replacement of rock associations of Novokryvorizka Suite by parageneses of Skeliuvatska suite.

The stage of regional tectonic stabilization, which began during the finalization of deposition of Novokryvorizka suite continued during sedimentation of the lower subsuite of Skeliuvatska suite. It is proved by the oligomictic composition of terrigenous material of the latter and supported by the coefficients of weathering intensity (W) and sedimentary differentiation (d) of different types of zones of tectonic regimes (Table 2) developed by O. A. Predovskyi. The analysis of these factors shows that the stabilization regime was moderately changeably activated during the deposition of the rock parageneses of the upper subsuite of Skeliuvatska suite, i. e. at the transition between the regression of the Skel-evatskyi paleobasin, which took place during the forma-

Table 2

Comparison of the approximate quantitative estimates of weathering intensity and degree of sedimentary differentiation of metasedimentary deposits of various paleotectonic regimes within the Skeliuvatska suite

Types of zones of tectonic regimes	Standard indicators		Indicator of Skeliuvatska suite formation	
	W	d	W	d
Stabilized subsidence	80	17	96*	—
Moderately active subsidence	58	2.4	79**	2.55
Average and strongly active subsidence	40	1.6	—	—
Moderately active uplifting	48	1.6	—	—

Footnote: W – weathering intensity; d – degree of sedimentary differentiation; * the lower subsuite; ** the upper subsuite

tion of rock associations of Novokryvorizka suite and the lower subsuite of Skeliuvatska suite, and transgressive conditions, during which there was accumulation of rocks of the upper subsuite. Increased significance of the tectonic activity at the time of deposition of the rock parageneses of the latter is also proved by a low degree of maturity of pelitic material of the phyllite-like schists ($Al_2O_3 : Na_2O = 23.3$; $K_2O : Na_2O = 6.85$) and by an increase in the Al-Si module from 0.07 (metasandstones of the lower subformation) up to 0.09 for psammites and 0.32 for pelites of the upper subsuite. This fact indicates a relatively high degree of differentiation of psammites from the lower subsuite. The degree of maturity of sedimentary material gradually increased from Novokryvorizka suite towards the upper subsuite of Skeliuvatska Suite. This fact may also support the conformable boundary between these stratigraphic units.

The metaconglomerates of Skeliuvatska suite refer to the inter-formational conditions rather than basal as it is traditionally considered.

This assumption is not only indicated by their position within the profile, confined to the border of two micro-cycles of the transgressive-regressive macro-cycle, but also by their paragenetic relation with other rocks of the suite [6], which is also a confirmation of the continuous accumulation of rock associations of Novokryvorizka and Skeliuvatska suites.

Conclusions. The composition of the profiles of the Novokryvorizka and Skeliuvatska suites combined with paleotectonic and paleoenvironmental features of the rock association deposition shows the conformable character of their contact and excludes the assumption that the metaconglomerates refer to the basal formations.

References / Список літератури

1. Yesypchuk, Yu. K., Bobrov, O. B. and Stepaniuk, L. M., 2004. *Koreliatsiina khronostratyhrafichna shkhema rannioho dokembriuu Ukrainskoho shchuta*

[Correlative chrono-stratigraphic scheme of Early Precambrian Ukrainian Shield]. Kyiv: UkrDGRI.

Кореляційна хроностратиграфічна схема раннього докембрію Українського щита / [Єсипчук Ю. К., Бобров О. Б., Степанюк Л. М. та ін.] – К.: УкрДГРІ, 2004. – 30 с.

2. Paranko, I. S. and Matishchuk, O. A., 2014. To the question of stratigraphic dismemberment of Skeliuvatska Suite of Kryvyi Rih series. *Zbirnyk naukovykh prats of UkrDHRI*, No. 1, pp. 140–150.

Паранько І. С. До питання про стратиграфічне розчленування скелюватської світи Криворізької серії / І. С. Паранько, О. А. Матишук // Збірник наукових праць УкрДГРІ. – 2014. – № 1. – С. 140–150.

3. Paranko, I. S., Butyrin, V. K. and Kozar, M. A., 2005. To the question of stratigraphic dismemberment of meta-volcanic sediments of Kryvyi Rih structure. *Mineralni resursy Ukrainy*, No. 3, pp. 35–40.

Паранько І. С. До питання про стратиграфічне розчленування метавулканогенно-осадових відкладів Криворізької структури / І. С. Паранько, В. К. Бутирін, М. А. Козар // Мінерал. ресурси України. – 2005. – № 3. – С. 35–40.

4. Paranko, I. S., 2005. Formational types of Proterozoic stratigraphic complexes of the Ukrainian shield. *Visnyk Lviv'skoho universytetu. Seriya heolohichna*. Vol. 19, pp. 100–110.

Паранько І. С. Формацийні типи стратигенних комплексів протерозою Українського щита / І. С. Паранько // Вісник Львівського університету. Серія геологічна. – 2005. – Вип. 19. – С. 100–110.

5. Deriabin, N. I., 2008. About the Skelevatska suite (complex) of Kryvbas. *Heolohichnyu zhurnal*, No. 2, pp. 100–107.

Дерябин Н. И. О скелеватской свите (комплексе) Кривбасса / Н. И. Дерябин // Геологический журнал. – 2008. – № 2. – С. 100–107.

6. Matishchuk, O. A., 2016. Paleogeographic peculiarities of the formation of a conglomerate enclosing strata of Kryvyi Rih structure. *Zbirnyk naukovykh prats of UkrDHRI*, No. 1, pp. 48–64.

Матишук О. А. Палеогеографічні особливості формування конгломератовміщуючих товщ криворізької структури / О. А. Матишук // Збірник наукових праць УкрДГРІ. – 2016. – № 1. – С. 48–64.

7. Deriabin, N. I., 2008. Once again about the formation of the rock of Kryvyi Rih structure. *Heolohichnyu zhurnal*, No. 1, pp. 102–110.

Дерябин Н. И. Еще раз о формировании пород Криворожской структуры / Н. И. Дерябин // Геологический журнал. – 2008. – № 1. – С. 102–110.

8. Pokaliuk, V. V. and Sukach, V. V., 2014. Sedimentation in the Early Precambrian kryvbas: lithogeochemical types and MINLITH-normative composition of metasediments. *Naukovyi Visnyk Natsionalnoho Hirnychoho Universytetu*, No. 6, pp. 5–14.

Покалюк В. В. Седиментогенез в раннем докембрии Криворожского железорудного бассейна: литохимические типы и MINLITH-нормативный состав метаосадков / В. В. Покалюк, В. В. Сукач // Научный вестник НГУ. – 2014. – № 6. – С. 5–14.

Мета. Дослідити особливості будови та взаємовідношення характеру залягання новокриворізької та скелюватської світ.

Методика. Авторами використувався аналіз розрізів світ, польові дослідження. Результати геохімічних аналізів були використані для визначення величини відношення вмісту елементів-індикаторів та фаціальних умов осадконакопичення порід, кількісних оцінок інтенсивності вивітрювання та ступеня осадової диференціації метаосадових відкладів різних палеотектонічних режимів з метою палеотектонічної реконструкції.

Результати. Результати геолого-формаційних досліджень конгломератовмісних товщ Кривбасу вказують на те, що в нижній частині розрізу Криворізької серії присутні два різних за складом та умовами утворення типи метаконгломератів – сланцеві та олігомиктові. Перші є складовою метаконгломерат-сланцевої формації, котра відповідає обсягу новокриворізької світи в сучасному її трактуванні, а другі – метаконгломерат-пісковико-сланцевої, що об'єднує метатеригенну частину розрізу скелюватської світи. Розріз верхньої частини новокриворізької світи репрезентований асоціацією різноманітних за складом хлоритових сланців і кварцових метапісковиків з підпорядкованим поширенням сланцевих метаконгломератів. При цьому кількість прошарків метапісковиків і їх потужності збільшуються вгору за розрізом. Нижня частина розрізу скелюватської світи представлена ритмами, складеними парагенезисом метапісковик + метагравеліт. При цьому метапісковики залягають в основі ритмів і за мінеральним складом та структурно-текстурними особливостями аналогічні метапісковикам верхньої частини розрізу новокриворізької світи. Це вказує на поступовий перехід між зазначеними світами та спростовує припущення щодо базального характеру кварцових метаконгломератів скелюватської світи, так як вони властиві для її центральної частини розрізу, де беруть участь у будові ритмів, складених асоціацією метапісковик ± метагравеліт + метаконгломерат. Тобто, розріз низів скелюватської світи має не трансгресивний, як вважається, а регресивний характер.

Наукова новизна. Був досліджений характер контакту новокриворізької та скелюватської світ, порівняні особливості їх речовинного складу та палеотектонічні особливості їх формування

Практична значимість. Результати дослідження можна використовувати для стратиграфічного розчленування розрізів; методики, використанні у статті, можна використовувати для палеотектонічних реконструкцій

Ключові слова: *світа новокриворізька, скелюватська, Криворізька серія*

Цель. Исследовать особенности строения и взаимоотношения характера залегания новокриворожской и скелюватской свит.

Методика. Авторами использовался анализ разрезов свит, полевые исследования. Результаты геохимических анализов были использованы для определения величины отношения содержания элементов-индикаторов и фациальных условий осадконакопления пород, количественных оценок интенсивности выветривания и степени осадочной дифференциации метаосаточных отложений различных палеотектонических режимов с целью палеотектонической реконструкции.

Результаты. Результаты геолого-формационных исследований конгломератосодержащих толщ Кривбасса указывают на то, что в нижней части разреза Криворожской серии присутствуют два различных по составу и условиям образования типа метаконгломератов – сланцевые и олигомиктовые. Первые являются составляющей метаконгломерат-сланцевой формации, которая соответствует объему новокриворожской свиты в современной ее трактовке, а вторые – метаконгломерат-песчаник-сланцевой, которая объединяет метатеригенную часть разреза скелюватской свиты. Разрез верхней части новокриворожской свиты представлен ассоциацией различных по составу хлоритовых сланцев и кварцевых метапесчаников с подчиненным распространением сланцевых метаконгломератов. При этом количество слоев метапесчаников и их мощность увеличиваются вверх по разрезу. Нижняя часть разреза скелюватской свиты представлена ритмами, сложенными парагенезисом метапесчаник + метагравелит. Метапесчаники залегают в основе ритмов и по минеральному составу и структурно-текстурным особенностям аналогичны метапесчаникам верхней части разреза новокриворожской свиты. Это указывает на постепенный переход между указанными свитами и опровергает предположение о базальном характере кварцевых метаконгломератов скелюватской свиты, так как они характерны для ее центральной части разреза, где участвуют в строительстве ритмов, сложенных ассоциацией метапесчаник ± метагравелит + метаконгломерат. То есть, разрез низов скелюватской свиты имеет не трансгрессивный, как считается, а регрессивный характер.

Научная новизна. Исследован характер контакта новокриворожской и скелюватской свит, сравнены особенности их вещественного состава и палеотектонические особенности их формирования.

Практическая значимость. Результаты исследований можно использовать для стратиграфического расчленения разрезов; методики, данные в статье, можно использовать для палеотектонических реконструкций.

Ключевые слова: *світа новокриворожская, скелюватская, Криворожская серія*

Рекомендовано до публікації докт. геол. наук А. А. Березовським. Дата надходження рукопису 01.12.15.

УДК 552.323.6:553.495:550.83

А. А. Калашник¹, д-р геол. наук, старш. научн. сотр.,
 Ю. И. Федоришин², д-р геол. наук, старш. научн. сотр.,
 А. В. Кузьмин³,
 Н. Н. Кирьянов⁴

1 – Кировоградская летная академия Национального авиационного университета, г. Кропивницкий, Украина, e-mail: kalashnik_anna1@mail.ru
 2 – Национальный университет водного хозяйства и природопользования, г. Ровно, Украина
 3 – Казенное предприятие „Кировгеология“, г. Киев, Украина
 4 – Геологоразведочная экспедиция № 37 Казенного предприятия „Кировгеология“, г. Кропивницкий, Украина

ПРЕДПОСЫЛКИ ФОРМИРОВАНИЯ И КРИТЕРИИ ПРОГНОЗИРОВАНИЯ АЛМАЗОНОСНЫХ СТРУКТУР НА УКРАИНСКОМ ШИТЕ

Н. А. Kalashnyk¹, Dr. Sc. (Geol.), Senior Research Fellow,
 Yu. I. Fedoryshyn², Dr. Sc. (Geol.), Senior Research Fellow,
 A. V. Kuzmin³,
 M. M. Kirianov⁴

1 – Kirovohrad Flight Academy Of National Aviation University, Professor of the Aeronavigation Department, Kirovohrad, Ukraine, e-mail: kalashnik_anna1@mail.ru
 2 – National University of Water Industry and Nature Management, Rivne, Ukraine
 3 – “Kirovheolohiia” State enterprise, Senior Geologist, Kyiv, Ukraine
 4 – Exploration expedition № 37, “Kirovheolohiia” State enterprise, Chief Geologist, Kirovohrad, Ukraine

PRECONDITIONS OF FORMATION AND CRITERIA FOR PREDICTION OF DIAMONDIFEROUS STRUCTURES ON THE UKRAINIAN SHIELD

Цель. Выявление новых закономерностей пространственного размещения разноранговых таксонов продуктивного кимберлит-лампроитового магматизма на территории Украинского щита (УЩ) и их отражение в геолого-геофизических материалах. Обоснование новых критериев локализации разномаштабных алмазоносных структур на основе системного подхода.

Методика. Выполнен комплексный анализ большого объема геофизической, геологической, петрогеохимической информации по УЩ для изучения изменчивости параметров глубинной среды, которые определяют возможность возникновения алмазоносных кимберлит-лампроитовых расплавов в литосфере и подъем флюидо-магматических колонн на верхние структурные горизонты земной коры с формированием продуктивных алмазоносных структур.

Результаты. Установлены новые закономерности, отражающие специфику формирования продуктивного алмазоносного кимберлит-лампроитового магматизма на основе многоуровневой обобщенной многофакторной модели природного алмазообразования. Определены новые критерии прогнозирования разноранговых потенциально алмазоносных кимберлитовых, лампроитовых таксонов территории УЩ в геолого-геофизических материалах. Это дало возможность осуществить обоснованные прогнозные оценки потенциальной алмазопродуктивности проявлений кимберлит-лампроитового магматизма сегментов литосферы УЩ, значительно минимизировать площади для дальнейших поисковых работ.

Научная новизна. Определен новый комплекс критериев прогнозирования разноранговых таксонов проявления продуктивного кимберлит-лампроитового магматизма Украинского щита, который учитывает обобщенную многофакторную модель природного алмазообразования. Указанный комплекс критериев позволяет выполнять последовательную системную локализацию разноранговых потенциально алмазоносных структур на поверхности фундамента.

Практическая значимость. На основе использования геолого-геофизических и петрогеохимических материалов выполнен комплексный геологический анализ территории УЩ и оценены ее перспективы на коренную алмазоносность, выделены площади наиболее вероятной локализации продуктивных проявлений кимберлит-лампроитового вулканизма. Это позволяет существенно повысить эффективность прогнозно-поисковых работ и достоверность полученных результатов.

Ключевые слова: алмазоносные структуры, литосфера, прогнозно-поисковые критерии, Украинский щит

Общая постановка проблемы и связь с практическими заданиями. За всю историю эксплуатации кимберлитовых трубок и их россыпей (более 125 лет) традиционными объектами добычи алмазов являлись, главным образом, месторождения Африки, Индии, Бразилии, позднее – Якутии. Однако, хронологически весьма непродолжительный период, включающий в себя последние 25 лет XX века, был ознаменован выдающимися открытиями новых алмазоносных провинций мира: в конце 70-х годов – лампроитовой алмазоносной провинции северо-запада Австралии; в начале 80-х годов – Архангельской алмазоносной провинции; в начале 90-х годов – крупной алмазоносной провинции северо-запада Канады. Благодаря этому активизировались и интенсивно развивались поисковые работы на алмазы на Урале, Тимане, в Карелии, на Кольском полуострове, в Финляндии, в Белоруссии, в Украине. Результаты работ значительно расширили исследования происхождения алмазов и их источников. Пока однозначным фактом явилось то, что только кимберлитовые и лампроитовые породы содержат алмазы в значительно больших концентрациях, чем другие их источники. Тем не менее, даже в традиционных алмазоносных районах геологи часто сталкиваются с тем, что источниками алмазов являются не классические кимберлитовые трубки взрыва. Например, в Заире разрабатываются аллювиальные россыпи, не имеющие кимберлитовых коренных источников. Продолжает дискутироваться проблема источников алмазов в месторождениях Красновишерского района Пермской области, которые разрабатываются более пятидесяти лет и не имеют связи с кимберлитопоявлениями. Заслуживают упоминания алмазы в россыпях острова Тасмания, которые залегают в долинах рек, дренирующих мощный массив серпентинов. Продолжается длительная попутная добыча алмазов из платиноносных россыпей на Аляске, которые образовались за счет массива ультраосновных пород, достаточно хорошо изученного как источник платинометаллической минерализации.

Нарастающее количество противоречивых фактов в истолковании источников алмазов в россыпях также привело к расширению исследований по этой проблеме. Крупномасштабные работы, проводившиеся в разных странах, увенчались открытием новых генетических типов коренных месторождений этого минерала. В настоящее время в общий список могут быть включены следующие коренные источники алмазов: кимберлитовые трубки взрыва, лампроиты, кимберлитовые дайки, ультрабазиты, метаморфиты, импактиты, алмазоносные конгломераты, флюидиты, ультраосновные коматииты.

Дискуссионным также является и вопрос о причинах, по которым не все кимберлитовые поля и трубки являются алмазоносными. В Якутской алмазоносной провинции только 13 трубок

из выявленных 800 являются алмазоносными [1]. В Канадской провинции Слейв из 150 кимберлитовых трубок только 50 содержит алмазы [1]. Из 22 кимберлитовых полей Канадского щита только 6 характеризуются высокими и средними содержаниями алмазов в трубках и 5 – низкими содержаниями алмазов [1].

Вышеприведенный фрагментарный обзор основных коренных источников алмазоносности, их разнообразие дает основание разносторонне подходить к оценке перспектив конкретных регионов, что само по себе затрудняет выбор оптимальных технологий поисков и разведки территорий. До сих пор отсутствует в практике универсальная технология оконтуривания рудных (кимберлитовых) полей для всех регионов, хотя в этом плане имеются достаточно значительные наработки. В этом кроется практически главная причина длительных неудач проведения поисковых работ на коренную алмазоносность в пределах Украинского щита и его склонов.

Анализ последних исследований и публикаций, выделение нерешенных частей проблемы. Украинский щит рассматривается как потенциально алмазоносная субпровинция. На территории Украинского щита и его склонов выявлены кимберлитовые трубки, лампроитовые трубки, кимберлитопоявления дайковой фации, проявления алмазов кимберлитового, метаморфогенного и лампроитового типов, россыпи мелких алмазов в отложениях чехла [2] (рис. 1). Однако месторождений алмазов пока в Украине нет. Для решения алмазной проблемы Украины в 70-е годы начали использовать минералогический способ поисков индикаторных минералов кимберлитов (ИМК), проверенный практикой и традиционный для Якутской алмазоносной провинции путь поисков алмазных месторождений кимберлитового типа. Однако, в условиях Украины, такой способ геологических поисков оказался не информативным.

Использование на территории УЩ в качестве главного аргумента перспективности территории такого минералогического признака как наличие „в разновозрастных породах алмазов различных (всех известных) генетических типов“ [3], который работает в Якутской алмазоносной провинции, на наш взгляд, явилось неправомерным. Результаты выполненных на территории Украины работ по изучению перспектив коренной алмазоносности [4] показали, что это, скорее всего, свидетельство повсеместной зараженности неогеновых и четвертичных отложений осадочного чехла россыпными переотложенными алмазами. Выявленное при этом нахождение в разновозрастных кластических образованиях широко распространенных в них алмаза и пиропы позволяют сделать заключение о множественности их первоисточников и существовании нескольких эпох кимберлитового магматизма и россыпеобразования.

Анализ современных представлений о тектонических условиях формирования алмазоносных

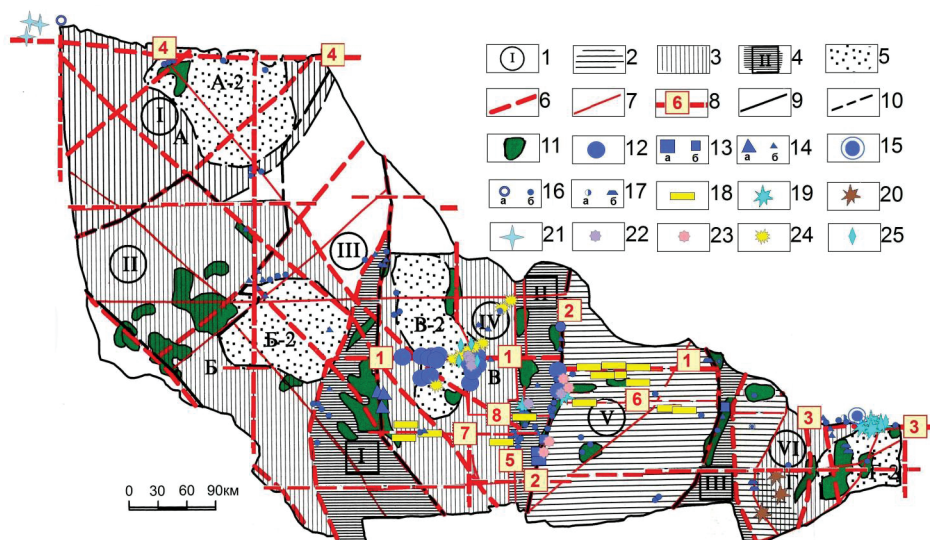


Рис. 1. Схема расположения проявлений кимберлитового и лампроитового магматизма, месторождений и рудопроявлений урана, размещения потенциально ториеворудных районов, зон и узлов, минерагенических зон с установленным пространственным и временным сопряжением кимберлитопоявлений и урановорудных объектов на территории Украинского щита:

1 – мегаблоки УЩ: I – Волынский, II – Днестровско-Бугский, III – Росинско-Тикичский, IV – Ингульский, V – Среднеприднепровский, VI – Приазовский; 2 – протоплатформенный массив мезоархейского заложения; 3 – протоплатформенные массивы палеопротерозойского заложения: А – Волынский, Б – Подольский, В – Кировоградский, Г – Приазовский; 4 – шовные зоны: I – Голованевская, II – Западно-Ингулецкая, III – Орехово-Павлоградская; 5 – мезопротерозойская фаза развития мантийных диапиров: А-2 – Коростенский вулканоплутонический комплекс, Б-2 – Гайсинская криптоинтрузия, В-2 – Корсунь-Новомиргородский плутон, Г-2 – Восточно-Приазовский плутон; 6 – осевые линии глубинных разломов I порядка; 7 – осевые линии разломов II порядка; 8 – осевые линии минерагенических разломных зон с региональным контролем уранового оруденения различного генезиса: 1 – Субботско-Мошоринская, 2 – Криворожско-Кременчугская, 3 – Южнодонецкая, 4 – Полесская (Припятская), 5 – Западно-Ингулецкая; 6 – Девладовская; 7 – Братская; 8 – Софиевско-Криничеватская; 9 – граница Украинского щита; 10 – границы мегаблоков; 11 – потенциально ториеворудные районы, зоны и узлы; 12–17 – эндогенные урановорудные объекты различных генетических типов: 12 – месторождения гидротермально-метасоматического типа в среднетемпературных карбонатно-натриевых метасоматитах, 13 – осадочно-метаморфогенные в конгломератах и песчаниках кристаллического фундамента: а – месторождения, б – рудопроявления; 14 – гидротермально-метасоматические в калиевых метасоматитах и пегматоидных гранитах: а – месторождения, б – рудопроявления; 15 – Николаевское месторождение гидротермального типа в минерализованных зонах; 16 – рудопроявления: а – типа „несогласия“, б – гидротермального типа в минерализованных зонах дробления пород кристаллического фундамента; 17 – рудопроявления: а – гидротермальные уранбитумные в зонах дробления пород кристаллического фундамента и складчатых областей, б – магматические в интрузивных массивах щелочных сиенитов, лейкократовых гранитов и карбонатитов; 18 – инфильтрационные месторождения („песчаникового“ типа), 19 – кимберлитовые трубки, 20 – взрывные лампроитопоявления (трубки); 21 – участки с находками обломков кимберлитовых пород; 22 – кимберлитопоявления дайковой фации; 23 – лампроитопоявления в виде жил и даек; 24 – алмазоперспективные взрывные структуры; 25 – находки коренных алмазов

пород [5, 6] позволил выделить наиболее популярные гипотезы: 1) наличие архейского литосферного корня (киля) под древними кратонами, проникающего вглубь мантии до 400 км; 2) корреляция между типом мантии, фрагменты пород которой выносятся кимберлитами, и временем формирования древней коры; 3) РТ-условия, необходимые для генерации кимберлитовых пород и алмазов (глубина более 150 км, давление более 40 кбар, температура 900–1200 °С).

По данным С. И. Хаггерти [7], кимберлитовый расплав, который образуется вследствие подплавления наиболее глубоко погруженной алмазоносной части литосферы под действием газонасы-

щенного флюида, проникает в хрупкую среду истощенной (деплетированной) литосферы, достигая, таким образом, поверхности Земли. Толчком к развитию этого процесса являются мантийные плюмы, которые зарождаются в зоне перехода от верхней к нижней мантии (400–650 км) или глубже [7].

Таким образом, на первый план при изучении перспектив формирования алмазоносных структур, на наш взгляд, выступает анализ глубинного строения литосферы. Основной отправной точкой при определении перспектив алмазоносности различных территорий не могут служить все чаще встречающиеся варианты правила Клиф-

форда, которое гласит, что „области древней стабилизации, по крайней мере, от 1500 млн лет и древнее, являются источниками большей части африканского золота, хрома, платины, асбеста, алмазов“ [8]. В последнее время открытие районов с алмазоносными трубками взрыва закономерно возрастает в пределах протерозойских подвижных поясов, спаивающих архейские блоки. Классическими примерами таких районов являются поля Эллендейл и Аргайл, где внедрение лампроитов приурочено к подвижным зонам Кинг-Леопольд и Холс-Крик на границе с блоком Кимберли (северо-западная Австралия) [9]. Здесь количество трубок превышает 50 (возраст от 20 до 1200 млн лет).

Аналогичная обстановка наблюдается в провинции Центральный Саскачеван (Канада), где кратоны Сьюпериор и Херн спаяны подвижной зоной протерозойского возраста [10]. Район Глены (количество трубок 70, возраст трубок – меловой). Район Северное Колорадо, включающий трубку Слоан (Канада) [10] и др., расположен на краю протерозойского кратона Центральных Равнин на границе архейского блока Вайоминг, где надвиговой пояс Чейенн образует орогенный шов.

Результаты ранее проведенных исследований алмазоносности территории Украины [4] и современных представлений об условиях формирования алмазоносных пород позволяют сделать вывод, что важнейшими типами объектов, которые могут иметь практический интерес, на УЩ являются месторождения алмазов в коренных кимберлитовых и лампроитовых породах.

Поэтому, на наш взгляд, очень важным является анализ связи выявленных проявлений ко-

рренной алмазоносности, а также кимберлитового и лампроитового магматизма в тесной связи с особенностями глубинного строения литосферы Украинского щита независимо от возраста стабилизации его мегаблоков. Определенный интерес имеют и нетрадиционные источники алмазов, прежде всего, флюидизиты, на чем неоднократно акцентировал внимание Г. М. Яценко [2].

Тенденции размещения проявлений кимберлитового и лампроитового магматизма, предпосылки формирования алмазоносных трубок. Высокая степень зрелости литосферы, мощностью более 150 км, является главным фактором возможности создания петрологических условий для обеспечения в подошве сегмента литосферы условий для стабильного существования графита и алмаза [7].

Канадская кимберлитовая провинция Слейв, в пределах которой выявлено максимальное количество трубок на Канадском щите (150), по данным сейсмотомографии, характеризуется мощностью современной литосферы 250 км [10]. Наряду с этим, данные термобарометрии ультраосновных ксенолитов из среднеюрских алмазоносных трубок указывают на глубину их образования в этом регионе, составляющую 190 км [10]. Представительные сейсмические исследования [10] свидетельствуют о неравномерно слоистой структуре литосферы Канадского щита и об отсутствии глубоко погруженного литосферного корня под продуктивным контуром, включающим алмазоносные трубки кратона Слейв.

Современная мощность литосферы центральной Сибирской платформы, включающей районы Далдынского, Алакитского и Малоботуобинского кимберлитовых полей, указывают на современную мощность литосферы, которая колеблется от 200 до 230 км. В ксенолитах кимберлитовых трубок Сибирской платформы, в частности „Удачная“, „Мир“, „Обнаженная“, совмещаются породы „разноглубинных“ парагенезисов (от 40 до 225 км по оценке РТ-условий литостатической нагрузки) [11]. При этом гранатовые перидотиты и эклогиты этих трубок, по данным термобарометрии, образовались в интервале глубин 200–225 км [11].

Изучение пространственного размещения кимберлитовых трубок в различных алмазоносных провинциях указывает на их приуроченность к определенным линейным зонам в земной коре – глубинным разломам транслитосферного проникновения, способным достигать гипсометрического уровня астеносферных областей масштабной генерации кимберлитовых магм. И это является определяющим структурным фактором для реализации процесса формирования промышленных месторождений алмазов в аномальных сегментах литосферы высокой степени зрелости. Прямая связь кимберлитов с глубинными разломами подтверждается линейно ориентированным расположением кимберлитовых трубок в

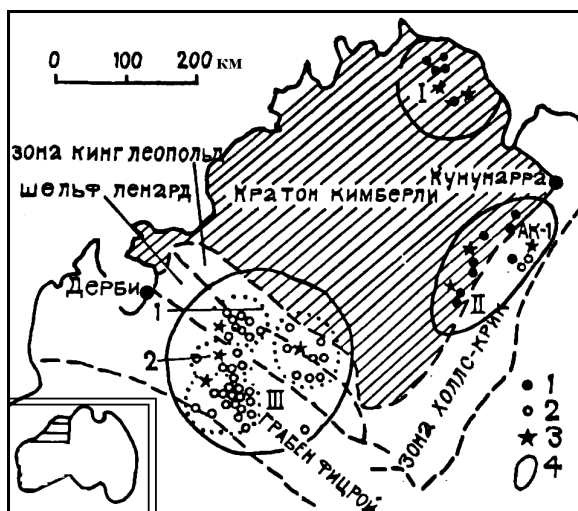


Рис. 2. Лампроитопоявления, кимберлитопоявления и алмазопоявления района кратона Кимберли Западной Австралии (по А. Джейку и др. [9]):

1 – кимберлитопоявления; 2 – лампроитопоявления; 3 – алмазопоявления; 4 – районы: I – Северный Кимберли, II – Восточный Кимберли, III – Западный Кимберли

виде цепочек и целых серий даек, секущих кристаллическое основание. Необходимым условием является (в сочетании с тектоническими факторами) развитие в особых зонах сверхвысоких давлений, которые способствуют образованию в кимберлитах алмаза и его спутников. Присутствие таких давлений в кимберлите является главным условием образования промышленных концентраций алмаза [5]. При этом скорость подъема магматической колонны прямо пропорциональна давлению, существующим в кимберлитовом очаге. При относительно меньших давлениях движение расплава к земной поверхности замедляется, при этом изначально кимберлитовый расплав может быть самопроизвольно раскислен, алмазы графитизируются еще на глубине в промежуточных очагах.

Возникает необходимость научно обоснованного анализа реальных перспектив промышленной алмазности отдельных регионов УЩ, который бы учитывал петрологические предпосылки формирования алмаза и особенности глубинного строения литосферы и земной коры.

Закономерности размещения коренных кимберлитов- и лампроитопоявлений на УЩ

в связи с глубинным строением. На сегодняшний день, на УЩ участки развития коренных кимберлитовых и лампроитовых пород выявлены только в пределах Ингульского и Приазовского мегаблоков (рис. 1).

Вопрос о мощности литосферы УЩ является дискуссионным. В основу анализа изучения глубинного строения литосферы УЩ нами были положены материалы интерпретации данных глубинного сейсмического зондирования (ГСЗ) [12] и сейсмомографии [13]. Для объективного анализа алмазопродуктивности литосферных сегментов УЩ были использованы данные мощности литосферы по ГСЗ (рис. 3), скорректированной по результатам петрологических исследований глубинных ксенолитов и минералов-спутников алмаза районов проявления мантийных пород (рис. 4).

Для Ингульского мегаблока характерна максимальная в пределах УЩ мощность литосферы, достигающая по данным ГСЗ 250 и более километров. Мощность коры в пределах мегаблока изменяется от 35 до 45 км с валообразным поднятием в Ингуло-Ингулецкой шовной зоне. Поверхность Мохо (М), по сравнению с соседними мегаблока-

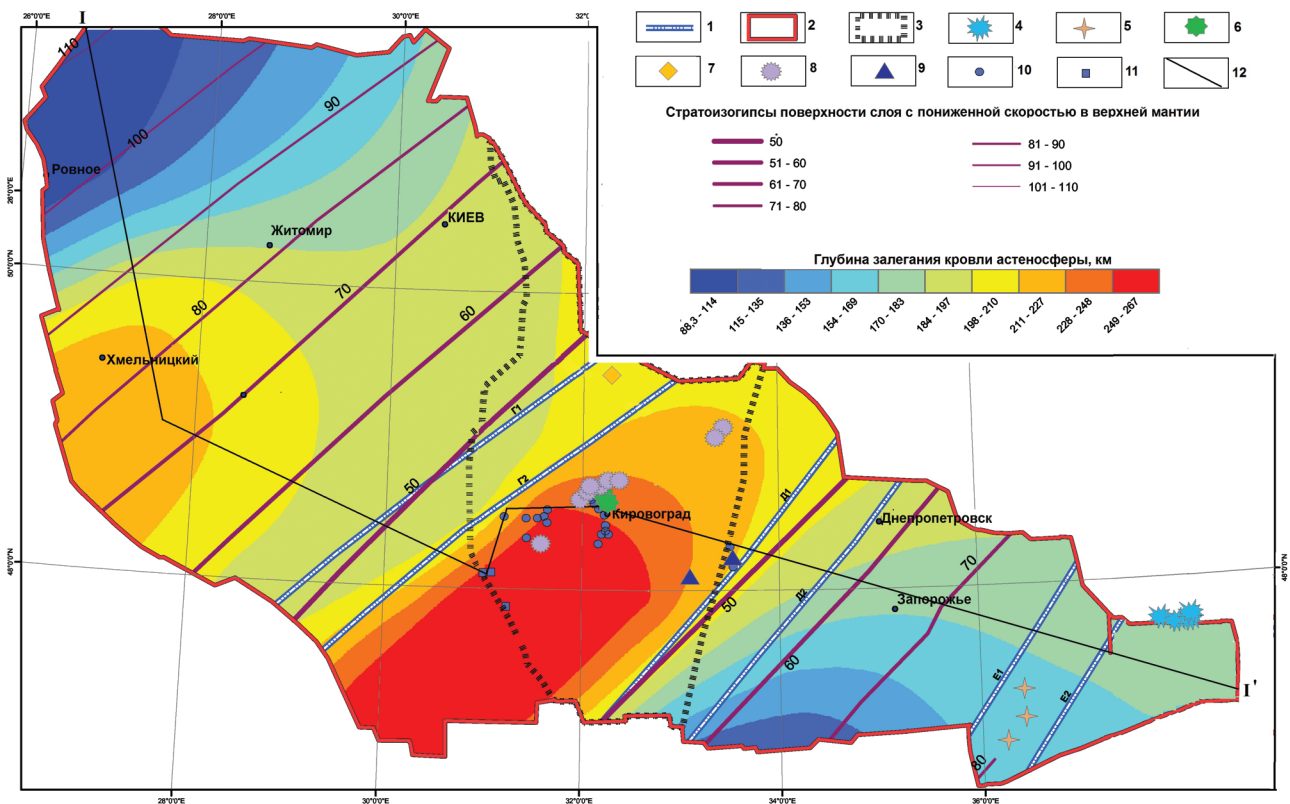


Рис. 3. Схема поверхности астеносферы в пределах Украинского щита (по Соллогубу В. Б. [12]) с данными по кимберлитовым и лампроитопоявлениям, промышленному урановому оруденению:

- 1 – трансрегиональные мантийные линейменты северо-восточного простирания; 2 – контур УЩ; 3 – контур Ингульского мегаблока; 4 – кимберлитовые трубки; 5 – взрывные лампроитопоявления (трубки); 6 – кимберлитопоявления дайковой фации; 7 – лампроитопоявления в виде жил и даек; 8 – алмазоперспективные взрывные структуры; 9 – кимберлитоподобные породы; месторождения урана: 10 – в среднетемпературных карбонатно-натриевых метасоматитах; 11 – калий-урановой формации; 12 – линия разреза I-I'

ми, образует поднятие, своеобразный приподнятый блок, в пределах которого в желобообразной впадине в поверхности М, совпадающей с Субботско-Мошоринской разломной зоной по данным ГСЗ, зафиксированы контрастно выраженные вертикальные расслоения коры (профиль XXIV), которые также отмечены и в зоне Кировоградского разлома (геотраверс IV) (рис. 4).

В пределах Ингульского мегаблока выделяют мантийный диапир (рис.1), который находится в основании Новоукраинского гранитного массива и Корсунь-Новомиргородского плутона габбро-анортозит-рапакиви. Кировоградский мантийный диапир коррелирует с Корсунь-Новомиргородской трансформовой акустической аномалией и Кировоградско-Новоукраинским гравитационным минимумом [13]. На глубине 200–400 км в этом районе выделяется большая зона пониженных скоростей сейсмических волн, связанная с резервуаром частично расплавленных пород (рис. 5). В восточной части Корсунь-Новоукраинского двухфазного плутона выявлена Кировоградская аномалия теплового потока и электропроводности, которая имеет тепловую природу [14]. Корреляция аномалии теплового потока, зоны электропроводности, пониженных скоростей сейсмических волн и наличие плотностной аномалии в едином сегменте Ингульского литосферного мегаблока позволяет рассматривать этот район как область длительной активизации мантии. Кировоградский мантийный диапир имел длительное прерывисто-пульсационное развитие, что свидетельствует о стабильности глубинного энергетического теплового источника, обусловившего его образование.

Проникновение мантийного диапира сопровождалось мощным гранитообразованием чарнокит-гранитовой стадии с формированием Новоукраинского массива в период от 2025 ± 48 до 2039 ± 6 млн лет [15]. Со вторым этапом развития мантийного диапира связано появление наиболее древних дайковых поясов, которые вмещают кимберлиты с изотопным возрастом 1800 и 1770 ± 9 млн лет [16] (рис. 6), образование анортозит-рапакиви-гранитной формации с модалным изотопным возрастом от 1725 ± 11 до 1754 ± 4 млн лет (U–Pb метод) [15], проявленность интенсивной флюидизатно-эксплозивной деятельности в разломных структурах с формированием тектоно-метасоматических зон, вмещающих масштабное урановое оруденение в натриевых метасоматитах с изотопным возрастом 1800–1750 млн лет [17].

Знаменско-Устиновское дайковое поле включает серию даек лампрофиров и кимберлитоподобных пород с изотопным возрастом 1600–1200 млн лет [2]. Боковянское поле (Западно-Ингулецкая минерагеническая зона) включает эксплозивные структуры и дайки кимберлитоподобных пород. Родионовское поле включает трубки взрыва, дайки. Дальнейший этап активизации в

Ингульском мегаблоке проявился развитием даек, в том числе лампроитовых, на северном фланге Корсунь-Новомиргородского плутона с изотопным возрастом 1370–1330 млн лет [16]. Герцинская эпоха диасторозизма в пределах региона выразилась образованием Ровенской эруптивной структуры с изотопным возрастом 350–275 млн лет [2], а в узле пересечения Криворожско-Кременчугского и Девладовского разломов образовалась группа вулканотектонических структур, среди которых самой крупной является Терновская с изотопным возрастом 250 млн лет [2]. В этот период активизации в Кировоградской зоне разломов образовалось жильное урановое оруденение возраста 380–350 млн лет. К альпийскому периоду тектонических движений относится образование райгородской и смелянской толщ, ряда эксплозивных структур в северной и северо-восточных частях Ингульского мегаблока (рис. 6). Основными магмо- и флюидопроводящими каналами в Ингульском мегаблоке были зоны глубинных разломов, активизация которых, в различной мере, возобновлялась во все основные эпохи диасторозизма.

Кимберлитовые дайки протерозойского этапа тектонической активизации (1800 и 1770 ± 9 млн лет) [16] в Ингульском мегаблоке впервые были выявлены при проведении разведки Щорсовского и Лелековского месторождений урана. Они установлены на участке Лелековского разлома в тектонических узлах, образованных нарушениями северо-западного, широтного и северо-восточного простирания (рис. 6). Дайки кимберлитов расположены по периферии локальной гравитационной аномалии трубчатого типа интенсивностью 0,5 мГал размером 600×500 –400 м.

Для изучения параметров кимберлитопроявления и отбора технологической пробы с целью определения их алмазоносности на Лелековском участке был пробурен куст буровых скважин из 31 скважинного пересечения (скв. 4095-31). Всего было получено 41 пересечение кимберлитов. Средняя стволовая мощность по всем пересечениям составляет 3,1 м и колеблется от 0,1 до 7,8 м. Вертикальный размах тел кимберлитов 91,6 м. Дайки встречены в пределах абсолютных отметок –159,5––251,1 м (абсолютная отметка устья скважины 4095 составляет +147,4 м). По простиранию кимберлитопроявление прослежено на 29 м и не оконтурено. Простирание кимберлитовых даек 315 и 45° . Падение тел субвертикальное. Вмещающими породами являются лелековские мелко-среднезернистые биотитовые граниты кировоградского комплекса. Порода даек представлена брекчированными слюдистыми и интенсивно измененными кимберлитами с порфириковой структурой, которая обусловлена фенокристами оливина и флогопита. Зерна оливина полностью серпентинизированы, флогопита также часто полностью замещены хлорит-рудным агрегатом с тонкой оторочкой карбонатных выделений по пери-

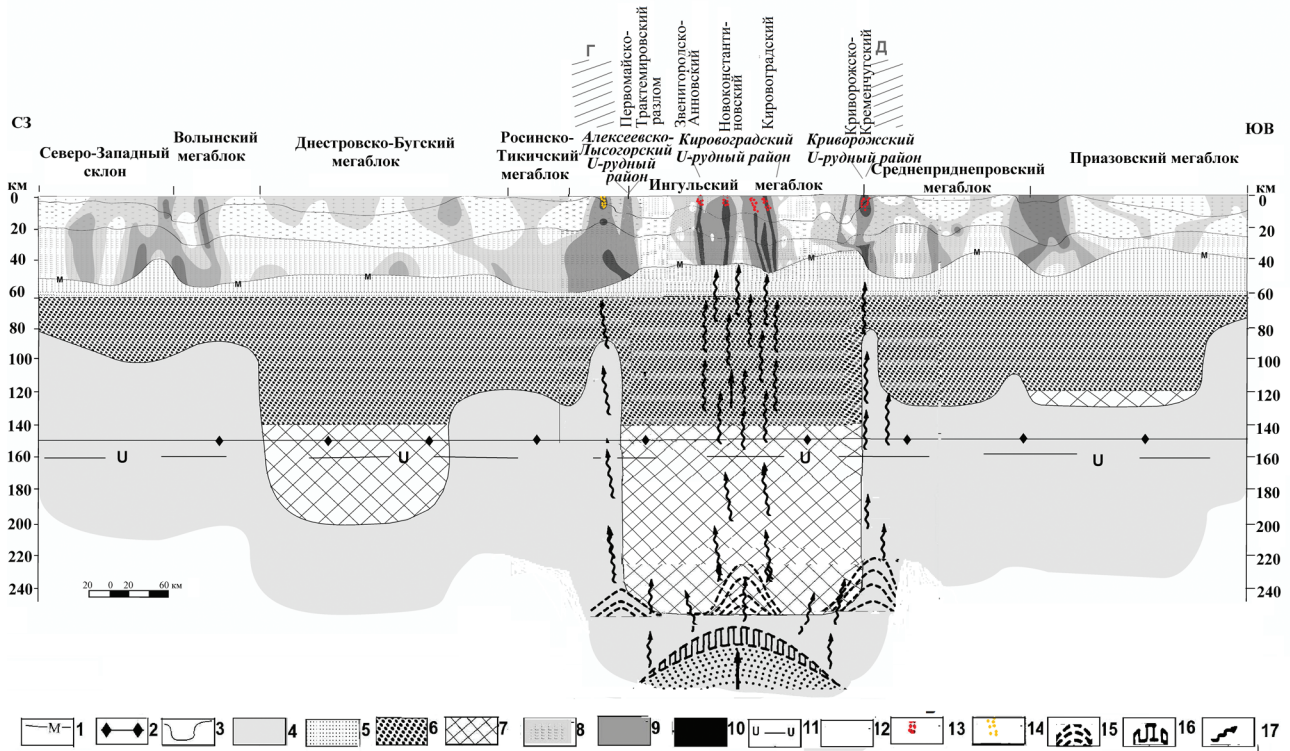


Рис. 4. Разрез литосферы в пределах Украинского щита по профилю I-I:

1 – граница Мохо; 2 – граница стабильности графит-алмаз; 3 – граница литосфера-астеносфера; 4 – астеносфера; 5 – железистые ультрабазиты (железистые дуниты, ильменит-флогопит-гранат-оливиновые породы); 6 – амфиболовые и пироксеновые глиммериты, шпинель-гранатовые, гранатовые лерцолиты; 7 – хромшпинелевые гарцбургит-лерцолитовая и дунит-перидотитовая серии с реликтами деформированных структур, гранатовые лерцолиты с реликтами деформированных структур; зоны дислокаций с различной степенью проницаемости: 8 – низкой, 9 – средней, 10 – высокой; 11 – уровень формирования очаговых потоков ураноносных трансмагматических флюидов; 12 – проекция положения литосферных линейментов (по В. Б. Соллогубу [12]); 13 – месторождения урана в альбититах; 14 – месторождения урана калий-урановой формации; 15 – локальные астеносферные ловушки на границе литосфера-астеносфера; 16 – термобарогradientный фронт глобальной астеносферной ловушки, сформированный вследствие импульсной дегазации ядра и мантии; 17 – астеносферные флюидопотоки

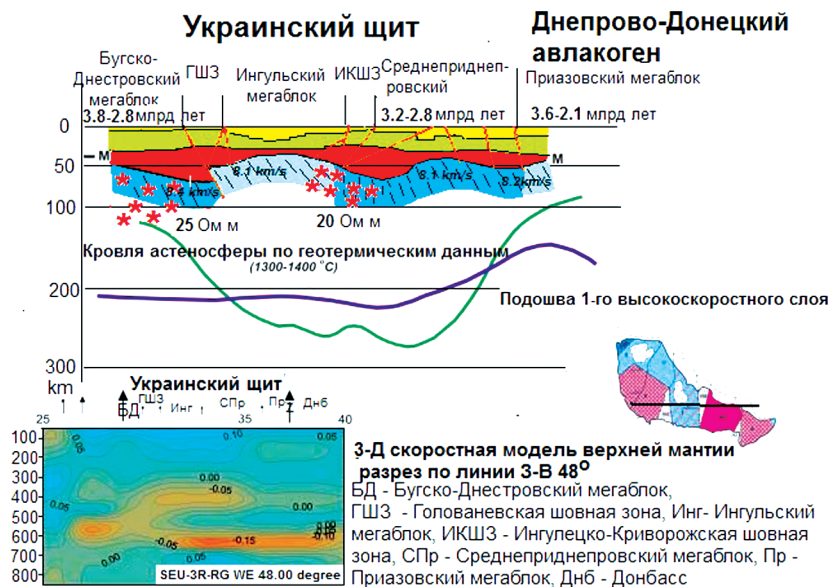


Рис. 5. Структура верхней литосферы Украинского щита и мантийные неоднородности по данным сейсмической томографии вдоль широтного геотраверса IV (по Богдановой и др. [14])

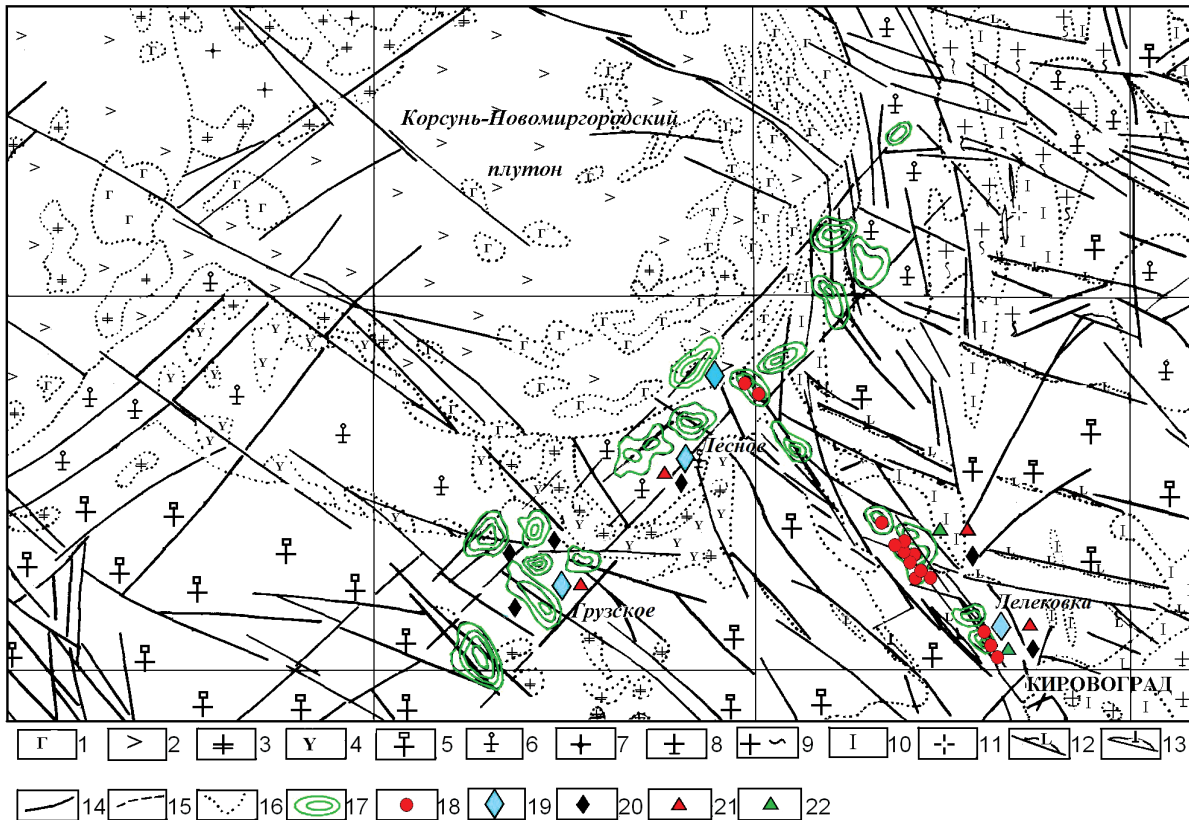


Рис. 6. Структурно-тектоническая схема расположения эксплозивных структур Кировоградского участка Ингульского мегаблока УЩ:

1 – габбро, габбро-нориты; 2 – анортозиты; 3 – монцониты; 4 – сиениты; 5 – граниты биотитовые, порфиробластические; 6 – граниты рапакиви; 7 – граниты контаминированные пироксен-роговообманковые; 8 – граниты равномернзернистые биотитовые; 9 – мигматиты; 10 – гнейсы биотитовые; 11 – граниты пегматоидные; 12 – внемасштабные дайки диабазов; 13 – внемасштабные дайки пикритовых порфиритов; 14 – тектонические нарушения; 15 – границы разновозрастных геологических отделов; 16 – границы одновозрастных литологических и фациальных отделов; 17 – контуры отрицательных гравианомалий, контролирующих эксплозивные структуры; 18 – проявления кимберлитов дайковой фаши нижнепротерозойского возраста; 19 – находки кимберлитовых алмазов; находки минералов-спутников алмаза; 20 – хромшпинелидов; 21 – пиропы; 22 – хромдиопсидов

ферии. Вещество, цементирующее порфиоровые выделения оливина и флогопита, представлено смесью серпентина, хлорита, рудного минерала и карбоната.

В кимберлитах встречены глубинные ксенолиты размером 2–8 мм до нескольких сантиметров, сложенные, в основном, вторичными продуктами – смесью пластинчато-волокнистого серпентина, бастита, рудного минерала. Ксенолиты глубинных пород по петрографическим особенностям соответствуют гранатовым дунитам (рис. 7) и гарцбургитам.

Из керна куста буровых скважин 4095 были сформированы технологическая проба Т-96-1 весом 280 кг и две лабораторные минералогические пробы весом 22 и 6,6 кг, которые изучались в Крымском отделении УкрГГРИ, Львовском Национальном университете (ЛНУ) и компании „Де Бирс“.

В пробе Т-96-1 в Крымском отделении УкрГГРИ было установлено два кристалла алмаза перидотитового парагенезиса. Кроме кристаллов ал-

маза, в пробе были выявлены зерна хромдиопсидов (содержание Cr_2O_3 в трех из них колеблется от 0,98 до 1,29 %) и хромшпинелиды. По данным

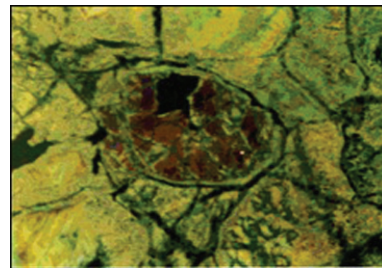


Рис. 7. Микрофотография образца кимберлита Лелековского участка (скв. 4095-2, гл. 348.2 м). Серпентинизированный ксенолит гранатового дунита. Реликт зерна оливина окружен серпентин-тальковым агрегатом. В оливине включения келифитизированного ксенокристалла граната. Николи +. Ув. 100 (материалы КП „Кировгеология“)

электронно-зондового анализа шести зерен хромдиопсидов содержание Cr_2O_3 в них колеблется в пределах 12,35–33,57 % и MgO 16,61–18,64 %. Также выделены гранаты, соответствующие гроссуляр-пироп-альмандинам. В образце Т-96-1/5 установлено преобладание пиропового минала над гроссуляровым и альмандиновым компонентами.

Более полные данные о концентрации Cr_2O_3 и MgO в хромшпинелидах получены по пробе весом 6,6 кг, исследованной лабораторией компании „Де Бирс“. Выполнено 377 электронно-зондовых анализов. По полученным данным содержание Cr_2O_3 в хромшпинелидах из этой пробы изменяется от 10 до 47 % (в 26 случаях оно превышает 40 %), а содержание MgO варьирует в пределах 14–20 %.

По текстурно-структурным особенностям и вещественному составу щорсовские кимберлиты близки к кимберлитам Лелековского участка.

На Щорсовском участке получено 23 пересечения по кимберлитам. Стволовая мощность кимберлитовых даек изменяется от 0,5 до 18,2 м. Падение тел вертикальное, простирание 305° . Дайки встречены в пределах абсолютных отметок +28 – –218 м (абсолютная отметка устья скважины 4097 составляет +155,0 м). По простиранию дайки кимберлитов вскрыты на протяжении 80 м. Вмещающими их породами являются лелековские мелко-среднезернистые биотитовые граниты Кировоградского комплекса.

Из кимберлитов слюдяного типа была отобрана технологическая проба весом 229 кг. Кроме того, отобраны минералогические пробы весом 21,3 и 4,5 кг. В пробах кристаллы алмаза не установлены. Во всех пробах был обнаружен полный комплекс ИМК: пиропы, пикроильмениты, хромшпинелиды, хромдиопсиды, высокомагнезиальный оливин. Однако по химическому составу минералов-спутников эти кимберлиты не могут быть отнесены к алмазоносной фации (содержание Cr_2O_3 в хромшпинелидах изменяется в пределах 31–50 %, содержание MgO – в пределах 10–17 %).

В Ингульском мегаблоке широко проявлены взрывные процессы. Наиболее продуктивным в проявлении взрывных процессов в Ингульском мегаблоке является нижнепалеогеновый этап тектонической активизации, он чрезвычайно плодотворен и во всем мире. Взрывные продукты этого этапа принадлежат, большей частью, к формации брекчиевых и взрывно-осадочных образований, которые в северо-восточной части Ингульского мегаблока УЩ ассоциируются, в основном, с райгородской толщей. Основная часть ореола указанной толщи тяготеет к приконтактовым частям Корсунь-Новомиргородского массива габбро-анортозит-рапакиви (рис. 8).

Райгородские слои образованы из обломков вмещающих пород кристаллического фундамента на фоне мощных автономных тектонических под-

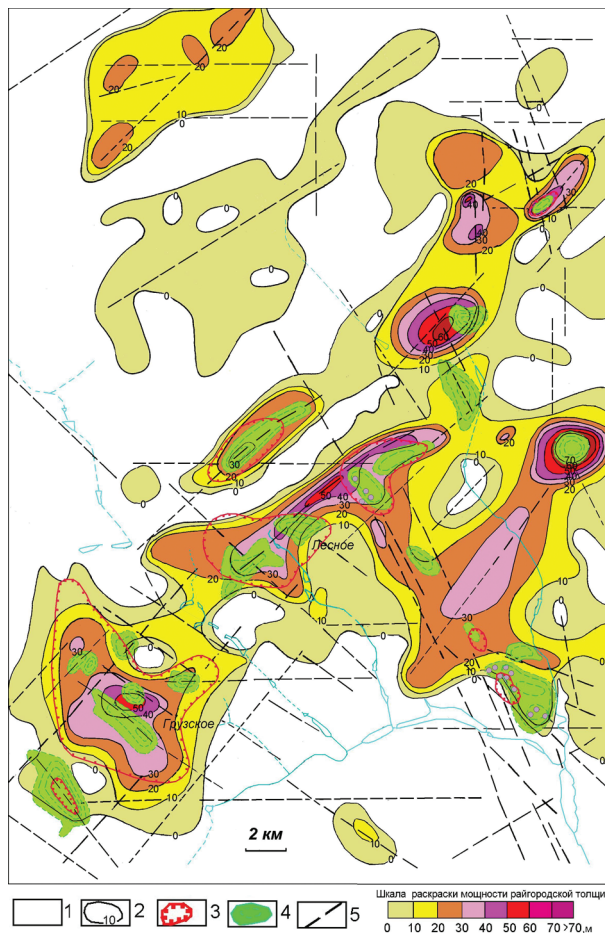


Рис. 8. Схема изопакит райгородских отложений (Pg_1). Кировоградский участок, Ингульский мегаблок УЩ:

- 1 – площадь отсутствия райгородских отложений;
- 2 – изопакиты райгородских отложений;
- 3 – ореолы развития автолитовых ксенофобрекчий кимберлита;
- 4 – отрицательные гравитационные аномалии, контролируемые взрывные структуры;
- 5 – разрывные нарушения

вижек с эффектами маарового вулканизма. На многих участках в пределах райгородской толщи выявлены прямые признаки кимберлитового магматизма. К ним отнесены проявления автолитовых брекчий кимберлита (скв. 4074, 4076 (структура Грузская-Южная), 4061, 4067, 4052, 4053, 4055 (участок Лесной)), алмазы и ИМК в породах, образующих кольца выброса взрывных диаметров. Размер взрывных структур – первые сотни метров (рис. 6, 8). Общий ореол распространения райгородской брекчированной толщи составляет 25×40 км только в центральной части, где она имеет сплошное развитие. Ореол образован вдоль серии тектонических узлов, которые являются следствием пересечения Захаровской зоны разлома северо-восточного простирания, идущей по экзоконтакту плутона рапакиви в его юго-западной части, с субпараллельными разломами северо-западного простирания, которые

упираются в плутон (рис. 6, 8). В материале лабораторно-технологической пробы весом 237 кг с автолитовых брекчий кимберлита Грузской-Южной структуры были выявлены 10 зерен хромшпинелидов размером от 0,08 до 0,15 мм в форме октаэдров и сростков кристаллов.

Микрозондовыми исследованиями зерен хромшпинелей определено содержание в них Cr_2O_3 от 30 до 62,17 % и MgO от 7,3 до 12,5 %. В минералогической пробе 4087/1 были установлены кимберлитовые алмазы – шпинелевый двойник кристалла переходной формы октаэдр-ромбододекаэдр $1,4 \times 1,2 \times 0,9$ мм и 6 осколков одного кристалла (октаэдр-ромбододекаэдр с полосами пластической деформации) размерами от 0,1 до 0,25 мм, мантийные пиропы – 150 обломков ($\text{Cr}_2\text{O}_3 = 6,1-7,1$ %, $\text{MgO} = 19,33-20,01$ %, $\text{CaO} = 4,14-4,38$ %, с содержанием кноррингитового компонента у большинства зерен >10 мол. %).

Петрологические характеристики кимберлитов Ингульского мегаблока УЩ (наличие нодулей гранатовых дунитов и гарцбургитов в кимберлитах Лелековского и Щорсовского участков, присутствие в них алмазов перидотитового парагенезиса, полного комплекса индикаторных минера-

лов кимберлитов (ИМК), химический состав ИМК, в частности Грузского участка – пиропов ($\text{Cr}_2\text{O}_3 = 6,1-7,1$ %, $\text{MgO} = 19,33-20,01$ %, $\text{CaO} = 4,14-4,38$ %, с содержанием кноррингитового компонента у большинства зерен >10 мол. %), хромшпинелидов ($\text{Cr}_2\text{O}_3 = 45,32-62,17$ %, $\text{MgO} = 7,3-12,5$ %), часть из которых относится к алмазной ассоциации, позволяют оценить глубину генерации отдельных очагов кимберлитовых магм в регионе не менее чем 140–150 км. Этот уровень генерации отдельных очагов кимберлитовых магм в регионе близкий по глубине к уровню, благоприятному для генерации алмазов. Одной из главных наблюдаемых особенностей химического состава ИМК из эксплозивных структур Ингульского мегаблока УЩ является сходство с таковыми из мантийных модулей дунит-гарцбургитового состава алмазоносных кимберлитов Якутии. Это может свидетельствовать о близких физико-химических условиях формирования тех и других ИМК (табл. 1, 2).

По данным ГСЗ мощность литосферы в пределах Приазовского мегаблока составляет 150–170 км (рис. 3), земной коры – 35–47 км. В северной части Центрально-Приазовской зоны разло-

Таблица 1

Химический состав хромшпинелей из кимберлитов и эруптивных брекчий Ингульского мегаблока УЩ [18] и кимберлитов Якутии [19]

Компонент	Ингульский мегаблок					Якутия	
	Щорсовский участок (кимберлит)	Лелековский участок (кимберлит)	Грузской участок (кимберлит)	Зеленогайская структура (кимберлит)	Ровенский участок (эруптивные брекчи)	Трубки Айхал, Удачная (гарцбургит-дуниты)	Трубка Удачная (лерцолиты)
Ст-компонент	35,3–41,1	17,4–39,3	35,3–84,0	76,4–83,9	65,0–78,1	83,4	41,0
Al-компонент	52,9–63,2	81,2–61,8	14,1–45,6	11,9–20,2	7,2–13,3	12,4	42,1
Ульвошпинель	0,1–0,6	0,2–0,5	0,5–5,2	0,1–0,6	1,3–1,8	0,4	2,8
<i>f</i> , %	29,2–41,9	28,0–23,5	58,9–64,3	40,9–51,9	46,8–73,0	45,1	41,0
<i>K_o</i>	43,8–75,7	9,4–20,7	3,4–50,5	27,3–28,6	38,2–45,0	11,3	0

Таблица 2

Химический состав гранатов из кимберлитов Ингульского мегаблока УЩ [18] и Якутии [19]

Компонент	Ингульский мегаблок		Якутия	
	Щорсовский участок	Грузской участок	Трубки Айхал, Удачная (гарцбургит-дуниты)	Трубка Удачная (лерцолиты)
Са-компонент	12,9–17,5	10,9–11,4	1,8–11,2	13,3–16,5
Mg-компонент	28,3–66,6	71,3–73,7	76,0–87,7	61,6–75,2
Ст-компонент	0,1–0,6	18,5–20,9	11,2–40,2	4,5–16,7
<i>f</i> , %	36,3–76,8	17,9–18,4	11,7–16,2	14,1–27,8

мов наблюдается валообразное поднятие границы М северо-западного направления. В северной части восточной половины мегаблока наблюдается ровообразное понижение границы М. В восточной части Приазовского мегаблока выделяется Приазовская мегаструктура, охватывающая одноименный мантийный диапир (рис. 1). На поверхности фундамента он выражен образованиями хлебодаровского и более поздних (южно-кальчикского, октябрьского и каменно-могильского) комплексов. Образования этих комплексов формируют единый плутон длительного образования

на площади от р. Каратыш (на западе) до р. Грузской Еланчик (на востоке) (рис. 9). Этот плутон расположен непосредственно над мантийным диапиром. В пределах плутона установлен ряд проявлений, которые могут быть отнесены к ультраосновной с карбонатитами формаций и связанных с ней фенитов (Петрово-Гнутовский, Хлебодаровский, Дмитровский).

На проявленность в пределах Приазовского мегаблока мантийных процессов кроме щелочных и субщелочных породных комплексов также указывают установленные штоки и дайки лам-

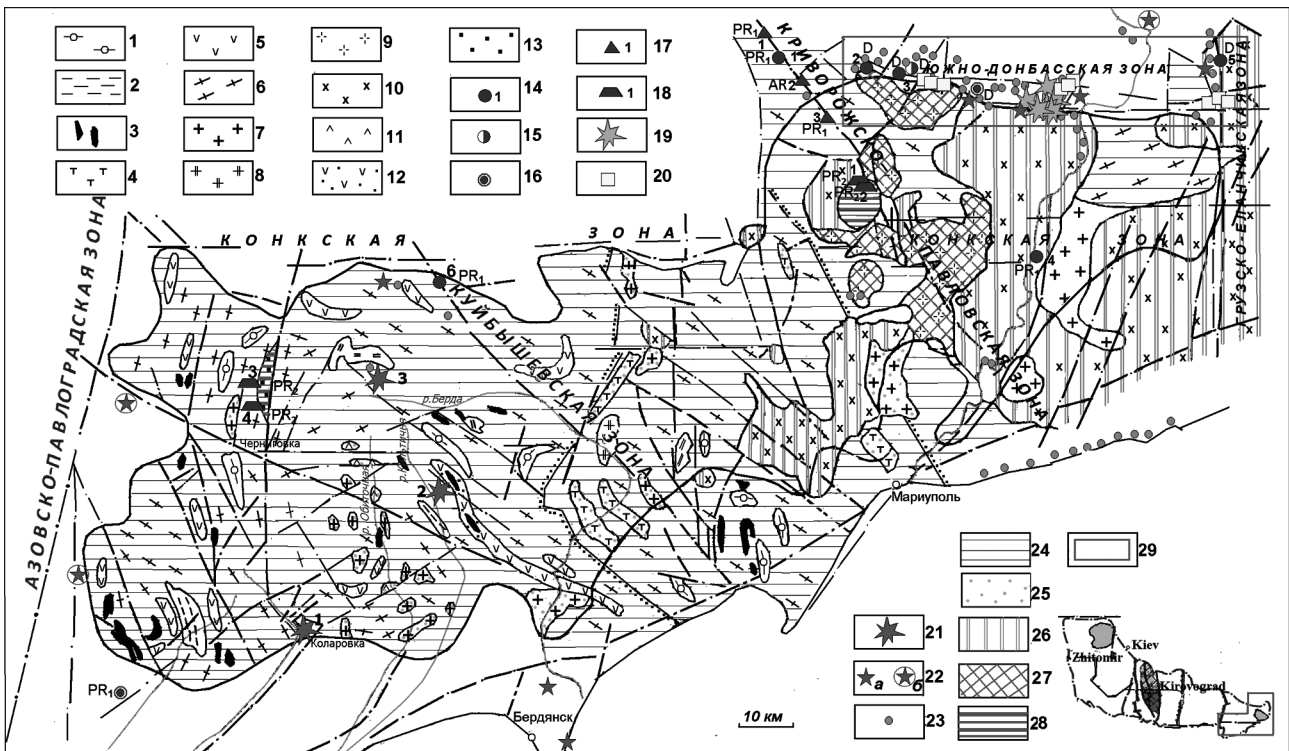


Рис. 9. Схема критериев и признаков алмазности (по материалам Приазовской ГРЭ), размещения урановородных объектов и распределение урана в породах Приазовского мегаблока (по материалам КП „Кировгеология“):

1 – гнейсы пироксеновые и амфибол-пироксеновые; 2 – гнейсы биотитовые; 3 – кварциты железистые; 4 – гнейсы биотит-графитовые, биотит-силлиманитовые и др. породы пестрой толщи р. Берды; 5 – амфиболиты; 6 – мигматиты существенно плагиоклазовые по разным породам; 7 – породы гранодиоритового комплекса; 8 – граниты плагиоклазовые р. Каратюк (Захарьевский массив); 9 – анадолевские граниты; 10 – породы граносиенитового комплекса, 11 – обиточненский интрузивный комплекс (кварцевые диориты, тоналиты, диориты и габбро-диориты); 12 – гуляйпольский метаморфизованный комплекс (высокоглиноземистые ставролит-, кордиерит-, андалузит-, силлиманитвещающие и двуслюдяные кристаллосланцы, мраморы и графитвещающие гнейсы, метаконгломераты); 13 – черниговский карбонатитовый комплекс (карбонатиты и ассоциирующие с ними нефелиновые и щелочные сиениты, щелочные ультрабазиты). Эндеогенные рудопроявления урана: 14 – гидротермальные в минерализованных зонах: 1 – Васильевское, 2 – Балка Большая Барсукова, 3 – Балка Мандрыкина, 4 – Балка Барбасова, 5 – Еланчикское (Покрово-Киреевское); 6 – Куйбышевское; 15 – Николаевское непромышленное месторождение в базальных отложениях; 16 – гидротермальные уранитумные в зонах дробления пород кристаллического фундамента; 17 – гидротермально-метасоматические в пегматоидных гранитах: 1 – Павловское, 2 – Ново-Андреевское, 3 – Валерьяновское; 18 – магматического типа в массивах сиенитов и карбонатитов: 1 – Мазуровское, 2 – Рудник „Циркон“, 3 – Новополтавское, 4 – Черниговское; 19 – кимберлитопроявления; 20 – находки жильных пикритов; 21 – взрывные лампроитопроявления: 1 – Мрия, 2 – Камыши, 3 – Конка; 22 – находки кристаллов алмазов: а – в современном аллювии, б – в отложениях мезокайнозойского возраста; 23 – находки пиропов в современном аллювии. Среднее содержание урана в породах (в 10^{-4} %): 24 – менее 2,5; 25 – от 2,5 до 5; 26 – от 5 до 8; 27 – от 8 до 10; 28 – более 10, 29 – контур Волновахской площади

проитов (трубки „Мрия“, „Конка“ и др.) возраста 1970–1950 млн лет (по флогопиту К-Аг метод) [16], серия малых интрузий кимберлит-лампроитового ряда коларовского комплекса возраста 1900–1760 млн лет [16], Мариупольское поле лампрофиров (рис. 9). В бассейне р. Лозоватка были выявлены высокомагнезиальные слюдяные ультрабазиты лампроитовой серии (1970–1950 млн лет) [16], залегающие в виде маломощных даек. В зоне Южно-Донбасского разлома (Волновахская площадь) установлен ряд кимберлитовых трубок и даек (рис. 9). Дайки якупирангитов мощностью до 2,5 м образуют пояс северо-западного простирания длиной 35 км при ширине 10 км, который прослеживается от с. Елисеевка до Соркинской зоны севернее с. Осипенки в направлении, перпендикулярном Черниговской зоне.

В кимберлитах трубок Волновахской площади пиропы являются продуктами дезинтеграции разноглубинных и разных по составу перидотитов графит-пироповой фации глубинности. Пиропы гарцбургитового парагенезиса алмаз-пироповой фации глубинности встречаются крайне редко [4].

Хромшпинелиды, выявленные в кимберлитовых трубках и дайках Приазовья, по особенностям химического состава делятся на три группы: 1) с низкой хромистостью ($Cr_2O_3 < 45\%$) и титанистостью ($TiO_2 < 1\%$), повышенной глиноземистостью и магнезиальностью, соответствующие лерцолитам с умеренным или повышенным содержанием клинопироксена; 2) соответствующие по составу высокохромистым ($Cr_2O_3 = 48–60\%$), низкоглиноземистым низкожелезистым магнезиохромитам, первоисточником которых были пироповые лерцолиты с низким содержанием клинопироксена (количеством существенно преобладают над другими разновидностями); 3) в знаковых количествах присутствуют высокохромистые ($Cr_2O_3 = 60–64\%$), низкоглиноземистые ($Al_2O_3 = 6–9\%$) магнезиохромиты, близкие по составу к алмазной ассоциации [2, 4].

Присутствие в преимущественном количестве хромшпинелидов второй группы позволяет отнести кимберлиты Волновахской площади к образованиям преимущественно лерцолитового состава, образование хромшпинелидов в диапазоне давлений 30–32 кбар, т. е. в условиях графит-пироповой фации глубинности (125–130 км). Единичные находки пиропов и хромшпинелидов алмазной ассоциации, мелких алмазов позволяют предполагать мелкие локальные очаги генерации кимберлитовых магм на границе алмаз и графит-пироповой фации глубинности.

В пределах Днестровско-Бугского мегаблока по данным ГСЗ мощность литосферы составляет 180–200 км (рис. 3), увеличиваясь в юго-восточном направлении до 200–250 км. Отмечается контрастное разделение структуры подошвы литосферы мегаблока на северо-западную (Подольский блок) и юго-восточную (Бугский блок) части. В Бугском блоке зафиксировано контрастное

погружение границы Мохо в северо-западном направлении. В общем, для поверхности Мохо мегаблока фиксируется наличие троговой структуры северо-западного простирания, в разрезе выделяется мощный (до 30 км) слой коромантийной смеси [12]. Данные петрологических исследований мантийных ксенолитов из пород в коренном залегании отсутствуют. Однако в осадочном чехле (главным образом, в отложениях балтской свиты) Подольского блока Днестровско-Бугского мегаблока, при проведении алмазопроисковых работ ПДГРП „Північгеологія“, были обнаружены ореолы индикаторных минералов кимберлитов (ИМК). Наибольшее развитие в ореолах имеют пиропы лерцолитового парагенезиса. Пиропы представлены, преимущественно, низкохромистыми ($Cr_2O_3 = 1–2.5\%$) разновидностями (до 95%), среднехромистые ($Cr_2O_3 = 2.5–5.0\%$) встречаются редко, высокохромистые ($Cr_2O_3 > 5.0\%$) – очень редко. Содержание кноррингитового компонента в них не превышает 10 мол.%, следовательно, основная масса их образовалась при давлениях меньше 30 кбар [4]. Среди пиропов идентифицированы лишь единичные зерна, характерные для вебстеритов. Имеющиеся минералогические данные [2, 4] дают основания прогнозировать возможное наличие вблизи областей сноса выявленных ИМК кимберлитовых тел дайкового типа, обогащенных ксенолитами и продуктами дезинтеграции верхнемантийных лерцолитов, эклогитов (малоглубинная ассоциация) с глубиной генерации не более 120 км.

В пределах Днестровско-Бугского мегаблока широко развиты проявления глубинного магматизма и флюидизатно-эксплозивных процессов. По данным Яценко Г. М. и др. [2], в районе с. Вороновник выявлены жильные кимберлиты и eksploзивные брекчии, у с. Брацлав – eksploзивные брекчии с флюидизатно-эксплозивным материалом.

В южной части Днестровско-Бугского мегаблока, в области сочленения Голованевской шовной зоны и Ингульского мегаблока, при проведении ГГК-50 выявлены слабоконтрастные ореолы ИМК в четвертичных и неогеновых отложениях [4] и алмазы в приплотиковом аллювии в бассейнах рек Синюха, Ятрань. Подавляющее большинство пиропов по химическому составу отнесены к разновидностям лерцолитового и вебстеритового парагенезисов графит-пироповой фации глубинности с кноррингитовым компонентом до 10 мол.%, что позволяет определять диапазон давлений их генерации в 30–35 кбар. Часть выявленных хромитов по составу близка к алмазной ассоциации ($Cr_2O_3 = 61.5–63.5\%$), ($TiO_2 < 1\%$), ($Al_2O_3 = 6–8\%$) и встречается совместно с наиболее высокохромистыми пиропами [2]. Учитывая это обстоятельство, глубина генерации коренных источников, указанных ранее ИМК в южной части Днестровско-Бугского мегаблока в зоне сочленения Голованевской шовной зоны и Ингульского мегаблока, может быть около 150 км.

По данным ГСЗ мощность литосферы в пределах Среднеприднепровского мегаблока составляет от 150 до 200 км и лишь на юге мегаблока уменьшается до 100 км (рис. 3). Поверхность Мохо представляет собой линейно-вытянутое в субмеридианальном направлении валообразное поднятие в центральной части мегаблока глубиной до 32 км, которое ограничено с востока и запада понижениями границы М до 50–55 км. Петрологические материалы относительно мощности литосферы для Среднеприднепровского мегаблока очень ограничены. Веских оснований для выделения в пределах мегаблока района развития кимберлит-лампроитового магматизма нет. Характерные для кимберлитов и лампроитов минералы-спутники алмаза в Волчанской и Самотканской россыпях не установлены. По мнению С. Н. Цымбала [20], наиболее вероятным первоисточником хромшпинелидов Самотканской россыпи были ультрабазиты и базиты зеленокаменных структур центральной части Среднеприднепровского мегаблока, а хромшпинелидов Волчанской россыпи — ультрабазиты и базиты восточной части этого мегаблока. Отсутствие находок глубинных ксенолитов, подобных выявленным в Восточном сегменте, широкое развитие железистых базит-ультрабазитовых серий пород с графитом и повышенным содержанием СаО, широкое развитие продуктов коматиитового вулканизма, отсутствие в породах минералов глубоких горизонтов, объективное наличие погрешности сейсмического метода, дали основание считать максимально возможной мощностью развития литосферы в этом сегменте около 120 км.

Мощность литосферы по данным ГСЗ в пределах Росинско-Тикичского мегаблока составляет 185–200 км (рис. 3). Глубина залегания поверхности Мохо колеблется от 40 до 60 км. В центральной части мегаблока в Зеленоярской и Тарасовской рутил-циркон-ильменитовых россыпях выявлены мелкие кристаллы алмазов, однако считается, что областью питания этих россыпей является Бердичевское поднятие Подольского блока Днестровско-Бугского мегаблока [20]. В северной части Росинско-Тикичского мегаблока развиты массивы ультраосновных пород (Чипыженский, Юровский и другие) с повышенной щелочностью, в том числе и калиевой специализации, сложенных апоперидотитовыми серпентинитами, дунитами, лерцолитами, гарцбургитами, горнблендитами [2]. Ряд исследователей относят данные массивы к предкимберлитовой стадии магматизма, соответствующей глубинам генерации не более 120 км [20]. Хромшпинелиды из перидотитов Чепыженского массива имеют сравнительно высокую хромистость ($Cr_2O_3 = 40–47\%$, низкую глиноземистость ($Al_2O_3 = 7–12\%$) и магnezальность ($MgO = 3–5\%$) [4].

Мощность литосферы Волынского мегаблока по данным ГСЗ непостоянна: в северо-западной части менее 100 км, в южной и центральной ча-

стях — от 100 до 200 км (рис. 3). Глубина верхней кромки мантии изменяется от 35 до 62 км [4]. Северная и северо-западная части мегаблока характеризуются широко проявленным базальтоидным магматизмом, широким проявлением ореолов ИМК в осадочных отложениях. Имеющиеся данные результатов исследований обломков кимберлитов из брекчий и мантийных минералов позволяет предполагать, что верхняя мантия в пределах Воляно-Подольского района Волянского мегаблока выполнена эклогитами, пироксенитами, лерцолитами, гарцбургитами с резким преобладанием в разрезе лерцолитов графит-пироповой фации глубинности [16]. Гарцбургиты алмаз-пироповой фации глубинности развиты крайне редко. Породы верхней мантии, по данным химического состава ИМК, формировались в широком интервале температур (от 700 до 1500 °С) и давления (от 17–20 до 55–60 кбар) [20]. При этом в „алмазное окно“ попадают лишь значительная часть пиропов *из обломков кимберлитов* Кухотско-вольского и Серховского брекчиепроявлений Припятского вала.

Минимальная глубина залегания поверхности Мохо от 40 до 28 км характерна для Ингульского и Приазовского мегаблоков (рис. 4). Согласно флюидной теории, эти районы потенциально ассоциируют с литосферными сегментами масштабного мантийного теплопереноса и, соответственно, высокой степени рудогенерирующей способности верхней мантии. Максимальной и повышенной мощностью гранито-гнейсового слоя, отражающей уровень энергопереноса и латеральную изменчивость степени зрелости коры, выделяются Ингульский мегаблок и в контуре Коростенского плутона — фрагмент Волянского мегаблока [21]. Ингульский мегаблок, характеризуясь минимальным погружением границы Мохо на УЩ, одновременно выделяется максимальными и средними мощностями гранито-гнейсового слоя, что также отражает особенности энергопереноса и, как следствие, высокую степень гранитизации коры (рис. 4).

При установленной пестрой радиогеохимической специализации мегаблоков УЩ, породы Ингульского мегаблока, по результатам изучения в 4л геометрии, характеризуются аномально высоким региональным содержанием калия среди пород остальных мегаблоков УЩ (среднее 3,6 %, максимальное до 4,1 %) [22] и это указывает на то, что Ингульский мегаблок является сегментом наиболее интенсивного дифференцированного энергопереноса вследствие привноса флюидов из астеносферы и обусловленной этим повышенной калиевостью пород верхней части земной коры.

Нами в качестве основных предпосылок формирования алмазоносных структур на УЩ рассматриваются следующие: 1) высокая зрелость литосферы; 2) мощность литосферы не менее 150 км, которая определяет в подошве литосферного сегмента условия стабильного существова-

ния графита и алмаза; 3) гранито-гнейсовый слой высокой (10–15 км) или повышенной мощности (> 15 км); 4) аномально выраженная радиогеохимическая калиевая специализация метаморфического субстрата верхней части земной коры; 5) структурный фактор – наличие разломов транслитосферного проникновения. Информативным критерием локализации кимберлитопоявлений в сегментах литосферы высокой степени зрелости является развитие в районе исследований зон глубоких разломов мантийного проникновения, способных достигать гипсометрического уровня астеносферных областей генерации кимберлитовых магм и кристаллизации алмаза. Проявленность ослабленных мест в литосферных блоках высокой степени зрелости, являющихся благоприятным фактором внедрения кимберлитовых флюидо-магматических колонн, определяют мантийные диапиры и сформированные над ними крупные тектонические узлы, образованные глубинными разломами, которые в различные периоды геологического развития района активизировались в режимах сжатия и растяжения и характеризуются проявленностью разновозрастных даек.

Связь проявлений ультраосновного щелочного магматизма с промышленными эндогенными месторождениями урана на УЩ. В процессе проведения исследований нами была выявлена закономерная пространственная связь проявлений ультраосновного щелочного магматизма (кимберлиты, кимберлитоподобные породы, лампроиты, слюдяные пикриты и пр.) и гидротермальных месторождений урана в Кировоградском и Криворожском урановорудных районах УЩ, Приазовской потенциально урановорудной области. Это объясняется физико-химической связью процессов их рудогенерации, обусловленной, в частности, возникновением в астеносфере, при определенных РТ-условиях, мощного источника углекислотных мантийных флюидов, а в литосфере – проницаемых зон, по которым с мантийных глубин осуществлялся подъем ураноносных флюидных потоков и кимберлитовых флюидо-магматических колонн [22].

Проявляется и временная сопряженность формирования кимберлитов и урановорудных объектов. Кимберлиты Кировоградского урановорудного района с изотопным возрастом 1800 ± 9 млн лет [16] сопряжены в разломных структурах с формированием тектоно-метасоматических зон, вмещающих масштабное урановое оруденение в натриевых метасоматитах с изотопным возрастом 1800–1750 млн лет [17].

Возраст кимберлитов Восточного Приазовья, полученный Rb-Sr изохронным методом по макрокристам неизмененного флогопита, составляет для трубки Новолашпинская – 380–391 млн лет, для трубки Южная – 383–389 млн лет (лаборатория Витватерсрандского университета ЮАР (F. Kruger, J. Holtzhausen)) [16]. Возраст урановой

минерализации по наиболее богатым ураном пробам Николаевского непромышленного месторождения урана по величине $^{207}\text{Pb}/^{235}\text{U}$ составляет 390 ± 40 млн лет.

Выявленная пространственная и временная связь проявлений кимберлитового магматизма и промышленного эндогенного уранового оруденения, несомненно, обусловлена сходными структурными, петрологическими, физико-химическими факторами их образования и может использоваться в качестве дополнительного регионально-поискового критерия при прогнозировании алмазоперспективных структур в урановорудных районах.

Критерии прогнозирования алмазоносных структур в условиях УЩ. Теперь уже не вызывает сомнений факт закономерного развития алмазоносных кимберлитовых формаций только в пределах древних щитов с мощной литосферой. Однако, отнесение отдельных регионов или областей к перспективным на коренные источники алмазов возможно лишь при условии использования всех имеющихся геолого-поисковых критериев. Выполненный нами сравнительный анализ региональных прогнозно-поисковых критериев и признаков алмазоносных структур Якутской, Западно-Австралийской алмазоносных провинций и выделенные критерии для потенциально алмазоносной субпровинции Украинский щит представлены в табл. 3.

Проблема выделения различных иерархических таксонов кимберлитового магматизма наиболее дискуссионная. Признавая их приуроченность к древним платформам, исследователи расходятся в вопросе главнейших факторов локализации кимберлитов. На первый план при изучении перспектив формирования алмазоносных структур, на наш взгляд, выступает анализ глубинного строения литосферы и структурный анализ. В пределах литосферных сегментов высокой степени зрелости с проявленным комплексом предпосылок, в качестве минерагенических зон, потенциально перспективных на обнаружение алмазоносных структур, могут выступать глубинные разломы транслитосферного проникновения (разломы первого порядка), сформированные в режиме растяжения и характеризующиеся насыщенностью разновозрастными дайками основного, ультраосновного и щелочно-основного состава, образующими пояса магматопроявлений. Основанием отнесения их к категории алмазоносных (потенциально-алмазоносных) является: наличие пород щелочно-ультраосновного состава – прежде всего самих кимберлитов и/или лампроитов; наличие линейно сгруппированных ореолов ИМК, включая минералы алмазной ассоциации и алмазы [23].

В качестве кимберлитового и/или лампроитового поля принимается группа пространственно сближенных кимберлитовых и/или лампроитовых тел, приуроченная к участку пересечения ми-

Региональные прогнозно-поисковые критерии и признаки алмазоносных провинций и потенциально алмазоносной субпровинции Украинский щит (с использованием [1, 3, 9, 11, 16, 18, 20, 21, 23, 24])

Прогнозно-поисковые критерии и признаки	Якутская провинция	Западно-Австралийская провинция	Субпровинция Украинский щит
Геотектоническая позиция	Центральная часть Сибирской платформы: Вилуйский, Оленекский, Тюнгский и другие архоны	Северо-западная окраина Австралийской платформы; протерозойские (1880–1850 млн лет) мобильные пояса Холлс-Крик и Кинг-Леопольд, обрамляющие кратон Кимберли	Юго-западная окраина Русской платформы; консолидированные массивы и окаймляющие мобильные пояса: Ингульский метаблок палеопротерозойского возраста стабилизации
Региональные кимберлитоконтролирующие структуры	Мощность литосферы 220–250 км. Кимберлитовые зоны и поля приурочены к бортам авлакогенов, синеклиз, палеорифтовых структур; в платформенном чехле им соответствуют малоамплитудные купола, осложненные концентрически-радиальными дизъюнктивными нарушениями	Мощность литосферы 200–250 км. Дислокационные сбросо-сдвигово-складчатые зоны глубинного (мантийного) заложения; региональные воскалчатые зоны милонитизации, расланцевания. Характерна неоднократная ремобилизация дислокационных зон; современная сейсмичность	Сегменты литосферы высокой степени зрелости с мощностью литосферы 220–250 км, гранито-гнейсовый слой высокой и повышенной мощности (10–15 км), преимущественно калиевая специализация метаморфического субстрата верхней части земной коры. В качестве минерогенических зон, перспективных на обнаружение алмазоносных структур, выступают транзитосферные разломы, сформированные в режиме растяжения и характеризующиеся насыщенностью разновозрастными дайками основного, ультраосновного и щелочно-основного состава, образующими пояса магматопоявлений. Пространственно-временная близость формирования кимберлитопоявлений и урановорудных объектов в единых минерогенических зонах
Региональные геофизические поля	Кимберлитовым зонам и полям соответствуют перегибы и воздымания поверхности М (30–40 км), минимумы гравитационного поля, совпадающие с пониженными значениями мозаичного магнитной скорости с повышенной электропроводимости и аномальной сейсмической скоростью трубок и локальные трубки Гравитационной съемки трубок и локальные трубки выделяются локальными близометричными гравитационными аномалиями –0,5 – –0,7 мГл, формирующими вдоль контролирующего их разлома дискретную цепь (кусты) структур. Отдельные тела кимберлитов отмечаются локальными близизометричными положительными магнитными аномалиями	Линейно-овоидная (150 × 70 км) положительная гравитационная аномалия в пределах мобильного пояса Холлс-Крик, на окраине ее расположена лампроитовая трубка Аргайл. Сейсмическими методами прослежены лампроитоконтролирующие сбросо-сдвиговые и надвиговые зоны до основания земной коры и верхней мантии	Валообразные поднятия поверхности М в пределах метаблоков высокой степени зрелости. Минимумы гравитационного поля, совпадающие с пониженными значениями мозаичного магнитного поля; зоны повышенной электропроводимости и аномальной сейсмической скоростью трубок и локальные трубки Гравитационной съемки трубок и локальные трубки выделяются локальными близометричными гравитационными аномалиями –0,5 – –0,7 мГл, формирующими вдоль контролирующего их разлома дискретную цепь (кусты) структур. Отдельные тела кимберлитов отмечаются локальными близизометричными положительными магнитными аномалиями
Сопутствующие коматитные комплексы пород	Кимберлиты, альнеиты, пикриты, пикритовые порфириты, траппы, щелочно-ультраосновные породы, карбонатиты центрального типа на периферии провинции	Лампроиты, кимберлиты, их туфы, щелочные пикриты, ультраосновные лампрофиты (оливин-лампроитовые, гранат-флогопитовые)	Кимберлиты, лампроиты, пикриты, одиниты, вогезиты, лампрофиты, щелочные базальтоиды, щелочно-ультраосновные породы

Индикаторные минералы (спутники)	Пироп высокохромистый ($Cr_2O_3 > 5,4\%$) низкокальциевый, пикроильменит ($Fe_2O_3 > 5,0\%$), хромшпинель, хромдиопсид, перовскит	Хромшпинель (2-х генераций), пироп высокохромистый (Cr_2O_3 до 6%) низкокальциевый, вэйдит, прайдерит, рутил, анатаз, пикроильменит ($(Cr_2O_3$ до 3,2%), циркон	Для Кировоградских – продукты дезинтеграции разноглубинных пород верхней мантии, преимущественно, графит-пироповой фации глубинности; в отдельных структурах присутствие пиропов ($Cr_2O_3 = 6,1–7,1\%$, $MgO = 19,33–20,01\%$, $CaO = 4,14–4,38\%$, с содержанием кноррингитового компонента у большинства зерен >10 мол %), хромшпинелидов ($Cr_2O_3 = 45,32–62,17\%$, $MgO = 7,3–12,5\%$), часть из которых относится к алмазной ассоциации. Для приазовских – пиропы гарцбургитового парагенезиса алмаз-пироповой фации глубинности встречаются крайне редко, хромшпинели, преимущественно, лерцолитового состава (высокохромистые ($Cr_2O_3 = 48–60\%$), низкоглиноземистые низкожелезистые магнезиохромиты)
Постмагматические процессы	Свежие конгломераты почти отсутствуют. Главные процессы – серпентинизация и карбонатизация, бруситизация, амакинитизация	Изменения незначительны, часто локальны: серпентинизация, карбонатизация, оталькование, хлоритизация, окремнение	Изменения весьма интенсивны: серпентинизация, карбонатизация, монтмориллонитизация, хлоритизация, сапонитизация, вермикулитизация, иногда оталькование и окварцевание. Свежие кимберлиты не вскрыты
Петрохимические особенности кимберлитов пород	Широкий спектр типичных кимберлитов с ультраосновным уклоном (II петрохимическая модель кимберлитовых магм: высокие значения MgO , низкие – TiO_2 , Al_2O_3 , K_2O)	Высокотитанистые и высококальциевые кимберлиты и лампроиты с пониженной железистостью (IV петрохимическая модель магмы). Влияние вмещающих пород, местами существенная контаминация	Кировоградские кимберлиты – относительно высокая железистость ($Fe+Fe_2O_3 = 7–14\%$), повышенная щелочность (до 4%, Na_2O до 0,5%), значительное обогащение фосфором (P_2O_5 до 1–2%), Cr , Ni , Nb , Zr , Va , Sr , P_3O_3 , Th , U (до 18–20 г/т), Ta . Приазовские кимберлиты – высокое содержание TiO_2 (до 5,4%), K_2O (до 2%), P_2O_5 (до 1,7%), Nb , Zr , Va , Sr , Ta , P_3O_3 , Th , U (до 14 г/т.)
Наличие ксенолитов и глубинных пород	Характерны повышенные количества, разнообразны по составу: от алмаз-пироповой субфации до шпинель-пироксеновой	Пониженные количества, ограниченное разнообразие ксенолитов ультраосновного состава, вплоть до алмаз-пироповой субфации	Пониженные количества, разнообразный состав: для кировоградских – обломки альбитов, гранулиты, для приазовских – ильменитовые желваки, слюдиты, перидотиты
Морфология кимберлитовых тел	Трубчатые, уплощенно-трубчатые, конусовидные тела, дайки	Уплощенно-трубчатые тела, трубки, нежки, дайки	Трубки, дайки, жилы
Эпохи кимберлитово- и лампроитовообразования	Верхняя Юра 159–145 млн лет; Пермь-Триас – 233–217 млн. лет; Верхний девон – нижний карбон – 361,5–340 млн лет; Верхний ордовик – силур – 450–400 млн лет	Миоцен – 24–17 млн лет; Юра – 160 млн лет; Протерозой – 1580–1800 млн лет; Трубка Аргайл – 1048–1153 млн лет	Нижний палеоген ~ 65 млн лет; Средний-верхний девон; Протерозой. Лелековские и шорсовские кимберлиты (1800 и 1770 ± 9 млн лет) Лампроитовые трубки Приазовья – Мрия, Конка (1970–1950 млн лет); Русскополянское лампроитопроявление (1370–1330 млн лет)

нерагенической зоны разломами, сформированными в режиме растяжения, либо разломами с существенными латеральными сдвигами, сформированными в режиме сжатия или растяжения. Как правило, кимберлитовые поля будут представлять собой высокопроницаемые локальные зоны, сформированные узлами пересечения глубинных разломов различного геодинамического режима (сжатия, растяжения) различных систем (сформировавших ослабленные зоны и послуживших выводными каналами для кимберлитовых колонн). В пределах кимберлитовых полей кусты трубок и локальные трубки можно выделить по наличию локальных близоземетричных гравитационных аномалий интенсивностью $-0,5$ – $-0,7$ мГл, которые могут быть связаны с кимберлитопоявлениями взрывного типа (трубчатое тело), формирующими вдоль контролирующего их разлома дискретную цепь (куст) структур.

Выводы и перспективы дальнейшего развития. Ингульский мегаблок по выделенным глубинным предпосылкам и критериям, а также ряду прямых признаков алмазоносности, является единственным литосферным сегментом на УЩ, который можно отнести к перспективным на выявление промышленно алмазоносных структур, несмотря на палеопротерозойский возраст стабилизации фундамента.

Кировоградский урановорудный район Ингульского мегаблока однозначно определился и как кимберлитовый район. Однако вопрос об отнесении этого района в разряд алмазоносного минерагенического требует уверенного подтверждения алмазоносности выявленных кимберлитов и автолитовых брекчий кимберлитов. Объем выполненного опробования недостаточен для оценки ранга алмазоносности.

В целом, Ингульский мегаблок может оцениваться как перспективный на выявление коренных месторождений алмазов в кимберлитах и лампроитах. На сегодняшний день в северо-восточной части Ингульского мегаблока мы последовательно провели специализированные на алмазы региональные прогнозные работы масштаба 1 : 200 000, поисковые работы на алмазы на лелековском и щорсовском кимберлитопоявлениях, на девяти из 27 выделенных алмазоперспективных взрывных структурах. Это позволило получить позитивные геологические результаты. В настоящее время, в условиях отсутствия государственного заказа на целенаправленные поиски алмазов на территории Украины и усилившейся тенденции к сокращению бюджетного финансирования геологоразведочных работ, главная задача – *сохранение должным образом геологической и минералогической документации для лучших времен*. При этом следует помнить, что на территории Ингульского мегаблока УЩ проявлен набор позитивных критериев и признаков (минералогических, петрологических, геохимиче-

ских, тектонических, геофизических, геодинамических) для открытия здесь месторождений алмазов. Актуальной в Ингульском мегаблоке является и проблема поиска и прогноза нетрадиционных некимберлитовых источников алмазов, связанных с проявлениями взрывных образований (брекчий, туфов, флюидизитов, лампроитов).

References / Список літератури

1. Сусов М. В. Неизвестные страницы в истории открытия якутских алмазов / Сусов М. В. – М.: Гидропроект, 2002. – 147 с.

Susov, M. V., 2002. *Neizvestnyie stranitsy v istorii otkrytiia yakutskikhalmazov* [Unknown pages in history of Yakutia's diamond discovering]. Moscow: Gidroproekt.

2. Алмазоносные формации и структуры юго-западной окраины Восточно-Европейской платформы (Опыт минерагении алмаза) / [Яценко Г. М., Гурский Д. С., Сливко Е. М. и др.]; под ред. Г. М. Яценко, Д. С. Гурского. – К.: УкрГГРИ, 2002. – 331 с. – ISBN 966-78-96-04-8

Yatsenko, G. M., Gursky, D. S., Slivko, E. M., Heiko, Yu. V. and Prykhodko, V. L., 2006. *Almazonosnyie formatsii i struktury yugo-zapadnoi okrainy Vostochno-Yevropeiskoi platformy (Opyt mineragenii almaza)* [Diamond-bearing formation and structure of the south-western margin of the East European Platform (Experience diamond mineralization)]. Kyiv: UkrGGRI.

3. Милашев В. А. Геология кимберлитов / Милашев В. А. – СПб.: ВНИИОкеангеология, 2010. – 334 с. – ISBN 978-5-88994-097-5.

Milashhev, V. A., 2010. *Geologia kimberlitov* [Geology of kimberlites] St. Petersburg: VNIIOkeanologia.

4. Перспективы коренной алмазоносности Украины / [Гейко Ю. В., Гурский Д. С., Лыков Л. И. и др.]. – Киев-Львов: Из-во „Центр Европы“, 2006. – 200 с.

Geiko, Y. V., Gursky, D. S., Metalidi, V. S., Pavlyuk, V. N., Prykhodko, V. L., Tsymbal, S. N. and Shymkiv, L. M., 2006. *Perspektivy korennoi almazonosnosti Ukrainy* [Perspectives of basement diamond productivity of Ukraine]. Kyiv: Izd-vo “Tsentr Evropy”.

5. Сорохтин О. Г. Глобальная эволюция Земли и происхождение алмазов / Сорохтин О. Г., Митрофанов Ф. П., Сорохтин Н. О. – М.: Наука, 2004. – 269 с.

Sorokhtin, O. G., Mitrofanov, F. P. and Sorokhtin, N. O., 2004. *Globalnaia evolutsiia Zemli i proiskhozheniiealmazov* [The Global Evolution of the Earth and the origin of diamonds]. Moscow: Nauka.

6. Доусон Дж. Кимберлиты и ксенолиты в них / Доусон Дж. – М.: Мир, 1983. – 300 с.

J. Dawson, 1983. *Kimberlites and xenoliths in them*. Translated from English by F. V. Kaminskii. Moscow: Mir.

7. Хаггерти С. И. Алмазоносность Западной Африки: структурное положение и продуктивность кимберлитов / С. И. Хаггерти // Геология и геофизика. – 1992. – № 10. – С. 44–60.

- Haggerty, S., 1992. Diamondiferous West Africa: structural position and productivity of kimberlites. *Geologiya i Geophysica*, No. 10, pp. 44–60.
8. Clifford, T.N., 1966. Tectono-metallogenic units and metallogenic provinces of Africa. *Earth Planet. Sci. Lett.*, Vol. 1, pp. 421–434.
9. Джейкс А. Кимберлиты и лампроиты Западной Австралии / Джейкс А., Луис Дж., Смит К. — М.: Мир, 1989. — 430 с.
- Jakes, A., Lewis, J., Smith, K., 1989. *The kimberlites and lamproites of Western Australia*. Translated from English by Gornaia E. N. Moscow: Mir.
10. Полигенность алмазов из кимберлитового района Снеп-Лейк (Кратон Слейв, Канада): результаты исследования оливина и изотопного состава углерода / В. Н. Реутский, Н. П. Похиленко, А. Е. Холл, Н. В. Соболев // Доклад РАН. — 2002. — Т. 386. — № 11. — С. 94–97.
- Reutsky, V.N., Pohilenko, N.P., Holl, A.E. and Sobolev, N.V., 2002. Polygenic diamonds from kimberlite district Snap Lake (Slave Craton, Canada): results of a study of olivine and isotopic carbon composition. *Doklady RAN*, Vol. 386, No. 11, pp. 94–97.
11. Глуховский М. З. Гигантские рои мафических даек докембрия и вопросы алмазоносности древних платформ / М. З. Глуховский // Геотектоника. — 2006. — № 1. — С. 14–30.
- Glukhovskii, M.Z., 2006. Huge swarms of Precambrian mafic dikes and issues of diamond content of ancient platforms. *Geotectonica*, No. 1, pp. 14–30.
12. Соллогуб В. Б. Литосфера Украины / Соллогуб В. Б. — К.: Наук. думка, 1986. — 184 с.
- Sollogub, V.B., 1986. *Litosfera Ukrainy* [Lithosphere of Ukraine]. Kyiv: Naukova Dumka.
13. Оровецкий Ю. П. Мантийный диапиризм / Оровецкий Ю. П. — К.: Наук. думка, 1990. — 172 с.
- Orovetskii, Yu.P., 1990. *Mantiyni diaperism* [Mantle diapirism]. Kyiv: Naukova Dumka.
14. Bogdanova, S., Tsymbal, S., Shumliansky, L., Tsymbal, Yu., Pashkevich, I., Tsvetkova, I., 2007. Heterogeneity of the subcontinental mantle beneath the Ukrainian Shield. In: *European Mantle Workshop*, Ferrara, Italy, 29–31 August 2007, pp. 28–30.
15. Геохронология раннего докембрия Украинского щита. Протерозой / [Щербак Н. П., Артеменко Г. В., Лесная И. М. и др.]. — К.: Наук. Думка, 2008. — 240 с.
- Shcherbak, N.P., Artemenko, G.V., Lesnaya, I.M., Ponomarenko, A.N. and Shumlyanskiy, L.V., 2008. *Geokhronologia rannego dokembria Ukrainського shchita. Proterozoi*. [Geochronology of early Precambrian of the Ukrainian Shield. Proterozoic]. Kiev: Naukova dumka.
16. Цымбал С. Н. Особенности вещественного состава кимберлитов Украины: матер. научн.-техн. совещания „Стан, перспективи та напрямки геологорозвідувальних робіт на алмази в Україні“ (Київ, 19–22 мая 2003 г.) / С. Н. Цымбал, С. Г. Кривдик — К.: УкрДГРІ, 2003. — С. 22–31.
- Tsymbal, S.N. and Kryvdik, S.G., 2003. Features of the material composition of Ukraine’s kimberlites. In: *Mater. Naukovo-tekhnichnoi narady “Stan, perspektivy ta napriamky heolohorozviduvальnykh robіt na almayı v Ukraini”*. Kyiv.: UkrDGRI, pp. 22–31.
17. Радиогеохронология процессов метасоматозу у кристаллических породах УШ: тези доповідей наукової конференції „Теоретичні питання і практика дослідження метасоматичних порід і руд“, (Київ 14–16 березня 2012 р.) / О. М. Пономаренко, Л. М. Степанюк, С. Г. Кривдик, В. О. Синицин // ИГМР. — 2012. — С 64–66.
- Ponomarenko, O.M., Stepaniuk, L.M., Kryvdik, S.G. and Sinitsin, V.O., 2012. Radiogeochronology of metasomatic processes in crystal rocks of the UkrSh. In: *tezy dopovidey naukovoi konferentsii “Teoretychni pytannia i praktyka doslidzhennia metasomatychnykh porid i rud”*, (Kyiv, 14–16 berезnya 2012). — *IGMR*, pp. 64–66. (in Ukrainian)
18. Калашник А. А. Алмазоперспективные структуры Ингульского мегаблока Украинского щита / А. А. Калашник, Е. Ю. Палкина, Н. Н. Кирьянов // Наукові праці УкрНДМІ НАН України. — 2013. — Т. 10. — Ч. II. — С. 39–48.
- Kalashnik, A.A., Palkina, E.Yu. and Kirianov, N.N., 2013. Diamondiferous structures of the Ingulsky megablock of the Ukrainian Shield. *Naukovi pratsi UkrNDMI NAN Ukrainy*, Vol. 10, Part II, pp. 39–48.
19. Афанасьев В. П. Морфология и морфогенез индикаторных минералов кимберлитов / Афанасьев В. П., Зинчук Н. Н., Похиленко Н. П. — Новосибирск, 2001. — 275 с.
- Afanasiev, V.P., Zinchuk, N.N. and Pokhilenko, N.P., 2001. *Morfologiya i morfogenez indikatorykh mineralov kimberlitov* [Morphology and morphogenesis of kimberlite indicator minerals]. Novosibirsk: Nauka.
20. Цымбал С. Н. Алмазоносность территории Украины в свете идей Н. П. Семененко / С. Н. Цымбал // Минералогический журнал — 1996. — № 2. — С. 12–13.
- Tsymbal, S.N., 1996. Diamond content of Ukraine’s territory in relation to N.P.Semenenko’s ideas. *Mineralohichnyi Zhurnal*, No. 2, pp. 12–13.
21. Федоришин Ю. І. Просторова модель глибинної будови літосфери Українського щита у зв’язку з перспективами промислової алмазоносності / Ю. І. Федоришин, О. В. Фесенко, О. Б. Денега // Мін. ресурси України. — 2006. — № 3. — С. 8–12.
- Fedoryshyn, Yu. I., Fesenko, O. V. and Deneha, B., 2006. The spatial model of the deep structure of the lithosphere of the Ukrainian shield at the prospect of industrial diamond. *Mineralny Resursy Ukrainy*, No. 3, pp. 8–12.
22. Калашник А. А. Предпосылки формирования и критерии прогнозирования промышленных эндогенных месторождений урана на Украинском щите / А. А. Калашник // Науковий вісник НГУ. — 2015. — № 4. — С. 12–21.
- Kalashnik, A.A., 2015. Precondition of formation and criteria for prognostication of industrial endogenous uranium deposits of the Ukrainian Shield.

Naykovyi Visnyk Natsionalnoho Hirychoho Universitetu, No. 4, pp. 12–21.

23. Ваганов В. И. Алмазные месторождения России и мира / Ваганов В. И. – М.: Геоинформмарк, 2000. – 371с.

Vaganov, V. I., 2000. *Almaznyie mestorozhdeniia Rossii i mira* [Diamond deposits in Russia and the world]. Moscow: Geoinformmark.

24. Зинчук Н. Н. Тектоника и алмазоносный магматизм / Н. Н. Зинчук, А. Д. Савко, Л. Т. Шевырев – Воронеж: Воронежский ГУ, 2004. – 282 с.

Zinchuk, N. N., Savko, A. D. and Shevyrev, L. T., 2004. *Tektonika ialmazonosnyi magmatizm* [Tectonics and diamondiferous magmatism]. Voronezh: Voronezhskiy Gosudarstvennyi Universitet.

Мета. Виявлення нових закономірностей просторового розміщення різнорангових таксонів продуктивного кимберліт-лампроїтового магматизму на території Українського щита (УЩ) та їх відображення в геолого-геофізичних матеріалах. Обґрунтування нових критеріїв локалізації різномасштабних алмазоносних структур на основі системного підходу.

Методика. Виконано комплексний аналіз великого обсягу геофізичної, геологічної, петрогеохімічної інформації по УЩ для вивчення мінливості параметрів глибинного середовища, що визначають можливість виникнення алмазоносних кимберліт-лампроїтових розплавів у літосфері та підйом флюїдо-магматичних колон на верхні структурні горизонти земної кори з формуванням продуктивних алмазоносних структур.

Результати. Встановлені нові закономірності, що відображають специфіку формування продуктивного алмазоносного кимберліт-лампроїтового магматизму на базі багаторівневої узагальненої багатофакторної моделі природного алмазоутворення. Визначені нові критерії прогнозування різнорангових потенційно алмазоносних кимберлітових, лампроїтових таксонів території УЩ у геолого-геофізичних матеріалах. Це дало змогу здійснити обґрунтовані прогнозні оцінки потенційної алмазопродуктивності проявів кимберліт-лампроїтового магматизму сегментів літосфери УЩ, значно мінімізувати площі для подальших пошукових робіт.

Наукова новизна. Визначено новий комплекс критеріїв прогнозування різнорангових таксонів прояву продуктивного кимберліт-лампроїтового магматизму Українського щита, що враховує узагальнену багатофакторну модель природного алмазоутворення. Зазначений комплекс критеріїв дозволяє виконувати послідовну системну локалізацію різнорангових потенційно алмазоносних структур на поверхні фундаменту.

Практична значимість. На основі використання геолого-геофізичних та петрогеохімічних матеріалів по УЩ виконано комплексний геологічний аналіз території УЩ та оцінено її перспективи на корінну алмазоносність, виділено площі

найімовірнішої локалізації продуктивних проявів кимберлітово-лампроїтового вулканізму. Це дозволяє суттєво підвищити ефективність прогнозно-пошукових робіт і достовірність отриманих результатів.

Ключові слова: алмазоносні структури, літосфера, прогнозно-пошукові критерії, Український щит

Purpose. Identify new laws of spatial distribution of different rank taxons of diamondiferous productive kimberlite-lamproitic magmatism in the territory of the Ukrainian Shield and its reflection in the geological and geophysical data. The research is devoted to studying the new criteria for localization of multiscale diamondiferous structures on the base of system approach.

Methodology. Complex analysis of a large amount of geophysical, geological, petrogeochemical information on the Ukrainian Shield was made. The variability of the deep environmental parameters that determine the possibility of occurrence of diamondiferous kimberlite-lamproitic melts in the lithosphere and the rise of fluid-magmatic columns on the upper structural horizons of the Earth's crust to the formation of the diamond-producing structures was studied.

Findings. New laws, reflecting the specific formation of productive diamondiferous kimberlite and lamproitic magmatism on the base of multilevel generalized multifactor models of natural diamond forming were discovered. New prognostication criteria of varying in ranks potentially diamondiferous kimberlite, lamproitic taxons of the Ukrainian Shield's (UkrSh's) territory in geological and geophysical materials were supported. This gave the opportunity to make reasonable forecasts of the potential manifestations of diamondiferous kimberlite-lamproitic magmatism in the UkrSh's segments of lithosphere and significantly minimize the area for further exploration works.

Originality. The new complex of forecasting criteria of different rank taxons of diamondiferous productive kimberlite-lamproitic magmatism of the Ukrainian Shield, which is based on multilevel generalized multifactor models of natural diamond forming, was defined. This complex of criteria allows for a consistent system localization of different ranks of potentially diamond-bearing structures on the surface of the foundation.

Practical value. On the basis of the use of geological, geophysical and petrogeochemical data the comprehensive geological analysis of the Ukrainian Shield was made. Moreover, its perspectives on the root of diamonds were evaluated; areas of most probable localization of productive manifestations of kimberlite-lamproitic volcanism were localized. This can significantly increase the effectiveness and validity of forecasting and prospecting geological works.

Keywords: diamond structure, lithosphere, forecasting and prospecting criteria, Ukrainian Shield

Рекомендовано до публікації докт. геол. наук М.М.Довбничем. Дата надходження рукопису 29.11.15.

РОЗРОБКА РОДОВИЩ КОРИСНИХ КОПАЛИН

UDC 622.271

В. Ю. Собко¹, Dr. Sc. (Tech.), Prof.,
О. В. Ложніков¹, Cand. Sc. (Tech.), Assoc. Prof.,
А. М. Гайдін², Cand. Sc. (Geol.-Mineral.),
О. М. Лазніков³

1 – State higher educational institution “National Mining University”, Dnipro, Ukraine, e-mail: sobko.boris.nmu@gmail.com

2 – JSC “GIRKHIPROM”, Lviv, Ukraine

3 – Motronivskiy MPP, Vilnohirs'k, Ukraine

SUBSTANTIATION OF RATIONAL MINING METHOD AT THE MOTRONIVSKYI TITANIUM-ZIRCONIUM ORE DEPOSIT EXPLORATION

Б. Ю. Собко¹, д-р техн. наук, проф.,
О. В. Ложніков¹, канд. техн. наук, доц.,
А. М. Гайдін², канд. геол.-мінер. наук,
О. М. Лазніков³

1 – Державний вищий навчальний заклад „Національний гірничий університет“, м. Дніпро, Україна, e-mail: sobko.boris.nmu@gmail.com

2 – ВАТ „ГІРХІМПРОМ“, м. Львів, Україна

3 – Мотронівський ГЗК, м. Вільногірськ, Україна

ОБҐРУНТУВАННЯ РАЦІОНАЛЬНОГО СПОСОБУ РОЗРОБКИ МОТРОНІВСЬКОГО РОЗСИПУ ТИТАНО-ЦИРКОНІЄВИХ РУД

Purpose. Substantiation of effective ways of mining titanium-zirconium ores deposits with high levels of flooding at the exploration Motronivskiy site of Malyshevskiy Deposit.

Methodology. The correct definition of hydrogeological parameters on Motronivskiy site by constructing wells in the relief depressions for the establishment of an average filtration coefficient in Miocene aquifer complex with the graphic-analytical method. The digital model of the area of Motronivskiy placers is based on the publicly available software package “VISUAL MODFLOW” considering laboratory and field studies. Substantiation of effective technology of overburden operations and underwater ore extraction, based on the received digital model of the area was carried out using a technical and economic analysis.

Findings. The technological scheme of underwater mining of mineral deposits at Motronivskiy deposit allows refusing from the use of wells for pit dewatering. The capital cost of the facility amounts to 10.5 million Euros, according to the bankable feasibility study by “Vattenfall” company. There is also a reduction in the cost of mining Sarmatian sands and spreading it in the basis of internal dump. Instead of loading into trucks and transporting around the quarry at a distance of about 2 km, Sarmatian sand, in the proposed scheme, is pumped to a distance 300 m in the slurry form.

Originality. The results of studies to establish the dependency of the average filtration coefficient of the Miocene aquifer on the parameters of the field are promising for the use in underwater mining operations, especially in case when the level of groundwater in the Neogene-Paleogene aquifer remains unchanged.

Practical value. Determination of hydrogeological parameters on Motronivskiy deposit and creation of the area digital model allows substantiating the choice of the efficient technology of overburden and mining minerals from previously used schemes with shovel and road trucks and new schemes for mining titanium-zirconium ores with the use of dredgers and hydraulic transport.

Keywords: *placer deposits, hydrogeological parameters, dredger*

Introduction. The exploitation of placer titanium-zirconium deposits in Ukraine began more than half a

century ago. For this time various methods and technological schemes of mining operations have been implemented. As a result of researchers and production workers' creative efforts, a technology was found

and brought to a high productive performance, which includes mining ore with dragline, transporting it to points of the integrated hydraulic ripping, washing-out with a hydraulic giant and pumping as slurry (pulp) to the concentrator.

Successful use of this technology gave rise to the idea of its perfection and universality. Therefore, this technology was proposed in the drafts for mining Motronivskiy site (MS) of Malyshevskiy deposit as well as weathering crust of Stremyhorodske magmatic deposits.

However, the experience of practical application of the above technology while developing a particular field indicates its incapability. This is due to the unique hydrogeological conditions and engineering geological properties of rocks in the Motronivskiy site of Malyshevskiy Deposit. Therefore, there is an urgent issue which is to develop a new technology for developing titanium-zirconium ore at Motronivskiy site deposit [1].

Analysis of the recent research. Hydrogeological conditions in the period of exploration Motronivskiy titanium-zirconium placer were not studied sufficiently. The source of information for the development of the project documentation was the report of "Tsentrkrheolohiia", a subsidiary of NAK "Nadra Ukraine" in 2002.

The seventies of the last century saw active improvement of mining technology for placer mineral resources with a high degree of irrigation. Thus, an underwater method was proposed to develop the mineral, which was also used for Irshanskyy deposits of continental origin. Stripping was performed with a dragline, and the ore sand was removed with bucketline dredges. Due to the complexity of the ore deposit shape and mutability of the minerals content, the control over the pulp composition was insufficient [2]. This led to increased losses and mineral dilution.

The world practice of open cast mining has also dealt with solving this problem. While analyzing research works, we considered the experience of the mining of coastal placer deposits in Australia, India,

America, and New Zealand, where the minerals are extracted from the water by dredgers or drags. Typically, dredgers for ore extraction are installed with dressing tools, which are mounted on barges. Only rough concentrate is transported to the coast. The experience of dredger application to dewater Lebedinsky iron ore pit was analyzed as well.

Unsolved aspects of the problem. Existing developments in the local and foreign scientific-research and design works does not allow applying known solutions while mining the Motronivskiy placer without a detailed substantiation of the hydrogeological conditions of the deposit. This is explained by the fact that Motronivskiy site is an ancient marginal-marine deposit. The field is different from continental ones by the flat roof surface. The sole of ore deposits is determined by the conditioning of the mineral content and varies little in space.

The identification of Motronivskiy placers hydrogeological parameters allows moving on to the technological component of the task, which is to select effective technological schemes of mining flooded placer deposits of titanium-zirconium ores.

Objectives of the article. The definition of correct hydrogeological parameters of Motronivskiy placer due to the construction of wells in a lower part of relief allows establishing the average filtration coefficients of the Miocene aquifer complex. The development of digital models of Motronivskiy placers based on public software package "VISUAL MODFLOW" was made according to laboratory and field studies. Substantiation of effective technology of overburden and under water ore mining was based on the obtained digital models of the deposit area.

Presentation of the main research. The area of the deposit field features spreading water in the cracks of the primary igneous rocks and in sediments of the Kyivskiy, Buchatskiy, Kharkivskiy, Poltavskiy and Sarmatian ages (Fig. 1).

The last two horizons are identified as Miocene aquifer system. Glauconite sand of the Kharkivskiy

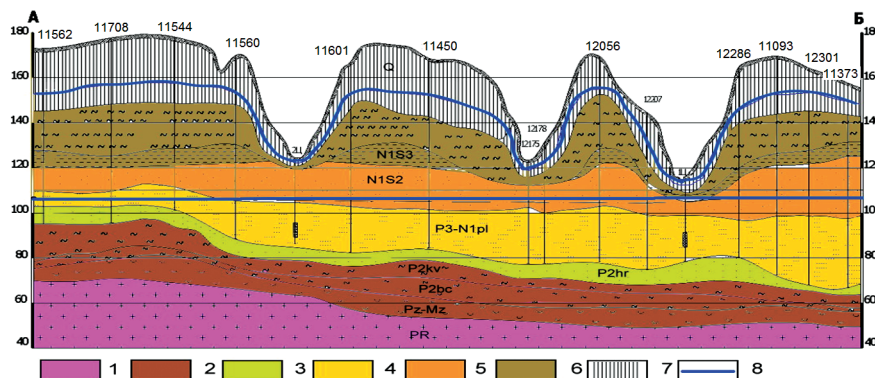


Fig. 1. Schematic hydrogeological section of Motronivskiy-Annovskiy site:

1 – water in fractured crystalline basement rocks; 2 – water in the crust of weathering, the sand of buchatskiy and kyivskiy layers; 3 – relatively aquifuge sand of kharkivskiy layer; 4 – sands of the poltavskiy series; 5 – sarmatian sands; 6 – seat clay; 7 – partially flooded loess loams; 8 – groundwater levels in the quaternary sediment and in the Miocene aquifer complex

layer in this area of clay has a firm consistency. It is adopted for aquifuge bed that divided Miocene aquifer complex from aquifers which are located below.

To determine the hydrogeological parameters, two welt clusters were built in depressions of relief – beams. The Central borehole was drilled with a diameter of 600 mm and equipped with filter columns of pipes with a diameter of 219 mm. The filters were installed in the layer of the Poltava deposits. The space between the side of the hole and the filter was filled with gravel. During the experiment test pumping of water was carried out with a constant flow at one fall. The results showed the average filter factor of the Miocene aquifer complex, equal to 3 m/day.

The obtained parameters were taken as the basis in the calculation of dewatering system within the feasibility study for MS mining by German engineering company “Vattenfall”. The planning schemes of deposits dewatering due to dewatering well with filters were installed in the bottom of the Poltavskiy and Kharkivskiy sediments. The complexity for the proposed systems has caused the need for detailed analysis of existing materials and additional hydrogeological investigations.

To refine the hydrogeological parameters, the filtration properties of rocks are determined using different methods: 1) the calculation according to the results of granulometric analysis; 2) studies with laboratory instruments; 3) field experimental-filtration works; 4) the solution of inverse problems according to digital simulation models.

Granulometric composition of the ore sands are given in Table 1.

As we can see from the data given in Table 1, ore “sand” contains 74 % of very fine sand, 17.8 % of dust, and 8.2 % of clay.

According to the engineering-geological classification of rocks [3] regarding grain-size composition ore sand is not sand, it is light dust loam. The filtration coefficient is a function of granulometric composition and porosity. For the well-known empiric formulas

their filtration coefficient is 0.0034 m/day, which is three orders of magnitude smaller than adopted in the design.

Sarmatian Sands are more coarse-grained than Poltavskiy sands.

Granulometric composition of the Sarmatian stage sands is given in Table 2.

According to the granulometric analysis, the filtration coefficient of Sarmatian sands is from 1.4 to 12.4 m/day.

For better certainty, laboratory measurement of the filtration coefficient Sarmatian sands was conducted using a modified device of G. N. Kamensky. The obtained values of filtration coefficient are 2–6 g/day. Laboratory testing of permeability coefficient of sands ore was not possible because they have water loss close to zero. The water in them has a bound form.

The obtained results of calculations and laboratory studies allow conducting an alternative interpretation of the pumping test results from well made by different organizations previously.

Although the filters of central welt cluster were located in the interval of Poltavskiy sands, the occurrence of gravel between the wall of the borehole with a diameter of 600 mm and pipes with a diameter of 250 mm has stipulated the free water flowing in the filter interval of the Sarmatian deposits (Fig. 2).

The water conductivity ($k \cdot m$) designed by the graphic-analytical method was 70 m/day. This means that the parameters do not refer to Poltavskiy, but refer to the Sarmatian sediments. If the resulting water conductivity – 70 m/day is attributed to the layer of flooded Sarmatian sands – 5.5 m, we will receive a filter factor of 12.7 m/day.

Refinement of hydrogeological parameters is made while observing pumping water out of the trench in size of 36×77 m, mined by the Esh10/50 Dragline to a depth of 3 m below the water level. In the trench, a pump was installed and water pumping was done with a flow rate of 40 m³/hour.

Table 1

Granulometric composition of the ore sands

Parameters	Size fractions, mm								Total
	-0.800 +0.500	-0.500 +0.250	-0.250 +0.100	-0.100 +0.050	-0.050 +0.010	-0.010 +0.050	-0.005 +0.001	<0.001	
Content, %	0.01	3.61	20.73	49.21	6.44	7.27	3.94	8.19	100

Table 2

Granulometric composition of the Sarmatian stage sands

Parameters	Size fractions, mm						Slope angle	
	0.5–2	0.25–0.5	0.1–0.25	<0.1	d60	D10	Dry soil	Under water
Content, %	1.3	39.2	45.4	14.1	0.2–0.26	0.04–0.12	32	29

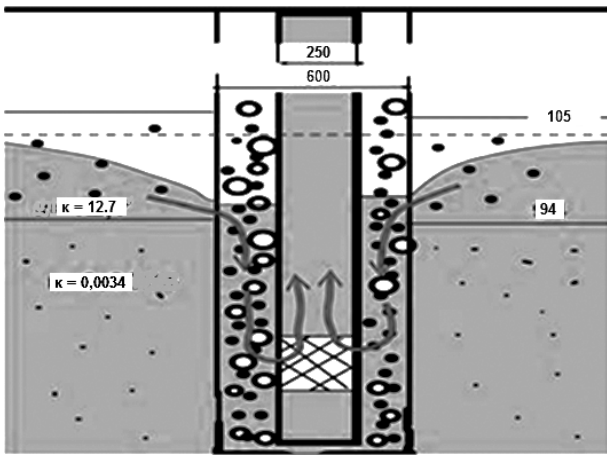


Fig. 2. Diagram of the water flow through gravel strew while conducting pumping tests

The filtration coefficient was determined according to the formula of Theis for non-stationary mode, m/day

$$K = Q \cdot \ln(2,25 \cdot a \cdot t/r^2) / 4\pi \cdot S,$$

where Q is the pumping flow rate, m^3/h ; a is the coefficient of piezoconductivity of bed, m^2/h ; t is time, h; r is given radius of the excavation, m; S is demotion, m.

Since the formula is not solved regarding filter coefficient explicitly, the method of iteration is applied, which results in a value of $K = 13.2$ m/day. This result almost coincides with the results of calculations of the pumping tests (12.7 m/day).

Considering laboratory and field studies the digital model of the area Motronivskiy placers was developed. It is based on publicly available "VISUAL MODFLOW". software package. Solving the inverse problem, we found the following filtration characteristics of the key rocks of the Miocene aquifer: 1) the deposits of the Poltava series – filtration coefficient 0.0034 m/day,

Sarmatian sand in beams – 12.7 m/day, the rest of the area – 1.4 m/day. The water loss equals 0.1.

These parameters were adopted in prediction calculations of water inflow into a prospective quarry with the open method of drainage. The simulation results in the flow of water are not more than $1000 m^3/day$, $50 m^3/hour$. To pump this amount of water would not present any problems. However, to drain the deposits in Poltava series is not possible due to the lack of water loss.

The establishment of geotechnical properties of rocks was performed using analysis of geological documentation of the deposits in the Poltava series, where it is listed as sand. However, according to the engineering-geological classification of rocks according to grain-size composition, they are light dust loam [3].

Such water-saturated soils are thixotropic, under the action of dynamic loads or hydrodynamic pressure they deliquesce. In mining and construction, they are defined as the quicksand [3]. They outpour from the excavator bucket and the truck body. The walls of boreholes are become swollen.

This is confirmed by the fact that the selection of technological samples of titanium-zirconium ore was conducted from the wells using an auger, and notably 75 tons of sand was produced from bore No. 2 [3]. Under the action of gradient filtering on trickling sites, water depth career become swollen. As a result, a swollen niche is formed, which provokes the collapse of the thicker Sarmatian sediments lying above the ore deposits. In such rocks, the excavation of drainage ditches and sumps is not possible. The only possible way is the underwater excavation of ore.

The first industrial tests of the underwater mining method for Motronivskiy placers were held at the authors' suggestion in 2015.

To master the underwater technology a dredger of ZGM-2m 42·8 type has been installed with the following technical data: performance of the dredge pump for slurry $2000 m^3/h$, for solid $300 m^3/h$. Normal depth of excavation is 11 m, the maximum one reaches 18 m.



Fig. 3. Dredge in Motronivskiy open cast mine

The movement of the dredge is of an anchor type. Fig. 3 shows a photo of the dredger working in Motronivskiyi cast.

The dredger is mounted in the pit with a depth of about 1.6 m from the water level and a volume of 9600 m³ which was built using the dragline. The first test run of the dredge was held in late August, 2015. When trying to start the operation, the available supply of water in the pit was nearly exhausted within three hours and a dredger ran aground. The groundwater inflow was scanty and further dredging work was not possible. In this regard, the technology needs the reverse water supply and recharge from an external source. After that the pit was expanded and filled with water collected in a temporary pond. At a distance of about 300 m from the excavation, a temporary hydraulic-mine dump was built.

From October, 2015 the regular dredger works started. It was found that the sand of Sarmatian horizon was washed out quite effectively. The swath walls, which a dredger forms, are first held in a vertical position, but within a few hours they become swollen. The maximum angle of bottom inclination after passage of the dredge is 28–32°.

Mining ore while deepening the working body of the dredge below the base of Sarmatian sand is easy. By the end of November a trench was formed with a width of 100 m and a length of about 200 m. The depth map of the pit, which was formed as of 19 November, 2015, is shown in Fig. 4.

The maximum depth of excavation, reached on November 23, 2015, was 8 m at a distance of 50 m from the shore. The tangent of the bottom slope was equal 0.18, which corresponded to the angle of 10°.

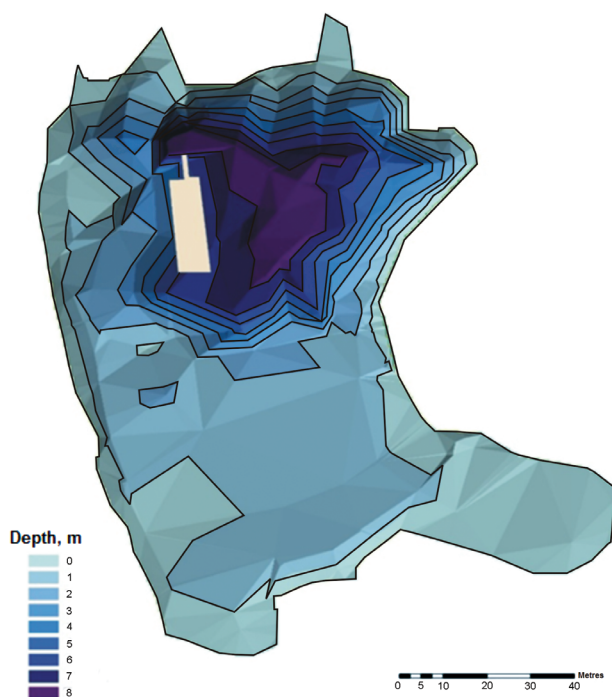


Fig. 4. The map of the open-cast mine depths in November 2015

While trying to deepen the excavation to the roof of the ore sand, the internal erosion takeaways occurred that led to the leveling of the pit bottom. Along the side on the surface cracks appeared, indicating a drawdown of thickness of Sarmatian sand over the flow core in the ore sand. Overall, the experience with the use of a dredger to conduct stripping and mining operations gave a positive result. Further, it is worth mastering the system practice determining the optimal producing cards size, organization of dredgers movements, etc.

After the establishment of the basic hydrogeological parameters of the Motronivskiyi placer, the sequence of mining works was defined. According to the concept of the authors, the technology of overburden and mining minerals from the underwater condition can be implemented in several different ways.

According to the first method, the Sarmatian deposits are developed in a mechanical way, according to the second one in a hydromechanic way. To implement the first method it is necessary to construct a pit and reduce the water level in the roof of ore deposits using a dredger (Fig. 5). The dragline is placed on berm in the sandstones above the water level and protects the roofing of ore formation, creating a berm on the roof of the ore. The width of the berm must be such that with the displacement of the ore ledge, the line of the cliff does not reach the soles of the Sarmatian sands and with the collapses in the Sarmatian sands, the products of the collapse do not reach the sand ore.

The water level in the pit should be at a few decimeters below the roof of ore deposits, for visual inspection when cleaning the roof with an excavator. In the case of water level rise due to heavy precipitation, the dredge elevates a suction pipe and pumps the water into the reservoir. At the lowering of water level, water is supplied from the storage pond. The first method implementation is complicated by the fact that the Sarmatian sand below the water level also has properties of quicksand. Another negative factor is the large cost of transportation of Sarmatian sand inside the internal dump with dump trucks, due to the considerable distances, because the full development of the quarry will reach a width of over 1.5 km.

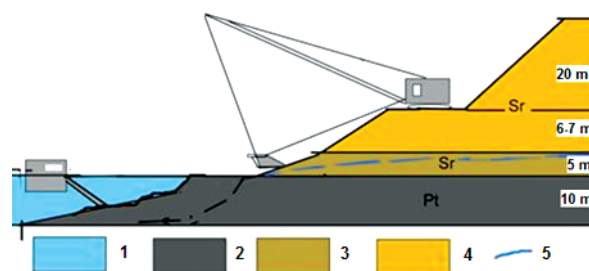


Fig. 5. The scheme of stripping and mining ore (method 1):

1 – water; 2 – ore; 3 – water-bearing Sarmatian sand; 4 – dry Sarmatian sandstone; 5 – aquifer

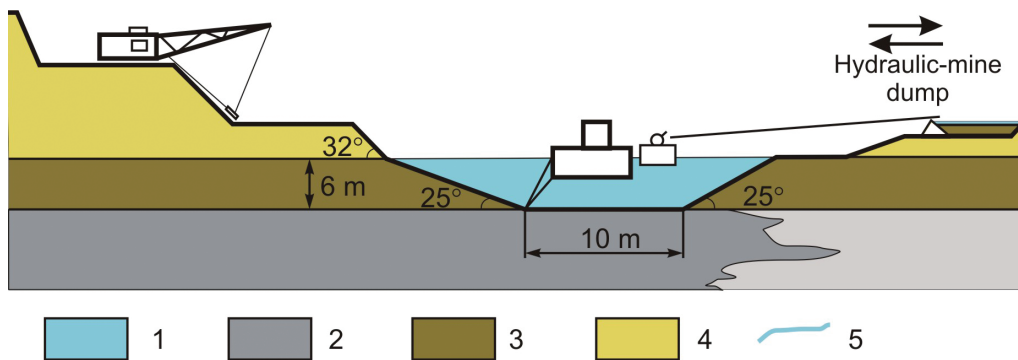


Fig. 6. The scheme of excavation of flooded Sarmatian rocks with a dredge:
1–5 are the same parameters (Fig. 5)

As for the second method, the flooded and later above-water part of the Sarmatian sand is also mined with a dredger (Fig. 6). The water level in the open cast mine corresponds to the natural one.

There are several stages in the development of mining operations. At the first stage, initial excavation, in which a dredger is installed, is constructed using the dragline. The dry part of the bench surface is left of minimum height that allows the vehicles to move. The dragline develops Sarmatian sand, which is delivered by road to the external dump. The dredger works out the Sarmatian Sands within the interval from water level to the roof of ore deposits. The slurry is fed to a temporary dump. Water from the hydraulic-mine dumps returns to the pit.

The first phase continues until the width of the pit bottom reaches 60 m. This width is determined from the condition that with the width of the berm of 30 m

Sarmatian sand does not float to the extractive slaughter.

When a berm with a width of about 30 m between the mining face and the slope of Sarmatian sand is formed, we proceed to the second stage: to install a second dredger and begin the mining of the ore (Fig. 7). Extracting dredger forms a trench with a depth equal to the thickness of the ore seam and then expands it after the promotion of dredger, which performs opening.

Upon reaching the mining trench width of 30–50 m, the third stage of mining operations begins. At the same time the dragline mining of over-ore bench with Sarmatian sands is finished (Fig. 8).

The dredger is equipped with a giant monitor for wash-out of the surface ledge. The installation of a slurry pipeline is carried out for reclamation of Sarmatian sand in dump from the opposite side of the pit.

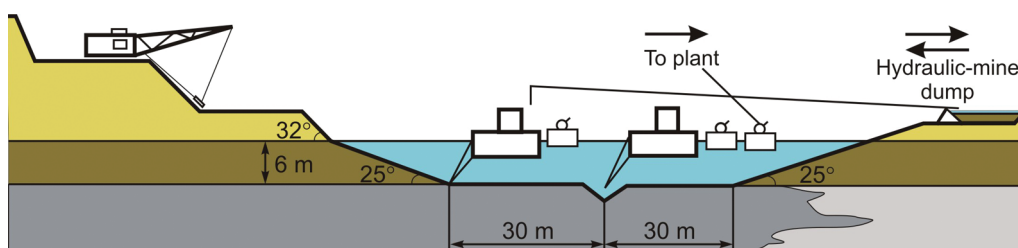


Fig. 7. The scheme of excavation of flooded Sarmatian sands and ore with dredges

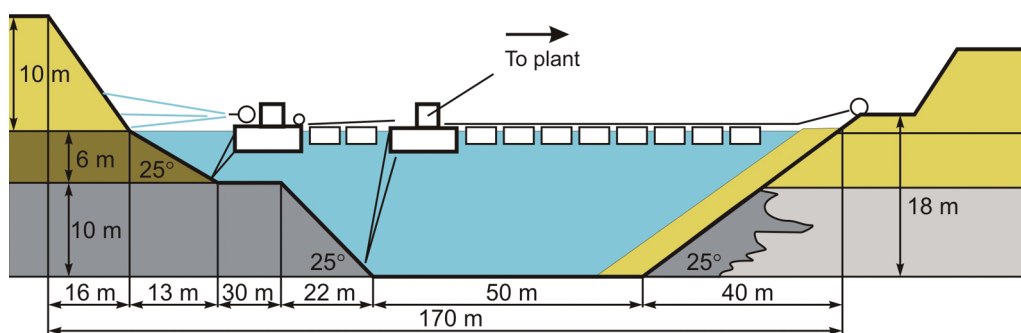


Fig. 8. Mining scheme for over-ore bench with Sarmatian sands and ore by dredges

The dredgers are moving in the direction of the front works. The worked-out area is filled with sand of Sarmatian horizon. The latter should serve as the basis for dumping rocks in the internal dumps in a mechanical way.

In order to make the height of the sand deposit greater than the excavation depth (from the water level to the soles of ore deposit), the first dredger is to develop a Sarmatian sand bench with a height of 16 m of which 6 m is under the water and 10 m is above the water.

The fourth stage of mining differs in the fact that overburden rocks which are developed for the road transport system, begin to store the rocks of the overburden into the mined-out space on the surface of washed beach with Sarmatian sand.

The fifth stage occurs after the storage of tailings on the surface of internal dumps becomes possible.

The research aimed at the use of the worked-out area and the internal dump pits for the placement of tailings started in Ukraine in the seventies of the last century. On the basis of scientific research [4], the project of the tailings dumps in the internal dump of Nikopol manganese pits was developed and in 1975 the first phase of the tailings was brought into the operation.

The technological scheme for the development of Irshanskyi ore field placers is given in [2]. After the formation of a sufficient space of mined-out areas, the refinement tailings are placed between the internal dumps. The latter are formed in a ridge shape dumps, which serve as fences dams. For conditions of Malyshivskyi titanium-zirconium deposits, these proposals are formulated in the patent [5].

The main conditions for placing the tailings on dumps surface are presented in the following way.

The dump relief is formed in such a way as to serve as tailings dams in the future. The tops of the dams correspond roughly marks a natural watershed.

Considering the fact that the volume of overburden is 4 times as large as the amount of waste, the dams should be formed with large margin of safety.

The building of dams and tailings alluvium is completed synchronously. The water discharge is provided through stoplog wells and pipes, which are laid under the dams.

As a result, landscape is formed from the system of the tailings which is similar to a system of beams blocked by dams.

Conclusions. The application of the proposed technology of mining the Motronivskyi placer allows refusing from draining careers using water depression wells. According to the bankable feasibility study developed by the "Vatenfall" company, the capital cost on the wells system construction for dewatering of the quarry would amount 10.5 million Euros. Moreover, there is no need for the construction of temporary dams in the beam to intercept and pump surface water with the subsequent dismantling of dams when the mining operations area approaches them.

The proposed technology allows rejecting the ore excavation of sand, transportation of ore to the "pulp"

knot, with subsequent erosion, because ore is eroded directly by dredger. Instead of excavators and dump trucks dredges, which cost much less, are used.

Benefits from the introduction of underwater mining of minerals at the Motronivskyi placer include the reduction of costs on overburden of the Sarmatian sands and its storing in the basis of an internal dump. Instead of loading into trucks and transporting around the pit at a distance of about 2 km, Sarmatian sand in the form of slurry is pumped to a distance of 300 meters only. The power costs for pumping tailings from the mine to the concentrator decrease significantly provided the factory of preliminary ore dressing is installed on the pontoons. According to preliminary estimates, the conventional method being used, these costs reach 130 million kW-hours per day. When placing an ore dressing plant on the pontoons, the costs reduce by 10 times.

The obtained results are promising regarding the use in underwater mining of minerals, particularly when the level of groundwater in the Neogene-Paleogene aquifer remains unchanged. This helps to prevent the development cone of influence and depletion of groundwater resources. In the process of deposits exploitation the very fine-grained ore sand is replaced by coarser sand of the Sarmatian horizon in which additional reserves of groundwater are generated.

References/Список літератури

1. Sobko, B. Yu., Melnikov, A. M., Pundiak, N. B., 2012. Comparative analysis of changes of market environment and development strategies of mining enterprises. *Naukovyi Visnyk Natsionalnoho Hirnychoho Universytetu*, No. 5, pp. 121–126.
2. Sobko B. Yu. Аналіз тенденцій змін ринкового середовища та напрямки формування стратегії розвитку гірничого підприємства / Н. Б. Собко, А. М. Мельников, Н. Б. Пундяк // Науковий вісник НГУ. – 2012. – № 5. – С. 121–126.
3. Golovach, N. A. and Volovik, V. P., 2008. Substantiation of the parameters of mining in Irshansky open pits MPP in account with environmental requirements. In: NMU (National Mining University), "Forum of miners – 2008". Dnipropetrovsk, Ukraine, 14–17 October 2008. Dnipropetrovsk: NMU.
4. Головач Н. А. Обоснование параметров горных работ на карьерах Иршанского ГОКа с учётом экологических требований: материалы международной конф. „Форум горняков – 2008“ / Н. А. Головач, В. П. Воловик – Днепропетровск: НГУ, 2008. – С. 158–163.
5. De Vallejo, L. G. and Ferrer, M., 2011. *Geological Engineering*. London: CRC Press.
6. Де Валеджо Л. Ж. Інженерна геологія / Де Валеджо Л. Ж., Феррер М. – Лондон: СРС Пресс, 2011. – 700 р.
7. Pivnyak, G. G., Gumenik, I. L., Drebenshtedt, S. and Panasenko, A. I., 2011. *Nauchnyie osnovy ratsyonalnogo prirodopolzovaniia pri otkrytoi razrabotke mestorozhdenii* [Scientific bases of rational nature

management at the deposits open cast mining]. Dnepropetrovsk: NМУ.

Научные основы рационального природопользования при открытой разработке месторождений: монография / Пивняк Г. Г., Гуменик И. Л., Дребенштетт К., Панасенко А. И. – Днепропетровск: НГУ, 2011. – 568 с.

5. Drizenko, A. Y., Lasnikov, O. M., Nikiforova, N. A., 2006. Method of tailings building on in-pit dump surface. – *The Patent Of Ukraine* No. 107586.-IE21C 41/26 (2006.01).

Патент України. Спосіб будівництва хвостосховища на внутрішньому відвалі в кар'єрі / Дріженко А. Ю., Лазніков О. М., Нікіфорова Н. А. та ін.; № 107586; Клас E21C 41/26 (2006.01).

Мета. Обґрунтування ефективного способу розробки родовищ титано-цирконієвих руд з великим рівнем обводнення на прикладі Мотронівської ділянки Малишевського родовища.

Методика. Визначення коректних гідрогеологічних параметрів Мотронівського розсипу шляхом спорудження свердловин у пониженнях рельєфу для встановлення середнього коефіцієнта фільтрації міоценового водоносного комплексу за графоаналітичним методом. Цифрова модель району Мотронівського розсипу складена на основі загальнодоступного пакету програм „VISUAL MODFLOW“ з урахуванням лабораторних і польових досліджень. Обґрунтування ефективної технології розкриття та видобутку руди з-під води на основі отриманої цифрової моделі району виконувалося з використанням техніко-економічного аналізу.

Результати. Розроблені технологічні схеми підводної розробки корисної копалини Мотронівської ділянки дозволяють відмовитися від використання свердловин для осушення кар'єру, капітальні витрати на спорудження яких становлять 10,5 млн євро, відповідно до розробленого фірмою „Ватенфаль“ банківського ТЕО. Також відбувається зменшення витрат на розкриття сарматських пісків і їх укладку в основу внутрішнього відвалу. Замість навантажування до самоскидів та транспортування навколо кар'єру на відстань біля 2 км, сарматський пісок, при запропонованій схемі, у вигляді пульпи перекачується на відстань до 300 м.

Наукова новизна. Отримані результати досліджень зі встановлення залежностей середнього коефіцієнта фільтрації міоценового водоносного комплексу від параметрів родовища перспективні до застосування при підводному видобутку корисних копалин, особливо у випадку коли рівень підземних вод неоген-палеогенового водоносного горизонту залишається незмінним.

Практична значимість. Визначення гідрогеологічних параметрів Мотронівського розсипу та створення цифрової моделі району дозволяє обґрунтувати вибір ефективної технології розкриття та видобутку корисної копалини з раніше відомих екскаваторних і автотранспортних схем та

схем видобування титано-цирконієвих руд з використанням земснарядів і гідротранспорту.

Ключові слова: *розсипні родовища, гідрогеологічні параметри, земснаряд*

Цель. Обоснование эффективного способа разработки месторождений титано-циркониевых руд с высоким уровнем обводнения на примере Мотроновского участка Малышевского месторождения.

Методика. Определение корректных гидрогеологических параметров Мотроновской россыпи путем сооружения скважин в понижениях рельефа для установления среднего коэффициента фильтрации миоценового водоносного комплекса по графоаналитическому методу. Цифровая модель района Мотроновской россыпи составлена на основе общедоступного пакета программ „VISUAL MODFLOW“ с учетом лабораторных и полевых исследований. Обоснование эффективной технологии вскрышных работ и добычи руды из-под воды, на основе полученной цифровой модели района, выполнялось с использованием технико-экономического анализа.

Результаты. Разработанные технологические схемы подводной разработки полезного ископаемого Мотроновского участка позволяют отказаться от использования скважин для осушения карьера, капитальные затраты на сооружение которых составляют 10,5 млн евро, согласно разработанного фирмой „Ватенфаль“ банковского ТЕО. Также происходит уменьшение расходов на вскрытие сарматских песков и их укладку в основу внутреннего отвала. Вместо погрузки в самосвалы и транспортировки вокруг карьера на расстояние около 2 км, сарматский песок, при предложенной схеме, в виде пульпы перекачивается на расстояние до 300 м.

Научная новизна. Полученные результаты исследований по установлению зависимостей среднего коэффициента фильтрации миоценового водоносного комплекса от параметров месторождения перспективны к применению при подводной добыче полезных ископаемых, особенно в случае, когда уровень подземных вод неоген-палеогенового водоносного горизонта остается неизменным.

Практическая значимость. Определение гидрогеологических параметров Мотроновской россыпи и создание цифровой модели района позволяет обосновать выбор эффективной технологии вскрышных и добычных работ из применяемых ранее экскаваторных и автотранспортных схем и схем по добыче титано-циркониевых руд с использованием земснарядов и гидротранспорта.

Ключевые слова: *россыпные месторождения, гидрогеологические параметры, земснаряд*

Рекомендовано до публікації докт. техн. наук А. Ю. Дріженком. Дата надходження рукопису 22.11.15.

UDC 622.235.5/.62

V. P. Kurinnyi¹, Dr. Sc. (Tech.), Prof.,
I. P. Garkusha¹, Cand. Sc. (Phys.-Math.), Prof.,
V. O. Nikiforova², Cand. Sc. (Tech.), Senior
Research Fellow

1 – State Higher Educational Institution “National Mining University”, Dnipro, Ukraine e-mail: nmu@nmu.org.ua
2 – M. S. Polyakov Institute of Geotechnical Mechanics under the NAS of Ukraine, Dnipro, Ukraine, e-mail: office.igtm@nas.gov.ua

PROCESSES OF INITIAL STAGE OF EXPANSIONS OF EXPLOSIVE CAVITY IN BLASTHOLE CHARGE

В. П. Курінний¹, д-р техн. наук, проф.,
І. П. Гаркуша¹, канд. фіз.-мат. наук, проф.,
В. О. Нікіфорова², канд. техн. наук, старш.
наук. співроб.

1 – Державний вищий навчальний заклад „Національний гірничий університет“, м. Дніпро, Україна, e-mail: nmu@nmu.org.ua
2 – Інститут геотехнічної механіки ім. М. С. Полякова НАН України, м. Дніпро, Україна, e-mail: office.igtm@nas.gov.ua

ПРОЦЕСИ ПОЧАТКОВОЇ СТАДІЇ РОЗШИРЕННЯ ПОРОЖНИНИ ВИБУХУ СВЕРДЛОВИННОГО ЗАРЯДУ

Purpose. Research into processes that occur in the blasthole and rock during the first 300 μ s after a detonation wave passing the given blasthole cross-section and determine the effectiveness of rock fracture.

Methodology. The analytical method of research based on fundamental positions of solid medium mechanics was applied.

Findings. The mechanisms of rock fracture in fine-dispersed crushing zone were considered. The valuation of dependences versus time of the blasthole radius increase, the displacement velocity of blasthole walls and of the detonation products pressure changing during the first 300 μ s after the explosion, was fulfilled. It is shown that the pressure in fine-dispersed crushed zone decreases exponentially and is inversely proportional to the square root of the distance to the blasthole axis.

Originality. It was found that the main mechanism in the fine-dispersed destruction zone is instantaneous rock destruction by shear stress. The particles size, into which the rock breaks down, is directly proportional to the width of chemical reaction zone in the explosive. Dependencies of explosion cavity radius, rock fracture velocity at the contact with detonation products and detonation products pressure on time are estimated using the adiabatic equation for detonation products with a constant index, taking into account that a strong compression wave is formed in the rock. It is shown that pressure decreases exponentially from the distance to the borehole axis in the fine-dispersed destruction zone.

Practical value. The result of this work makes it possible to develop explosives with small fine-dispersed destruction zone and substantiate charges parameters with inert and water interval, thus reducing the size of a fine-dispersed destruction zone.

Keywords: *explosion, fine-dispersed crushed zone, shock waves, pressure and rarefaction waves*

Introduction. More than 90 % of explosive energy is spent on the blasting destruction of rocks in the explosion near zone. Pressure jumps after explosion, at the rock-explosive contact, overcoming the rock mass resistance to uniform compression, crush and grind rocks, increasing the size of the charging cavity. After initial increase in charge cavity volume, the pressure of detonation products (DP) decreases, but still remains high enough and acts on the enlarged cavity walls and cracks, made after explosion.

By reducing energy consumption for grinding in the near zone of an explosion, this energy can be redistributed over the entire volume of destruction and thus enhance explosive destruction efficiency. Therefore, it is important to consider processes that take place in a charge chamber and in the rock during the first 300 μ s after a detonation wave passes a borehole of a given

section. There are many complex wave processes that pass through a borehole, which largely determine the effectiveness of rock destruction and are difficult to describe. Currently, the equation of detonation products state does not consider the interaction of their constituent molecules; correlation between adiabatic value and DP volume is not considered. Moreover, processes of formation and propagation of shock waves (SW) and compression waves (CS) in the rocks, and processes of wave energy absorption as they propagate are poorly investigated.

Therefore, consideration of the processes which occur in the near zone of explosion at its initial stage and their parameters estimation appears relevant.

Analysis of the recent research and publications. A number of studies [1] review explosive mining operation processes and assume that a shock wave is formed in the rock. In our opinion, this is not entirely

true. Moreover, in this case the authors do not take into account the relation between the volume and adiabatic value of detonation products; nor they regard the fact that formulas for shock waves are obtained for isentropic processes, i.e. the dissipation of mechanical energy in isentropic processes is not considered. In many publications stress field is reviewed as being stationary or quasi-stationary [2]. They assume that the initial pressure is equivalent to the detonation pressure. As shown by the authors, the initial pressure (or σ_{rr}) is about 20 % less. Furthermore, in the zone of fine-dispersed destruction, the rock behaves as a quasi-liquid ratio and charge cavity surface tension relation $|\sigma_{rr}/\sigma_{00}|$ is not 3.5, as in [2], but approximately 1. Therefore, the objective of this article is to remedy these shortcomings and to research processes at the initial stage of the deep-hole charge explosion cavity expansion.

Presentation of the main research. As indicated earlier by the authors of this article, pressure p_s is needed to form the shock wave in the rock, and can be calculated by the formula

$$p_s = \frac{2\rho_0 c_l^2}{m+1}, \quad (1)$$

where ρ_0 and c_l are, respectively, the density and the velocity of longitudinal stress waves in the rock; m is coefficient of rock shock compressibility in the Tait equation.

A range of pressures, required for shock wave formation, $p_s = 25-90$ GPa is calculated from (1). This is confirmed by experiments in granite ($\rho_0 = 2610$ kg/m³; $c_l = 5870$ m/s; $m = 4$) at pressures $p_s \leq 33$ GPa. Only acoustic wave at velocity c_l was recorded. Equation (1) gives the value of $p_s = 35.97$ GPa. Pressure values difference p_s is easy to explain. The shock wave only occurs when the compression wave velocity increases along with pressure increase. The compression wave velocity is determined by the formula $c_r = \sqrt{dp/d\rho}$. Given that the rock pressure and density are related by Tait equation

$$p = A \left(\left(\frac{\rho}{\rho_0} \right)^m - 1 \right),$$

where ρ is the density of the rock at the pressure p , then

$$c_r = \sqrt{\frac{Am}{\rho_0} \left(\frac{\rho}{\rho_0} \right)^{\frac{m-1}{2}}} = c_{r0} \left(1 + \frac{p}{A} \right)^{\frac{m-1}{2m}}, \quad (2)$$

where c_{r0} and c_r are, respectively, wave velocity in the rock at atmospheric pressure and at the pressure p .

This implies that p_s must be greater than 33 GPa. Compression waves propagating with velocity $c_r > c_{r0}$, are called strong (SCW).

Unlike the shock wave, the strong compression wave has shock pressure surge. During this surge pressure increases to the shock wave pressure at the interval of about 1 nanometer. In addition, the substance behind the wavefront of a plane shock wave moves with the same mass flow rate and particles displacement rate

in medium in the SCW decreases from maximum to zero in the wavefront. It can be argued, that if rock breaks into particles larger than 0.1 mm after the wavefront, then it is not a shock wave. Increased particle size is specified because the pressure in the damped shock wave is lower than the pressure p_s . In this case, rock begins to break down due to its kinetic energy and the wavefront width increases. When the pressure in the wave reaches the rock dynamic yield strength, the shock wave transforms in the compression wave.

Let us review the rock destruction processes near the borehole walls. With the detonation wave (DW) propagation in a borehole, the pressure in the area of chemical reactions increases over time τ to pressure p_d . A strong compression wave is formed in rock after that, with the frontal stress gradient average module in the front which equals (Pa/m)

$$\langle \partial\sigma/\partial r \rangle = \frac{p_d}{c \cdot \tau} \approx (3 \div 5) \times 10^{11},$$

where c is the SCW velocity. Rock shearing

Stress gradient leads to deformations, which are parallel to the wavefront, and causes rock shear. Since the critical stress levels arise simultaneously on the surface of the shear, the destruction occurs instantly. Minimal particle size d can be estimated by the formula (mm)

$$d \sim \sigma_s / (p_d / c \cdot \tau) \leq 0,$$

where σ_s is the dynamic tensile strength of rock shear.

Considering the friction force, the size of subsequence particles will increase.

With SCW propagation, the rock moves in the radial directions, which leads to the radial cracks increase, with the minimal distance order of magnitude between them akin to the minimal particle size d .

Because there are many complex wave processes (dilution and compression waves) in the plane which is perpendicular to the borehole plane, propagation of the SCW in rock is faster than propagation of the detonation wave in the borehole. The components of the tensor compression wave, propagating in the rock, depend highly on the time. The greater the amplitude of the stress in the compression wave, inhomogeneity and rate of change of the stress field are, the smaller the particle sizes into which the rock breaks are. In the near zone of explosion, the rock breaks not only in a compression wave, but also in the quasi-static stress field, created by the expanding detonation products. The rock breaks in the quasi-static field, if the field change during the time of destruction of rock element is substantially smaller than the limit of rock strength. The rock breaks into particles with a size less than 1 mm in the examined zone. The time of destruction in this case, is several micro-seconds, and during this several microseconds the pressure in the rock changes by an amount less than 10 MPa. It can be said that rock, in any sufficiently strong dynamic stress field, collapses in a quasi-static field starting from a certain element. At a pressure of 4-7 GPa the rock density increases by 4-7 %. If the rock is polycrystal, non-uniform according to its com-

pressibility and durability, then stress concentrators arise in rock, which contribute to the destruction level.

It is necessary to know dependence of near borehole wall rock movement speed on time to evaluate the destructive effectiveness of explosion. Since there are no sufficiently accurate state equations for detonation products and rocks, only movement speed of near borehole walls rocks, can be estimated, assuming that the expansion of the detonation products is adiabatic

$$p_1 V_1^n = p_2 V_2^n, \quad (3)$$

where V_1 and V_2 are initial and final volumes of detonation products; p_1 and p_2 are corresponding pressures; n is an adiabatic index.

During expansion of detonation products the adiabatic index decreases from $n = 3$ to $n = 1.33$. Since it is not possible to take into account the dependence of the adiabatic index on the DP volume, it is generally believed that n is constant.

With the actual loading densities of 500–1000 kg/m³, a major role is played by the volume of detonation products molecules (covolume). Work [3] substantiates that equation (3) can be re-written as

$$p_1 \left(\frac{V_1}{V_0} - b \right)^\gamma = p_2 \left(\frac{V_2}{V_0} - b \right)^\gamma, \quad (4)$$

where γ is the adiabatic index which does not depend on the DP volume; $\frac{V_1}{V_0}$ and $\frac{V_2}{V_0}$ are dimensionless quantities if $V_0 = 1 \text{ m}^3$; b is inaccessible to molecules part of the volume in 1 m³ of DP at a chemical spike pressure.

The adiabatic index can be expressed through the average number of freedom degrees of \bar{i} molecules, constituting the detonation products

$$\gamma = \frac{\bar{i} + 2}{\bar{i}}.$$

The average number of freedom degrees, contained in the detonation products of gases, is

$$\bar{i} = \frac{\sum v_k i_k}{v},$$

where v_k is the number of moles of k gas in DP; i_k is the freedom degree of k gas molecules; v stands for DP moles.

Covolume value can be calculated by the formula

$$b = 1 - \frac{\gamma}{n}.$$

If the detonation products contain solid particles, then their volume is added to b .

When $V_1 = 1 \text{ m}^3$ and p_1 corresponds to the detonation wave front p_d , equation (4) can be re-written as

$$p_d (1 - b)^\gamma = p (V - b)^\gamma. \quad (5)$$

If DP volume is expressed through the borehole radius (r_0), then equation (5) takes the form

$$p_d (1 - b)^\gamma = p \left(\left(\frac{r}{r_0} \right)^2 - b \right)^\gamma, \quad (6)$$

where r is the borehole radius at pressure p .

The pressure in the detonation products was calculated according to the formulas (6) and (3). The pressure, calculated by the formula (6), is about four times as large as the pressure, calculated by the formula (3).

The strong compression wave is formed in the rock with detonation wave propagation in the given section of the borehole. The initial rock velocity u_1 at the borehole wall can be calculated by the formula

$$u_1 = \frac{2c_{r0}}{m-1} \left(\frac{c_r}{c_{r0}} - 1 \right), \quad (7)$$

where c_{r0} and c_r are the compression wave velocities at the atmospheric pressure p_0 and at pressure p accordingly.

Velocities ratio $\frac{c_r}{c_{r0}}$ can be determined from the equation (2)

$$\frac{c_r}{c_{r0}} = \left(1 + \frac{p}{A} \right)^{\frac{m-1}{2m}}.$$

Detonation products velocity on the DP-rock boundary, if dilution wave is formed in the DP, is

$$u_2 = \frac{2c_d}{\gamma-1} \left(1 - \frac{c}{c_d} \right),$$

where c_d and c are the dilution wave velocities at pressures p_d and p accordingly.

Velocities ratio $\frac{c}{c_d}$ can be determined from the equation

$$\frac{c}{c_d} = \left(\frac{p}{p_d} \right)^{\frac{\gamma-1}{2\gamma}}.$$

Considering that $u_1 = u_2$ at the borehole wall

$$u_1 = u_2 = \frac{2c_d}{\gamma-1} \left(1 - \left(\frac{p}{p_d} \right)^{\frac{\gamma-1}{2\gamma}} \right) = \frac{2c_{r0}}{m-1} \left(\left(1 + \frac{p}{A} \right)^{\frac{m-1}{2m}} - 1 \right). \quad (8)$$

Acquired equation (8) allows evaluation of the initial pressure and the rock speed at the borehole wall.

Formula (7) is obtained on the assumption that at the pressures rock behaves as a liquid, i.e. from hydrodynamic equations. SW equations do not take into account that the medium resists the wave and that SW is formed at a pressure more than p_s . From these equations, it follows that SW can occur at any pressure. Given that SW and SCW equations are obtained from the laws of conservation of mass and momentum, the initial values of the substance velocity and pressure in the SWC and SW will match with a sufficiently accurate precision. Assuming that the shock wave is formed at

the borehole wall after explosion, it is possible to determine the initial rock displacement speed and the pressure on the borehole wall using the formula for the mass velocity in the shock wave. Then $u_1 = u_2$ equation is

$$u_1 = u_2 = \frac{2c_d}{\gamma - 1} \left(1 - \frac{p}{p_d}\right)^{\frac{\gamma-1}{2\gamma}} = \sqrt{\frac{p}{\rho_0} \left(1 - \frac{p}{A}\right)^{\frac{1}{m}}}, \quad (9)$$

where ρ_0 is rock density.

The following values were acquired for granite using formulas (8) and (9): $\rho_0 = 2610 \text{ kg/m}^3$; $c_d = 3750 \text{ m/s}$; $\gamma = 1.4$; $A = 23 \text{ GPa}$; $m = 4$. With explosive minimum value $p_d = 4 \text{ GPa}$, the pressure on the borehole walls and borehole wall displacement speed, calculated by the formula (8) are: $p = 3.653 \text{ GPa}$ and $u = 222.4 \text{ m/s}$, and by the formula (9) are: $p = 3.65 \text{ GPa}$ and $u = 224.6 \text{ m/s}$. Reasonably good match of pressure and velocity values confirms the validity of the formula (7).

Wave processes, which are propagating along and perpendicular to the borehole axis, must be considered when determining dependence of DP pressure and rock velocity on time, as well as superposition of compression and dilation waves in rock, coming at the relevant cross-section from the adjacent charge sites. Instantaneous detonation must be considered to estimate $p(t)$ and $u(t)$. It is generally believed, that the initial pressure in the borehole at the instantaneous detonation is $\bar{p} = p_d/2$. Given that only the initial stage of the explosion ($t = 300 \mu\text{s}$) is reviewed, p and u real values will be slightly greater. Let the borehole radius increase abruptly, so that during this leap changes of the rock pressure and velocity can be neglected. Rock velocity at the borehole wall and DP pressure in the borehole at $(j + 1)$ extension leap can be expressed through pressure and velocity values at leap j

$$u_{j+1} = \frac{2c}{\gamma - 1} \left(\frac{p_j}{p}\right)^{\frac{\gamma-1}{2\gamma}} \left(1 - \left(\frac{p_{j+1}}{p_j}\right)^{\frac{\gamma-1}{2\gamma}}\right) = \frac{2c_{r0}}{m-1} \left(\left(1 + \frac{p_{j+1}}{A}\right)^{\frac{m-1}{2m}} - 1 \right),$$

where j is leap index number; p_j and u_j are pressure and mass velocity of rock after extension leap j ; c is dilution wave velocity in DP at the pressure p ; p_{j+1} and u_{j+1} are pressure and mass velocity of rock after extension leap $j + 1$.

The radius of the explosion chamber (borehole radius) after leap $j + 1$ can be found from equation (6)

$$r_{j+1} = r_0 \sqrt{\frac{p_j}{p_{j+1}} \left(\left(\frac{r_j}{r_0}\right)^2 - b \right)} + b.$$

J -th leap time is $\Delta t_j = (r_{j+1} - r_j)u_j$.

The results of calculations are presented in Fig. 1–3. They were obtained with explosive minimum value $p_d = 4 \text{ GPa}$, dilution wave velocity in DP at pressure p is $c_d = 3750 \text{ m/s}$; DP adiabatic value $\gamma = 1.4$.

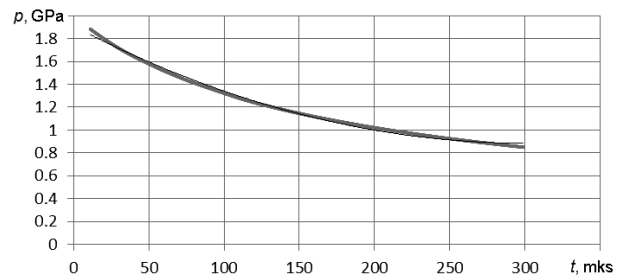


Fig. 1. Dependence of detonation (p) product pressure in the borehole on time (t):

$$p = 10^{-5}t^2 - 0.0068t + 1.9076; R^2 = 0.9956 - \text{correlation relation}$$

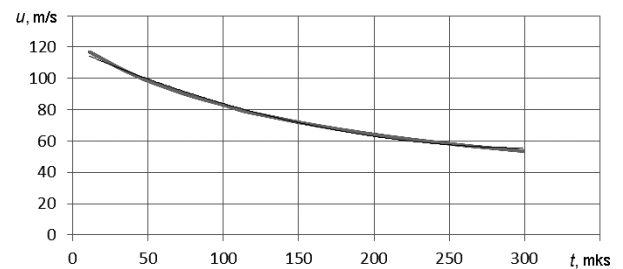


Fig. 2. Dependence of displacement (u) velocity of the rock at the borehole wall on time (t):

$$u = 0.0007t^2 - 0.4162t + 118.71; R^2 = 0.9957 - \text{correlation relation}$$

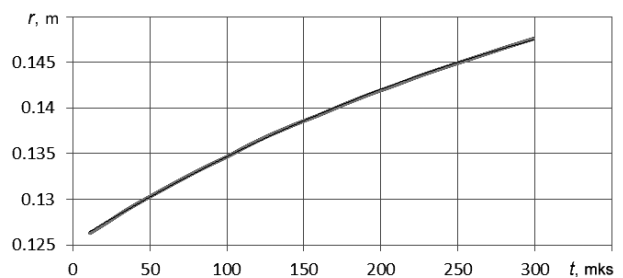


Fig. 3. Dependence of the borehole radius (r) on time (t):

$$r = -10^{-7}t^2 + 0.0001t + 0.125; R^2 = 0.9998 - \text{correlation relation}$$

Granite was taken as a rock sample with density $\rho_0 = 2610 \text{ kg/m}^3$, longitudinal wave velocity $c_{r0} = 5789 \text{ m/s}$; Teit equation coefficients $A = 23 \text{ GPa}$, $m = 4$. By the formula $u_x = up_{dx}/p_d$, where p_{dx} is another value of detonation pressure, the borehole walls velocity u_x in the same rock can be estimated with an error of less than 10 % for other values of p_d .

The compression wave damps in the zone of fine destruction according to the power and exponential functions. Indeed, if wave energy absorption coefficient depends only on wave amplitude, then the following equation is true for the plane wave

$$dJ = -\mu(r)Jdr,$$

where dJ is wave intensity change on the rock layer; $\mu(r)$ is linear coefficient of absorption; J is wave intensity at the $[r, r + dr]$ interval.

An expression for the compression wave intensity at the distance r from the borehole axis can be written after integration and consideration of axial symmetry

$$J(r) = J_0 e^{-\mu r} \cdot \frac{r_0}{r},$$

where J_0 is the initial intensity of the wave; μ is the average value of the absorption linear coefficient; r_0 is the borehole radius.

Since the wave intensity is proportional to the square of the pressure, the pressure decrease in the rock with a distance is determined by the formula

$$p(r) = p_0 \sqrt{\frac{r_0}{r}} e^{-\frac{\mu r}{2}}.$$

At a distance $r \leq r_0$ size d of particles, into which the rock breaks down, is less than 1 mm, so the coefficient μ is large enough, and DP pressure will be comparable to the dynamic tensile strength at uniform compression after 300–500 μ s.

Conclusions. The main mechanism in the fine-dispersed destruction zone – instantaneous rock destruction by shear stress – was found. The size of the particles, into which the rock breaks down, is inversely proportional to the chemical reactions zone width in the explosive. Dependencies of explosion cavity radius, rock velocity at the contact with detonation products and detonation products pressure on time are estimated using the adiabatic equation for detonation products with a constant index, taking into account that the strong compression wave is formed in the rock. It is shown that pressure decreases exponentially from the distance to the borehole axis in the fine-dispersed destruction zone.

The result of this work makes it possible to develop explosives with small fine-dispersed destruction zone and substantiate parameters of charges with inert and water interval, thus reduce the fine-dispersed destruction zone size.

References/Список літератури

1. Menzhulin, M.G. and Brovin, V.E., 2007. Energy efficiency of rocks destruction by blasting of explosives with different detonation characteristics. *Blasting affair*, No. 98/55, pp. 55–62.

Менжулин М.Г. Энергетическая эффективность разрушения горных пород при взрыве ВВ с различными детонационными характеристиками / М.Г. Менжулин, В.Е. Бровин // Взрывное дело. – М.: ЗАО „МВК по ВД“, 2007. – № 98/55. – С. 55–62.

2. Kryukov, G.M., 2009. Evaluation of the time of rocks destruction by blasting the long charges of industrial explosives. *Mining informational and analytical bulletin*, Vol. 1, pp. 8–15.

Крюков Г.М. Оценка времен разрушения породы при взрыве в ней удлиненного заряда промышленных взрывчатых веществ / Г.М. Крюков // ГИАБ. – 2009. – № 1. – С. 8–15.

3. Kurinnoy, V.P and Garkusha, I.P., 2012. On the adiabatic equation for detonation products of explo-

sive. In: International Scientific School named after Academician S.A. Khristianovich *The International scientific conference “Deformation and destruction of materials with defects and dynamic phenomena in rocks and workings”*. Tavria National University named after V.I. Vernadskyi, Simferopol, pp. 193–196.

Куриной В.П. Об уравнении адиабаты для продуктов детонации взрывчатых веществ: материалы XXII международной научной школы им. академика С.А.Христиановича „Деформация и разрушение материалов с дефектами и динамические явления в горных породах и выработках“ / В.П. Куриной, И.П. Гаркуша – Симферополь: Таврический нац. ун-т, 2012. – С. 193–196.

Мета. Дослідження процесів, що протікають у свердловині та породі в перші 300 мкс після проходження детонаційною хвилею заданого перетину свердловини та визначаючих ефективність руйнування породи.

Методика. Використано аналітичний метод досліджень, заснований на фундаментальних положеннях механіки суцільних середовищ.

Результати. Розглянуто механізми процесів руйнування породи в зоні дрібнодисперсного руйнування. Виконано оцінку залежностей від часу збільшення радіусу свердловини, швидкості зміщення її стінок і зміни тиску продуктів детонації за перші 300 мкс. Показано, що в зоні дрібнодисперсного руйнування тиск убуває по експоненті та обернено пропорційний до кореня квадратного з відстані до осі свердловини.

Наукова новизна. Встановлено, що основним механізмом у зоні дрібнодисперсного руйнування є миттєве руйнування породи від зсувних напружень. Розмір частинок, на які руйнується порода, прямо пропорційний ширині зони хімічних реакцій у вибуховій речовині. Використовуючи рівняння адиабати для продуктів детонації з постійним показником, при врахуванні збудження в породі сильної хвилі стиснення, оцінені залежності зміни від часу радіуса порожнини вибуху, швидкості руйнування породи на контакт з продуктами детонації та тиск продуктів детонації. Показано, що в зоні дрібнодисперсного руйнування тиск убуває по експоненціальній залежності від відстані до осі свердловини.

Практична значимість. Результати роботи дозволяють розробити вибухові речовини з малою зоною дрібнодисперсного руйнування, обґрунтувати параметри зарядів з інертними й водними проміжками, що дає можливість знизити величину зони дрібнодисперсного руйнування.

Ключові слова: вибух, зона дрібнодисперсного руйнування, хвилі розрідження та стиснення, ударні хвилі

Цель. Исследование процессов, протекающих в скважине и породе в первые 300 мкс после прохождения детонационной волной заданного сечения скважины и определяющих эффективность разрушения породы.

Методика. Использован аналитический метод исследований, основанный на фундаментальных положениях механики сплошных сред.

Результаты. Рассмотрены механизмы процессов разрушения породы в зоне мелкодисперсного разрушения. Выполнена оценка зависимостей от времени увеличения радиуса скважины, скорости смещения ее стенок и изменения давления продуктов детонации за первые 300 мкс. Показано, что в зоне мелкодисперсного разрушения давление убывает по экспоненте и обратно пропорционально корню квадратному из расстояния до оси скважины.

Научная новизна. Установлено, что основным механизмом в зоне мелкодисперсного разрушения является мгновенное разрушение породы от сдвиговых напряжений. Размер частиц, на которые разрушается порода, прямо пропорционален ширине зоны химических реакций во взрывчатом веществе. Используя уравнение адиабаты для продуктов детонации с постоянным показате-

лем, при учете возбуждения в породе сильной волны сжатия, оценены зависимости изменения от времени радиуса полости взрыва, скорости разрушения породы на контакте с продуктами детонации и давление продуктов детонации. Показано, что в зоне мелкодисперсного разрушения давление убывает по экспоненциальной зависимости от расстояния до оси скважины.

Практическая значимость. Результаты работы позволяют разработать взрывчатые вещества с малой зоной мелкодисперсного разрушения, обновлять параметры зарядов с инертными и водными промежутокками, что дает возможность снизить величину зоны мелкодисперсного разрушения.

Ключевые слова: взрыв, зона мелкодисперсного разрушения, волны разрежения и сжатия, ударные волны

Рекомендовано до публікації докт. техн. наук В.Д. Петренко. Дата надходження рукопису 15.12.15.

UDC 622.02:539.4.011.25

**O. M. Shashenko, Dr. Sc. (Tech.), Prof.,
O. S. Kovrov, Cand. Sc. (Tech.), Assoc. Prof.**

State Higher Educational Institution "National Mining University", Dnipro, Ukraine, e-mail: shashenko@nmu.org.ua; kovrova@nmu.org.ua

COMPARATIVE ANALYSIS OF TWO FAILURE CRITERIA FOR ROCKS AND MASSIFS

**O. M. Шашенко, д-р техн. наук, проф.,
O. С. Ковров, канд. техн. наук, доц.**

Державний вищий навчальний заклад „Національний гірничий університет“, м. Дніпро, Україна, e-mail: shashenko@nmu.org.ua; kovrova@nmu.org.ua

ПОРІВНЯЛЬНИЙ АНАЛІЗ ДВОХ КРИТЕРІЇВ РУЙНУВАННЯ ГІРСЬКИХ ПОРІД І МАСИВІВ

Purpose. The analysis of two failure criteria for rocks being in the stress-strain state.

Methodology. The study is based on an integrated approach with the use of analysis and synthesis of the literature sources on the topic related to failure of the rocks with heterogeneous structure, and use of analytical and empirical failure criteria to assess the strength of rocks.

Findings. The analysis of the two failure criteria for compliance with the results of laboratory testing of rocks in the volumetric stressed state is carried out. It is established that the expressions of both analytical criteria reflect the process of rock failure by introducing factors that take into account the mining and geological conditions and mining technology: in the Hoek-Brown criterion – m_b, s, a, D, GSI ; in the O. M. Shashenko criterion – ψ, η_0, I_r . Both criteria meet the results of laboratory tests provided m_i coefficient from the Hoek-Brown analytical expression, which takes into consideration rock structure and genesis, should not exceed 4 ($m_i \leq 4$).

Originality. Analytical comparison of two criteria has shown that, taking into consideration scattering experimental points obtained as a result of laboratory testing of rocks in the volumetric stressed state when $0 \leq m_i \leq 4.0$, they reflect the fact of the destruction of structurally inhomogeneous rock quite well. However, the Hoek-Brown criterion does not fully take into account the components of the spherical stress tensor ($I = \sigma_1 + \sigma_3$) and if the $m_i > 4$ its application requires additional study.

Practical value. Comparison of the analytical criterion with the results of laboratory testing of structurally heterogeneous materials in the volumetric stressed state allows predicting the rock failure in the massif with the precision of 94 %.

Keywords: rock failure criterion, Hoek-Brown criterion, A. N. Shashenko criterion, strength in uniaxial compression, geological strength index, coefficient of structural attenuation, coefficient of brittleness

Introduction. Choosing an adequate failure criterion for evaluation of rock destruction is one of the key points in geomechanical analysis. Priority is given to those criteria which sufficiently describe the behavior of both homogeneous and inhomogeneous rock mass being in the volumetric stressed state.

Analysis of recent research and objectives of the article. Despite some discrepancies between failure criteria and the data obtained from testing rocks in 3D compression state, lots of scientists have proposed analytical equations to fit the available laboratory data. Thus, P. R. Sheorey et al. presented the manner in which five parameters obtained from the triaxial compression test, in particular the compressive strength, tensile strength and shear strength, friction coefficient and cohesion can be interconnected by three equations (Sheorey, Biswas & Choubey). Compliance of the failure criterion has been studied in a rock mass of coal seams, mine workings and pillars.

A. Jaiswal and B. K. Shrivastva proposed a new generalized criterion for solving the problems of rock failure in the volume that takes into consideration the expansion effect and allows describing three-dimensional state of the rock massif [1]. Comparative analysis with the Hoek-Brown criterion has shown that σ_c and m_i are the most essential parameters for assessment of intact rock failure.

The experimental data revealed that strength of geo-materials, such as soil and rocks, largely depends on the intrinsic anisotropy, and other factors, such as layering and the effect of the intermediate principal stress, which is not always sufficiently described by isotropic failure criterion. Z. Gao et al. presented a generalized failure criterion for geo-materials with transverse anisotropy for predicting the strength of clay, sand and some rocks with complex strength characteristics caused by the massif anisotropy [2].

Despite the destruction of a large number of criteria used for geomechanical analysis of rocks, the issue of the most optimal and adequate criteria remains open. Thus, according to the forecast of the rock failure while drilling with the use of thirteen criteria, R. Rahimi et al. established that the most appropriate failure criteria are modified Lade, modified Wiebols-Cook and Mogi-Coulomb [3]. In comparison with the above mentioned the Tresca, von Mises and Drucker-Prager criteria yield higher values of rock strength and, as a consequence, the need for large amount of mud.

A. Elyasi and K. Goshtasbi presented a comparative analysis of the failure criteria to assess the stability of boreholes at two oil fields in Iran [4]. The maximum and minimum allowable values of the drilling fluid pressure in two wells were calculated in Fish module of the FLAC engineering software using the Mohr-Coulomb, Mogi-Coulomb, Hoek-Brown criteria. According to the results of calculations, the Mogi-Coulomb criterion is recommended to evaluate the stability of the wells, since it most adequately describes the geo-

mechanical processes during drilling, which satisfactorily agrees with the data of field research.

The parameters of the Hoek-Brown criterion (σ_{ci} , m_i and s) are significantly affected by the strength of anisotropic intact rock mass. In the study of H. Saroglou and G. Tsiambaos the criterion was modified to include a new parameter ($K\beta$) for taking into account the impact of the strength of anisotropic rock under load at different positions of the plane anisotropy (Saroglou & Tsiambaos). The range of $K\beta$ parameter for specimens of metamorphic rocks (gneiss, schist, marble) has been tested analytically and investigated by triaxial testing with different orientations of the layers.

Many types of natural rocks have inherent anisotropic plane, such as bedding, layering, etc. These structural features are responsible for the anisotropy of rock strength and deformation properties. The Hoek-Brown failure criterion takes into account the anisotropy through the special parameter $K\beta$. M. A. Ismael et al. proposed a simplified method of accounting for the influence of the rock anisotropy directly from uniaxial compression tests instead of triaxial tests to determine the anisotropy parameter K_{min} and reduce the volume of experimental work [5].

In the case when several parameters influence the total stability of the rock mass or geotechnical constructions, the application of probabilistic analysis with a random distribution of the rock massif properties to improve the durability of geotechnical design is proper. So, the probability of the rock failure and effectiveness of technology during underground mining depends on the depth of coal layers and moisture of the rock massif [6].

Currently, there are a number of studies devoted to the impact of intermediate stress σ_2 on the stress-strain state of the tested solid medium, which conceptually can be divided into 2 directions. Thus, A. D. Alekseev and N. V. Nedodayev have proved that the influence of σ_2 on the material deformation behavior does not exceed 8.5 % (Alekseev & Nedodayev). However, there are studies that show a significant impact of σ_2 on development of deformations in the solid. Thus L. B. Colmenares and M. D. Zoback consider seven different failure criteria, comparing them with available test data for five different rock types in volumetric compression ($\sigma_1 > \sigma_2 > \sigma_3$) under various stress conditions (Colmenares & Zoback). It was established that modified criteria Wiebols and Lode showed good agreement for the most of the test data with high dependence on intermediate stress σ_2 (dolomite, limestone). This statement requires serious analysis, since it does not fit well confirmed Mohr's hypothesis. These results give rise to logical questions concerning the design of the machine (device) for measuring the stress-strain state of the tested specimen and the experiment procedure.

However, for some rocks (sandstone, slate) intermediate stress has almost no effect on the failure process and the Mohr-Coulomb and Hoek-Brown criteria reflect the test data under volumetric compression better than other criteria [7].

The presented above analysis of various failure criteria shows their ambiguous application for description of the rock massif behavior.

The objective of this paper is to analyze two failure criteria of Hoek-Brown and A.N. Shashenko to describe the behavior of a rock mass under the conditions of volumetric stress-strain state.

Comparative analysis of two criteria. All known failure criteria can be divided into two major groups according to the way of their obtaining: analytical and empirical ones. Thus, the analytical criteria include those proposed by A. Griffith, Tresca-Saint Venant, Yu. I. Yagna, P. P. Balandin, I. N. Miroyubov, A. N. Shashenko, and many others (Shashenko et. al.).

The analytical failure criterion proposed by A. N. Shashenko in many respects is similar to the A. Griffith failure criterion (Griffith), the general formula for which looks as follows

$$4\tau^2 - 2a\sigma R_c - bR_c^2 = 0. \quad (1)$$

When $a = 1 - \psi$ and $b = \psi$, we obtain the dependence proposed by A. N. Shashenko, but when $a = 1$ and $b = 0.25$ we obtain the formula proposed by A. Griffiths. Here $\psi = \frac{R_p}{R_c}$ is brittleness index, R_p and R_c are uniaxial tensile and uniaxial compression strengths respectively, $\tau = \frac{\sigma_1 - \sigma_3}{2}$, $\sigma = \frac{\sigma_1 + \sigma_3}{2}$, σ_1 , σ_3 are maximum and minimum principal stresses.

Transition from the R_c strength of rock specimens to the R_m strength of objects much larger in size (rock massif) is carried out through the coefficient of structural attenuation (Shashenko et al.)

$$k_c = \frac{R_m}{R_c} = 1 - \sqrt{0.5\eta} \exp(-0.25\eta),$$

where η is coefficient of rock mass strength variation, determined according to the formula

$$\eta = \sqrt{\frac{l_t - l_0}{l_t} (\eta_0^2 + 1)} - 1.$$

Here l_t is the average distance between the cracks; l_0 is a typical rock sample size; η_0 is uniaxial compression strength variation coefficient for rock specimens.

Among the most popular and well-known empirical failure criteria, those proposed by O. Mohr, Z. T. Bieniawski, Hoek-Brown and others are widely used in geotechnical calculations. The empirical strength criteria are obtained through the processing results of laboratory testing of rocks under complex stress-strain states and related field measurements. In the strict sense, their use should be limited to those rocks and geological conditions of the experiment, which are subsequently subjected to generalization on the basis of statistical and mathematical analysis of measurement results.

Let us consider the empirical failure criterion proposed by Evert Hoek and Edwin T. Brown (Hoek),

which is very popular in geomechanics. Its generalized formula looks as

$$\sigma_1 = \sigma_3 + R_c \left(m_b \frac{\sigma_3}{R_c} + s \right)^a, \quad (2)$$

where m_b is the Hoek-Brown constant, taking into account the genesis and state (quality) of the rock mass, s and a are constants arising from the approximation of the power function of the envelope of limit stress circles obtained by bulk sample compression.

For intact (undisturbed) rock mass, the dependence (2) is transformed into the following formula

$$\sigma_1 = \sigma_3 + R_c \left(m_i \frac{\sigma_3}{R_c} + 1 \right)^{0.5}. \quad (3)$$

Here the m_i constant, unlike the m_b constant, considers the genesis and structure of the rock mass ($0 \leq m_i \leq 33$). A larger m_i value corresponds to fragile rocks, and a smaller m_i value corresponds to plastic rocks respectively. The stress state when $m_i = 0$ corresponds to the state of perfect plasticity ($R_c = R_p$). The equivalents of the m_i constant in the failure criterion (1) are the variation coefficient η_0 and brittleness coefficient ψ . In fact, the equation (3) reflects the pattern of rock specimen failure in laboratory testing.

For disturbed rock mass m_b constant is defined as follows

$$m_b = m_i \exp\left(\frac{GSI - 100}{28}\right),$$

where GSI (Geological Strength Index) presents a parameter that takes into account geological features of rock mass, in particular, its structure and occurrence of cracks ($5 \leq GSI \leq 100$). The GSI parameter is very similar to the RMR parameter (Rock Mass Rating) proposed by Z. T. Bieniawski.

For the rock mass of "good quality" ($GSI > 25$) we obtain the following values of s and a

$$s = \exp\left(\frac{GSI - 100}{9}\right), \quad a = 0.5.$$

Respectively, for the rock mass of "poor quality" ($GSI < 25$) the values are

$$s = 0, \quad a = 0.65 - \frac{GSI}{200}.$$

In order to smooth the transition from the solid rocks (with "good quality") to very poor (with "poor quality"), an additional parameter D (as "disturbance factor") has been taken into consideration. D takes into account the disturbance of the rock mass, for example, as a result of blasting. Thus, the constants m_b , s and a can be expressed through the D parameter by the following relationships

$$m_b = m_i \exp\left(\frac{GSI - 100}{28 - 14D}\right);$$

$$s = \exp\left(\frac{GSI - 100}{9 - 3D}\right);$$

$$a = \frac{1}{2} + \frac{1}{6}\left(e^{-GSI/15} - e^{-20/3}\right).$$

The D parameter possesses the values in the range from 0 for an intact rock to 1.0 for a very disturbed rock. The values of the D parameter are selected on the basis of visual observation of rocks "in situ" and assessment of their quality and disturbance degree.

It should be noted that the failure criterion (1), the characteristics of the rock mass (genesis, disturbance, structure, etc.) are considered by introducing three parameters of ψ , η_0 , l_r . The values of these parameters are obtained quite objectively through the results of laboratory testing and geological surveys. The generalized Hoek-Brown failure criterion suggests introduction of five parameters of m_b , s , a , GSI , and D , the definition of which has to some extent a subjective procedure. In an attempt to take into account all peculiarities of the rock mass in analytical expression inevitably makes empirical relations more cumbersome and less accurate due to the value dispersion for each of the input parameters. The error inevitably arises in the calculation of geotechnical constructions due to uncertainty when choosing initial parameters. Its value is smaller for more plastic rocks, and respectively larger for more brittle rocks.

The considered above criteria, even though they were obtained from various preconditions, are very similar. Equations (1) and (3) in relation to the rock specimen failure made of very brittle materials ($\psi = 0$, $m_i = 33$), can be reduced to the following form

$$\sigma_1 = \sigma_3 + \sqrt{0.25(2\sigma_3 + R_c k_c)^2 - \sigma_3^2 + \sigma_3 k_c + 0.5 R_c k_c}; \quad (4)$$

$$\sigma_1 = \sigma_3 + R_c \sqrt{\frac{m_i \sigma_3}{R_c} + 1}. \quad (5)$$

In order to compare criteria (4) and (5), the two of their parts should be divided by R_c .

As a result, the following expressions are obtained

$$\bar{\sigma}_1 = \frac{\sigma_1}{R_c} = \frac{\sigma_3}{R_c} + \sqrt{0.25\left(\frac{2\sigma_3}{R_c} + k_c\right)^2 - \frac{\sigma_3^2}{R_c^2} + \frac{\sigma_3 k_c}{R_c} + 0.5 k_c};$$

$$\bar{\sigma}_1 = \frac{\sigma_1}{R_c} = \frac{\sigma_3}{R_c} + \sqrt{\frac{m_i \sigma_3}{R_c} + 1},$$

or

$$\bar{\sigma}_1 = \bar{\sigma}_3 + \sqrt{0.25(2\bar{\sigma}_3 + k_c)^2 - \bar{\sigma}_3^2 + \bar{\sigma}_3 k_c + 0.5 k_c}; \quad (6)$$

$$\bar{\sigma}_1 = \bar{\sigma}_3 + \sqrt{m_i \bar{\sigma}_3 + 1}. \quad (7)$$

For plastic materials (e.g., wet clays) under $\psi = 1$ and $m_i = 0$ the expressions (1) and (3) become identical

$$\sigma_1 - \sigma_3 = R_c k_c;$$

$$\sigma_1 - \sigma_3 = R_c.$$

For brittle rocks $\psi = 0$ and $k_c = 1$ in the criteria (1), and $m_i = 33$ for the criteria (3) should be accepted. Then from the equations (6) and (7), we obtain

$$\bar{\sigma}_1 = \bar{\sigma}_3 + \sqrt{0.25(2\bar{\sigma}_3 + 1)^2 - \bar{\sigma}_3^2 + \bar{\sigma}_3 + 0.5}; \quad (8)$$

$$\bar{\sigma}_1 = \bar{\sigma}_3 + \sqrt{33\bar{\sigma}_3 + 1}. \quad (9)$$

The Figure presents the results of laboratory testing of various rocks in the volumetric stressed state obtained by A. N. Stavrogin and A. G. Protosenya (Stavrogin & Protosenya). These curves correspond to the dependencies (8) and (9). It is implied that both criteria fully coincide for plastic rocks ($\psi = 1$, $m_i = 0$). For brittle rocks ($\psi = 0$, $m_i = 33$), the curve corresponding to the dependence (8), coincides with the results of laboratory tests with an accuracy of $R_2 = 0.90$. The curve corresponding to equation (8), when $m_i = 33$ lies far away from the results of rock testing and agrees fairly well with them when $m_i = 3$. Since there is no reason not to trust the test data obtained by A. N. Stavrogin and A. G. Protosenya for rocks in volumetric stressed state, this circumstance requires additional analysis. Perhaps the reason lies in an incomplete account of the components of spherical stress tensor in the basic equation (2).

The difference in the structure of formulas (1) and (3) can be explained by the fact that the first case completely considers the fact of material failure by shear ($\sigma_1 - \sigma_3$) and separation ($\sigma_1 + \sigma_3$), while in the second case the failure is not entirely considered by its shear ($\sigma_1 - \sigma_3$) and the value of σ_3 . The extent to adequacy of analytical criteria to the failure of such structurally inhomogeneous materials as rocks can be determined only on the basis of compliance with the results of laboratory testing of rocks in non-uniform stressed state ($\sigma_1 > \sigma_2 = \sigma_3$).

The Figure presents such comparison of two criteria for adequacy, from which it follows that taking into

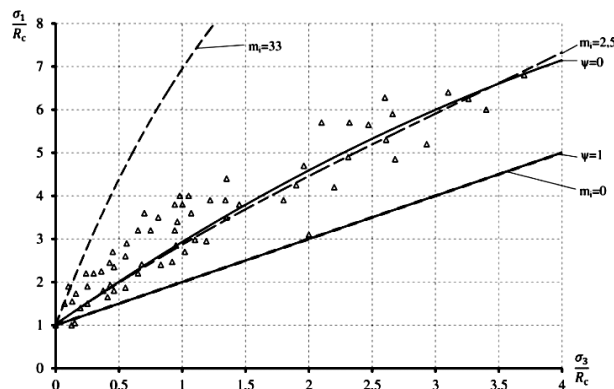


Fig. Comparison of analytical equations of failure criteria (4) and (5) with results of laboratory testing of rocks (by A. N. Stavrogin A. G. Protosenya)

account the scattering experimental points obtained as a result of testing rock specimens in volumetric stressed state at $0 \leq m_i \leq 4.0$, they reflect quite well the fact of the destruction of such structurally inhomogeneous materials as rocks. However, at the values of $m_i > 4.0$ the curves that correspond to the Hoek-Brown failure criterion are located substantially above the experimental points [8, 9]. Considering the popularity of this criterion, this fact requires further investigation.

Conclusions.

1. Two failure criteria (A. N. Shashenko and Hoek-Brown) for compliance with the results of rock specimen laboratory testing in the volumetric stressed state has been analyzed.

2. Matching both criteria with analytical expressions for a particular rock type and geological conditions is carried out by introducing special coefficients: m_b, s, a, D, GSI – for the Hoek-Brown criterion; ψ, η_0, l_t – for the A. N. Shashenko criterion. In this case, the D parameter takes into account the disturbance of rock mass during blasting operations ($0 \leq D \leq 1$).

3. It is shown that the structure of analytical expressions of both criteria is similar; however, the Hoek-Brown criterion does not fully consider the components of the stress spherical tensor ($I = \sigma_1 + \sigma_3$).

4. Both criteria match the results of laboratory tests provided the m_i coefficient, which takes into account the structure and genesis of rocks in analytical equation of the Hoek-Brown criterion, does not exceed 4 ($m_i \leq 4$).

5. Guidelines of Hoek and Brown in the case for $m_i > 4$ require further study and substantiation.

References/Список літератури

1. Jaiswal, A. and Shrivastva, B. K., 2012. A generalized three-dimensional failure criterion for rock masses. *Journal of Rock Mechanics and Geotechnical Engineering*. [online] Available at: <<http://dx.doi.org/10.3724/SP.J.1235.2012.00333>>.
2. Gao, Z., Zhao, J. and Yao, Y., 2010. A generalized anisotropic failure criterion for geomaterials. *International Journal of Solids and Structures*. [online] Available at: <<http://dx.doi.org/10.1016/j.ijsolstr.2010.07.016>>
3. Rahimi, R. and Nygaard, R., 2015. Comparison of rock failure criteria in predicting borehole shear failure. *International Journal of Rock Mechanics and Mining Sciences*, [online] Available at: <<http://dx.doi.org/10.1016/j.ijrmms.2015.08.006>>
4. Elyasi, A. and Goshtasbi, K., 2015. Using different rock failure criteria in wellbore stability analysis. *Geomechanics for Energy and the Environment*. [online] Available at: <<http://dx.doi.org/10.1016/j.gete.2015.04.001>>.
5. Ismael, M. A., Imam, H. F. and El-Shayeb, Y., 2014. A simplified approach to directly consider intact rock anisotropy in Hoek-Brown failure criterion. *Journal of Rock Mechanics and Geotechnical Engineering*. [online] Available at: <<http://dx.doi.org/10.1016/j.jrmge.2014.06.003>>.
6. Vlyadyko, O. B., Kononenko, M. M. and Khomenko, O. Ye., 2012. Imitating modeling stability of mine

workings. In: *Geomechanical Processes during Underground Mining: School of Underground Mining*. Dnipropetrovsk / Yalta, 24–28 September 2012. CRC Press Balkema.

7. Shashenko, O. M. and Kovrov, O. S., 2016. Failure criteria for structurally heterogeneous materials. *Mining of Mineral Deposits*, Vol. 10, No. 3, pp. 55–63.

Шашенко А. Н. Критерий разрушения структурно неоднородных материалов / А. Н. Шашенко, А. С. Ковров // Разработка месторождений полезных ископаемых. – 2016. – Т. 10. – № 3. – С. 55–63.

8. Sobolev, V. V. and Starikov, A. P., 2012. *Fizika gornykh porod* [Physics of mine rocks]. Donetsk: Donbass.

Соболев В. В. Физика горных пород / Соболев В. В., Стариков А. П. – Донецк: Донбасс, 2012. – 465 с.

9. Sdvizhkova, Ye. A., Babets, D. V. and Smirnov, A. V., 2014. Support loading of assembly chamber in terms of western Donbas plough longwall. *Naukovyi Visnyk Natsionalnoho Hirnychoho Universytetu*, No. 5, pp. 26–32.

Сдвижкова Е. А. Анализ закономерностей формирования нагрузки на крепь при проектировании монтажных камер струговых лав в условиях шахт Западного Донбасса / Е. А. Сдвижкова, Д. В. Бабец, А. В. Смирнов // Науковий вісник Національного гірничого університету. – 2014. – № 5. – С. 26–32.

Мета. Аналіз двох критеріїв руйнування гірських порід, що знаходяться в об'ємному напружено-деформованому стані.

Методика. Дослідження базуються на комплексному підході з використанням аналізу та узагальнення літературних джерел з тематики руйнування гірських порід з неоднорідною структурою, застосуванні аналітичних і емпіричних критеріїв руйнування для оцінки міцності гірських порід.

Результати. Виконано аналіз двох критеріїв руйнування на предмет їх відповідності результатам випробувань гірських порід в об'ємному напруженому стані. Встановлено, що аналітичні вирази обох критеріїв відображають процес руйнування гірських порід за допомогою введення коефіцієнтів, які враховують гірничо-геологічні умови та технологію розробки родовища: у критерії Хоека-Брауна – m_b, s, a, D, GSI ; у критерії О. М. Шашенка – ψ, η_0, l_t . Результатам лабораторних випробувань у повній мірі відповідають обидва критерії за умови, що коефіцієнт m_i , який враховує структуру та генезис порід в аналітичному виразі Хоека-Брауна, не повинен перевищувати 4 ($m_i \leq 4$).

Наукова новизна. Аналітичне порівняння двох критеріїв показало, що, з урахуванням розкиду експериментальних точок, отриманих у результаті лабораторних випробувань гірських порід в об'ємному напруженому стані при

$0 \leq m_i \leq 4.0$, вони досить добре відображають факт руйнування структурно неоднорідних гірських порід. Однак, критерій Хоека-Брауна не в повній мірі враховує компоненти кульового тензора напружень ($I = \sigma_1 + \sigma_3$) і при $m_i > 4$ його застосування вимагає додаткового обґрунтування.

Практична значимість. Порівняння аналітичних критеріїв з результатами лабораторного тестування зразків гірських порід в об'ємному напруженому стані дозволяє з точністю 90 % прогнозувати руйнування гірських порід у масиві.

Ключові слова: критерій руйнування гірських порід, критерій Хоека-Брауна, критерій О. М. Шашенка, межа міцності на однісіне стиснення, коефіцієнт геологічної міцності, коефіцієнт структурного ослаблення, коефіцієнт хрупкості

Цель. Анализ двух критериев разрушения горных пород, находящихся в объемном напряженно деформированном состоянии.

Методика. Исследования базируются на комплексном подходе с использованием анализа и обобщения литературных источников по тематике разрушения горных пород с неоднородной структурой, применении аналитических и эмпирических критериев разрушения для оценки прочности горных пород.

Результаты. Выполнен анализ двух критериев разрушения на предмет их соответствия результатам испытаний горных пород в объемном напряженном состоянии. Установлено, что аналитические выражения обоих критериев отражают процесс разрушения горных пород посредством введения коэффициентов, учитыва-

ющих горно-геологические условия и технологию разработки месторождения: в критерии Хоека-Брауна – m_b, s, a, D, GSI ; в критерии А. Н. Шашенко – ψ, η_0, I_r . Результатам лабораторных испытаний в полной мере соответствуют оба критерия при условии, что коэффициент m_i , учитывающий структуру и генезис пород в аналитическом выражении Хоека-Брауна, не должен превышать 4 ($m_i \leq 4$).

Научная новизна. Аналитическое сравнение двух критериев показало, что, с учетом разброса экспериментальных точек, полученных в результате лабораторных испытаний горных пород в объемном напряженном состоянии при $0 \leq m_i \leq 4.0$, они достаточно хорошо отражают факт разрушения структурно неоднородных горных пород. Однако, критерий Хоека-Брауна не в полной мере учитывает компоненты шарового тензора напряжений ($I = \sigma_1 + \sigma_3$) и при $m_i > 4$ его применение требует дополнительного обоснования.

Практическая значимость. Сравнение аналитических критериев с результатами лабораторного тестирования образцов горных пород в объемном напряженном состоянии позволяет с точностью 90 % прогнозировать разрушение горных пород в массиве.

Ключевые слова: критерий разрушения горных пород, критерий Хоека-Брауна, критерий А. Н. Шашенко, предел прочности на одноосное сжатие, коэффициент геологической прочности, коэффициент структурного ослабления, коэффициент хрупкости

Рекомендовано до публікації докт. техн. наук О. О. Сдвижковою. Дата надходження рукопису 14.12.15.

UDC 622.278.273.2

P. B. Saik¹, Cand. Sc. (Tech.),
R. O. Dychkovskiy¹, Dr. Sc. (Tech.), Prof.,
V. H. Lozynskiy¹, Cand. Sc. (Tech.),
Z. R. Malanchuk², Dr. Sc. (Tech.), Prof.,
Ye. Z. Malanchuk², Dr. Sc. (Tech.), Assoc. Prof.

1 – State Higher Educational Institution “National Mining University”, Dnipro, Ukraine, e-mail: saik.nmu@gmail.com
 2 – National University of Water Management and Nature Resources Use, Rivne, Ukraine, e-mail: malanchyk@ukr.net

REVISITING THE UNDERGROUND GASIFICATION OF COAL RESERVES FROM CONTIGUOUS SEAMS

П. Б. Саїк¹, канд. техн. наук,
Р. О. Дичковський¹, д-р техн. наук, проф.,
В. Г. Лозинський¹, канд. техн. наук,
З. Р. Маланчук², д-р техн. наук, проф.,
Є. З. Маланчук², д-р техн. наук, доц.

1 – Державний вищий навчальний заклад „Національний гірничий університет“, м. Дніпро, Україна, e-mail: saik.nmu@gmail.com
 2 – Національний університет водного господарства та природокористування, м. Рівне, Україна, e-mail: malanchyk@ukr.net

ХАРАКТЕРИСТИКА ПІДЗЕМНОЇ ГАЗИФІКАЦІЇ ЗАПАСІВ ВУГІЛЛЯ ЗБЛИЖЕНИХ ПЛАСТІВ

Purpose. Substantiating of contiguous coal seams coefficient during application of borehole underground coal gasification technology based on dependences of interstratium rocks subsidence on gasification duration.

Methodology. Using stand experimental research and methods of computer modeling we obtained the dependences of interstratium rocks subsidence in terms of their thickness change, alternating thickness of coal seams and duration of the gasification process. To reflect the geomechanical situation of rock mass around underground gasifier, license software Flac 5.00 was used. For data processing and building of synthesis dependences, the method of multiple regression using generally accepted data processing systems – Excel-2013 was used.

Findings. The obtained inequality allows setting the coefficient of contiguous coal seams during the application of underground gasification technology. Setting this factor makes it possible to assess mining and geo-logical conditions of coal seams occurrence with further rational order of their gasification. For values of contiguous coefficient 5.5–5.7, gasification of coal seams can be carried out both in ascending and descending sequence. In this case, there is no need to preserve the allowable distance between combustion faces on adjacent seams.

Originality. To determine the contiguous of coal seams, a mathematical mechanism was developed, whose effectiveness is confirmed by computer simulation of rock massif that contains an underground gasifier and by research on a special test bench installation. The difference between the results was less than 24 %.

Practical value. Dependence of interstratium rocks subsidence at changing duration of the gasification process describing the development of possible formation of gas-permeable cracks in interstratium rocks ensuring technological process was established. The obtained conditions of contiguous coal seams allow providing rational order of mine workings.

Keywords: *stand research, underground coal gasification, contiguous coal seams, coefficient of contiguity*

Introduction. In Donetsk and Lvivsko-Volynskiy coal basin the majority of reserves is located in contiguous coal seams. Analysis of domestic and international experience has shown that extraction of such reserves using conventional mining methods is uneconomical because of the negative manifestation of rock pressure in working faces. This situation greatly affects the cost of coal produced and mining accidents. It is possible to avoid this situation by improving conventional technologies of extraction, at least by changing the process of extraction. According to the opinion of leading specialists in the field of fuel and energy complex, this problem can be solved by implementing a radically new technology of development and process-

ing of coal in place of its occurrence in a closed technological cycle – borehole underground coal gasification (BUCG). To carry out this technology, it is necessary to drill two boreholes toward the coal seams with subsequent linking. Then the coal seam must be ignited, which promotes creation a controlled combustion face with balanced oxidation and reduction zones. This makes it possible to obtain a mixture of combustible gases and then use them as a source of electricity and chemicals. In this way, the development of mining coal deposits for obtaining energy and innovation of the product in an environmentally closed cycle is classified as “Clean Coal Technology” (CCT) and “High Technologies” (HT).

Analysis of the recent research and publications. Over the last decade, the global energy market has shown growing interest in the technology of un-

derground coal gasification, as evidenced by the number of developed projects and an increasing share of patents and security documents (according to Worldwide European Patent Office). New technological solutions of the process execution and new designs of gasifiers appear.

A team of researchers developed innovative technological solutions related to ensuring the effectiveness and efficiency of gasification technology application based on performed scientific and experimental study. A particularity of these technological solutions of coal seams gasification is that they are adapted to one productive horizon or the coal fields, where the works of minerals extraction have not been carried out. Therefore, it is necessary to consider a further possibility of expanding the technology for other coal seams. Today the question concerns a transfer of the results in terms of real mines, the creation of power and chemical complex of processing the received energy and chemical products. This requires the development of spatial representations of the state of the rock mass during the process of underground gasification and creation of efficient modes of operation [1], studying the balance of physical and chemical reactions [2], which will expand the use of the technology of borehole underground coal gasification and conduct rational management planning of mining, locating underground gasifiers with a focus on required final energy product. The technology of underground gasification of contiguous coal seams is being paid increasing attention due to reducing the volume of drilling operations and improving the productivity of a gasifier plant. Simultaneous extraction of coal reserves in contiguous seams results in a significant reduction of costs of the received final product.

In manuscript [3] the method of underground gasification of contiguous coal seams which involves their preliminary degassing through horizontal or inclined boreholes drilled on the upper and lower layers, is suggested. In the process of gasification, degassing of above layering strata of rocks is conducted. The period of degassing of the zone of upper layer discharge is regulated by changing the speed of combustion face advance along the bottom layer. Underworked coal seam and rock massif can completely give almost all methane only in unloading zone.

The period of gas recovery can be called a degassing interval. In the area of drainage, discharge efficiency is increased up to 78–88 %. The implementation of this method of gasification prevents drainage of methane into the atmosphere (if any) from rock massif around underground gasifier, and escape of combustible gases through underworked rock massif. During this technology, methane is viewed not as an independent energy product, but as an additional product of underground gasification gases.

While using the “UCG-methane” technology, proportion of methane in the initial combustible gas is increased to 26–44 %. This technology can increase the energy indicators of degassing gases from coal seams in the closed cycle and receive a comprehensive

energy products and fertilizers. The downside of this technology is the low efficiency of degassing 15–20 % when the coal seam is intact. The occurrence of excess pressure in the gasifier leads to the escape of methane and gasifier gas on the Earth's surface, polluting the atmosphere and hydrosphere.

Another variant of underground gasification of contiguous coal seams is a technology described in the paper [4]. This technology provides, firstly, gasification of upper layering coal seam, formation of a gathering collector in a goaf. Its hermetization is done from outside of the earth's surface and gasification of other coal seams in ascending order. Methane outlet released from the rock massif, goes along degassing wells. The peculiarity of this gasification technology is that after creating a gathering collector other contiguous coal seams can be gasified in advance of each combustion face on the bottom layer relative to the top. The main disadvantages, as in the first case, can be low indicators of coal seams degassing process and the need for complex degassing of wells.

The closest technical solution of contiguous coal seams gasification is a method of underground gasification of solid fuels described in the paper [5]. The advantages of this technological scheme include reducing the cost of preparing and opening the coal seam, increasing the area of the gasifier, reducing air blast and gasification products escape. The following can be referred to as its disadvantages: the difficulty of breaking into layers of the coal seam and the inability to hold the opposite gasifier through design features of a vertical shaft.

Unsolved aspects of the problem. Analysis of the above technological solutions showed that the mechanism for setting conditions for coal gasification of contiguous seams has not been developed yet. The following restrictive factors have been hardly considered: structural change of the rock mass, thickness, the angle of the seam, the length of the combustible face and extraction pillar; occurrence of geological faults; the variation of parameters of the gasification process; design features of underground gasifier; different ways of managing rock pressure, etc. The authors of this work, see the need to investigate the effect of geometrical parameters of coal seams and changes in quality of the contiguous rocks on quality indicators of the gasification process as the primary task.

Presentation of the main research and explanation of scientific results. With interstratial rocks lowering, the probability of the vertical cracks formation in the rock massif increases [6]. It should be noted that during coal seam gasification the fracturing formation is related primarily to rock pressure. Uneven distribution of temperature field around underground gasifier is a secondary factor. During gasification of contiguous coal seams, forming of the vertical cracks is even more evident. These discontinuous formations turn into gas channels in the rocks. Vortices of blowing and gaseous mixtures of lower and upper underground gasifiers can occur there. This situation leads to destabilization of the whole system.

In undisturbed rock massif, natural cracks are under stresses caused by mining pressure and reservoir pressure of gas in the cavities of the cracks [7].

The possibility of formation of gas channels in interstratified rocks has been based on a subsidence on the coal bottom of the upper coal seam. The formation of vertical cracks is observed in the rock layers with horizontal deformation $\xi > 5 \text{ mm/m}$ [8]. Based on the study of the stress-strain state of the rocks of the main roof, a strain graph of the main roof depending on the size of subsidence was built (Fig. 1).

Analyzing this dependence (Fig. 1), we can conclude that the subsidence of the main roof by over 200 mm results in increase of vertical through-cracks ($\xi > 5 \text{ mm/m}$). This makes it possible to predict the probability of formation of these cracks based on the values of coal bottom subsidence of the upper layer.

During the process of experimental research three models of rock and coal massif around ex-situ gasifier were formed. The transition from the model size to natural conditions occurred using the relevant similarity criteria. Thickness of the coal seam in each model was the same – 1.2 m. Thickness of interstratified rocks ranged from 3.6 to 6.6 m. Three layers represented interstratified rocks. Thickness of the first layer was 0.7 m, the second ranged from 2.3 to 5.3 m, and the third was 0.6 m. Modelled physical and geometrical parameters

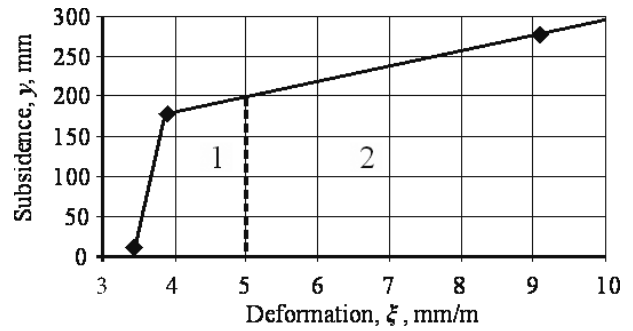


Fig. 1. Graph of behavior of the main roof depending on the size of subsidence:

1 – the zone in which there are no vertical through cracks formation; 2 – the zone of vertical through cracks formation

corresponded to geological conditions of selected areas of mine fields of SE “Lvivuhillia”.

Monitoring of the subsidence of interstratified rocks and their collapse was carried out for 18 measuring points (reference sensors) in three rows in terms of underground gasifier area. They were placed at the bottom of the upper coal seam (6), as shown in the technological diagram in Fig. 2.

The nature of the rocks subsidence in each model had both their own and common features.

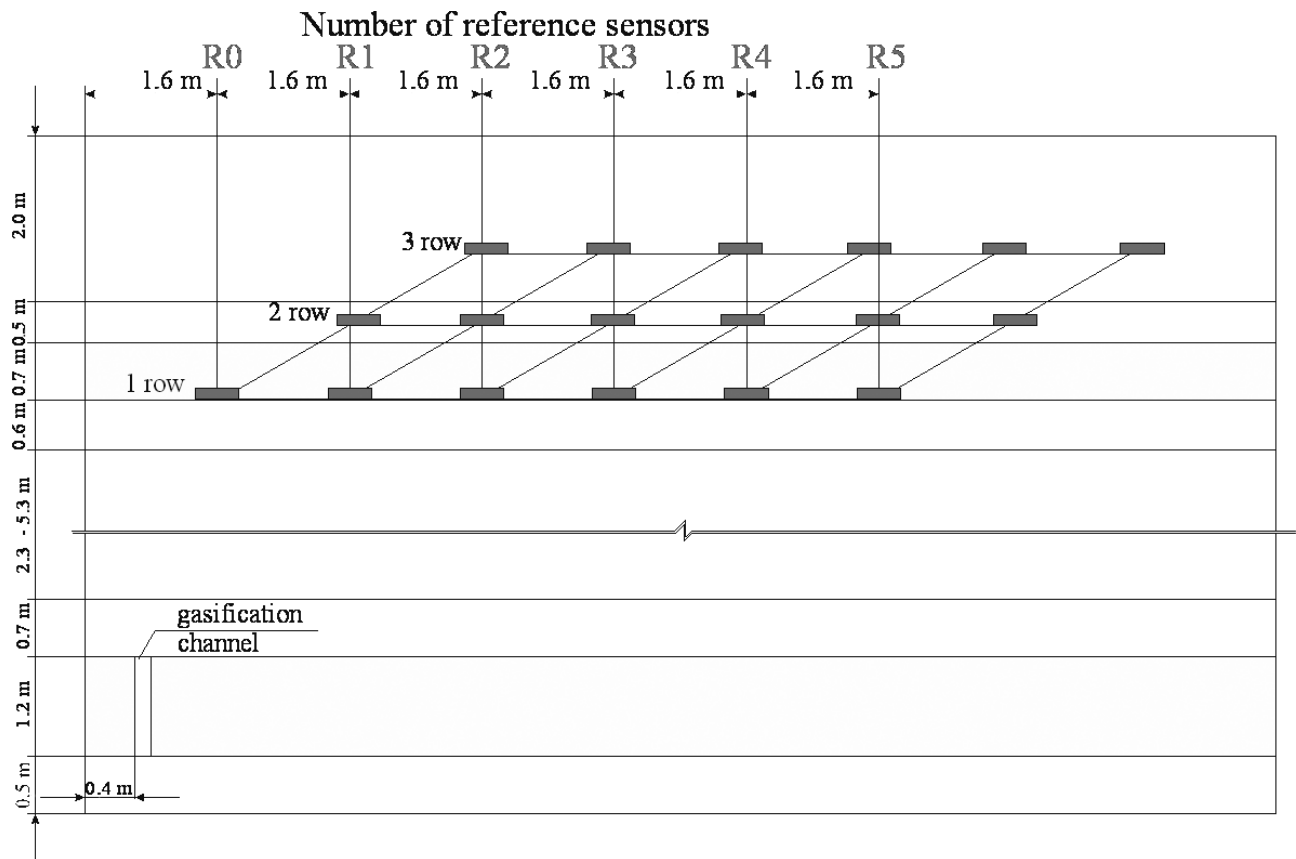


Fig. 2. Scheme of reference sensors installation:

1 – the bottom of lower coal seam 2; 3–5 – interstratified rocks; 6 – upper coal seam; 7, 8 – rocks of the roof of upper coal seam 6; 9 – reaction (gasification) channel; 10 – reference sensors

As a result of studies, dependences of rock layers subsidence with lithological differences were defined. These dependences were set using a measuring ruler and a system of optical sensors. With the transition to the full-scale gasification process, through the established scale factors, the distance between the reference sensors (R1–R6) equals 1.6 m. The distance to the first row of reference sensors along the length of the column gasification (R1) of man-made reaction channel (9) is equal to 1.2 m. During the research, we conducted gasification of the lower coal seam (2).

Fixation of subsidence that corresponds to natural conditions was held daily. Total observation time was 6 days. Dependencies of bottom subsidence at the top coal seam during variable thickness of interstratal rocks (3.6 and 6.6 m) and thickness of lower coal seam 1.2 m on the duration of the gasification process is shown in Fig. 3.

In this figure, horizontal line 7 shows a critical border of subsidence, below which the formation of through vertical cracks starts. The maximum subsidence of reference sensors with a thickness of interspatial rocks $h = 3.6$ m was observed on day 5 of gasification and made 0.46 m, $h = 5.4$ –0.28 m, $h = 6.6$ –0.21 m.

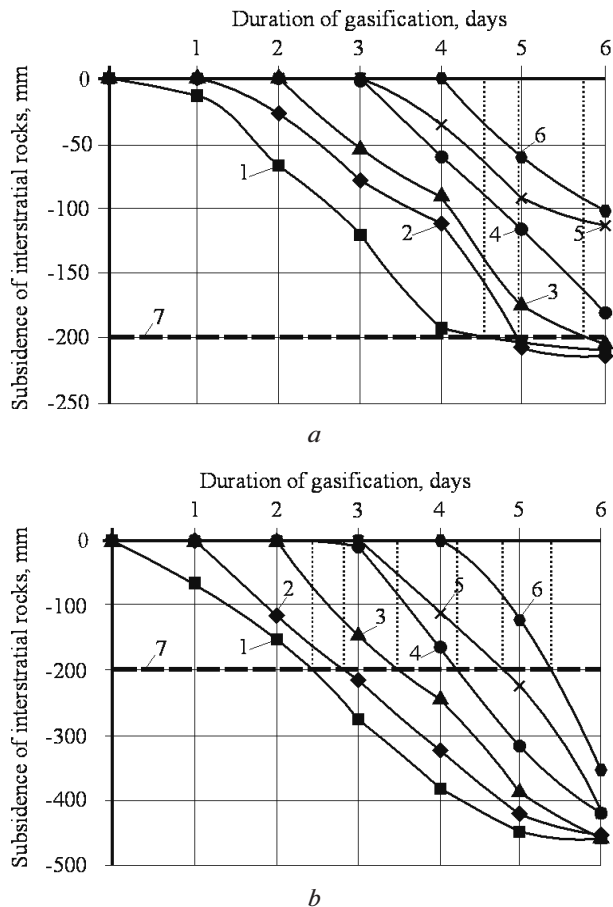


Fig. 3. Diagram of interstratal rocks subsidence with a thickness of 3.6 m (a) and 6.6 m (b) depending on the gasification duration:

1–6 – subsidence values of reference sensors; 7 – a critical border of subsidence, below which the formation of through vertical cracks occurs

The main feature during underground coal gasification is the presence of high temperatures in the combustion face > 1000 °C [9]. The values of temperature decrease with distance from the combustion face. At a distance of coal seam roof of 3.6 meters above combustion face, the maximum temperature is in the range of 200–300 °C, while in the rocks of the bottom at the same distance it is 53–82 °C. The degree of the roof rocks exposure to heat depends on blast pressure in the underground gasifier. With the pressure increasing from 0.15 to 0.35 MPa, the heat of roof rocks increases by 70–100 °C. This change in temperature is due to convection penetration of combustible gases mixture through artificial gas channels (vertical through cracks). This problem can be solved by using stoichiometric conditions for the dual fuel system [10].

The results of the research (Fig. 3) prove that provided the advance of the lower combustion face over the upper one, it should be before the area of formation of vertical through cracks. Based on the results the of bottom subsidence of the upper coal seam and the rate of combustion face advance, the dependence of the possible delay of upper combustion face on the lower one with variable interspatial rocks thickness was obtained (Fig. 4).

From the studies, it is clear that the maximum allowable distance of upper combustion face delay from the lower combustion face with the thickness of lower coal seam of 1.2 m changes under linear dependence and can be written as

$$L_{ek} = 1.55h - 2.93,$$

where L_{ek} is the value of the combustion face delay of the upper coal seam with compared to the lower coal seam; h is the thickness of interstratal rocks.

In the area of SC “Lvivuhillia” mines, the thickness of coal seams varies from 0.6 to 1.2 m, and the thickness of interstratal rocks reaches up to 28 meters. Therefore, for these parameters, given the technical and economic characteristics of experimental studies, the coefficient of contiguity of coal seams was analyzed using available information packets that form the basis of computer modeling.

During coal seams gasification, the space of gasification area increases, resulting in destruction of above

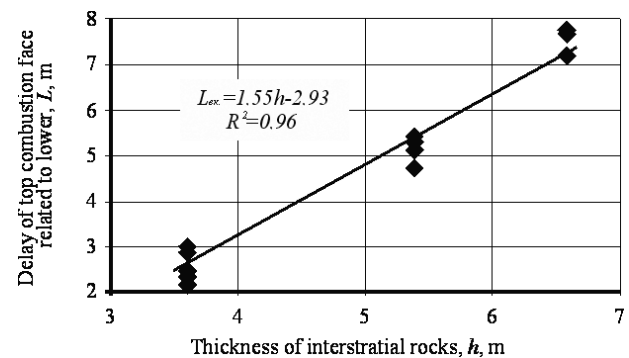


Fig. 4. Change dependency of the upper combustion face delay on the lower one under variable thickness of interstratal rocks

rock mass. A mechanism of rock mass destruction allows observing its subsidence in concrete span point.

During simultaneous gasification of contiguous coal seams, an important element is to establish the value of the first combustion face delay regarding the second one. Determining this value excludes mutual and simultaneous influence of the underground gasifier on interstratial rocks. The underground gasifier can work both in ascending and in descending sequence. The delay in the lower coal seam does not virtually affect the top coal seam, whereas delay in the upper coal seam can create substantial effect on blowing flow.

During our research, 27 models were processed using methods of computer simulation. As a result, graphs of top coal seam subsidence at different values of interstratial rocks were obtained. Fig. 5 shows received graphs of subsidence of upper coal seam at interstratial rocks with a thickness of 3.6 m and a thickness of the lower coal seam of 1.2 m.

Based on Fig. 5, primary rock subsidence of the upper coal seam occurs at point 1Y (x = 39, y = 33), in 0.2 days of gasification process. In 1.6 days, at a value of goaf of 3.5 m, subsidence value made 200 mm. This makes it possible to predict the position of the upper combustion face, provided its delay from the lower seam. Construction of models was performed until the maximum lowering of the bottom of the lower seam did not exceed 200 mm.

At the first stage of modeling with the thickness of coal seam of 1.2 m, a step of interstratial rock thickness was 0.2 m. The acceleration of the process of this model was increased by up to 0.4 m. With the coal seam

thickness decreasing to 0.6 m, and interstratial rocks decreasing to 3.6 m, subsidence does not exceed 200 mm.

According to the results of computer simulation it was found that subsidence of rocks of the bottom of the upper coal seam > 200 mm was observed with the studied coal seam thickness of 1.2 m at the level of 6.9 m, 1.0–5.6 m, 0.8–4.4 m and at 0.6–3.4 m. This does not contradict the experimental research conducted in the laboratory. The discrepancy between the results of all kinds of research does not exceed 24 %.

Accordingly, we can get dependences in which we can assume when the coal seams are contiguous during underground gasification (Fig. 6). The main parameters that influence contiguity will be thickness of coal seams and interstratial rocks.

Consequently, during underground coal gasification coal seams can be related as contiguous under the inequality

$$\frac{h}{m} \leq 5.5 - 5.7,$$

where h is thickness of interstratial rocks, m; m is thickness of the lower coal seam, m.

The ratio $\frac{h}{m}$ reflects the contiguous coefficient of coal seams during underground coal gasification (k_c). For values of the coefficient $k_c \geq 5.5 - 5.7$, gasification of coal seams can be conducted in descending and ascending sequence.

Research conclusions and recommendations for further research in this area. The study of si-

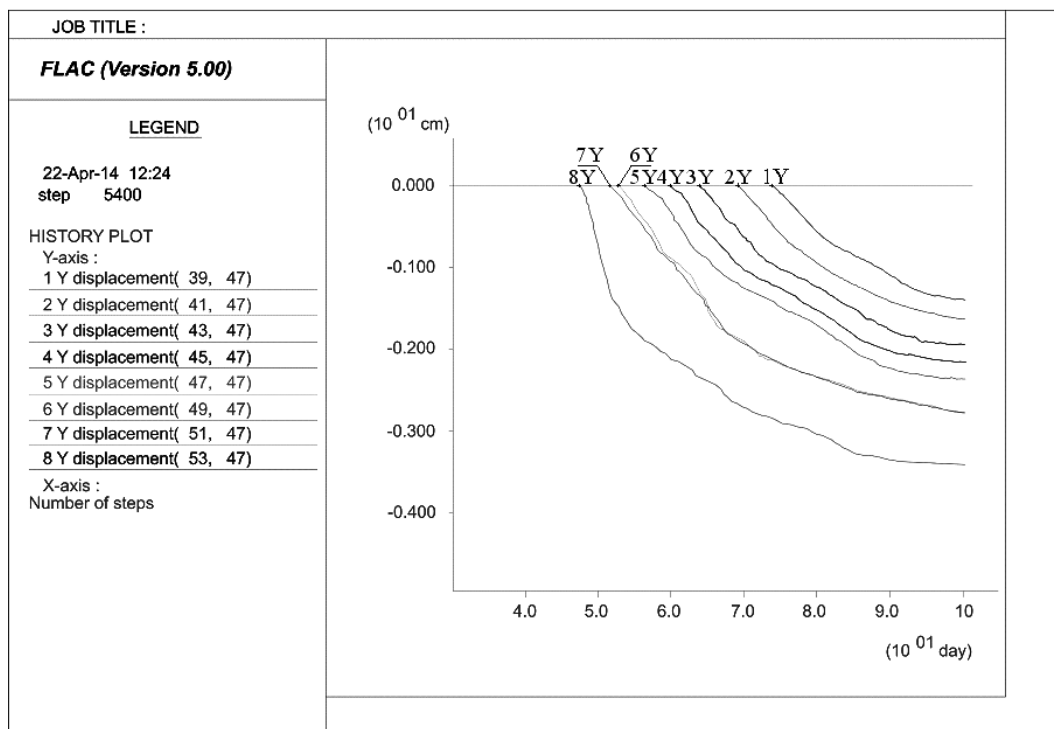


Fig. 5. Graphs of subsidence of the upper coal seam (Y, cm) depending on time (x, days) at interstratial rocks thickness of 3.6 m

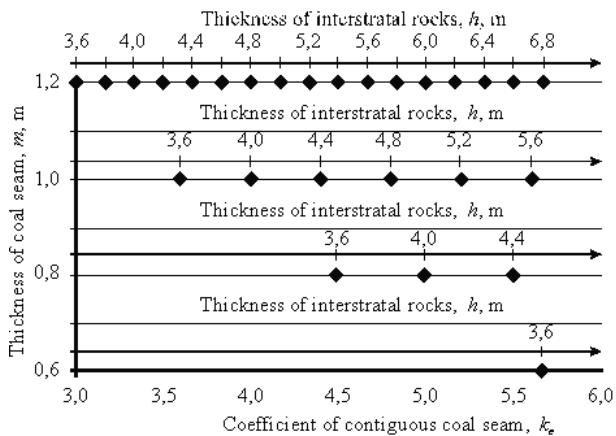


Fig. 6. Formation of data field for determination of contiguous coefficient of coal seams depending on interstratal rocks and coal seam thickness

multaneous multi-level gasifiers shows that existing approaches to determining the coefficient of contiguous coal seams during underground gasification require significant adjustments. Unfortunately, existing methods for determining the parameters used in the complex mechanized coal extraction are not suitable when applying the borehole underground coal gasification technology. Using experimental tests research and computer simulations, the authors, have attempted to establish the degree of influence of underground gasification gases in ascending and descending sequence of coal gasification. The basis of research was mining and geological conditions of mines SE "Lviv-vuhillia".

According to the results of these studies, dependence that reflects the condition of coal seam being contiguous was obtained. Considering this dependence makes it possible to ensure the stable coal gasification process and avoid destabilization zones of thermochemical reactions in an underground gasifier.

References / Список літератури

1. Lozynskiy, V.H., Dychkovskiy, R.O., Falshtynskiy, V.S. and Saik, P.B., 2015. Revisiting possibility to cross disjunctive geological faults by underground gasifier, *Naukovyi Visnyk Natsionalnoho Hirnychoho Universytetu*, No. 4, pp. 22–28.
2. Falshtynskyy, V., 2012. New method for justification of the technological parameters of coal gasification in the test setting. In: *Geomechanical Processes During Underground Mining – Proceedings of the School of Underground Mining*. CRC Press/Balkema, The Netherlands, pp. 201–208.
3. Trizno, S.K. and Lazarenko, S.N., 2007. *Sposob podzemnoy gazifikatsii svity ugol'nykh plastov*. Pat. 2307244 RF MPK E21V43/295.
Патент № 2307244 РФ МПК E21V43/295. Способ подземной газификации свиты угольных пластов / С. К. Тризно, С. Н. Лазаренко и др. – Оpubл. 27.09.2007.
4. Trizno, S.K., Lazarenko, S.N. and Fedorin, V.A., 2009. *Sposob podzemnoy gazifikatsii svity krutykh i*

krutonaklonnykh ugol'nykh plastov. Pat. 2347070 RF MPK E21V 43/295.

Патент № 2347070 РФ МПК E21V 43/295. Способ подземной газификации свиты крутых и крутонаклонных угольных пластов / С. К. Тризно, С. Н. Лазаренко, В. А. Федорин. – Оpubл. 20.02.2009.

5. Falshtynskiy, V.S., Dychkovskiy, R.O. and Tabachenko, M.M., 2010. *Sposib pidzemnoyi hazyfikatsiyi potuzhnykh plastiv tverdoho palyva*. Ukraine. Pat. 50753 MPK E21V 43/00.

Патент № 50753 Україна, МПК E21V 43/00. Спосіб підземної газифікації потужних пластів твердого палива / В. С. Фальштинський, Р. О. Дичковський, М. М. Табаченко та ін. – Оpubл. 25.06.2010.

6. Sakhno, S., Kobylanskiy, B. and Sakhno, I., 2016. Destruction of rocks by the non-explosive depleting compounds during mining. *Mining of Mineral Deposits*, No. 10(1), pp. 25–30.

7. Rakishev, B., Seituly, K. and Kovrov, O., 2014. Physical modeling geomechanical stability of open-cast slopes and internal overburden dumps. In: *Legislation, Technology and Practice of Mine Land Reclamation*, pp. 583–588.

8. Savostianov, O.V., 2016. *Metody prohnozu heomekhanichnykh protsesiv dlia vyboru tekhnolohichnykh parametriv vidpratsiuwannia polohykh plastiv* [Methods for forecasting geomechanical processes for selecting technological parameters for working flat seams]. Dnipropetrovsk: NМУ.

Савостьянов О.В. Методи прогнозу геомеханічних процесів для вибору технологічних параметрів відпрацювання пологих пластів: монографія / Савостьянов О.В. – Днепропетровск: НГУ, 2016. – 246 с.

9. Falshtynskiy, V., 2013. Justification of the gasification channel length in underground gas generator. In: *Annual Scientific-Technical Collection – Mining of Mineral Deposits 2013*, CRC Press/Balkema, The Netherlands, pp. 125–132.

10. Postrzednik, S., Przybyla, G. and Zmudka, Z., 2015. Main conditions and effectiveness of gas fuel use for powering of dual fuel IC self-ignition engine. *Transport Problems*, Vol. 10, Iss. 3, pp. 99–111.

Мета. Обґрунтування коефіцієнта зближення вугільних пластів при застосуванні технології свердловинної підземної газифікації, виходячи зі встановлених залежностей опускань міжпластових порід від тривалості газифікації.

Методика. Стеновими експериментальними дослідженнями та методами комп'ютерного моделювання встановлені залежності опускання міжпластових порід при змінній їх потужності та потужності вугільних пластів від тривалості процесу газифікації. Для відображення геомеханічної ситуації гірського масиву навколо підземного газогенератора застосовано пакет ліцензійної прикладної програми Flac 5.00. Для обробки даних та побудови узагальнюючих залежностей викорис-

тано метод множинної регресії із застосуванням загальноновизнаної системи обробки даних Excel-2013.

Результати. Отримана нерівність, що дає можливість встановлювати коефіцієнт зближення вугільних пластів при застосуванні технології підземної газифікації. Встановлення даного коефіцієнта дозволяє проводити оцінку гірничо-геологічних умов залягання вугільних пластів з подальшим раціональним порядком їх газифікації. При значеннях коефіцієнта зближення більших 5,5–5,7 газифікацію вугільних пластів можна проводити як у висхідному, так і низхідному порядках. При цьому не потрібно витримувати допустиму відстань між вогневими вибоями, що працюють на зближених пластах.

Наукова новизна. Запропоновано математичний механізм для визначення коефіцієнта зближення вугільних пластів, ефективність якого підтверджена комп'ютерним моделюванням стану гірського масиву, що вміщує підземний газогенератор, та дослідженнями на спеціальній стендовій установці.

Практична значимість. Встановлено залежності опускань міжпластових порід від тривалості газифікації, що характеризують утворення газопровідних каналів у породах міжпласта для забезпечення технологічності процесу. Отримана умова зближення вугільних пластів дозволяє проводити раціональний вибір порядку відпрацювання запасів вугілля.

Ключові слова: *стендові дослідження, підземна газифікація, зближені пласти, коефіцієнт зближення*

Цель. Обоснование коэффициента сближения угольных пластов при применении технологии скважинной подземной газификации, исходя из установленных зависимостей опускания межпластовых пород от продолжительности газификации.

Методика. Стеновыми экспериментальными исследованиями и методами компьютерного моделирования установлены зависимости опускания межпластовых пород при изменении их мощ-

ности и мощности угольных пластов от продолжительности процесса газификации. Для отображения геомеханической ситуации горного массива вокруг подземного газогенератора применен пакет лицензионного приложения Flac 5.00. Для обработки данных и построения обобщающих зависимостей использован метод множественной регрессии с применением общепризнанной системы обработки данных Excel-2013.

Результаты. Полученное неравенство дает возможность устанавливать коэффициент сближения угольных пластов при применении технологии подземной газификации. Определение данного коэффициента позволяет проводить оценку горно-геологических условий залегания угольных пластов с последующим рациональным порядком их газификации. При значениях коэффициента сближения больше 5,5–5,7 газификацию угольных пластов можно проводить как в восходящем, так и нисходящем порядках. При этом не нужно выдерживать допустимое расстояние между огневыми забоями, которые работают на сближенных пластах.

Научная новизна. Предложен математический механизм для определения коэффициента сближения угольных пластов, эффективность которого подтверждена компьютерным моделированием состояния горного массива, вмещающего подземный газогенератор, и исследованиями на специальной стендовой установке.

Практическая значимость. Установлены зависимости опускания межпластовых пород от продолжительности газификации, характеризующие образования газопроводных каналов в породах междупластья для обеспечения технологичности процесса. Полученное условие сближения угольных пластов позволяет проводить рациональный выбор порядка отработки запасов угля.

Ключевые слова: *стендовые исследования, подземная газификация, сближенные пласти, коэффициент сближения*

Рекомендовано до публікації докт. техн. наук І. А. Ковалевською. Дата надходження рукопису 15.01.16.

ФІЗИКА ТВЕРДОГО ТІЛА, ЗБАГАЧЕННЯ КОРИСНИХ КОПАЛИН

A. Chaib,
M. Bounouala, Dr. Sc. (Tech.),
S. Bouabdallah, Dr. Sc. (Tech.),
A. Benselhoub, PhD

Annaba University, Annaba-Algeria, e-mail: achaib_as@yahoo.fr

NEW CONDITION FOR SEPARATION OF ORTHOCLASE FROM QUARTZ BY FLOTATION; CASE OF AIN BARBAR QUARRY (ALGERIA)

А. Шаїб,
М. Бунуала, д-р техн. наук,
С. Буабделла, д-р техн. наук,
А. Бенселгуб, PhD

Університет Аннаба, м. Аннаба, Алжир, e-mail: achaib_as@yahoo.fr

НОВІ УМОВИ СЕПАРАЦІЇ ОРТОКЛАЗУ ІЗ КВАРЦЮ МЕТОДОМ ФЛОТАЦІЇ НА ПРИКЛАДІ КАР'ЄРУ АЙН-БАРБАР (АЛЖИР)

Purpose. The preliminary study of Ain Barbar (Algeria) feldspar quality improvement is aimed to obtain high purity of feldspar (orthoclase) without iron oxides and quartz to meet the standards of glass manufacturing and ceramics.

Methodology. The feldspar of Ain Barbar quarry was crushed and sieved. The mineral was characterized by X ray diffraction and chemical analyses with X ray fluorescence. The material ($-250 +45 \mu\text{m}$) was washed followed by physico-chemical concentration (magnetic separation and flotation) by new condition. The study of the main parameters of magnetic separation and flotation process in different ranges was realized.

Findings. Washing and high intensity magnetic separation (12 Ampere) afford to reduce the iron-bearing impurities up to 0.09 % Fe_2O_3 , and the flotation is the best way for the separation of K-feldspar from quartz by appropriate reagents for this purpose (HBr, amine).

This method for beneficiation of feldspar ore (orthoclase) assaying on average, 15.16 % Al_2O_3 , 70.40 % SiO_2 , 0.03 % total iron oxides, 13.51 % K_2O and 0.14 % Na_2O , provided several types of products which can be used in the ceramic and glass making.

The most striking result in this experimental study is the depressive effect of HBr on quartz and activation of the orthoclase, HBr addition controls amine adsorption on k-feldspar through adsorption of Br^- ions onto mineral surfaces.

The use of HBr in flotation was found to increase the K-feldspar (orthoclase) grade in the concentrate. This study clearly demonstrates an effective separation of feldspar (orthoclase) from quartz.

Originality. The originality of this study consists in the use of hydrobromic acid as a new reagent to activate orthoclase and depress the quartz in the flotation process, with a comparison of the obtained results with the use of hydrofluoric acid or hydrobromic acid in orthoclase flotation, showing that the use of hydrobromic acid (800 g/t of HBr) gives a concentration of 90 % orthoclase and 8 % quartz with 13.51 % K_2O , while in feed it is 56 % orthoclase and 39 % quartz with a K_2O content of 7.78 %. On the other hand, the use of hydrofluoric acid (800 g/t HF) provides a concentrate of 80 % orthoclase and 18 % quartz, with a grade of 9.52 % of K_2O in the same conditions.

Practical value. The results obtained with magnetic separation followed by the flotation method can be suitable specifications for ceramics and glass. Besides, the use of hydrobromic acid is economical and less threatening for the environment in comparison with the use of hydrofluoric acid.

Keywords: *Ain Barbar, K-feldspar, magnetic separation, flotation, glass, ceramics*

Introduction. Feldspar is extensively used in various industrial applications such as glass and ceramics due to its alumina and alkali contents. The mineralogical composition of most feldspar minerals can be expressed in terms of the ternary system: orthoclase (KAlSi_3O_8), albite ($\text{NaAlSi}_3\text{O}_8$) and anorthite ($\text{CaAl}_2\text{Si}_2\text{O}_8$). Chemically, the feldspars are silicates of aluminum, containing sodium, potassium, iron, calcium, barium or combinations of these elements [1].

In industrial applications, the removal of colored impurities and quartz affects the quality, but the ratio of $\text{K}_2\text{O}/\text{Na}_2\text{O}$ is more crucial for identifying the quality of the raw material. A ratio of 2/1 to 3/1 is required for ceramic products whereas for high-voltage insulators, abrasives and electrodes production, the ratio must be higher [2].

Feldspar is used in the manufacture of glass as a source of alumina and as a partial replacement for soda ash. It is also used in the production of ceramics. About 65 % of all feldspathic material is used in the glass industry, 30 % in ceramics and 5 % in fillers and other applications. Chemically, the specifications of feldspar products for application in both ceramic and glass industries are nearly the same, total SiO_2 65–68 %, free quartz < 8 %, Al_2O_3 18–19 %, K_2O and Na_2O 11.5–13.5 % and Fe_2O_3 0.08–0.2 %. However, the glass industry requires coarser feldspar concentrates ($420 \times 74 \mu\text{m}$) in comparison with those necessary for ceramic production (98 % < $74 \mu\text{m}$). Cengiz Demir [1], conducted differential flotation of Na–K feldspars by fluoride activation in the presence of 15 g/l NaCl and found an increase in the potassium content of the feldspar concentrate.

The best flotation results with Voineasa pegmatites containing equal amount of Na- and K-feldspars using amine collectors were achieved when Na-feldspar was depressed with NaCl [3]. Bayraktar et al studied Demirci-Turkey pegmatite containing 4.8 % K_2O and 2.40 % Na_2O ; mica and oxides were first removed followed by separation of Na- and K-feldspars and quartz using NaCl, these researchers achieved a concentrate assaying 3.3 % Na_2O and 13.10 % K_2O .

Gülsoy et al [4] studied the similar feldspar ore from the same region assaying 5.94 % K_2O , 3.14 % Na_2O using magnetic separation followed by flotation with HF and NaCl; a concentrate assaying 3.1 % Na_2O and 12.65 % K_2O was achieved. Boulos, and al [5], confirmed that Na^+ ions depress Na-feldspar in the presence of amine (G-TAP) at natural pH. Similarly, Na ions were found to be effective in the selective separation of feldspar minerals in HF medium.

Gülgönül [6] determined that various feldspar minerals particularly K-feldspars display different surface and floatability properties due to the presence of nano impurities on the mineral surface.

Demir and Gülgönül used mixtures of pure minerals to explain the separation mechanism of feldspar minerals by microflotation experiments. However, it was also observed that pure minerals do not always imitate real ores such as pegmatite, granite, syenite etc.

The formation conditions of feldspar ores particularly the existence of perthitic structure in the ore or rock greatly influence the separation conditions.

Materials and Methods. Characterization studies. The fieldstone (feldspathic rhyolites) sample used in these experiments was obtained from AinBarbar quarry of Annaba (East of Algeria). The ore sample of 90 Kg was reduced to <1 mm in size by a jaw crushers, mixing, quartering and dividing to obtain representative samples of 500 g.

All the ore samples were ground in a ball mill to produce a sample below $500 \mu\text{m}$, the particles of approximately $250 \mu\text{m}$ were separated by particle size analysis using a sieving device of RETSCH type with a diameter of $200 \times 50 \text{ mm}$, the particle size measurement range is from 0.045 to 4 mm on a vibratory sieve for 20 min at an amplitude of 60, which amounted to about 80 % by weight of particles in the size range from 250 to $45 \mu\text{m}$. The particle size analyses were carried out to determine the optimal mesh release.

The characterization was completed on representative samples by means of optic microscope, diffraction of ray X and X-ray fluorescence in order to better determine the aspect of the qualitative and quantitative characteristics of the feldspathic matter.

Experimental procedure. The separation of feldspar (orthoclase) from quartz is difficult because they reveal the similar surface properties. The froth flotation is one of the methods for feldspar separation from quartz. But all conditions of this method to get high selectivity are reported to be used in acidic medium with amine as collector and with addition of fluoride (hydrofluoric acid) as modifier; a shortcoming of this reagent system is that it is expensive and involves using environmental pollutants.

In our investigation, we applied physical and physico-chemical processes on samples for the reduction of iron oxides and quartz, the double sided linking by flotation with different collectors including petroleum sulfonate, diamine solution with HF and HBr as modifiers in order to obtain a quality product for ceramists. During this study, the examined parameters were effects of current intensity of the coil, pH, and concentration of different reagents used.

The material of 500 g of the size of fraction $250/45 \mu\text{m}$ was subjected to magnetic separation tests aimed to remove the ferriferous inclusions contained in the K-feldspar (orthoclase) material. The range of the current variation in the magnetic separator that was used is from 5 to 12 Amperes, and drum rotation rotor is 60 rpm.

The magnetic separation performance highly depends on the physical particle properties to be separated (and size of the magnetic nature), the quality of the applied magnetic field, and the difference in magnetic susceptibility between the separated particles. The magnetic separator of high intensity laboratory work dry is composed of three coils surrounding the electromagnet provided with a splined rotor rotating between the pole pieces of a magnetic circuit. The magnetic poles or pole pieces, between which

the rotor rotates, are subjected to a magnetic induction [7].

The main magnetic separator parameters are the magnetic flux density which varies from 1.2 to 2 Tesla. The next step is enrichment by flotation concentrates obtained by magnetic separation.

The first condition to obtain good flotation is to achieve a grinding of the maximum releasing minerals from each other; and a suitable release of the particles to float, in our case the mesh of 250/45 μm is estimated at the release. In some cases, it is necessary to deslime pulp before the float and to avoid the recovery of the mineral particle surfaces. The pulp containing 20 % solids mixture with water, is stirred in a conditioning tank to ensure the homogeneity of the medium. The first time round, dispersants AP 801 and AP 840 are added to avoid any kind of agglomeration before floating the concentrate (feldspar), then the hydrofluoric acid or hydrobromic acid is added to modify the surface feldspar particles during conditioning to be driven to the surface by the air bubbles; this process is repeated every time before flotation concentrates for 5 min. After that, a diamine or petroleum sulfonate agent is added to the collector.

The flotation operation is repeated for each collector and modifier. After flotation, washing, drying and filtering follows, (Table 1). The tests were performed in laboratory of valorization of mining resources and environment, Mining Department, Badji Mokhtar University, Annaba.

Results and Discussion. Chemical analysis and X-ray Diffraction analysis. The results of chemical and mineralogical analyses are shown in Table 2 and Fig. 1, 2 respectively, these results demonstrate that the ore contains quartz and orthoclase with minor amounts of albite, anorthite, and small quantities of clay minerals. The sample has K_2O and Na_2O contents of 7.78 and 0.33 % respectively.

The XRD spectrum and tme section confirm that orthoclase is the principal mineral and other minerals present are very minor to trace their amount.

Particle size analyses. The collected results from chemical analysis of size fractions reveal that the totals of SiO_2 contents vary from 70.89 to 75.61 %. As for the ferriferous inclusions, their contents of Fe_2O_3 are 0.18 to 1.06 % showing an excess of iron in the raw material which does not meet the required standard ($\text{Fe}_2\text{O}_3 < 0.03$ % and quartz < 8 %). Besides, we noted that the iron oxide content increases as the particles diminish. The contents of K_2O and Na_2O and SiO_2 are homogeneous almost in all size fractions. The results of the chemical analysis of size fractions are given in Table 3.

Evaluation of efficiency of iron removal. The efficiency of iron removal can be calculated by the following equation

$$E(\%) = \left[1 - \left(\frac{\text{Fe}_2\text{O}_3 \text{ content in concentrate}}{\text{Fe}_2\text{O}_3 \text{ content in feed}} \right) \right] \cdot 100.$$

Table 4 shows the effect of the current intensity on the effectiveness of iron oxide removal from feldspar,

Table 1

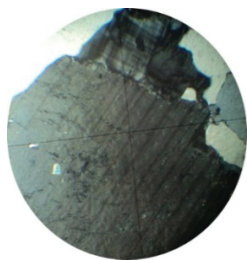
Conditions used in Denver flotation experiments

Parameters	Conditions
Temperature of medium	20–25 °C
Particle size	–250 +45 μm
Impeller speed	1200 rpm
Solids by wt. %	40
Collector type	Diamine, Petroleum sulfonate
Amount of collector	150 g/t
Frother type	Pine oil
Conditioning time for collector	5 min
pH	Acidic pH (1.5–4.0) HF, HBr
Conditioning time for HF	(300–1200 gr/t) H_2SO_4 as much as needed
Conditioning time for HBr	(300–1200 gr/t) H_2SO_4 as much as needed
Conditioning time for frother	3 min
Flotation time	5 min

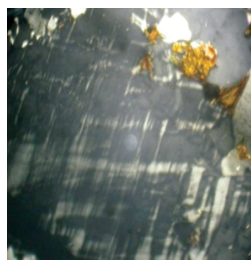
Table 2

Chemical composition of the fieldstone sample

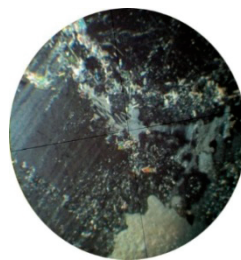
Oxides	SiO_2	Al_2O_3	K_2O	Na_2O	Fe_2O_3	CaO	P_2O_5	MgO	TiO_2	PbO	ZnO	MnO	PAF
Contents (%)	73.26	14.71	7.78	0.33	0.79	0.59	0.31	0.05	0.02	0.02	0.03	0.01	1.04



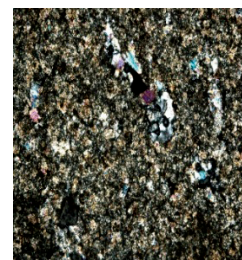
Plagioclase grains in contact with the quartz and orthoclase, +120



Alteration of plagioclase and orthoclase by sericite (mica), +120



Biotite aggregates on the contour of the grain of orthoclase, +120



Pate with feldspar porphyritic quartz and feldspar and mica inclusions, +60

Fig. 1. Tine sections

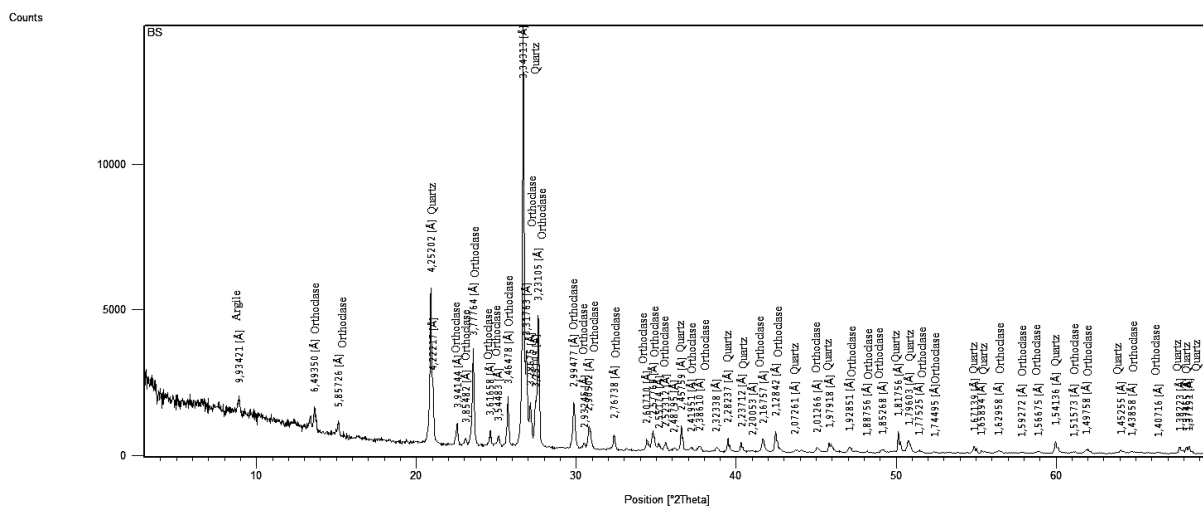


Fig. 2. XRD pattern of investigated fieldstone sample

Table 3

Results of chemical analysis of size fractions of *k*-feldspar sample

Fraction, mm	Yield (%)	SiO ₂	Al ₂ O ₃	K ₂ O	Na ₂ O	Fe ₂ O ₃	CaO	MgO	P ₂ O ₅	TiO ₂	MnO	PAF
+4	26.02	73.25	15.39	8.45	0.30	0.18	0.52	0.01	0.31	0.01	0.02	0.82
-4 +2	30.54	75.61	13.18	8.81	0.33	0.20	0.30	0.02	0.29	0.00	0.02	0.61
-2 +1	13.00	75.60	12.31	8.48	0.30	0.55	0.60	0.02	0.31	0.02	0.01	1.27
-1 +0.5	07.11	70.89	16.76	8.56	0.34	0.65	0.21	0.03	0.30	0.02	0.01	0.89
-0.5 +0.25	04.04	73.46	13.46	7.98	0.28	1.06	0.87	0.01	0.32	0.00	0.01	0.98
-0.25 + 0.125	03.52	73.56	13.62	8.20	0.36	0.96	0.89	0.02	0.28	0.00	0.02	1.24
-0.125 +0.063	04.03	72.40	15.75	7.60	0.35	0.76	0.59	0.01	0.34	0.07	0.01	1.04
-0.063 +0.045	01.82	74.61	14.52	7.37	0.27	0.57	0.05	0.01	0.35	0.05	0.01	1.04
-0.045	09.92	74.12	14.46	8.50	0.32	0.70	0.20	0.01	0.33	0.03	0.01	1.14

according to obtained results by high intensity magnetic separation (MSHI), we found a significant improvement in feldspar content and a remarkable decrease of impurities such as hematite was obtained in the range between 10 and 12 Amperes. With the increase in the intensity of the electric current at 12 Am-

peres, it is noted that the iron impurity content decreases from 0.32 to 0.09 %. The optimum efficiency of removal of iron oxide was obtained in the range of 71.81 %.

Effect of the pH on separation of *k*-feldspar (orthoclase). Separation of feldspar from quartz can be

Table 4

Reduction of iron content in size fractions of the 250/45 μm material, at different intensities of magnetic field

Intensity (A)	Fe ₂ O ₃ (%)	Fe ₂ O ₃ (%)	E (%)
5	0.32	0.28	06.6
7		0.24	25.0
9		0.19	40.7
10		0.11	65.7
12		0.09	71.81

achieved with cationic collectors in acid circuit at a pH value in the vicinity of 1.5 to 2.5. Other works, found that at the pH range of 2.5 to 3, a maximum selectivity could be reached [8].

Fig. 3 and 4 show a maximum selectivity at pH of 1.8 to 2 in both cases, when using the HF or HBr modifier and diamine as a collector, at concentration of 150 g/t. The contents and recovery of K₂O achieve a

maximum, when we use Diamine collectors and hydrobromic acid (HBr) as an activator of orthoclase and quartz depressor (12.65 %; 85 %) respectively.

The results obtained are justified by the point of zero charge of feldspar (1.5 to 2) and quartz varying from 2 to 3.7; at pH 1.5 to 2.5 above the value of the point of zero charge the surface orthoclase takes a positive sign whereas the quartz has a negative sign which allows creating new sites (a better surface activation of orthoclase) to increase the adsorption of collectors (diamine).

Considerable contents of SiO₂, more than 90.61 %, in tailing signify a better depress of the quartz when using HBr with 150 g/t Diamine at pH = 1.8. The use of HBr increases the quartz depression (increases the speed of sedimentation), compared with the use of HF because the molecular weight of HBr is greater than HF.

From Fig. 5 and 6 it is noted that the use of petroleum sulfonate as a collector in both cases (HF, HBr) reduces the recovery of K₂O, and the content of K₂O is almost constant when the pH ≥ 3, which means that the adsorption of the collector by the quartz surface is started (the start of flotation of quartz in this pH).

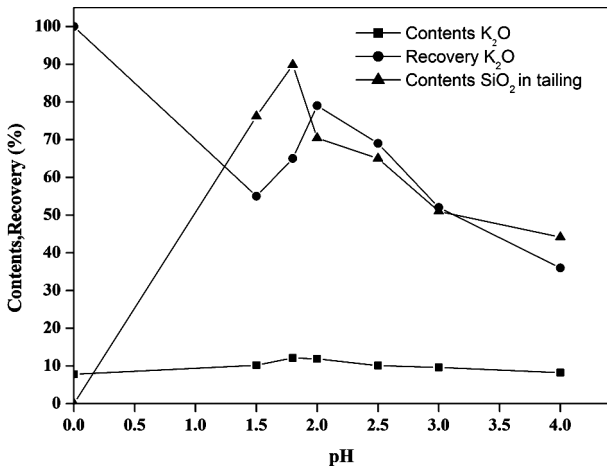


Fig. 3. Effect of pH on orthoclase separation with HF and Diamine (150 g/t)

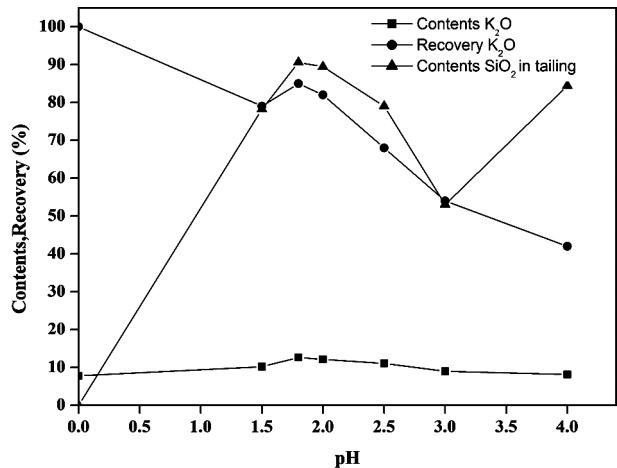


Fig. 4. Effect of pH on orthoclase separation with HBr and (150 g/t Diamine)

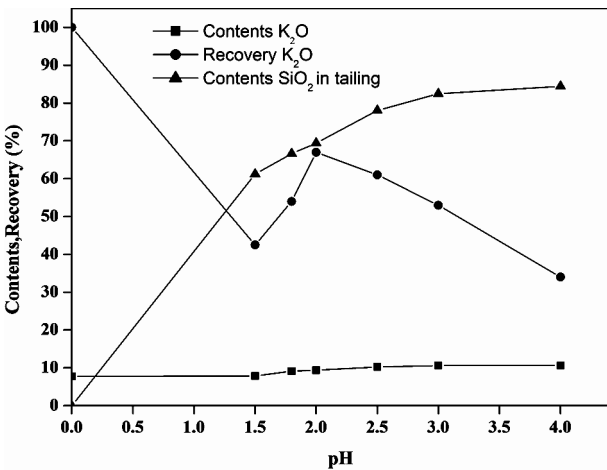


Fig. 5. Effect of pH on orthoclase separation with HF and petroleum sulfonate (150 g/t)

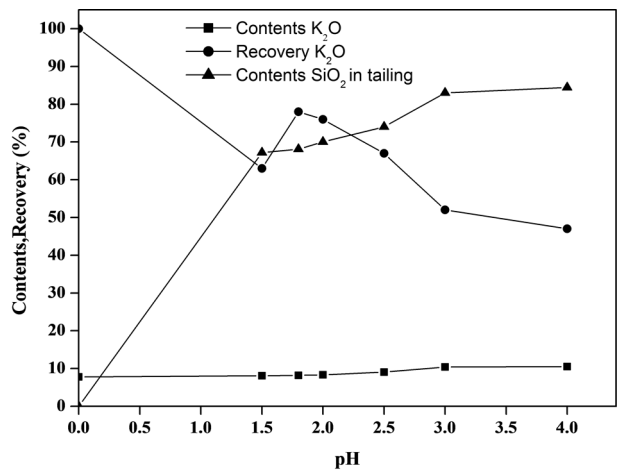


Fig. 6. Effect of pH on orthoclase separation with HBr and (150 g/t petroleum sulfonate)

Effect of the concentrate of hydrofluoric or hydrobromic acids on separation of orthoclase with pH = 1.8 : 2 and 150 g/t diamine. Flotation studies in acidic medium were carried out in two main parts: the amount of F⁻ and Br⁻ ions required to activate and depress the minerals (orthoclase) was systematically optimized by using 150 g/t of Diamine or petroleum sulfonate. All experiments were performed at pH 1.8 to 2 adjusted with H₂SO₄. Tables 5, 6 illustrate that some selective separation between K-feldspar (orthoclase) and quartz occurs at substantial recoveries.

It is also found in the present research that conditions of k-feldspar formation greatly affect the optimum dosage of HF and HBr. For instance, altered feldspar requires higher HF and HBr dosage for activation. HF and HBr removes altered layers and cleans the surface to facilitate the formation of alumina fluoride complexes.

Pine oil was added to the flotation cell as a frother because HF addition increases the collector consumption and deteriorates the quality of bubble.

The addition of either HF or HBr as pH regulators and modifiers increases the selectivity of the feldspar flotation and the quartz depression as shown in Table 5. The best results were recorded when we used HBr as a modifier with diamine as a collector at a concentration of 800 and 150 g/t respectively.

The use of petroleum sulfonate as a collector and HF or HBr as a modifier does not give satisfying results.

Comparison of obtained results with hydrofluoric or hydrobromic acids in orthoclase flotation. Comparing the obtained results with the use of hydrofluoric acid or hydrobromic acid in orthoclase flotation, shows that the use of hydrobromic acid (800 g/t of HBr) gives a concentration of 90 % orthoclase and 8 % quartz with 13.51 % K₂O, while in feed it is 56 and 39 % quartz orthoclase with a K₂O content of 7.78. On the other hand, the use of hydrofluoric acid (800 g/t HF) provides a concentrate of 80 % orthoclase and 18 % quartz, with a grade of 9.52 % of K₂O in the same conditions. Then the use 1200 g/t of HF gives concentrates of 86 % orthoclase and 12 % quartz with 12.55 % of K₂O as shown in Table 6.

Separation of orthoclase by magnetic separation followed by flotation. The operation of orthoclase processing from Ain Barbar quarry is diagrammed in Fig. 7.

Conclusion. The beneficiation of feldspar ore (orthoclase) assaying on average 15.16 % Al₂O₃, 70.40 % SiO₂, 0.03 % total iron oxides, 13.51 % K₂O and 0.14 % Na₂O, provide several types of products which can be used in the ceramic production and glassmaking.

Attrition by washing operation is necessary for the enrichment of K-feldspar, as well as magnetic separation is designed to remove the iron-bearing impurities as presented in our study.

The separation of orthoclase from quartz by flotation with conditions used in this study is very impor-

Table 5

Effect of the concentration of hydrofluoric or hydrobromic acids on orthoclase separation with pH = 1.8 to 2 and 150 g/t Diamine

Concentration of HF (g/t)	feed	300	500	800	1000	1200
Grade of K ₂ O (%)	7.78	8.92	10.70	11.32	12.50	12.55
Recover of K ₂ O (%)	100	56.41	63.25	70.0	76.92	78.00
Concentration of HBr (g/t)	feed	300	500	800	1000	1200
Grade of K ₂ O (%)	7.78	8.95	9.81	13.51	13.34	12.33
Recover of K ₂ O (%)	100	46.50	62.35	90.40	86.00	85.04
Feed: Condition without any addition (concentration of HBr and HF = 0 g/t); HBr: Hydrobromic acid; HF: Hydrofluoric acid; K ₂ O: Potassium oxide in concentrate						

Table 6

Effect of the concentration of hydrofluoric or hydrobromic acids on orthoclase separation with pH = 1.8 to 2 and 150 g/t petroleum sulfonate

Concentration of HF (g/t)	feed	300	500	800	1000	1200
Grade of K ₂ O (%)	7.78	8.92	9.50	9.52	9.65	9.66
Recovery K ₂ O (%)	100	56.41	63.25	70.0	76.92	78.00
Concentration of HBr (g/t)	feed	300	500	800	1000	1200
Grade of K ₂ O (%)	7.78	8.42	8.54	9.22	9.24	9.30
Recovery K ₂ O (%)	100	46.50	62.35	78.40	84.00	85.04
Feed: Condition without any addition (concentration of HBr and HF = 0 g/t); HBr: Hydrobromic acid; HF: Hydrofluoric acid; K ₂ O: Potassium oxide in concentrate						

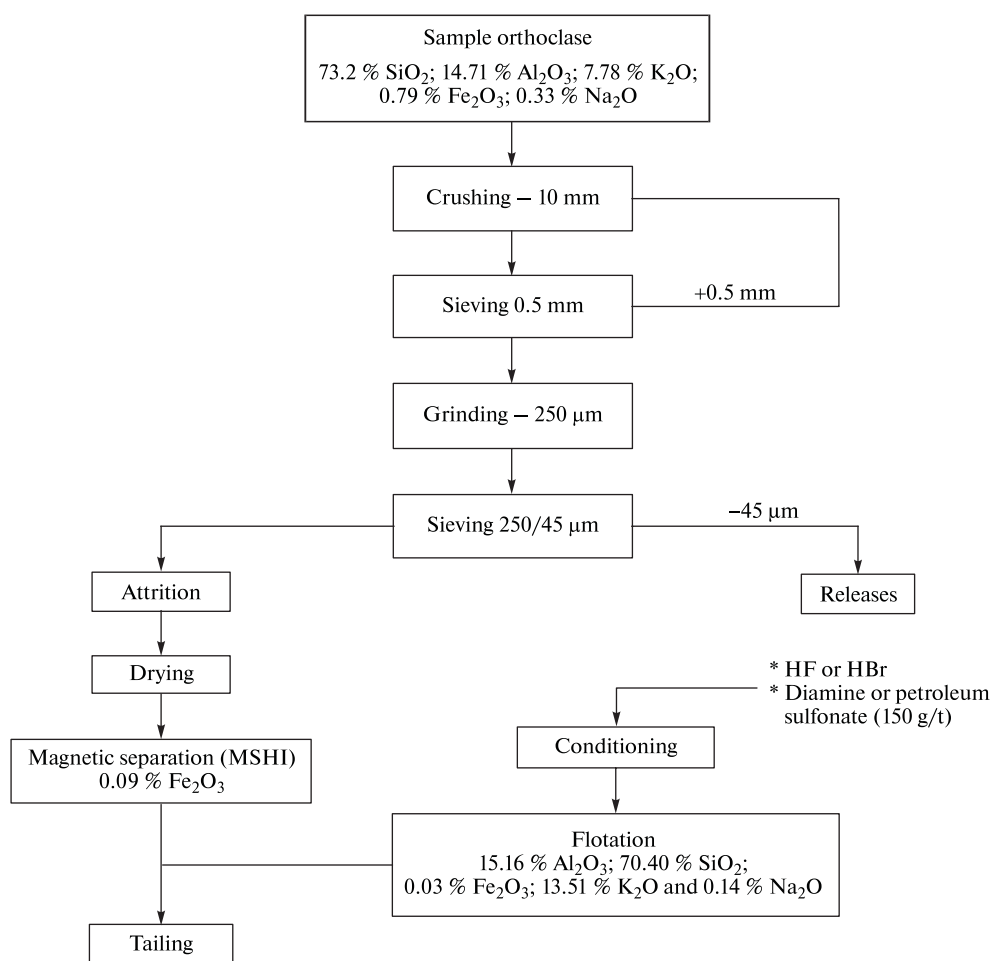


Fig. 7. Proposed flow sheet for orthoclase processing from Ain Barbar quarry

tant because it gives good results in terms of economic cost and protection of the environment (the use of HBr is economical and less hazardous than using HF).

Flotation of *K*-feldspar (orthoclase) with pH of 1.8; 2 by diamine as a collector and HBr as an activator at dosage of 800 g/t is better than the flotation by petroleum sulfonate and HF in the same conditions.

References/Список літератури

1. Demir, C., 2010. Selective separation of Na- and K-feldspar from weathered granites by flotation in HF medium. *Ceramics—Silikaty*, Vol. 54, No. 1, pp. 60–64.
2. Lewicka, E., 2010. Conditions of the feldspathic raw materials supply from domestic and foreign sources in Poland. *Gospodarka surowcami mineralnymi*, Vol. 26, pp. 5–19.
3. Heyes, G., Allan, G., Bruckard, W., and Sparrow, G., 2012. Review of flotation of feldspar. *Mineral Processing and Extractive Metallurgy (Trans IMM Section C)*, Vol. 121(2).
4. Gülsoy, O. Y., Can, N. M., and Bayraktar, I., 2005. Production of potassium feldspar concentrate from a low-grade pegmatitic ore in Turkey. *Mineral Processing and Extractive Metallurgy*, Vol. 114(2), pp. 80–86.
5. Boulos, T. R., Ibrahim, S. S., and Yehia, A., 2015. Differential Flotation of Some Egyptian Feldspars for Separation of Both Silica and Iron Oxides Contami-

nants. *Journal of Minerals and Materials Characterization and Engineering*, No. 3(06), pp. 435–443.

6. Demir, C., Bentli, I., Gülgönül, I., and Celik, M. S., 2003. Effects of bivalent salts on the flotation separation of Na-feldspar from K-feldspar. *Minerals Engineering*, Vol. 16(6), pp. 551–554.

7. Bouabdallah, S., Bounouala, M., Idres, A., and Chaib, A., 2015. Iron removal process for high purity silica production by leaching and magnetic separation technique. *Naukovyi Visnyk Natsionalnoho Hirnychoho Universytetu*, No. 5, pp. 47–52.

8. Soonthornwiphat, N., Saisinchai, S., and Parinayok, P., 2016. Recovery Slime Waste from Feldspar Flotation Plant at Attanee International Co. Ltd., Tak Province, Thailand. *Engineering Journal*, No. 20(4), pp. 69–78.

Мета. Попереднє вивчення покращення якості польового шпату родовища Айн-Барбар (Алжир) з метою отримання польового шпату (ортоклаза) високого ступеня чистоти, без оксидів заліза та кварцу, що відповідає стандартам виробництва скла та кераміки.

Методика. Польовий шпат з кар'єру Айн-Барбар був подрібнений та просяний. Отримана характеристика мінералу методами рентгеноструктурного аналізу (рентгенодифракційного аналізу), хімічного аналізу та рентгенофлуорес-

центного аналізу. Матеріал (-250 +45 мкм) піддавався промиванню з наступною фізико-хімічною концентрацією (магнітна сепарація та флотація) в нових умовах. Вивчені основні параметри процесів магнітної сепарації та флотації в різних діапазонах.

Результати. Промивання та високоінтенсивна магнітна сепарація (12 Ам) дозволяє зменшити долю залізовмісних домішок до 0,09 %, а флотація є кращим способом для відокремлення калієвого польового шпату від кварцу за допомогою відповідних реагентів (бромистий водень, амін).

У середньому, у пробі польового шпату, збагаченого цим методом, міститься 15,16 % Al_2O_3 , 70,40 % SiO_2 , 0,03 % оксидів заліза, 13,51 % K_2O та 0,14 % Na_2O , що дозволяє використовувати продукт у керамічній і скляній промисловості.

Найбільший інтерес представляє ефект, який бромистий водень здійснює на кварц (придушення) та ортоклаз (активація). Додавання бромистого водню дозволяє контролювати адсорбцію аміна калієвим польовим шпатом шляхом адсорбції іонів Вг до поверхні мінералу.

Було виявлено, що використання бромистого водню у процесі флотації збільшує вміст калієвого польового шпату (ортоклазу) в концентраті. Дослідження показало ефективність відокремлення польового шпату (ортоклазу) від кварцу.

Наукова новизна. Використання бромистоводневої кислоти в якості нового реагента для активації ортоклазу та пригнічення кварцу у процесі флотації. Проведене порівняння результатів дослідження фтористо-водневої та бромисто-водневої кислот у процесі флотації ортоклазу. При вмісті 56 % кварцу та 39 % ортоклазу, із вмістом K_2O у 7,78 % у вихідній сировині, застосування бромистоводневої кислоти (800 г/т.) дає на виході співвідношення 90 % ортоклазу, 8 % кварцу з 13,51 % K_2O . За аналогічних умов, використання фтористо-водневої кислоти (800 г/т.) забезпечує вміст 80 % ортоклазу та 18 % кварцу, з 9,52 % K_2O в концентраті.

Практична значимість. Продукт, отриманий за допомогою магнітної сепарації з наступною флотацією, відповідає специфікації для кераміки й скла. Крім того, використання бромистоводневої кислоти є економічно вигідним та менш шкідливим для навколишнього середовища у порівнянні з використанням фтористо-водневої кислоти.

Ключові слова: *Айн-Барбар, калієвий польовий шпат, магнітна сепарація, флотація, скло, кераміка*

Цель. Предварительное изучение улучшения качества полевого шпата месторождения Айн-Барбар (Алжир) с целью получения полевого шпата (ортоклаза) высокой степени чистоты, без окислов железа и кварца, соответствующего стандартам производства стекла и керамики.

Методика. Полевой шпат из карьера Айн-Барбар был измельчен и просеян. Получена характеристика минерала методами рентгеноструктурного анализа (рентгенодифракционного ана-

лиза), химического анализа и рентгенофлуоресцентного анализа. Материал (-250 +45 мкм) подвергался промывке с последующей физико-химической концентрацией (магнитная сепарація и флотація) в новых условиях. Изучены основные параметры процессов магнитной сепарації и флотації в различных диапазонах.

Результаты. Промывка и высокоинтенсивная магнитная сепарація (12 Ам) позволяет уменьшить долю железосодержащих примесей до 0,09 %, а флотація является лучшим способом для отделения калиевого полевого шпата от кварца с помощью соответствующих реагентов (бромистый водород, амин).

В среднем, в пробе полевого шпата, обогащенного этим методом, содержится 15,16 % Al_2O_3 , 70,40 % SiO_2 , 0,03 % оксидов железа, 13,51 % K_2O и 0,14 % Na_2O , что позволяет использовать продукт в керамической и стекольной промышленности.

Наибольший интерес представляет эффект, который бромистый водород оказывает на кварц (подавление) и ортоклаз (активация). Добавление бромистого водорода позволяет контролировать адсорбцию амина калиевым полевым шпатом путем адсорбции ионов Вг в поверхность минерала.

Было обнаружено, что использование бромистого водорода в процессе флотації увеличивает содержание калиевого полевого шпата (ортоклаза) в концентрате. Исследование показало эффективность отделения полевого шпата (ортоклаза) от кварца.

Научная новизна. Использование бромистоводородной кислоты в качестве нового реагента для активации ортоклаза и угнетения кварца в процессе флотації. Проведено сравнение результатов использования фтористо-водородной и бромисто-водородной кислот в процессе флотації ортоклаза. При содержании 56 % кварца и 39 % ортоклаза, с содержанием K_2O в 7,78 % в исходном сырье, применение бромисто-водородной кислоты (800 г/т.) дает на выходе соотношение 90 % ортоклаза, 8 % кварца с 13,51 % K_2O . При аналогичных условиях, использование фтористо-водородной кислоты (800 г/т.) обеспечивает содержание 80 % ортоклаза и 18 % кварца, с 9,52 % K_2O в концентрате.

Практическая значимость. Продукт, полученный с помощью магнитной сепарації с последующей флотацією, соответствует спецификации для керамики и стекла. Кроме того, использование бромисто-водородной кислоты является экономически выгодным и менее опасно для окружающей среды по сравнению с использованием фтористо-водородной кислоты.

Ключевые слова: *Айн-Барбар, калиевый полевой шпат, магнитная сепарація, флотація, стекло, керамика*

Рекомендовано до публікації докт. техн. наук О. Є. Хоменком Дата надходження рукопису 08.12.15.

UDC 621.7+539.63

V. V. Sobolev¹, Dr. Sc. (Tech.), Prof.,
O. S. Baskevych², Cand. Sc. (Phys.-Math.),
L. M. Shyman³, Corresponding Member of the
NAS of Ukraine, Dr. Sc. (Tech.),
S. M. Usherenko⁴, Dr. Sc. (Tech.), Prof.

1 – State Higher Educational Institution “National Mining University”, Dnipro, Ukraine, e-mail: valeriy Sobolev@rambler.ru

2 – State Higher Educational Institution “Ukrainian State University of Chemical Technology”, Dnipro, Ukraine, e-mail: abaskevich@ukr.net

3 – State Enterprise Research-Industrial Complex “Pavlograd Chemical Plant”, Pavlograd, Ukraine, e-mail: dirphz@pkhz.dp.ua

4 – Belarusian National Technical University, Minsk, Belarus, e-mail: usherenko@gmail.com

MECHANISM OF THICK METAL WALLS PENETRATION BY HIGH-SPEED MICROPARTICLES

В. В. Соболев¹, д-р техн. наук, проф.,
О. С. Баскевич², канд. фіз.-мат. наук,
Л. М. Шиман³, член-кор. НАН України, д-р
техн. наук,
С. М. Ушеренко⁴, д-р техн. наук, проф.

1 – Державний вищий навчальний заклад „Національний гірничий університет”, м. Дніпро, Україна, e-mail: valeriy Sobolev@rambler.ru

2 – Державний вищий навчальний заклад „Український державний хіміко-технологічний університет”, м. Дніпро, Україна, e-mail: abaskevich@ukr.net

3 – Державне підприємство „Науково-виробниче об'єднання „Павлоградський хімічний завод”, м. Павлоград, Україна, e-mail: dirphz@pkhz.dp.ua

4 – Білоруський національний технічний університет, м. Мінськ, Білорусь, e-mail: usherenko@gmail.com

ПРО МЕХАНІЗМ ПРОБИВАННЯ МЕТАЛЕВИХ ТОВСТИХ СТИНОК ВИСОКОШВИДКІСНИМИ МІКРОЧАСТИНКАМИ

Purpose. Analysis and estimation of physical parameters which create conditions for microparticles penetration into metal microstructure to abnormally big depth.

Methodology. Quantum mechanical three-site model has been used for studying the regularities of electron motion in the field of two Coulomb centres and numerical solution for the problem of the effect of external electrical charge on stability of the chemical bond. Solution was found for the equation of heat conductivity for estimating the temperature of microparticles heating under compression and acceleration by explosively driven accelerator. Stokes's law was used for estimating viscosity of hypothetical medium which can be penetrated by microparticle at a great speed and to a great depth. The research was done with the help of X-ray microanalysis, X-ray crystallography, micrographic investigation, mass-spectrometry and electronic spectroscopy.

Findings. Solution of the quantum mechanical model testifies that electric charges serve as catalysts responsible for the significant reduction of the energy barrier of chemical reactions. To ensure super deep penetration, it is necessary to achieve acceleration of a great number of microparticles in a special explosively driven accelerator. Heating, intensive stirring and friction result in electrification of the surface of the particles, which is known as triboelectric effect. The hypothesis about physical and chemical mechanism of particles penetration into metals resulting from high-speed impact has been put forward.

Originality. The research has established relationship between the sizes of microparticles accelerated by explosion and the density of electric charges on their surfaces, as well as the depth of their penetration into the metal barrier. By experimental research, it was proven that maximum depth of microparticles penetration is directly proportional to the maximum density of surface charges for the particles of the 50...80 μm size. It is assumed that particles penetration into metals to greater depths is conditioned by the reduction of the barrier material viscosity in the zone of particle-barrier contact due to quantum mechanical effects in the solid-state plasma.

Practical value. The value of the work includes creating a new generation of metal composites as well as new prospective technologies of reactive materials utilization.

Keywords: *microparticles, explosion, high-speed impact, crater, plasma, viscosity, penetration*

Introduction. Highly-energetic processing of materials together with other kinds of physical impacts is one of state-of-the-art scientific and technological researches aimed at creating innovative technologies and materials. Application of two or more simultaneous physical impacts can yield new fundamental knowledge and solutions to such cutting-edge tasks as creating innovative energy-saving technologies, developing new energy sources and materials with new physical and chemical properties.

The main idea of complex processing lies in physical impacts on preliminarily destabilized microstructure of materials. Such complex processing may produce the following results: synthesizing monocrystals of metastable diamond under impact compression of preliminarily destabilized graphite-metal system, transformation of graphite and zirconium into amorphous state under simultaneous impact of high pressure and exposure to radiation of heavy ions flows [1], abnormally deep penetration of microparticles into metals resulting in formation of chemical elements [2]. Standard experimental and processing methods were not reported to have yielded any of such results.

Solid bodies are distinguished by high degree of physical and chemical activity and increased scale of transformations in their microstructure even under weak energy impacts, but it is only the case when the initial state of the solid body is characterized by a great reserve of excessive inner energy. In view of this, it is especially interesting to study the effects discovered in metals after superdeep penetration of particles (S. Usherenko).

Analysis of recent research. Research into the collision of microparticles' flow and the metal barrier and into processes of their penetration to abnormally big depths is aimed at solving fundamental problems of substance stability and phase transformations. In the process of microparticles' penetration, we observed formation of nanomodified composite metal material which is in fact a massive metal matrix saturated with

parallel-oriented insertions of the new phase with the density $(300...1500) \times 10^6 \text{ m}^{-2}$ as shown in Fig. 1. Fig. 2 presents the remains of microparticles in the barrier microstructure. Such composite material with unique combination of physical, chemical and mechanical characteristics was used for manufacturing and testing the pilot batch of cutters used for destroying coal, pot-ash salt, cutting metals etc. (S. Usherenko).

Microparticles with the impact speed of 500...3000 m/s get into contact with a massive metal barrier and penetrate to more than 10^{-1} m deep. To compare: during detonation sputtering (approximately with the same velocities 300...1000 m/s), there appears a surface deposit [3], and the depth of microparticles' penetration into the barrier does not exceed 6×10^{-5} m, according to professor S. I. Buravova. Experiments established that conditions for microparticles' penetration to abnormally big depths arise due to a number of processes brought about by physical peculiarities of forming a bunch of microparticles in cumulative explosively driven accelerator. As a result of microparticles' hitting the surface of a massive metal barrier, there appear the so-called craters reaching 2×10^{-1} m deep. The traces of the penetrated particle have the form of a cavity with the length exceeding width by 10^5 times. During particles' penetration at the average impact pressure 0,2...1,0 GPa, the grain size of the metal barrier did not differ from the grain size of the same metal under shock-wave treatment at 50 GPa pressure. For both treatment methods, dislocation densities are nearly the same, which testifies to the same values of additional energy stored by microstructure of the given metal. Thus shock compression and additional high-volume alloying by elements of introduced microparticles dramatically changed the structure and chemical composition of initial metals which acquired principally new physical and chemical properties not to be achieved by any other methods of metal processing.

At present, researches into the studied problem are being conducted not only by the institutions represent-

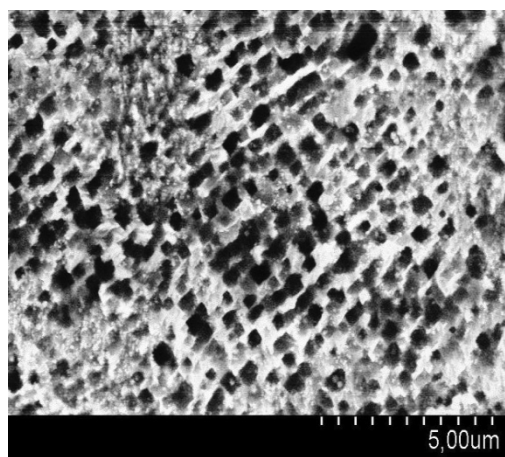


Fig. 1. Transverse section of the copper barrier near the surface. Observable craters of cubic beta-shape have been formed after the impact of silicon carbide particles

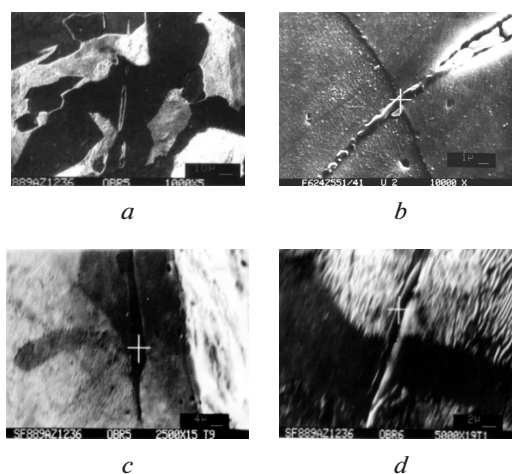


Fig. 2. Barrier microstructure of steel 45 with remains of penetrated microparticles:
a – $\times 1000$; b – $\times 10\ 000$; c – $\times 2500$; d – $\times 5000$

ed by the authors of this paper, but also by the Research Institute of Pulse Processes with Pilot Plant – SRI PIs OP (Belarus) and Samara University (Russia) [4].

In the field of fundamental sciences (synthesis of new materials), analogous results were obtained by the specialists of Scientific-research Electrodynamics Laboratory “Proton–21” (Ukraine) [5], Purdue University West Lafayette (USA); in the field of creating composite materials, new results were received by the team of National Research Center “Kurchatov Institute” (Russia), Polymate Ltd. – International Nanotechnology Research Center, Migdal Ha-Emek (Israel) and Kazan National Research Technological University (Russia) [6] etc. The above researches were related to small depths of particles’ penetration (Samara University) and small amounts of the processed material (“Proton–21”, “Kurchatov Institute”). Fundamentals for studying the mechanism of solid particles’ penetration into the solid body are presented in publications of scholars from SRI PIs OP, Belarus National Technical University, State Scientific Institution “The Institute of Metal Technology” (Belarus) and State Higher Educational Institution “National Mining University” (Ukraine).

Purpose of the research. Study of super deep penetration (SDP) of solid particles into metals is based upon a big amount of statistical experimental data. Various physical and mathematical models of this process developed by G. G. Chorny, S. S. Grigoryan, A. E. Rakhimov, G. P. Cherepanov, S. K. Andilevko, N. N. Sirot, A. A. Sivkov, L. G. Korshunov and others – do not provide credible arguments in favour of any SDP mechanism.

The present research aims at analysis and assessment of the physical parameters which create conditions for microparticles’ penetration into metal microstructure to abnormally big depths. We consider the depth of penetration abnormal if it constitutes $10^2 \dots 10^3$ of the initial diameter of a microparticle, while according to classical assumptions the penetration depth should not exceed 10^1 . The simplest estimation allows to conclude that the energy consumed by microparticles acceleration to the average velocity 1000 m/s is by several orders of magnitude smaller than the energy required for penetration of one percent of a microparticle to the depth of 10^3 diameters. Research into SDP phenomenon involves studying the previously unknown physical mechanism of a microparticle travel in the solid medium at distances that are sufficiently big in reference to the specific size of this particle.

Materials and equipment. Metal barriers were manufactured from copper, brass, aluminium, silicon-aluminium alloy AK-12, iron, structural steel P6M5. Blasting charges were made of ammonite № 6ЖВ. We also used powders containing microparticles (not bigger than 125 μm) of silicon carbide, lead, copper, and aluminium. The data was received from X-ray microanalysis (DS340 TESLA; Superprobe 733, JEOL), electronic spectroscopy (JAMP-10S, JEOL), mass spectrometry (MI-1201IG), secondary ion mass spec-

trometry (IMS-4f), X-ray crystallography, and transmission electron microscopy (JEOL JEM-2100). Surface charge density was measured by noncontact induction. Experimental data were processed on the basis of the theory of random errors. For the purpose of the research, we applied a quantum-mechanical model describing dynamics of chemical bond in the field of Coulomb centre (V. Sobolev et al.) and the technique for detecting ionizing radiation during microparticles’ penetration into the metal barrier (V. Ovchinnikov et al.).

Summary of the research. Microparticle travel in the solid medium at great distances cannot be presented in the form of conventional hydrodynamic models. The almost absent resistance to solid microparticles’ penetration can be related to abnormally low viscosity of the barrier metal. We assume that viscosity changes only within the zone limited by the contact surfaces of the barrier and microparticle. Hence it appears probable that the mechanism of plasma formation may be the reason for stepwise change of viscosity. Such inference is substantiated by the results of experimental research analysis which prove the feasibility of plasma hypothesis:

1. SPD is observed only in the case of acceleration of a great number of particles and does not take place if only one particle hits the barrier.

2. SDP is always accompanied by a strong electromagnetic radiation emitted by the metal barrier which can be explained by the movement of electric charges of high density in microstructure.

3. SDP is characteristic of microparticles with initial size not more than $\sim 100 \mu\text{m}$. The probability of SDP sharply drops if microparticle size exceeds a certain range (scale factor). The critical size for penetrating particles is $10^{-5}\text{m} > d_K > 2 \times 10^{-4} \text{m}$. If the barrier is hit by the flow of particles of $10^{-5}\text{m} > d_K$ size, SDP is not observed.

4. SDP does not take place if the speed of microparticles’ hitting the barrier exceeds a certain velocity range (0,5...3,0 km/s).

5. As microparticles penetrate the barrier, new phases are being crystallized in the resulting channels from the elements of the barrier, from microparticles and new chemical elements which were absent in the original materials.

Table (V. Sobolev, S. Usherenko) presents the chemical composition of the iron barrier microstructure in the zones adjacent to the channels formed by penetrating microparticles (analogous results have been obtained for copper aluminium and other metals). Element and isotope compositions have been investigated by X-ray microanalysis, laser mass spectrometry and other tools. Experiments showed that the pair of materials forming the barrier and microparticle interacting in the course of SDP determines what new (in respect to the initial ones) isotopes of chemical elements will be formed. Thus, is we used Pb + Fe and Fe + Fe, the resulting element was mostly manganese (up to 59 %). It was observed that the sulphur content has been always smaller than and proportional to man-

Chemical elements content in the iron barrier after lead microparticles' penetration

Analyzed sample or a fragment of its microstructure	Chemical elements, % mass						
	Cr	Fe	Al	Mn	S	Cu	Pb
Initial composition of microparticles	–	–	–	–	–	–	99.91
Initial composition of the barrier	0.004	99.58	–	–	0.007	–	–
Analysis at the depth of 15 mm (Fig. 2, a)	–	52.99	0.04	28.83	18.14	0.900	–
Analysis at the depth of 32 mm	–	28.61	13.99	39.17	–	0.55	17.68
Analysis at the depth of 47 mm	0.18	43.83	–	30.39	25.01	0.28	–
Analysis at the depth of 72 mm (Fig. 2, b)	–	41.64	0.22	45.74	–	0.12	12.27
Analysis at the depth of 116 mm (Fig. 2, c)	–	43.32	0.03	40.00	–	0.54	16.11
Analysis at the depth of 173 mm (Fig. 2, d)	–	46.50	0.14	36.22	–	0.43	16.71

ganese content. Stable appearance of new elements' isotopes (Mn, S, Na, Cu, Al, Ne, Rn and others) on a large scale can be caused only by nuclear processes (V. Sobolev, S. Usherenko). The hypothesis about probable nuclear transformations can be proved or disproved only after multiple experiments using maximum number of methods required and possible (for the present specification of experiments) to control intermediate and final results.

The energy consumed by microparticles' acceleration on the one hand, and by breaking chemical bonds between the barrier atoms and new elements' formation – on the other hand, differs by 10^5 times. This estimation could have become a serious reason for pessimism regarding the very possibility of SDP occurrence but for the stability of its effect substantiated by thousands of experiments conducted during the last four decades. The attempts to explain the obtained results using conventional hydrodynamic models usually end in a failure. Thus the task of searching for conspicuous physical processes serving as "supplementary energy sources" stimulating breakage of bonds in the barrier metal, especially – formation of initially absent elements – becomes especially topical.

Experiments proved that microparticles' penetration to great depths is stable if the acceleration velocity (kinetic energy) and microparticles' sizes are of definite boundary values. Another specificity is related to the conditions of forming a bunch of microparticles in the cumulative accelerator where they are subjected to compression, mixing, intensive friction and heating. Microparticles' acceleration in the bunch ensures continuous intensive friction of their surfaces. Maximum time required for microparticles' bunch formation in the cumulative accelerator does not exceed $10 \mu\text{s}$. The temperature of iron microparticles' (dia 60 and $120 \mu\text{m}$) heating was measured with the help of A. V. Lykov's method. Fig. 3 shows the relationship between microparticles heating and time. Taking into account the obtained regularities and physical properties of microparticles' material, we have selected a design

of blasting cumulative accelerator to form a bunch of microparticles in the given time span. All the further descriptions of properties and behaviour of a single microparticle relate to any particle penetrating metal microstructure. Peculiarities of microparticles' compression and acceleration in cumulative accelerator bring about triboelectric reaction. Microparticles' surfaces can be activated not only by reciprocal friction but also by increased temperature and pressure – the surfaces of tossed microparticles acquire electric charges during acceleration in the cumulative accelerator. The density of microparticles' bunch in cumulative accelerator does not differ much from the bulk density.

The average velocity of microparticles' movement is more than three times higher than the speed of sound in the air. High speed and density are the reasons why the known methods of diagnostics cannot be applied to the charged microparticles. Fig. 4 shows the relationship between the distribution of surface charges and microparticles' sizes (surface charges were ac-

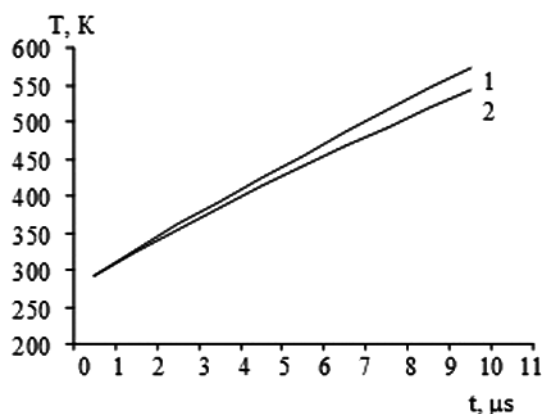


Fig. 3 Relationship between the heating temperature T of the outer layer $10 \mu\text{m}$ thick consisting of iron microparticles with dia $60 \mu\text{m}$ (1) and $120 \mu\text{m}$ (2) and time t

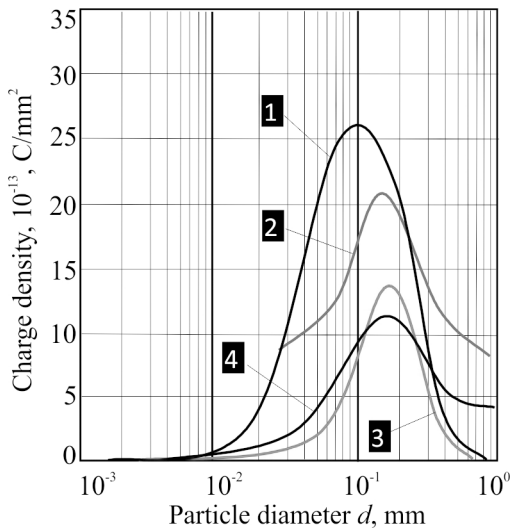


Fig. 4. Relationship between the charge density on the surface of mineral particles and their sizes during blowing:

1 – biotite; 2 – gypsum; 3 – calcite; 4 – microcline

quired by microparticles in “mild” conditions of mechanical interaction).

Hence the first condition for microparticles’ penetration to great depths is acquisition of maximum possible density of surface charges before hitting the barrier.

Decrease in stability of chemical bond and its subsequent breakage were studied by numerical modelling (V. Sobolev et al.). Figures 5 and 6 show the specificity of the bond agitation under the influence of negative and positive charges. Research into the system “CO ion-molecule” allows to state that under otherwise equal conditions any molecule’s bond is broken at a certain distance from an ion. For example, a strong bond of CO molecule at the temperature 0 K is broken by a point charge at the distance $0,16 \times 10^{-9}$ m. As the temperature rises to 600 K (Fig. 3), the distance increases to 2×10^{-9} m. The probability of the bond breakage increases sufficiently as the chemical bond energy decreases, or the temperature rises, ion charge and charge density distribution increase. When approaching charges at a critical distance, chemical bonds are broken with charged particles’ formation.

High-speed microparticles hitting the barrier produce shock waves in the front of which, according to W. F. Libby, the barrier substance enters the state of activated complex which is fundamentally different from the initial state. In the moment of each microparticle hitting the surface, there appear localities with newly formed thin plasma layer (P. A. Tissen et al.). After that, 1...3 % of microparticles continue penetrating destabilized mechanically activated microstructure. Microparticles’ smooth travel in metal is ensured by the plasma zone of ions and electrons of the barrier chemical elements limited by the surfaces of the barrier and microparticle. The hypothesized pattern of a microparticle penetration into the metal barrier is presented in Fig. 7. Fig. 8 shows the typical state of parti-

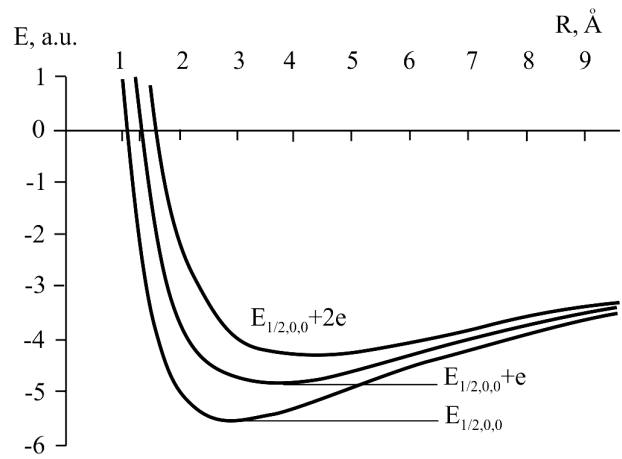


Fig. 5. Alteration of chemical bond energy E related to inter-atom distance R under the impact of one-valent and two-valent negative ion

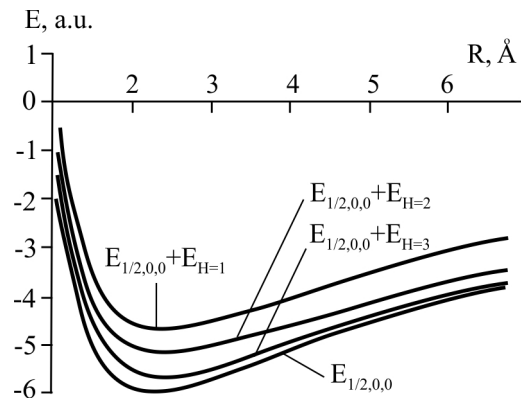


Fig. 6. Alteration of chemical bond energy E related to inter-atom distance R under the impact of one-valent, two-valent and three-valent positive ion

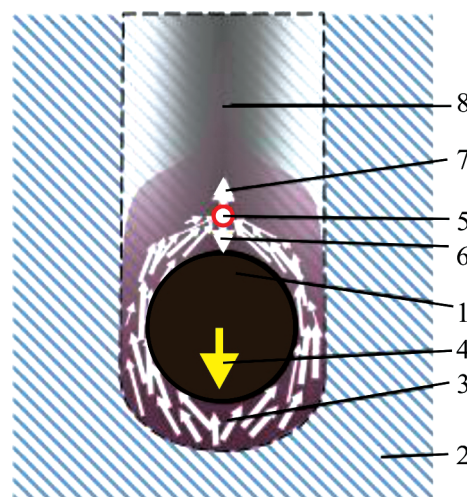


Fig. 7. Formation of the “barrier–penetrating microparticle” system:

1 – microparticle; 2 – metal barrier; 3 – plasma; 4 – direction of microparticle’s motion; 5 – “plasma focus”; 6, 7 – plasma jets; 8 – zone of a new phase crystallization

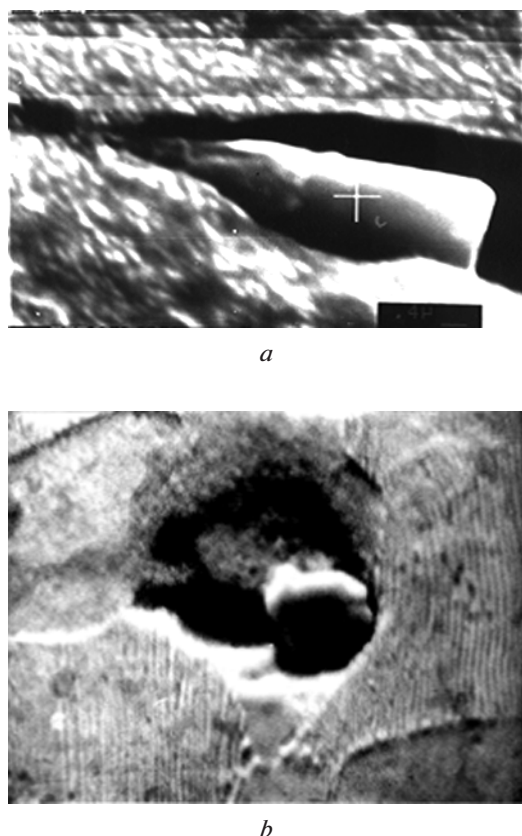


Fig. 8. The shape of some particles that stopped their motion in microstructure of the metal barrier:

a – longitudinal view in the channel; *b* – cross sectional view

cles at halt. It can be seen that the channel diameter in the area of braking is two times bigger than microparticle diameter.

Let us assume that the initial temperature of the plasma flowing around the microparticle is relatively small – about 1 eV (I. V. Sokolov). The so-called plasma focus is formed behind the microparticle where collisional plasma flows rise plasma temperature to the values of nuclear synthesis reactions – about 10^3 eV. Such temperature can be achieved as a result of redistribution and cumulation of plasma flows' internal energy.

Consequently, the second condition for microparticles' penetration to abnormally big depths is connected to decrease of dynamic viscosity in the localities of microparticles' contact to values approaching 10^{-3} .

Chemical bonds are broken during the period of $10^{-12} \dots 10^{-13}$ s. This time $(0,66 \dots 4) \times 10^{-13}$ s is enough for a microparticle moving at a speed of $(0,5 \dots 3,0) \times 10^3$ m/s to pass through one atom layer 2×10^{-10} m thick. Charged particles (ions, electrons) formed as a result of this passage fill the zone between the surfaces of the barrier and microparticle. The total mass of charged particles entering this zone is directly proportional to the crosswise size of the microparticle penetrating the barrier. New chemical bonds between ele-

ments are formed behind the microparticle that is the channel formed by the microparticle passing through the barrier is stopped with new phases.

According to V. Tzariov estimation, the time of charge relaxation in metals is $\sim 10^{-15}$ s that is why charge outflow from the zone cannot be compensated by incoming particles during the time of $\sim 10^{-13}$ s. If the plasma layer disappears, metal viscosity in the contact zone instantaneously drops to the initial value and the microparticle stops its further motion. For the effect to take place, it is necessary that the time of particles' discharge through metal exceed the time of new charges entering the zone.

Hence, the third condition is about selecting initial sizes of microparticles d_k taking into account the set range $10^{-5} \text{ m} > d_k > 2 \times 10^{-4} \text{ m}$ and the range of velocities of microparticles' hitting the barrier from 500 to 3000 m/s.

The discharge through the metal barrier is negligible when the barrier microstructure is strongly destabilized, or there appears conductivity of non-metallic type. Microparticles' bunch impact can cause the state of destabilization lasting from 0,2 to 1,2 ms. Dynamic treatment results in different forms of lability: e. g. deformational destabilization including displacement of dislocations and grain boundaries (P. Butiagin). Microstructure disorder brings about formation of strained bonds, new defects (point, linear and planar), which results in electron concentration decrease in conductivity zone.

Studies of magnetic and dynamic effects caused by the motion of ionized high-speed flow of Si_3N_4 microparticles allowed to establish the relationship between the value of magnetic induction and microparticle size (V. Ovchinnikov), Fig. 9. The graph illustrating the relationship between the magnetic induction value and the powder microparticles' sizes indirectly substantiates the particle size influence on the density of charge distribution on the surface and consequently on the probability of plasma emergence. The depth of microparticles' penetration related to their sizes has been many times proved experimentally, Fig. 10.

The character of relationship between the depth of barrier penetration and Si_3N_4 microparticle (Fig. 10) size is typical for other microparticles under study – SiC, Al, Cu etc. Maximum depth of penetration varies depending on the particles' material. One of the main premises of our hypothesis and a mandatory condition of penetrating thick-walled metal barrier is tossing of microparticles with surface charges. By definition [7], charged microparticles of condensed substance are dust plasma characterised by extremely high chemical activity, ability to self-organize and form ordered structures, by fluctuation of particle charges etc. Particles of dust plasma may be charged by the flows of electrons and ions, as well as by way of photo-, thermo-, or secondary emission of electrons from particles' surfaces [7]. If a microparticle captures electrons, the charge value may reach $\sim 10^2 \dots 10^5$ of elementary charges. Thus average Coulomb energy of particles' interaction greatly exceeds thermal energy. Theoretical

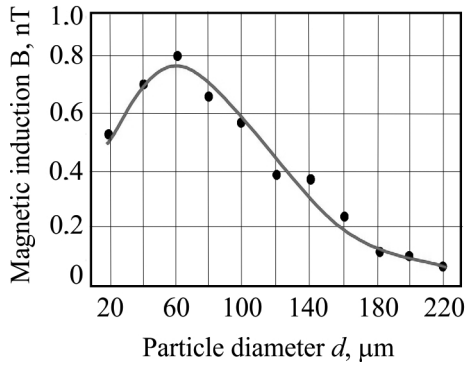


Fig. 9. Alteration of magnetic induction depending on the size of introduced Si_3N_4 particles (according to V. I. Ovchinnikov)

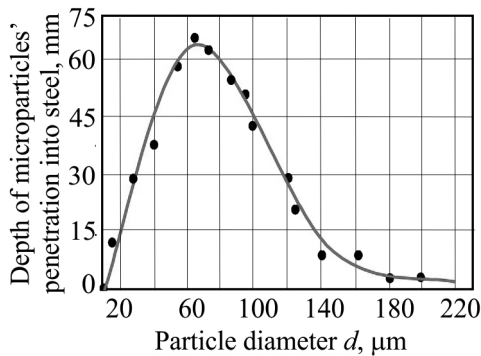


Fig. 10. Relationship between the depth of Si_3N_4 microparticles' penetration and their size

calculations of equilibrium properties of such plasma demonstrate that under certain conditions strong electrostatic particles' interaction and small energy of their thermal motion bring about formation of spatially-ordered structures in particles' location which are analogous to structures in liquids and solids [7]. Microstructure of the section near the barrier surface can testify to spatial orderliness of microparticles in a bunch, Fig. 1.

Stepwise decrease of viscosity is the consequence of quantum mechanical effects. As microparticles hit the barrier, there appears a shock wave propagating at the speed 5100 m/s (for technical iron), while phonons interact with free metal electrons and with electrons forming chemical bonds (P. Platzman, P. Wolf). The time of sound wave for microparticles of 20...120 μm dia is $(2...12) \times 10^{-8}$ s. Sound waves, advancing microparticles, interact with chemical bonds and free electrons (interaction between electrons and phonons). As a result, bound electrons and free electrons get agitated, that is go through upward transition. This means that energy of bond decreases by ΔE (Fig. 5). Electron transitions are possible from level 1/2 to 3/2, from 3/2 to 5/2 etc. These transitions are accompanied by emission of energy quanta. Electron transition (agitation) lasts for $t_{agit} = 10^{-12} - 10^{-13}$ s. Relaxation of valent electrons during downward transition lasts for $t_{relax} = 10^{-4} - 10^{-5}$ s and relaxation of free electrons takes $t_{fre} = 10^{-12} - 10^{-13}$ s (A. A. Vedenov). That is we can state

that free electrons act as donors of energy which goes onto chemical bonds and loosens them. Bonds receive additional agitation and get opened, while the particle start moving in the the plasma of solid body. Comparing t and t_{relax} , we can assert that not all chemical bonds go through relaxation during the time of microparticle motion. Using Stokes equation $ma = 6\pi\eta rv$, let us estimate the value of viscosity for a hypothetical medium so that a microparticle of 60 μm dia will penetrate to the depth 0,1 m at the average speed 1000 m/s, Figures 11 and 12. The obtained range of viscosity values for the hypothetical medium, which can in principle ensure microparticles' penetration to abnormally big depths, includes known values of water viscosity and low temperature plasma. The research results confirm the hypothesis of plasma formation during microparticles hitting the metal barrier surface that is SDP mechanism which is based on formation of Coulomb

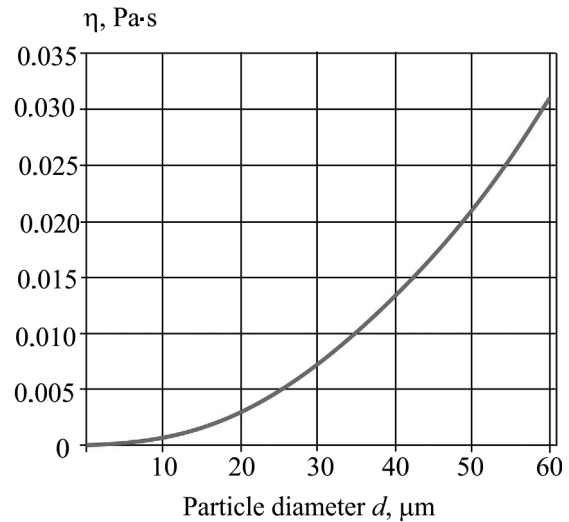


Fig. 11. Relationship between viscosity η and microparticles' size R ($v = 1000$ m/s) during their penetration to the depth 0,1 m

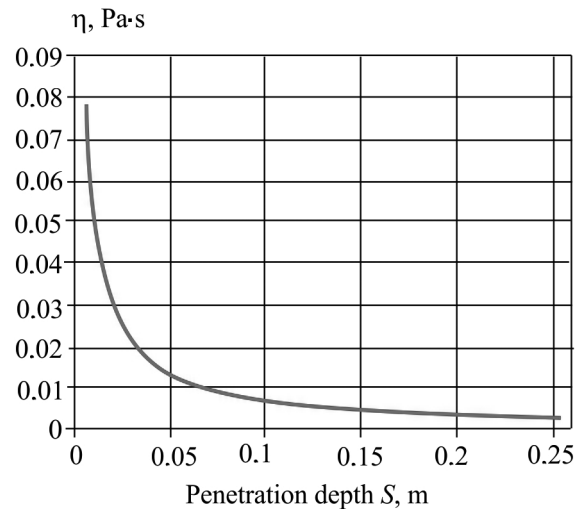


Fig. 12. Relationship between viscosity η and microparticles' penetration depth S . For the particles 60 μm and their velocity $v = 1000$ m/s

potential on microparticles' surfaces. It was experimentally found that microparticle travel in the barrier is accompanied by electromagnetic radiation registered as a light exposure on the X-ray film [8], which can be interpreted as movement of the system "penetrating microparticle – plasma layer" in metal microstructure.

Conclusions. The authors have developed a new physical and chemical model of microparticles' penetration to great depths in metal barriers. The main idea of the model is formation of continuously regenerating plasma between the contact surfaces of penetrating microparticle and the barrier.

Behaviour of conglomeration of charged microparticles is distinguished by the spatial orderliness whose character is analogous to the behaviour of well-studied dust plasma. However, most often we do not observe any signs of ordered disposition of craters in the target microstructure. This phenomenon is related to the value and sign of the charge, microparticle size and relationship between the force of electrostatic interaction of particles and energy of their thermal movement.

References / Список літератури

1. Glasmacher, U. A., Lang, M., Keppler, H., Langenhorst, F., Neumann, R., Schardt, D., Trautmann, C. and Günther, A. Wagner, 2006. *Phase Transitions in Solids Stimulated by Simultaneous Exposure to High Pressure and Relativistic Heavy Ions*. [online] Physical Review Letters. Available at <<http://journals.aps.org/prl/abstract/10.1103/PhysRevLett.96.195701>>.
2. Sobolev, V. V. and Usherenko, S. M., 2006. Shock-wave initiation of nuclear transmutation of chemical elements. *Journal de Physique. IV*, No. 134, pp. 977–982.
3. Malikov, L. P., 2012. Structure and properties of plasma-detonation coating. *Journal of physics and surface engineering*, Vol. 12, No. 2, pp. 550–555.
- Маликов Л. П. Структура и свойства плазменно-детонационного покрытия / Л. П. Маликов // Журнал физики и инженерии поверхности. – 2012. – Т. 12. – № 2. – С. 550–555.
4. Aleksentseva, S. E. and Krivchenko, A. L., 2012. Peculiarities of the Dynamic Interaction Between the Directed Stream of High Speed Particles and Metals. In: *Shock Waves in Condensed Matter*. Kyiv, Ukraine, 16–21 September 2012. Kyiv.
5. Adamenko, S. V., Selleri, F. and A. van der Merwe eds., 2007. *Controlled Nucleosynthesis. Breakthroughs in Experiment and Theory*. Springer.
6. Figovskiy, O., Gotlib, E., Ilicheva, E. and Mokeev, A., 2013. Super deep penetration – new method of nanoreinforced composites producing based on polymer matrixes. In: *High energy systems, processes and their models*. Dnipropetrovsk: AktsentPP. pp. 123–130.
- Super deep penetration – new method of nanoreinforced composites producing based on polymer matrixes / O. Figovskiy, E. Gotlib, E. Ilicheva, A. Mokeev // Сб. научн. трудов „Высокоэнергетические

системы, процессы и их модели“. – Днепропетровск: АкцентПП, 2013. – С. 123–130.

7. Fortov, V. E., Khrapak, A. G., Khrapak, S. A., Molotkov, V. I. and Petrov, O. F., 2004. Dust plasma. *Success of physical sciences*, Vol. 174, No. 5, pp. 495–544.

Пылевая плазма / В. Е. Фортов, А. Г. Храпак, С. А. Храпак [и др.] // Успехи физических наук. – 2004. – Т. 174. – № 5. – С. 495–544.

8. Ovchinnikov, V. I., 2007. Magneto-dynamic effects in cumulative processes of explosion. In: *Physics and technology of high energy material processing*. Dnipropetrovsk: Art-Press, pp. 134–143.

Овчинников В. И. Магнитодинамические эффекты в кумулятивных процессах взрыва // Сборник научн. трудов „Физика и техника высокоэнергетической обработки материалов“. – Днепропетровск: Арт-Пресс, 2007. – С. 134–143.

Мета. Аналіз і оцінка фізичних параметрів, що в комплексі створюють умови для проникнення мікрочастинок до мікроструктури металу на аномально великі глибини.

Методика. Використана квантово-механічна трицентрова модель для дослідження закономірностей руху електрона в полі двох кулонівських центрів і чисельного рішення задачі щодо впливу зовнішнього електричного заряду на стійкість хімічного зв'язку. Вирішувалося рівняння теплопровідності для оцінки температури нагрівання мікрочастинок при їх стисненні та розгоні вибуховим прискорювачем. Використовувалося рівняння Стокса для оцінки значення в'язкості гіпотетичного середовища, до якого на велику глибину й на високій швидкості здатна проникнути мікрочастинка. Проведене аналітичні дослідження із застосуванням мікрорентгеноспектрального, рентгеноструктурного й мікроструктурного аналізів; мас-спектрометрії, електронної спектроскопії та ін.

Результати. Рішення квантово-механічної моделі показує, що електричні заряди є катализаторами, які істотно знижують енергетичний бар'єр хімічних реакцій. Для реалізації надглибокого проникнення необхідно виконати обов'язкову умову, що полягає в розгоні великої кількості мікрочастинок у спеціальному вибуховому прискорювачі. У результаті нагрівання, інтенсивного перемішування та тертя відбувається електризація поверхні мікрочастинок – проявляється відомий трибоелектричний ефект. Висунута гіпотеза про фізико-хімічний механізм проникнення мікрочастинок у метали в результаті високошвидкісного удару.

Наукова новизна. Встановлено взаємозв'язок між розміром мікрочастинок, що розганяються вибухом, щільністю електричних зарядів на їх поверхні та глибиною проникнення мікрочастинок в металеву перешкоду. Експериментально встановлено, що максимальна глибина проникнення мікрочастинок прямо пропорційна найбільшій щільності поверхневих зарядів, характерних для

частинок розміром 50...80 мкм. Передбачається, що проникання мікрочастинок до металів на великій глибині обумовлене зменшенням в'язкості матеріалу перешкоди в зоні контакту мікрочастинки з перешкодою за рахунок прояву квантово-механічних ефектів у плазмі твердого тіла.

Практична значимість. Створення металевих композитів нового покоління. Перспективи пов'язані з новою технологією утилізації радіоактивних матеріалів.

Ключові слова: *мікрочастинки, вибух, високоскоростний удар, кратер, плазма, в'язкість, проникання*

Цель. Анализ и оценка физических параметров, которые в комплексе создают условия для проникания микрочастиц в микроструктуру металла на аномально большие глубины.

Методика. Использована квантово-механическая трехцентровая модель для исследования закономерностей движения электрона в поле двух кулоновских центров и численного решения задачи о влиянии внешнего электрического заряда на устойчивость химической связи. Решалось уравнение теплопроводности для оценки температуры нагревания микрочастиц при их сжатии и разгоне взрывным ускорителем. Использовалось уравнение Стокса для оценки значения вязкости гипотетической среды, в которую на большую глубину и на высокой скорости способна проникнуть микрочастица. Проведены аналитические исследования с применением микрорентгено-спектрального, рентгеноструктурного и микроструктурного анализом; масс-спектрометрии, электронной спектроскопии и др.

Результаты. Решение квантово-механической модели показывает, что электрические заряды являются катализаторами, существенно сни-

жающими энергетический барьер химических реакций. Для реализации сверхглубокого проникания необходимо выполнить обязательное условие, которое заключается в разгоне большого количества микрочастиц в специальном взрывном ускорителе. В результате нагревания, интенсивного перемешивания и трения происходит электризация поверхности микрочастиц – проявляется известный трибоэлектрический эффект. Выдвинута гипотеза о физико-химическом механизме проникания микрочастиц в металлы в результате высокоскоростного удара.

Научная новизна. Установлена взаимосвязь между размером микрочастиц, разгоняемых взрывом, плотностью электрических зарядов на их поверхности и глубиной проникания микрочастицы в металлическую преграду. Экспериментально установлено, что максимальная глубина проникания микрочастиц прямо пропорциональна наибольшей плотности поверхностных зарядов, характерных для частиц размером 50...80 мкм. Предполагается, что проникание микрочастиц в металлы на большие глубины обусловлено уменьшением вязкости материала преграды в зоне контакта микрочастицы с преградой за счет проявления квантово-механических эффектов в плазме твердого тела.

Практическая значимость. Создание металлических композитов нового поколения. Перспективы связаны с новой технологией утилизации радиоактивных материалов.

Ключевые слова: *микрочастицы, взрыв, высокоскоростной удар, кратер, плазма, вязкость, проникание*

Рекомендовано до публікації докт. фіз.-мат. наук А. В. Чернаєм. Дата надходження рукопису 11.01.16.

ГЕОТЕХНІЧНА І ГІРНИЧНА МЕХАНІКА, МАШИНОБУДУВАННЯ

UDC 621.436-55

J. A. Nechytailo¹,
T. O. Bazhynova¹,
M. A. Vesela²

1 – Kharkiv National Automobile and Highway University, Kharkiv, Ukraine, e-mail: julianatol@rambler.ru; tatyana2882@gmail.com

2 – State Higher Educational Institution “National Mining University”, Dnipro, Ukraine, e-mail: mariyakucheryava@mail.ru

THE ENERGY ESTIMATION OF TRANSPORTATION VEHICLES

Ю. А. Нечитайло¹,
Т. О. Бажинова¹,
М. А. Весела²

1 – Харківський національний автомобільно-дорожній університет, м. Харків, Україна, e-mail: julianatol@rambler.ru; tatyana2882@gmail.com

2 – Державний вищий навчальний заклад „Національний гірничий університет“, м. Дніпро, Україна, e-mail: mariyakucheryava@mail.ru

ЕНЕРГЕТИЧНА ОЦІНКА ТРАНСПОРТНИХ МАШИН

Purpose. The research features calculation of analytical methods of management tasks under the condition of rational energy consumption in the transport process performed by the car adhering to the high level of both traffic and environment safety. The work analyses analytical dependence of defining the quality of transportation vehicles which meet customer requirements based on quality performance according to energy estimation.

Methodology. Determination of the analytical model for the evaluation of the hybrid power plant technical condition of the test cycle mode velocities from 30 to 60 km/h is developed. It determines the operation completion of the electrical installation and operation start of the internal combustion engine (ICE) according to car speed motion by means of analyzing the energy loss of hybrid power plant depending on diverse operation conditions to engineering decision.

Findings. The choice of synergistic approach in research performing is grounded. The system of evaluation of technical condition of hybrid vehicles depending on the mode of their working conditions is improved. Simultaneous estimation of the performance of two power flows, from the ICE and electric motor drive, is also provided. The basis of the research of energy costs of electric power unit of a hybrid vehicle is characterized by the steady movement of the vehicle when the control loop based on the energy balance, depending on the average speed.

Originality. For the first time, the interrelation between the technical condition of the hybrid power plant (HPP) and working modes is determined on the basis of the energy principle.

Practical value. The method for determining the hybrid power plant boundary condition, which will improve the system of maintaining and repairing hybrid cars at service stations, is designed.

Keywords: *hybrid power plant, transport machine, energy estimation*

Introduction. The issue of energy saving is important in the energy usage for transportation. In this regard, a vehicle cannot be an exception. Moreover, for vehicles this question is of particular importance because nowadays a vehicle is becoming almost the

most common technical tool used by people in their practice.

It is generally accepted to consider that it is not wealth that makes us the great nation, but the way how efficiently we create it. In relation to the vehicle it is possible to say that “it is not about what volume of transportation we perform by car, but how efficiently we make it, what the energy costs are”. In this regard,

the approach to quality assessment of synergistic cars should be different.

Unsolved aspects of the problem. The works of the following authors are the most valuable for the formation of methodological framework of the diagnostics systems of vehicles:

- the general methodology outlined by Miroshnikov L. V. and used in the practice of technical operation, is taken as the basis while developing the methodology for assessing the technical condition of HPP;

- calculation methodology for the basic parameters of HPP designed by Surin E. I., Umniashkin V. A., Alexandrov A. K., and Vasiliev V. A., provided the basis for the mathematical model working to determine the reference values of diagnostic parameters.

Technical condition assessment and finding of HPP defects (based on the results of scanning of an electronic control system) is currently performed by the method of detailed test that does not provide high quality diagnosis, occurring in additional labor costs and the complexity of the diagnosis process. Insufficient level of validity in the diagnosis results in mistakes during repairs and damage of the expensive elements of hybrid drive. Repairs are complicated due to the lack of necessary diagnostic equipment.

Summarizing the existing experience, it is possible to make a conclusion that the developers of HPP diagnostics go through separate control of the technical condition of the internal combustion engine and electric drive systems, albeit without evaluation of their relationship.

The most common types of vehicles are those with HPP of mixed type (about 80 %). Information about HPP failures and the reason for their occurrence is not well known and virtually is not systematic. Since the mixed type scheme is the most common and the most difficult to diagnose, it is paid the largest attention while developing the methodology.

In the mixed HPP scheme the power generated by the internal combustion engine can be transmitted to vehicle wheels depending on the driving mode into two streams: mechanical stream, through the device of power distribution, and electric stream, through electric motors-generators and high-voltage battery. To build power to the drive wheels, the ICE and the high-voltage battery can work both separately and together, which makes the assessment of the technical condition of HPP difficult.

Analysis of the recent research and publications. As it is shown by various studies there is urgent necessity to measure simultaneously both the actual amount made by useful work of a vehicle and the quantity of energy expenditure, and according to it to assess the transport process as a whole with the most important criterion, which is the coefficient of efficiency.

In this regard, it is appropriate to remind the words of the great Italian scientist G. Galilei: “to measure everything that is measurable, and make measurable

what is not so”. The great Russian scientist D. I. Mendeleev clearly appreciated the role and importance of measurement and, pointed that “in the nature, the measure and weight are the essence of the main instruments of cognition. Science begins with measurement”.

Fuel oil as an energy source has very high specific characteristics: in particular, 1 kg of gasoline contains 11.6 kWh of energy. Batteries of any possible electro-chemical systems have the theoretical amount of energy which is 6–10 times as small. For this reason, the issues of rational use of available electric energy are essential for electric traction systems of all types.

Let us note that electric traction systems have much smaller energy losses than systems with heat engines, including internal combustion engines. The efficiency coefficient of existing heat engines is 25–30 %, so only about 3 kWh/kg of energy density of the fuel is effectively used at the output of the engine.

The energy consumed by one electric car would approximately be 3.4 MWh/year, or 9.3 Wh/day [1].

The efficiency degree of electrochemical accumulator energy (with the modern state of the equipment) can be much higher and the achieved level of electric motors efficiency is 85–90 %. Thus, the useful energy density level of the electro-chemical sources may reach 25–30 % of the above mentioned values of the heat engine output. The approximate calculation shows that while essentially losing the original theoretical energy of energy carrier, electric traction systems can partially compensate this in implementing existing opportunities for its more effective usage. This fact is important while assessing the prospects of development of environmental friendly vehicles.

Objectives of the article. The purpose of this work is investigation of the management objectives of a power plant with rational energy consumption in the transport process performed by a vehicle following the highest level of safety. The approach to the formation of the hauling rig structure is considered which allows reducing energy costs for transportation work significantly.

Presentation of the main research. In accordance with the principle of its action, a vehicle performs some mechanical work due to the thrust force applied to the drive wheels of the vehicle; based on the expanded equation of the traction balance of the vehicle, which is adopted in the theory of vehicle, for the common case of rectilinear motion of a vehicle the work should be determined by the formula

$$A = F_K \cdot S = [m \cdot g \cdot \psi + W_B(v_a \pm v_b)^2 \pm m \cdot r \cdot a] \cdot S,$$

where A is work, J ($N \cdot m$); F_K is traction force, H ; S is way, m ; $m = m_a + m_1$ stands for the gross weight of a vehicle, kg ; m_a is proper mass of a vehicle, kg ; m_1 is the mass of payload, kg ; $\psi = f \pm i$ stands for the coefficient of road resistance; f is rolling resistance coefficient; i is the longitudinal slope of the road (“+” mark corresponds to the movement on rise, “-” mark corre-

sponds to the downhill operation); W_B is factor of streamlining, $N \cdot s^2/m^2$; v_a is vehicle speed, m/s; v_b is wind speed, m/s (“+” mark refers to headwind, “-” mark is for tail-wind); $m \cdot r \cdot a$ stands for inertia force, N (“+” mark corresponds to acceleration, “-” mark corresponds to deceleration); r is the factor of the rotating masses of a car; $a = v_a/dt$ is the absolute value of acceleration or deceleration, m/s^2 .

Thus for a vehicle moving in a set mode (motion with constant speed) and while there is no wind, we have

$$A = F_K \cdot S = (m \cdot g \cdot \psi + W_B v^2) \cdot S.$$

Taking into account the fact that a vehicle is a power machine and, as it is known from physics, it is common practice to assess power machine performance according to their capacity, and based on the expanded power balance equation, adopted in the theory of the vehicle, it is necessary to take the power to the drive wheels of the vehicle as a vehicle performance measurement, which at any time of vehicle movement is equal to

$$P = N_K = F_K \cdot v_a \cdot 10^{-3} = [m \cdot g \cdot \psi + W_B(v_a \pm v_b)^2 \pm m \cdot r \cdot a] \cdot v_a \cdot 10^{-3} S,$$

where P is vehicle performance, kV; N_K is vehicle power (power on the drive wheels), kV.

As it is seen, the performance is equal to the product of the force (traction) by speed.

Thus for the case of vehicle movement at constant speed and absence of wind we get

$$P = N_K = F_K \cdot v_a \cdot 10^{-3} = (m \cdot g \cdot \psi + W_B \cdot v_a^2) v_a \cdot 10^{-3}.$$

Currently, among the performance indicators of a vehicle, special place should be taken by fuel efficiency. At the same time it is advisable to use the coefficient of efficiency (CE) as a generalizing (integral) indicator of fuel efficiency of the vehicle.

As it is known, the coefficient of efficiency is determined for any system by the formula

$$\eta = E_a/E,$$

where E_a is the energy absorbed by the system; E is the energy received by the system.

It should be recognized that the efficiency coefficient of a vehicle is a very necessary concept which allows not only estimating the fuel consumption, but also comparing the most completely and “fairly” the vehicles and choosing the right directions of their improvement.

The term the efficiency coefficient of a vehicle denotes the ratio of the power of the N_R , i.e. the power supplied to the drive wheels (developed by the vehicle power) consumed – power $N_K = q \cdot G$, i.e. the power supplied to a car. Therefore, the efficiency coefficient of a vehicle as the power plant is represented by the ratio of power N_R to power N_K

$$\eta = \eta_{cs} = \frac{N_R}{N_K} = \frac{N_R}{q \cdot G},$$

where η_{cs} – the efficient coefficient of a vehicle as a power plant.

Therefore, the fact that the power of N_R is useful is beyond question, if a car is considered as a power plant.

When considering car movement, it is deemed appropriate to deal with the rolling resistance coefficient f rather than with the coefficient of rolling friction f' , the former is defined by the formula

$$f = \frac{F_f}{P},$$

where F_f is power applied to the wheel, N; P is the gross vehicle weight, N.

In this approach, the force F_f , required to maintain even motion of a vehicle, should be determined by the formula

$$F_f = f \cdot P = f \cdot m \cdot g.$$

However, in reality the force prevents steady motion. Under real traffic conditions the lifting force and the drag force of the air environment occur.

In accordance with this approach, the common formula characterizing the process of vehicle steady motion, looks like this one

$$F_K = F_f + F_a + F_B = m \cdot g(f \pm i) + W_B \cdot v_a^2 = m \cdot g \cdot \psi + W_B \cdot v_a^2,$$

where F_K is force applied to the drive wheels of a vehicle, N; i is road slope; $\psi = f \pm i$ stands for the coefficient of road resistance.

As it is known, the equation represented by the formula, is called the equation of the traction balance.

As it is seen, the right side refers to the power load external to a vehicle rather than the magnitude of losses; to overcome the former, the force F_K is spent, and consequently a vehicle moves along the road.

If the left and right parts of the equation are multiplied by the value of $v \cdot 10^{-3}$, it is possible to obtain an equation that is called the power balance equation

$$N_R = (m \cdot g \cdot \psi + W_B \cdot v_a^3) \cdot 10^{-3}.$$

Based on the above mentioned material, the efficiency coefficient of a vehicle as a power plant should be determined by the formula

$$\eta = \eta_{cs} = \frac{N_R}{q \cdot G} = \frac{(m \cdot g \cdot \psi + W_B \cdot v_a^3) \cdot 10^{-3}}{q \cdot G}.$$

To substantiate the appropriateness of this approach to the calculation of the efficiency coefficient of a vehicle as power plant, let us consider the fuel consumption changes and electronics of hybrid car depending on the average vehicle speed [2].

Electric traction systems have much less energy loss than systems with internal combustion engines (ICE). The efficiency coefficient of existing internal combustion engine hybrid power units (HPP) is from 32 to 36 %, so only about 3 kWh/kg of energy density of the fuel is effectively used at the output of the internal combustion engine.

The degree of energy usage of an electrochemical battery is much higher, and the efficiency coefficient

of electric motors is 85...90 %. Thus, the level of efficiently used energy density of the electrochemical sources reaches 25...30 % of the present value at the internal combustion engine output. This calculation shows that it significantly loses in the original theoretical energy of energy carrier, electrical traction systems can partially compensate for. This occurs at realization of existing opportunities of its more effective usage. This fact is of great importance while assessing the prospects of development and assessing technical condition of electric traction systems and for hybrid approach of its creation.

The method of energy balance was used as the base of the energy cost research for the electric powertrain of a hybrid vehicle. From the analysis of HPP structures and schemes it follows that any electric power plant consists of the following power modules, carrying out consecutive energy conversion: traction batteries, inverter, controller, traction motor, and transmission.

The general equation of electrical power plant balance of a hybrid vehicle in a driving mode with the electric traction will be

$$E_b + E_r = P_a + P_i + P_m + P_r + P_d,$$

where E_b is power from the battery; E_r is energy recovery; P_a , P_i , P_m , P_r are energy losses in the power plant modules – accumulator battery, inverter, motor, and transmission; P_d is energy loss when driving a hybrid vehicle.

In addition to the energy balance, it is approved to consider the equations of power balance that is primary in relation to the energy balance. However, the test conditions of the power plant of a hybrid vehicle are characterized by the steady-state motion of a vehicle at given speed. In this regard, this is the energy balance of the hybrid power plant prepared for the control of the driving movement cycle which is of great value [3].

The most effective hybrid test cycle is within the real speeds of 30...60 km/h. Therefore, it is advisable to carry out assessment of the hybrid powertrain technical condition particularly for this cycle, which determines the powertrain work completion using the ve-

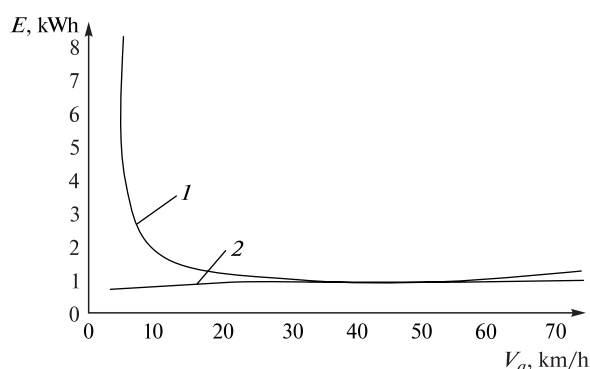


Fig. The energy E change received by vehicle, depending on the average speed V_a :
1 – while running with gasoline; 2 – in EV mode

hicle motion speed and the beginning of enabling ICE operation. The equation of energy balance gives much more information for cyclic calculations than the equation of power balance; in addition, the energy consumption per cycle is a very important indicator of assessing the technical condition of HPP. These are the graphs of power consumption depending on average speeds below (Figure).

As it follows from the Figure at average speed of 50 km/h the petrol consumption of the electric vehicle will be at low average speeds up to 40 km/h. At the average speed over 60 km/h it is efficient to use the vehicle in mode with a gasoline engine. This is because the efficiency coefficient of the electric engine reduces when the load is close to maximum, and the efficiency coefficient of a gasoline engine increases and will be maximum at medium loads.

Conclusions and recommendations for further research. On basis of the analysis of the energy loss of a vehicle with HPP, it follows that at low medium speeds of about 5...20 km/h it is very effective to use the driving mode on the electric range, and at medium speeds of above 60 km/h it is worth driving with the use of internal combustion engines. It is obvious that hybrid vehicles use the energy effectively to perform transport work unlike other types of vehicles.

References / Список літератури

1. Knez, M., Sternad, M., 2015. *Solar energized transport solution and customer preferences and opinions about alternative fuel vehicles – the case of Slovenia*. Transport Problems. Scientific Journal, Gliwice, Vol. 10, Issue 3, pp. 17–28.
2. Bazhinov, A. V., Smirnov, A. P., Serikov, S. A. and Dvadenko, V. J., 2011. *Synerhetychnyi avtomobil. Teoriia y praktika* [Synergy car. Theory and practice]. Kharkiv: KNASU.
- Синергетичний автомобіль. Теорія і практика / [О. В. Бажинов, О. П. Смирнов, С. А. Серіков та ін.]. – Харків: ХНАДУ, 2011. – 236 с.
3. Bazhinov, O. V., Smirnov, O. P., Serikov, S. A., Hnatov, A. V. and Kolesnikov, A. V., 2008. *Hybridni avtomobili* [Hybrid cars]. Kharkiv: KNASU.
- Гібридні автомобілі / [Бажинов О. В., Смирнов О. П., Серіков С. А. та ін.]. – Харків: ХНАДУ, 2008. – 327 с.

Мета. Дослідження особливостей розрахункових аналітичних методів задачі керування силовою установкою за раціональної витрати енергії при транспортному процесі, здійсненим автомобілем, дотримуючись високого рівня як безпеки руху, так і екологічної безпеки. Аналіз аналітичних залежностей визначення якості транспортних машин, що відповідають вимогам споживача на основі відбору показників якості за енергетичною оцінкою.

Методика. Визначення аналітичної моделі оцінки технічного стану гібридної силової установки для випробувального циклу в режимі швид-

костей руху 30...60 км/год, що за швидкістю руху автомобіля визначає закінчення роботи електроустановки та початок роботи двигуна внутрішнього згоряння (ДВЗ), за допомогою аналізу енергетичних витрат гібридної силової установки в залежності від різноманіття умов експлуатації к технічним рішенням.

Результати. Обґрунтовано вибір синергетичного підходу при виконанні досліджень. Удосконалена система оцінки технічного стану гібридних автомобілів у залежності від режиму та умов їх роботи. А також представлена одночасна оцінка роботи двох потоків потужності: від ДВС і від електроприводу. Основа дослідження енергетичних витрат електричної силової установки гібридного автомобіля характеризується сталим рухом транспортного засобу при контрольному циклі, виходячи з балансу енергії, у залежності від середньої швидкості руху.

Наукова новизна. Уперше на базі енергетичного принципу встановлено взаємозв'язок між технічним станом гібридної силової установки (ГСУ) і режимами роботи.

Практична значимість. Розроблено метод визначення граничного стану гібридної силової установки, що вдосконалив систему сервісного обслуговування та ремонту гібридних автомобілів на станціях технічного обслуговування.

Ключові слова: *гібридна силова установка, транспортна машина, енергетична оцінка*

Цель. Исследование особенностей расчетных аналитических методов задачи управления силовой установкой при рациональном расходе энергии при транспортном процессе, совершаемом автомобилем, соблюдая высокий уровень как безопасности движения, так и экологической безопасности. Анализ аналитических зависимостей определения качества транспортных машин, отвечающих требованиям потребителя, на основе системного отбора показателей качества по энергетической оценке.

Методика. Определение аналитической модели оценки технического состояния гибридной силовой установки для испытательного цикла в режиме скоростей движения 30...60 км/ч, который по скорости движения автомобиля определяет окончание работы электроустановки и начало работы двигателя внутреннего сгорания (ДВС), с помощью анализа энергетических потерь гибридной силовой установки, в зависимости от многообразия условий эксплуатации к техническим решениям.

Результаты. Обоснован выбор синергетического подхода при выполнении исследований. Усовершенствована система оценки технического состояния гибридных автомобилей в зависимости от режимов и условий их работы, а также предоставлена одновременная оценка работ двух потоков мощности: от ДВС и от электропривода. Основа исследования энергетических затрат электрической силовой установки гибридного автомобиля характеризуется установившимся движением транспортного средства при контрольном цикле, исходя из баланса энергии, в зависимости от средней скорости движения.

Научная новизна. Впервые на базе энергетического принципа установлена взаимосвязь между техническим состоянием гибридной силовой установки (ГСУ) и режимами работы.

Практическая значимость. Разработан метод определения граничного состояния гибридной силовой установки, который усовершенствует систему сервисного обслуживания и ремонта гибридных автомобилей на станциях технического обслуживания.

Ключевые слова: *гибридная силовая установка, транспортная машина, энергетическая оценка*

Рекомендовано до публікації докт. техн. наук О. Я. Ніконовим. Дата надходження рукопису 20.09.15.

UDC 534.1, 621.81-192

V. P. Shpachuk, Dr. Sc. (Tech.), Prof.

O. M. Beketov National University of Urban Economy in Kharkiv, Ukraine, e-mail: shpachukvp@mail.ru

EFFECT OF MUTUALLY AMPLIFYING ACTION OF TWO COORDINATE SHOCK LOADING IN PROBLEMS OF DYNAMICS OF KNOTS OF MACHINES

В. П. Шпачук, д-р техн. наук, проф.

Харківський національний університет міського господарства ім. А. Н. Бекетова, м. Харків, Україна, e-mail: shpachukvp@mail.ru

ЕФЕКТ ВЗАЄМОПІДСИЛЮЮЧОЇ ДІЇ ДВОКООРДИНАТНОГО УДАРНОГО НАВАНТАЖЕННЯ В ЗАДАЧАХ ДИНАМІКИ ВУЗЛІВ МАШИН

Purpose. To define and analyze patterns of influence on the qualitative and quantitative parameters of mutually reinforcing action of two components of the kinematic coordinate shock loading on the vibration amplitude of the object at the control points on the basis of two-parameter amplitude-down hole-time characteristics.

Methodology. The study is based on fundamental approaches of applied mechanics, theory of modeling and vibration reliability. The pre-set parameters include inertial, dissipative and elastic characteristics of the test object, coordinates of its reference points while varied parameters are time parameters of two-dimensional external mechanical shock action, design factors of a supporting structure as well of the object itself and its pre-set reference points.

Findings. Factors of influence of the parameters of the two coordinate impact while testing the facilities of the spatial structure for vibration reliability are introduced, dependence of the quantities and gradient signs of changes in these factors on the design parameters of the supporting structure of the test object and geometric coordinates of the reference point on the object and the supporting structure (e.g., a platform of a many coordinate shaker).

Originality. For the first time, quantitative and qualitative patterns of influence factors dependence on the parameters of the two coordinate external mechanical loading, the test object and the support structure are defined for objects of the spatial structure based on two-parameter amplitude-downhole-time characteristics. As a measure of mutually increasing action of parameters of two-coordinate shock loading, it is suggested to use the influence coefficients described through amplitudes, duration and inter-coordinate temporal delay of shock influences.

Practical value. The examined shock influences in practice result in the refuses of the real objects of mining machinery manufacturing, aviation, transport and space machinery regarding stability of functioning and durability. For the particular assembly machines, the results are used when determining the regulatory regime of bench tests for multicoordinate impact force, which improves durability and reliability in operation.

Keywords: *two-coordinate shock loading, vibration reliability, dynamics of knots of machines*

Introduction. Constructions of modern machines, equipment and mechanisms of mining machinery, aviation, transport and space engineering are continuously developed and improved in the direction of increasing the power, rapidity and accuracy. While seeking to reduce metal consumption and the size of metal, this leads to high dynamic loading, as well as to an increasing role of the vibrational movement of the machine knots [1]. Most of the units and components of such equipment make a set of nodes, blocks, and units installed on the supporting structure (housing) and belongs to a class of objects of the spatial structure (OSS), whose mechanical scheme is a system of spatially oriented inertial, elastic and dissipative elements.

Analysis of the recent research. Theoretical issues related to the peculiarities of manifestation of the synergistic action effects in the task to test the spatial structure objects for vibration reliability problems are solved in the works [1–3]. It was found that this excludes the underestimations of indicators of the vibratory activity of objects, diagnosed by at bench tests and, consequently, their unexpected failures at vibration reliability in use. Mutually reinforcing action of parameters of the deterministic multi-axis vibration was analyzed on the basis of amplitude – phase – frequency characteristics, and the effectiveness of OSS bench tests on the multi-axis forward angular vibrating tables was showed.

The objective of the article is to define influence patterns for the of qualitative and quantitative parameters of mutually reinforcing actions of constituting

two-coordinate kinematic mechanical shock loading on the vibration amplitude of the object at the control points, formalized on the basis of two-parameter amplitude-down hole-time characteristics.

Presentation of the main research. The present work is devoted to the numerical analysis of the mutually reinforcing action of the parameters of two-coordinate shock loading, formalized by means of two-parameter amplitude-downhole-time characteristics (ADTC) of the OSS through mechanical and geometric parameters of the supporting structure (housing products), as well as the object itself and its defined control points.

Fundamental equation of OSS vibrations in the time domain, produced in the control room and then in the normal forms, were the basis of research. This functional dependence of the vibration parameters of the object on the parameters of the external kinematic effects is analyzed based on the extremality properties [1, 2].

As a measure of the mutually reinforcing action of the parameters of the two-coordinate shock loading on the dynamic state of the OSS the coefficients of influence are accepted

$$\begin{aligned}
 K_{S_y} &= \frac{\max Y - \max Y^*}{\max Y^*} \cdot 100\%; \\
 K_{S_z} &= \frac{\max Z - \max Z^*}{\max Z^*} \cdot 100\%; \\
 K_{S_\theta} &= \frac{\max \theta - \max \theta^*}{\max \theta^*} \cdot 100\%; \\
 K_{S_r} &= \frac{\max r - \max r^*}{\max r^*} \cdot 100\%.
 \end{aligned}
 \tag{1}$$

Where $\max Y$, $\max Z$, $\max \theta$, $\max r$ are the maximum values of functions

$$\begin{aligned}
 \max_t |y(t, T, \tau)| &= f_1(T, \tau); \quad \max_t |z(t, T, \tau)| = f_2(T, \tau); \\
 \max_t |\theta(t, T, \tau)| &= f_3(T, \tau); \quad \max_t |r_{k1,2}(t, T, \tau)| = f_4(T, \tau),
 \end{aligned}$$

where r is the radius-vector of deviations of the control points of the test object from their positions in a state of static equilibrium of the object; τ , T is the duration and the XY time delay of shock impacts (the time interval between the leading edges of the rectangular shock pulse in the direction of the vertical and horizontal coordinates). Here, the quantities $\max Y^*$, $\max Z^*$, $\max \theta^*$, $\max r^*$ are determined by the expression $\max(y = f_1(5, 1))$, $\max(z = f_2(5, 1))$, $\max(\theta = f_3(5, 1))$, $\max(r = f_4(5, 1))$. In this case the maximum values for the submodular function in the version accepted as the parameters $\max X^*$ ($X = y, z, \theta, r$) when the OSS has time to come to a state of static equilibrium before the arrival of subsequent shock impacts. For the mechanical object analyzed in the experiment it was found that this occurs at magnitudes $\tau = 1s$ and $T = 5s$. The influence coefficients $K_{S_i}(T, \tau)$ ($i = y, z, \theta, r$) are zero at the action of indicated perturbations.

On the base of the two-dimensional ADTC ($f_k(T, \tau)$ ($k = 1-4$)), the work defines and analyzes quantitative and qualitative characteristics of the behavior of the influence coefficients (1) when changing the τ , T parameters of the two-coordinate kinematic shock impact of a rectangular shape, as shown in Fig. 1 where A is the pulse amplitude.

The kinematic excitation at an object is formalized as

$$\begin{aligned}
 V_{z_1}(t) = V_{z_2}(t) &= \begin{cases} A, t \in [0, \tau] \\ 0, t \in (\tau, +\infty) \end{cases}; \\
 V_{y_1}(t) = V_{y_2}(t) &= \begin{cases} 0, t \in (0, T) \cup (T + \tau, +\infty) \\ A, t \in [T, T + \tau] \end{cases}.
 \end{aligned}
 \tag{2}$$

The advantage of the considered two-dimensional ADTC over the uniform amplitude-boreholes and amplitude-time characteristics is their absolute informative value regarding the following basic characteristics of mechanical vibration systems [1, 2]: the number of the resonance peaks when $\tau = Var$ and $T = Var$; the values of the parameters of indicators of the mutually reinforcing action of the two-coordinate shock loading (coefficients of the influence $K_{S_i}(T, \tau)$). The mechanical scheme of the analyzed three-dimensional object under research is shown in Fig. 2. The following designations are adopted: 1-4 – structural elements, mod-

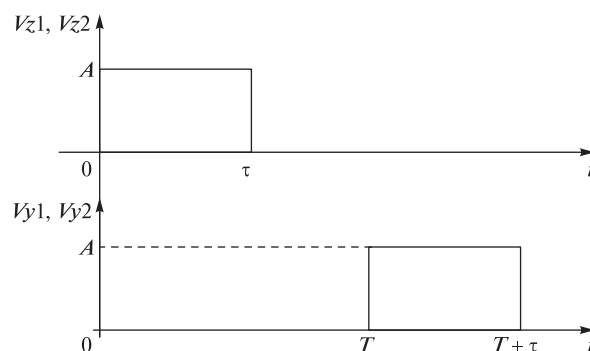


Fig. 1. Scheme of shock influence

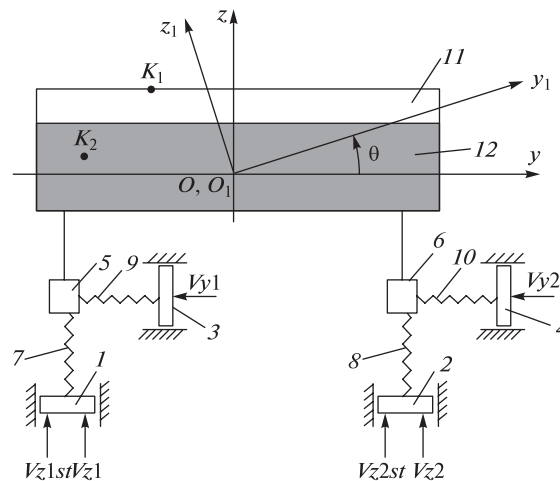


Fig. 2. Mechanical scheme of the object

eling supporting structure (body) of the item; 5, 6 – details of junction of the object with the product of housing; 7–10 – elastic-dissipative elements, modeling the generalized deformation characteristics of the suspension of the object in orthogonal directions; 11 – the basic constructive element of mass m_6 , modeling the inertial properties of the object; 12 – the inertial additive element of mass m_a ; V_{z1st} , V_{z2st} – vertical mounting displacement of constructive elements 1, 2, providing a static equilibrium of the object; Oyz , $O_1y_1z_1$ – fixed and movable system of coordinates accordingly, whose poles are the same in the position of static equilibrium. The feature of the object of research is a type of non-linear characteristics of the stiffness of elastic elements 7, 8 of its suspension bracket (Table Entry 8).

With the aim to facilitate the analysis and interpretation of results, as well as to make the results of studies of generalizing practical importance, the work represents the object as a set of basic inertial member 11 and the inertial additive element 12, which is embedded in the base, informing OSS the properties of the parametric irregularity of the dynamic model. In a particular case, the circuit of the research object, shown in Fig. 2, simulates the mining machinery units, seismic protection, aviation, space technology, as well as the crews of the rail and road transport. For example, with regard to mining and transport equipment it occurs when with machine working and the object moving along the route, the download changes; as for the aviation technology, the mounted unit is forcibly separated from the frame structure during the flight of the object. In this case, there obviously occurs a change of

mass characteristics of the object, its moment of inertia, as well as the coordinates of the points fixing elastic-dissipative elements, etc., that is, the parameters of the dynamic model. In the paper, this object property is defined by the term “the parametric infrequency of the dynamic model”.

As a result of the given shock impacts V_{z1} , V_{z2} , V_{y1} , V_{y2} of constructive elements 1–4 of the supporting structure of the item, the research object executes three-dimensional vibrations in yOz plane. It has three degrees of freedom: the ability to move in the direction of the axis Oy and Oz , and rotate around the point O_1 (the center of mass). In practice, the considered shock impacts lead to the denials of the real objects regarding the stability of functioning and strength. Particularly when they appear periodically. As part of the task, the design scheme of the object reflects the main features of the real mechanical system, affecting the evaluation of its dynamic response, the features of connectedness of vibration; it is correct and structurally sufficient, taking into account the two-parameters of the analyzed influence coefficients and XY of the considered kinematic impact excitation.

In a time domain the dynamic model of the object with two-coordinate shock loading of kind (2) considering [1, 3] has the form

$$W \cdot Q_1 = Q_2,$$

where $Q_1 = [y, z, \theta]$ is a vector of linear and angular displacements of the object together with the mass center and around it; $Q_2 = [q_1, q_2, q_3]$ is a vector of input actions;

Table

Geometrical and mechanical parameters of the object

No.	OSS Parameters	The Object of the first type	The Object of the second type
1	The Mass m_6 of basic inertial element, kg	17000	
2	The Mass m_a of additive element, kg	0	8050
3	The Mass of generalized inertial element, kg	17 000	25 050
4	The coordinates of the center of basic element's masses, m	(0; 0.57)	(0; 0.64)
5	The moment of inertia of the generalized element, $kg \cdot m^2$	250 692.67	251 589.33
6	The resistance ratios of elastic elements 7–10 of the suspension, $N \cdot s/m$	$24 \cdot 10^3$	
7	The coefficients of the stiffness of elastic elements 9, 10 of the parallel axes, Oy , N/m	$0.475 \cdot 10^5$	
8	The coefficients of the stiffness of elastic elements 7, 8 of the parallel axes, Oz , (z – dimension in the formula is in meters), N/m	$5 \cdot 10^4 \cdot \sqrt{6 \cdot 10^3 z + 1}$	
9	The Coordinates of the fixing points of elastic elements 7, 9 and 8, 10, m	(-3.2; -1.12); (3.2; -1.12)	(-3.2; -1.19); (3.2; -1.19)
10	The coordinates of the control points, m	K1 (-3.2; 2.0); K2 (-6.0; 0.5)	K1(-3.2; 1.93); K2(-6.0; 0.43)

$$\begin{aligned}
 q_1(t) &= (b_y \cdot P + c_y) \cdot V_{y_1}(t); \\
 q_2(t) &= b_z \cdot P \cdot V_{z_1}(t) + c_z V_{z_1}(t); \\
 q_3(t) &= b1_z \cdot P \cdot y_{11} \cdot V_{z_1}(t) + b2_z \cdot P \cdot y_{12} \cdot V_{z_2}(t) + \\
 &+ c1_z \cdot y_{11} \cdot V_{z_1}(t) + c2_z \cdot y_{12} \cdot V_{z_2}(t) - \\
 &- (b1_y \cdot P + c1_y) \cdot z_{12} \cdot V_{y_1}(t) - (b2_y \cdot P + c2_y) \cdot z_{13} \cdot V_{y_2}(t);
 \end{aligned}$$

$$W = \begin{pmatrix} W_y & 0 & -W_{y\theta} \\ 0 & W_z & W_{z\theta} \\ -W_{y\theta} & W_{z\theta} & W_\theta \end{pmatrix} \text{ is a matrix of transfer}$$

functions of the study object;

$$W_y = M \cdot P^2 + b_y \cdot P + c_y;$$

$$W_z = M \cdot P^2 + b_z \cdot P + c_z;$$

$$\begin{aligned}
 W_\theta &= I_c \cdot P^2 + (b1_y \cdot P + c1_y) \cdot z_{12}^2 + (b2_y \cdot P + c2_y) \cdot z_{13}^2 + \\
 &+ (b1_z \cdot P + c1_z) y_{11}^2 + (b2_z \cdot P + c2_z) y_{12}^2;
 \end{aligned}$$

$$W_{y\theta} = (b_y \cdot P + c_y) \cdot z_{12};$$

$$W_{z\theta} = b1_z \cdot P \cdot y_{11} + b2_z \cdot P \cdot y_{12} + c1_z y_{11} + c2_z y_{12},$$

where $M = m_b + m_a$ is the mass of generalized inertial element; $P = \frac{d}{dt}$ is the operator of differentiation; $c_y = c1_y + c2_y$; $c_z = c1_z + c2_z$; $b_y = b1_y + b2_y$; $b_z = b1_z + b2_z$; $c1_y, c2_y, b1_y, b2_y$ are the coefficients of stiffness and elastic-dissipative resistance of elements 9, 10; $c1_z, c2_z, b1_z, b2_z$ are the coefficients of stiffness and elastic-dissipative resistance of elements 7, 8; I_c is the moment of inertia of the object relative to the axis passing through its center of mass; y_{11}, y_{12} are coordinates of the points fixing the elastic elements 7, 8 accordingly; $z_{12} = z_{13}$ are the coordinates of points of fastening of the elastic elements 9, 10; $Vz1 = Vz2$; $Vy1 = Vy2$.

The dynamic model of the object of research is presented in the normal Cauchy form and solved by the Runge-Kutta method of fourth-order accuracy.

As in the expressions (1) the values $\max Y^*$, $\max Z^*$, $\max \theta^*$, $\max r^*$ are constant values for a particular object, the behavior of the coefficients of influence is uniquely determined by the character of variation of the corresponding functions of two variables

$$\max_t |y(t, T, \tau)| = f_1(T, \tau);$$

$$\max_t |z(t, T, \tau)| = f_2(T, \tau);$$

$$\max_t |z(t, T, \tau)| = f_2(T, \tau);$$

$$\max_t |r_{k1,2}(t, T, \tau)| = f_4(T, \tau).$$

They are analyzed in the work for the geometrical and mechanical OSS parameters shown in Table.

Here, the objects of type 1 and 2 differ in masses of the additive element, respectively, with $m_a = 0$ and $m_a = 8050$ kg.

For example, Fig. 3–4 for the type 1 object shows the characteristics of the maximum deviations of coordinates of its center of mass and the reference point K_2 from its equilibrium position while varying τ and T in the range (0–5) c, where the positions a, b, c show the variations in coordinate direction Y, Z, θ , respectively.

The same characteristics for OSS of the second type are shown in Fig. 5–6.

As a result of the cumulative behavior analysis for ADTC $f_1(T, \tau), f_2(T, \tau), f_3(T, \tau), f_4(T, \tau)$ we installed

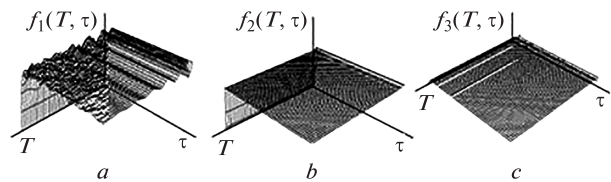


Fig. 3. Amplitude-downhole-time characteristics of the object:

a – deviations in the direction of Z coordinate; *b* – deviations in the direction of Y coordinate; *c* – deviations in the direction of θ coordinate

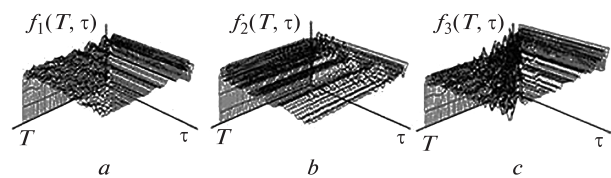


Fig. 4. Amplitude-downhole-time characteristics of the object:

a – deviations in the direction of Z coordinate; *b* – deviations in the direction of Y coordinate; *c* – deviations in the direction of θ coordinate

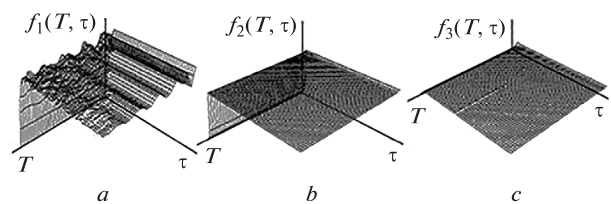


Fig. 5. Amplitude-downhole-time characteristics of the object:

a – deviations in the direction of Z coordinate; *b* – deviations in the direction of Y coordinate; *c* – deviations in the direction of θ coordinate

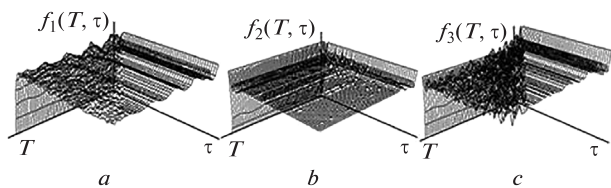


Fig. 6. Amplitude-downhole-time characteristics of the object:

a – deviations in the direction of Z coordinate; *b* – deviations in the direction of Y coordinate; *c* – deviations in the direction of θ coordinate

the qualitative and quantitative dependences of coefficients influencing $Ks_i(T, \tau)$ ($i = y, z, \theta, r$) from the effect of parametric irregularities of the OSS dynamic model. For the test object analyzed in the work with changing mass of the inertia additive element in the range of $m_a = [0 \div 8050]$ kg, the ranges of change of influence coefficients adopted the following values: for the center of mass of the generalized inertial element $Ks_y = [21.9 \div 9.3]$ %, $Ks_z = [5.3 \div 3.7]$ %, $Ks_\theta = [20.1 \div 14.9]$ %; for the control point $K_1 - Ks_y = [38.4 \div 26.1]$ %, $Ks_z = [0.6 \div 6.2]$ %, $Ks_r = [47 \div 40.4]$ %; for the control point $K_2 - Ks_y = [23.9 \div 11.9]$ %, $Ks_z = [35.2 \div 25.4]$ %, $Ks_r = [58.8 \div 48.5]$ %.

At the same time there occurs dependence of the signs of gradients of changing influence coefficients on the position of the analyzed point in the internal volume of the object hull. For example, at a reference point K_1 , for the vertical coordinate Z , as opposed to other considered points of the test object (point K_2 , and the center of mass) the effect of the positive dynamics of change of influence coefficient Ksz appears, while an increase in mass inertia of the additive element in the range $m_a = [0 \div 8050]$ kg leads to its increase in 10.3 times. Moreover, we installed quantitative and qualitative dependence of the time parameters τ , T of the two-coordinate shock loading of kinematic excitation of the object, with which the conditions of $Ks_i(T, \tau) = \max(i = y, z, \theta, r)$ are achieved, on the geometric coordinates of the analyzed point in the $O_1y_1z_1$ system. For example, at $m_a = 0$, the following quantities of durations τ and the time lag T of shock loadings are obtained: for the center of mass in the coordinate $y - \tau = 1.1$ s, $T = 0.6$ s, in the coordinate $z - \tau = 0.3$ s, $T = 1.3$ s, in the coordinate $\theta - \tau = 0.9$ s, $T = 1.3$ s; for the control point K_1 : for the coordinate $y - \tau = 0.9$ s, $T = 0.9$ s, for the coordinate $z - \tau = 0.6$ s, $T = 0.1$ s, for the radius-vector of the point $- \tau = 0.9$ s, $T = 0.4$ s; for the control point K_2 : for the coordinate $y - \tau = 0.9$ s, $T = 0.4$ s, for the coordinate $z - \tau = 0.9$ s, $T = 1.3$ s, for the radius-vector of the point $- \tau = 1.9$ s, $T = 1.6$ s. Thus, for example, for the radius-vector of the control point K_2 the condition $Ksr = \max$ is reached at values of the duration quantities τ and the time lag T , exceeding the similar for the control point K_1 , respectively by 2.1 and 4.0 times.

Conclusion. The importance of the studies carried out in the work, involves specifying the features of occurrence of effect of mutually reinforcing action of multi-coordinate mechanical shock loading from the supporting structure as applied to problems of the vibration reliability of the spatial structure of objects; the features are determined by coefficients influence. The obtained results should be considered when determining the normative operational mode of the object. Disregard of the established effect leads to a reduction of durability and reliability of an object in operation.

It should also be noted that with bench test for vibration reliability, the considered option of vibrations of the product hull is implemented by the platform of two-coordinate shock vibrating bench, whose devel-

opment and implementation relates to the topical problems of modern testing equipment.

The practical significance of the obtained results is shown while solving the problems of vibration resistance, vibration strength and vibration diagnostics of knots and units of machines relating to the objects of the spatial structure, designed for operation under conditions of multi-coordinate impact action, as well as in the synthesis of constructive schemes.

References / Список літератури

1. Shpachuk, V.P., Dudko, V.V. and Kostenko, I.V., 2015. Methods and installations for tests for multicoordinate external vibrational influence. *Komunal'ne gospodarstvo mist*, Issue 120, pp. 12–20.
- Шпачук В. П. Методи й установки для випробувань на багатокоординатний зовнішній вібраційний вплив / В. П. Шпачук, В. В. Дудко, І. В. Костенко // Комунальне господарство міст. — К.: Техніка, 2015. — Вип. 120. — С. 12–20.
2. Masich, P. and Kashapov, M., 2007. Electrodynamics test equipment from IMV. *Elektronika: Nauka, tekhnologiya, bisnes*, No. 2, pp. 90–95.
- Масич П. Електродинамические испытательные установки компании IMV / П. Масич, М. Кашапов // Электроника: Наука, технология, бизнес. — 2007. — № 2. — С. 90–95.
3. Halimand, D. and Cazzolato, B.S., 2006. A multiple-sensor method for control of structural vibration with spatial objectives. *Journal of Sound and Vibration*. Vol. 296, No. 1–2, pp. 226–242.

Мета. Встановити та проаналізувати закономірності впливу на якісні й кількісні параметри дії складових двокоординатного кінематичного ударного механічного навантаження, що взаємопідсилюється, на амплітуди коливань об'єкта в контрольних точках, формалізовані на базі двопараметричних амплітудно-шпаруватисно-часових характеристик.

Методика. Дослідження базуються на фундаментальних підходах прикладної механіки, теорії моделювання та вібронадійності. Заданими параметрами є інерційні, дисипативні й пружні характеристики об'єкта випробувань, координати його контрольних точок, варійованими — тимчасові параметри двомірної зовнішньої механічної ударної дії, конструктивні параметри несучої конструкції, а також самого об'єкта та його заданих контрольних точок.

Результати. Уведені коефіцієнти впливу параметрів двокоординатної ударної дії при випробуваннях об'єктів просторової структури на вібронадійність, встановлена залежність величин і знаків градієнтів зміни вказаних коефіцієнтів від конструктивних параметрів несучої конструкції, об'єкта випробувань і геометричних координат контрольної точки на об'єкті й несучій конструкції (наприклад, платформі багатокоординатного вібростенда).

Наукова новизна. Уперше для об'єктів просторової структури на базі двопараметричних амплітудно-шпаруватисно-часових характеристик встановлені якісна й кількісна закономірності коефіцієнтів впливу від параметрів зовнішнього двокоординатного механічного навантаження, об'єкта випробувань і несучої конструкції. В якості міри взаємопідсилюючої дії параметрів двокоординатного ударного навантаження запропоновано використовувати коефіцієнти впливу, що формалізовані через амплітуди, тривалість і міжкоординатне часове запізнювання ударних впливів.

Практична значимість. Ударні впливи, що розглядаються, призводять на практиці до відмов реальних об'єктів гірничого машинобудування, авіаційної, транспортної та космічної техніки за стійкістю функціонування й міцністю. Для конкретних вузлів машин отримані результати використовуються при визначенні нормативного режиму стендових випробувань на багатокординатну ударну дію, що забезпечує підвищення довговічності та надійності об'єкта в експлуатації.

Ключові слова: *двокоординатне ударне навантаження, вібронадійність, динаміка вузлів машин*

Цель. Установить и проанализировать закономерности влияния на качественные и количественные параметры взаимоусиливающегося действия составляющих двухкоординатного кинематического ударного механического нагружения на амплитуды колебаний объекта в контрольных точках, формализованные на базе двухпараметрических амплитудно-скважностно-временных характеристик.

Методика. Исследования базируются на фундаментальных подходах прикладной механики, теории моделирования и виброненадежности. Заданными параметрами являются инерционные, диссипативные и упругие характеристики объекта испытаний, координаты его контрольных точек, а варьируемыми – временные параметры двухмерного внешнего механического ударного воздействия, конструктивные параметры несущей

конструкции, а также самого объекта и его заданных контрольных точек.

Результаты. Введены коэффициенты влияния параметров двухкоординатного ударного воздействия при испытаниях объектов пространственной структуры на виброненадежность, установлена зависимость величин и знаков градиентов изменения указанных коэффициентов от конструктивных параметров несущей конструкции, объекта испытаний и геометрических координат контрольной точки на объекте и несущей конструкции (например, платформе многокоординатного вибростенда).

Научная новизна. Впервые для объектов пространственной структуры на базе двухпараметрических амплитудно-скважностно-временных характеристик установлены качественная и количественная закономерности зависимости коэффициентов влияния от параметров внешнего двухкоординатного механического нагружения, объекта испытаний и несущей конструкции. В качестве меры взаимоусиливающегося действия параметров двухкоординатного ударного нагружения предложено использовать коэффициенты влияния, формализованные через амплитуды, длительность и межкоординатное временное запаздывание ударных воздействий.

Практическая значимость. Рассматриваемые ударные воздействия на практике приводят к отказам реальных объектов горного машиностроения, авиационной, транспортной и космической техники по устойчивости функционирования и прочности. Для конкретных узлов машин полученные результаты используются при определении нормативного режима стендовых механических испытаний на многокоординатное ударное воздействие, что повышает долговечность и надежность объекта в эксплуатации.

Ключевые слова: *двухкоординатное ударное нагружение, виброненадежность, динамика узлов машин*

Рекомендовано до публікації докт. техн. наук В. І. Самусею. Дата надходження рукопису 12.11.15.

UDK 62-83:621.313.323

**O. Beshta¹, Korrespondierendes Mitglied der Nationalakademie der Wissenschaften der Ukraine, Dr. Sc., Prof.,
E. Nolle², Dr.-Ing., Prof.,
M. Kuvaiev¹**

1 – Nationale Bergbauuniversität, Dnipro, Ukraine, e-mail: beshtaa@nmu.org.ua; mykola.kuvaiev@ukr.net
2 – Hochschule Esslingen, Goeppingen, Bundesrepublik Deutschland, e-mail: Eugen.Nolle@hs-esslingen.de

ENTWURF EINER EINFACHEN UND MODIFIZIERTEN RASTMOMENTKOMPENSATION FÜR DIE PERMANENTERREGTE SYNCHRONMASCHINE

**O. Beshta¹, Corresponding Member of the National Academy of Sciences of Ukraine, Dr. Sci. (Tech.), Prof.,
E. Nolle², Dr.-Ing., Prof.,
M. Kuvaiev¹**

1 – State Higher Educational Institution “National Mining University”, Dnipro, Ukraine, e-mail: beshtaa@nmu.org.ua; mykola.kuvaiev@ukr.net
2 – Hochschule Esslingen (University of Applied Sciences), Goeppingen, Federal Republic of Germany, e-mail: Eugen.Nolle@hs-esslingen.de

THE DEVELOPMENT OF THE SIMPLE MODIFIED CONTROL LAW FOR THE COMPENSATION OF THE COGGING TORQUE IN THE SYNCHRONOUS MOTOR WITH PERMANENT MAGNETS

**O. С. Бешта¹, член-кор. НАН України, д-р
техн. наук, проф.,
О. Нолле², д-р-інж., проф.,
М. В. Куваєв¹**

1 – Державний вищий навчальний заклад „Національний гірничий університет“, м. Дніпро, Україна, e-mail: beshtaa@nmu.org.ua; mykola.kuvaiev@ukr.net
2 – Есслінгенський університет прикладних наук, м. Гьоппінген, Федеративна Республіка Німеччина, e-mail: Eugen.Nolle@hs-esslingen.de

РОЗРОБКА ПРОСТОГО МОДИФІКОВАНОГО ЗАКОНУ КОМПЕНСАЦІЇ ЗУБЦЕВОГО МОМЕНТУ СИНХРОННОЇ МАШИНИ З ПОСТІЙНИМИ МАГНІТАМИ

Ziel. Entwicklung einer einfachen und modifizierten Rastmomentkompensation für eine Transversalflussmaschine (TFM), die als Sonderbauform der permanenterregten Synchronmaschine (PMSM) zum Direktantrieb für C-Pressen in der Servo-Direkt-Technologie eingesetzt werden soll.

Methode. Nachfolgend werden Möglichkeiten der Rastmomentreduzierung vorgestellt, bei der man die Rastmomente durch eine geeignete Stromvorgabe reduziert bzw. weitgehend vermeidet.

Ergebnisse. Alternativ wird sowohl eine einfache als auch eine verbesserte, modifizierte Rastmomentkompensation für die TFM bzw. allg. für PMSM entwickelt.

Neuheit. Entworfen wird eine drehzahlabhängige Rastmomentkompensation, unter Berücksichtigung des Amplitudenverhältnisses und der Phasenverschiebung zwischen dem Kompensationsstromsignal und dem Drehmoment.

Vorteile, Anwendung. Verbesserung der Qualität bei Stanz- und Umformprozessen.

Stichworte: *permanenterregte Synchronmaschine, Transversalflussmaschine, Rastmoment, Drehmomentwelligkeit, Rastmomentkompensation, Amplitudenverhältnis, Phasenverschiebung*

Aufgabenstellung. Für eine neue Generation von Servopressen in der sog. Servo-Direkt-Technologie benötigt der Hersteller von Pressen möglichst kompakte, hochdynamische und hochüberlastbare elektrische Direktantriebe mit exzellentem Wirkungsgrad. Dazu werden bisher konventionelle permanenterrege, wassergekühlte Synchronmaschinen zugekauft und eingesetzt.

Der Pressenantrieb arbeitet dabei mit einer vorgegebenen variablen Belastung. Eine Momentwelligkeit des Antriebes kann sich daher nachteilig auf die Qualität des Umformprozesses auswirken. Eine Ursache für diese Drehmomentwelligkeit bei elektrischen Maschinen mit Permanentmagnetregung ist das Rastmoment. Dieses entsteht u. a. durch das Zusammenwirken des magnetischen Rotorfeldes mit dem Statoreisen. Je stärker daher das Rotormagnetfeld ist, desto größer kann auch der Spitzenwert des überlagerten Rastmomentes werden.

Dieses Rastmoment ist bei TFM, als Folge des dort starken Rotormagnetfeldes, oft sehr groß und die Auswirkungen sind insbesondere bei Direktantrieben mit ihrer typisch kleinen Drehzahl besonders störend.

Hauptteil. Zwar kann man das Rastmoment durch konstruktive Änderungen (z. B. eine andere Zahn- oder Magnetform, durch optimale Statorzahn- bzw. Magnetzahlen, etc.) reduzieren, was aber oft zu einem erhöhten Herstellungsaufwand und somit zu höheren Motorkosten führt. Daher wird hier nachfolgend eine andere Möglichkeit der Rastmomentreduzierung untersucht, bei der man deren Entstehung z. B. durch eine geeignete Stromvorgabe vermeidet [1, 2].

In [1] wurde die Einführung einer einfachen und modifizierten Rastmomentkompensation allg. für die permanenterrege Synchronmaschinen untersucht.

Darin wird gezeigt, dass der Verlauf des Rastmomentes bei PMSM allg. ausreichend genau mit Hilfe von FEM-Simulationen bestimmen werden kann.

Der so mittels 3D-FEM berechnete Verlauf des Rastmomentes für eine TFM ist in Bild 1 dargestellt.

Aus dem zeitlichen Verlauf des Rastmomentes nach Bild 1 lässt sich dann mit Hilfe einer Frequenzanalyse dessen Frequenzspektrum bestimmen. Diese Frequenzanalyse kann in Maxwell automatisch durchgeführt werden. Mit den so bekannten Werten der Amplituden und Phasen lässt sich der Verlauf des Rastmomentes schließlich als Fourier-Reihe (1) darstellen

$$M_R = M_{R0} + M_{R1} \cdot \cos(\theta_{el} + \gamma_1) + M_{R2} \cdot \cos(2 \cdot \theta_{el} + \gamma_2) + \dots + M_{Rk} \cdot \cos(k \cdot \theta_{el} + \gamma_k) + \dots, \quad (1)$$

wobei $M_{R0}, M_{R1}, \dots, M_{Rk}$ – die Amplituden und $\gamma_1, \dots, \gamma_k$ – die Phasen der Rastmomentharmonischen angeben; θ_{el} – der elektrische Winkel.

Bei der Rastmomentkompensation nach [1] mit Hilfe des Steuerungssystems wird ein geeigneter Hilfsstrom i_{qkom} zum Hauptstrom i_q vor dem Stromregler addiert, der die gleichen maßgeblichen Harmonischen wie das Rastmoment aufweist (Bild 2)

$$i_q^* = i_q + i_{qkom}. \quad (2)$$

Dieses Kompensationsstromsignal i_{qkom} wird dann auf den Eingang des Stromreglers gelegt, so dass die Simulation des Systems jetzt mit dieser Korrektur durchgeführt wird.

Die Ergebnisse dazu sind für die Bemessungsdrehzahl $n_N = 40$ U/min in Bild 3, a, und für eine kleine Drehzahl $n = 1$ U/min in Bild 3, b dargestellt.

Häufig bewertet man die Qualität eines Antriebes anhand der Drehmomentschwingungen, da deren Amplituden und Verläufe oftmals weitgehend von der Drehzahl unabhängig sind.

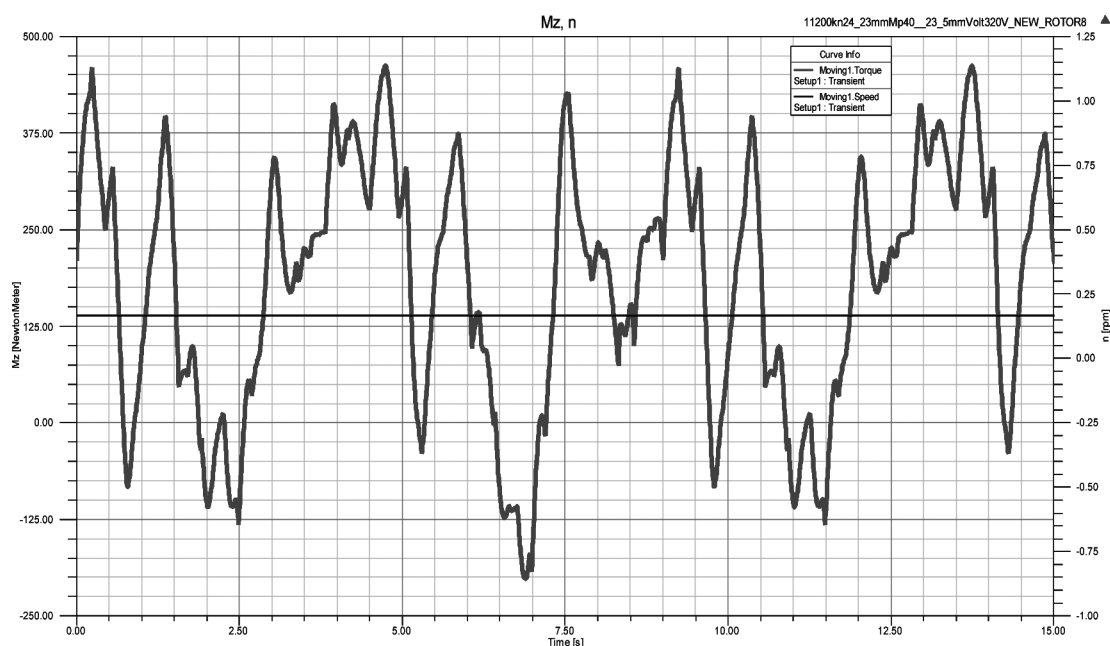


Bild 1. Mit Maxwell berechnetes Rastmoment einer TFM

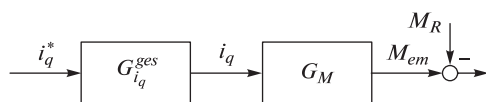


Bild 2. Strukturschaltbild des Glieds $G_{i_q}^{ges}$ und G_M :

$G_{i_q}^{ges}$ – die Übertragungsfunktion des geschlossenen Stromregelkreises und G_M – die Übertragungsfunktion für das Drehmoment

Dies zeigt sich auch bei einem Vergleich der Verläufe in den Bildern 3, a und 3, b bis jeweils 1,5 s, die sich mit dem überlagerten Rastmomentverlauf nach Bild 1 ja auffallend ähneln.

Allerdings weist dabei das maximale Rastmoment mit 450 Nm noch etwa 4 % des Bemessungsdrehmomentes auf, sollte aber laut Vorgabe des Anwenders hier 2 % des Arbeitsdrehmomentes nicht überschreiten. Dabei muss man noch berücksichtigen, dass das Arbeitsdrehmoment des Pressenantriebes betriebsbedingt (durch unterschiedliche konkrete Umformaufgaben) auch kleiner als das Bemessungsdrehmoment sein kann, wodurch sich die prozentualen Schwingweiten dann noch zusätzlich vergrößern.

Mit der einfachen Rastmomentkompensation halbiert sich etwa die Schwingungsamplitude des Drehmomentes bei Bemessungsdrehzahl nach Bild 3, a durch den Kompensationsstrom i_{qkom} und bei der kleinen Drehzahl nach Bild 3, b werden die Schwingungen praktisch vollständig eliminiert.

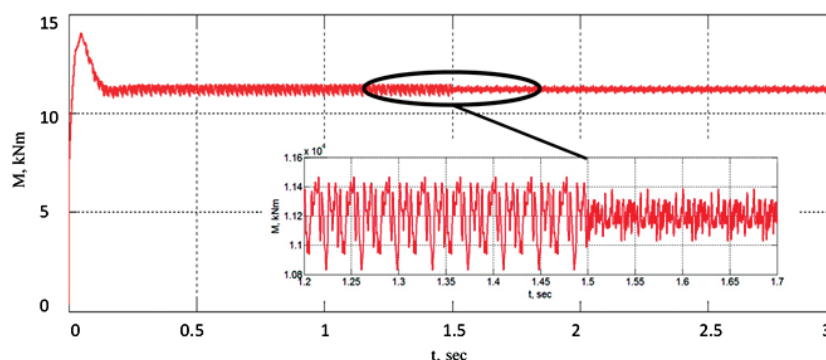
Das Ergebnis dieser Simulation, wie auch entsprechende Untersuchungen in [2] zeigen, dass die Wirksamkeit des Kompensationsstromes i_{qkom} drehzahlabhängig ist. Offensichtlich kompensiert dieser das Rastmoment besser bei kleiner Drehzahl, was eine Folge des aperiodischen Gliedes in der Übertragungsfunktion $G_{i_q}^{ges} \cdot G_M$ ist. Dieses bedeutet, dass sich das Amplitudenverhältnis und die Phasenverschiebung beim Übertragungsglied $G_{i_q}^{ges} \cdot G_M$ mit zunehmender Frequenz deutlich vergrößern.

Die Amplituden der Harmonischen des Hilfsstromes bestimmt man aus dem Amplitudenverhältnis mit Hilfe des Übertragungsgliedes [3, 4], wobei dieses Verhältnis zwischen dem Eingangs- und Ausgangssignal frequenzabhängig ist. Dabei kann man die Amplitude der n-ten Stromharmonischen (Stromwelle) i_{qkom-n} durch die entsprechende Rastmomentharmonische (Rastmomentwelle) M_{R-n} mit der nachfolgenden Formel berechnen

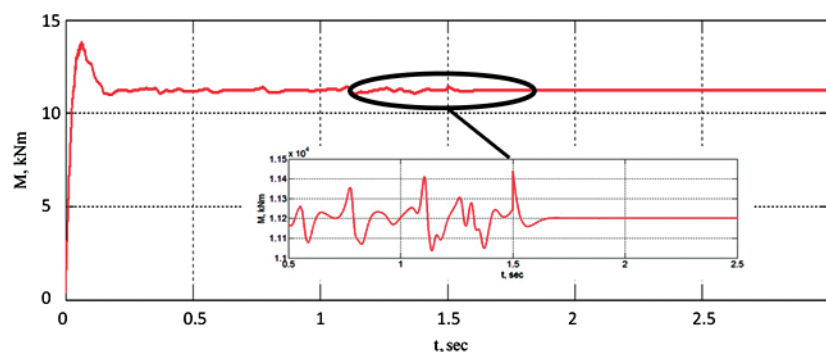
$$i_{qkom-n} = \frac{M_{R-n}}{A(\omega_{e-n})}, \quad (3)$$

mit $A(\omega_{e-n})$ – als Amplitudenverhältnis der n-ten Harmonischen und ω_{e-n} – als deren Eckfrequenz (Kreisfrequenz).

Dazu muss man zunächst die Übertragungsfunktion des Übertragungsgliedes bestimmen, wobei die Stromvorgabe i_{qkom} die Eingangsgröße und das Rastmoment M_R die Ausgangsgröße darstellt. Dazu werden aus dem



a



b

Bild 3. Simulierte Drehmomentverläufe eines TFM-Pressenantriebes bei a Bemessungsdrehzahl 40 U/min und b kleiner Drehzahl 1 U/min mit einfacher Rastmomentkompensation ab 1,5 s

Blockdiagramm in Bild 2 die Übertragungsfunktionen des geschlossenen Stromregelkreises $G_{i_q}^{ges}$ und die Übertragungsfunktion G_M verwendet.

Dieser geschlossene Stromregelkreis wird dann mit Hilfe des Betragsoptimums optimiert, wobei für $G_{i_q}^{ges}$ gilt

$$G_{i_q}^{ges} = \frac{1}{2 \cdot T_\mu^2 \cdot s^2 + 2 \cdot T_\mu \cdot s + 1}, \quad (4)$$

mit T_μ – als kleinster (nichtkompensierter) Zeitkonstante.

Dabei hat die Übertragungsfunktion G_M die Form

$$G_M = \frac{3}{2} \cdot p \cdot \Psi_{pm}, \quad (5)$$

wobei Ψ_{pm} – den verketteten magnetischen Fluss der Permanentmagnete und p – die Polpaarzahl angibt.

Aus den Gleichungen (4) und (5) folgt so für die benötigte Übertragungsfunktion

$$G_{i_q}^{ges} \cdot G_M = \frac{\frac{3}{2} \cdot p \cdot \Psi_{pm}}{2 \cdot T_\mu^2 \cdot s^2 + 2 \cdot T_\mu \cdot s + 1}. \quad (6)$$

Damit wird z. B. das Amplitudenverhältnis der Übertragungsfunktion (6) für die Grundwelle definiert

$$A(\omega_{e-1}) = \frac{\frac{3}{2} \cdot p \cdot \Psi_{pm}}{\sqrt{1 + 4 \cdot T_\mu^4 \cdot \omega_{e-1}^4}}. \quad (7)$$

Analog werden dann auch die Amplitudenverhältnisse der Übertragungsfunktionen für die anderen Harmonischen (Oberwellen, bei deren Frequenz) bestimmt. Die Ströme i_{qkom} zur Kompensation der Rastmomente müssen dann noch um 180° elektrisch (π , gegenphasig) gegenüber den Rastmomentanteilen M_R verschoben werden.

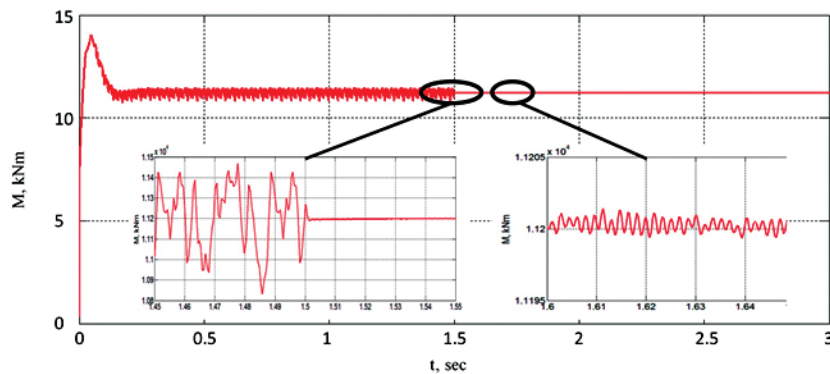
Diese Phasenverschiebung vergrößert sich deutlich beim Übertragungsglied $G_{i_q}^{ges}$ mit zunehmender Frequenz. Besonders starken Einfluss hat diese Phasenverschiebung bei den Oberwellen (höhere Harmonische), deren Frequenz (8) ja das n-fache der Grundwellenfrequenz aufweist

$$\omega_{e-n} = n \cdot \omega_{e-1}, \quad (8)$$

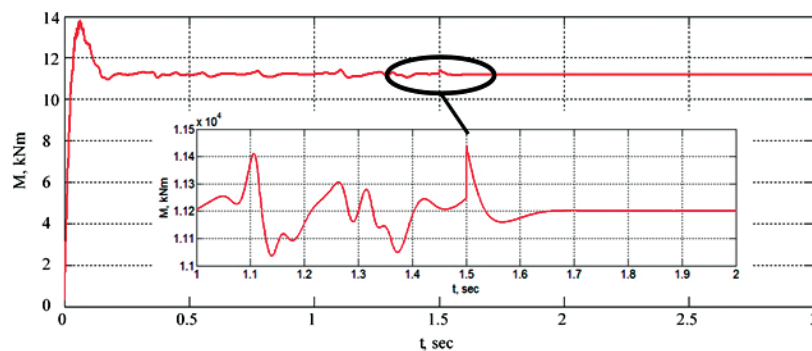
wobei n – die Ordnungszahl der betreffenden Oberwelle ist.

Damit kann die Phasenverschiebung (9) für jede einzelne Welle mit ihrer eigenen Frequenz angegeben werden, wobei nach der Steuerungstheorie [3] gilt

$$\varphi_n(\omega_{e-n}) = -\arctan \frac{2 \cdot T_\mu \cdot \omega_{e-n}}{(1 - 2 \cdot T_\mu^2 \cdot \omega_{e-n}^2)}, \quad (9)$$



a



b

Bild 4. Simulierte Drehmomentverläufe eines TFM-Pressenantriebs bei a Bemessungsdrehzahl 40 U/min und b kleiner Drehzahl 1 U/min mit modifizierter Rastmomentkompensation ab 1,5 s durch Berücksichtigung der Phasenverschiebung

mit $\varphi_n(\omega_{e-n})$ – als Phasenverschiebung der n-ten Oberwelle.

Auf diese Weise werden die Phasenverschiebungen der Übertragungsfunktion für alle Harmonischen (Oberwellen) berechnet. Zur Kompensation müssen die Kompensationsstromwellen i_{qkom-n} (10) dann den entsprechenden Rastmomentwellen M_{R-n} (1) um den zuvor berechneten Phasenverschiebungswert $\varphi_n(\omega_{e-n})$ voreilen

$$i_{qkom} = \frac{M_{R-1}}{A(\omega_{e-1})} \text{pos}(\theta_{el} + \gamma_1 + -\varphi_1(\omega_{e-1})) + \frac{M_{R-2}}{A(\omega_{e-2})} \text{pos}(2 \cdot \theta_{el} + \gamma_2 + -\varphi_2(\omega_{e-2})) + \dots + \frac{M_{R-k}}{A(\omega_{e-k})} \text{pos}(k \cdot \theta_{el} + \gamma_k + -\varphi_k(\omega_{e-k})) \dots \quad (10)$$

Mit diesem modifizierten Kompensationsstromsignal i_{qkom} nach (10) wird das System erneut simuliert. Die diesbezüglichen Ergebnisse sind in Bild 4, a (wieder für die Bemessungsdrehzahl $n_N = 40$ U/min) und in Bild 4, b (für die kleine Drehzahl $n = 1$ U/min) dargestellt, wobei die anderen Simulationsbedingungen ungeändert, wie bei den früheren Simulationen, gewählt sind.

In beiden Bildern sind die Verbesserungen durch die modifizierte Rastmomentkompensation M_R ab dessen Zuschaltung bei 1,5 s deutlich zu erkennen, was besonders bei Antrieben mit variabler Drehzahl wichtig ist.

Trotzdem sind auch dabei noch kleine Schwingungen möglich, da das aperiodische Glied $G_{i_q}^{ges} \cdot G_M$ hier wie ein Filter wirkt und deshalb die Oberwellen zur Kompensation bei höheren Drehzahlen, etwa ab der Ordnungszahl 20, infolge der dann sehr hohen Frequenz nicht übertragen werde.

Fazit. Im Rahmen einer Promotion an der NBU und der Hochschule Esslingen wurde, als eingebettete Teilaufgabe, sowohl eine einfache als auch eine modifizierte Rastmomentkompensation für TFM bzw. allg. PMSM entwickelt.

Mit der modifizierten Kompensation des Rastmomentes reduzieren sich die Momentenschwingungen auch bei hohen Drehzahlen (Bemessungsdrehzahl) auf unter 2 % und somit auf hier zulässige Werte. Bekanntlich werden die Schwingungen dann mit abnehmender Drehzahl noch kleiner und bei kleinen Drehzahlen daher wieder fast vollständig kompensiert.

Zusammenfassung. Transversalflussmaschinen als besondere Ausführung der permanentenregten Synchronmaschinen weisen oft ein großes Rastmoment auf, das sich sehr nachteilig auf die Regelgenauigkeit des Drehmomentes auswirken kann. Dieses Rastmoment bestimmt dann oft wesentlich die Drehmomentwelligkeit des Antriebes, welche oft zu Nachteilen, wie z. B. Vibrationen, Geräuschen etc., bei der Anwendung führt. Daher wurde in dieser Arbeit sowohl eine einfache als auch eine modifizierte Rastmomentkompensation zur Reduzierung bzw. Vermeidung der

Drehmomentwelligkeit allg. bei PMSM entwickelt. Dieses Verfahren wurde beispielhaft für den TFM-Direktantrieb einer C-Pressen in der Servo-Direkt-Technologie untersucht und hier mit konkreten Zahlenwerten vorgestellt.

Literatur/Список літератури

1. Nolle, E., Beshta, O. and Kuvaiev, M., 2015. Compensation of the cogging torque by means of control system for transverse flux motor. In: Power Engineering Control and Information Technologies in Geotechnical Systems. CRC Press/Balkema, Taylor & Francis Group, Leiden, The Netherlands, annual publication, pp. 21–25.
2. Bakutin, A., 2015. The electromechanical system of the turning machine tool. In: Power Engineering Control and Information Technologies in Geotechnical Systems. CRC Press/Balkema, Taylor & Francis Group, Leiden, The Netherlands, annual publication, pp. 201–210.
3. Schröder, D., 2009. Elektrische Antriebe – Regelung von Antriebsystemen. 3rd ed. Berlin; Heidelberg: Springer.
- Schroeder, D., Electric drives – Control of drive systems. Edition 3, Berlin, Heidelberg, Springer, 2009.
4. Bessekерskij, V. and Popov, E., 2003. Teoriia avtomaticheskogo upravleniia [Theory of automatic control]. Saint Petersburg: Professija.
- Бессекерский В.А. Теория систем автоматического управления / Бессекерский В.А., Попов Е. П. – СПб.: „Профессия“, 2003. – 752 с.

Purpose. The goal is to synthesize a simple way to suppress the cogging torque in the transverse flux motor (TFM), which is a special type of the synchronous motor with permanent magnet. This TFM is meant to be used in direct drive of the C-Press with ServoDirekt-technology.

Methodology. To justify the opportunity of the cogging torque compensation via a special harmonic component of stator current.

Findings. The simple modified way of the cogging torque compensation for transverse flux motor and the synchronous motor with permanent magnet has been proposed, which minimizes ripples of the torque in broad spectrum of the operation speeds.

Originality. The presented research shows that compensation of the cogging torque depends on rotation speed of the motor. Therefore the phase delay and the amplitude ratio factor between current reference and the reproduced electromagnetic torque must be taken into account.

Practical value. Using this control law in drive with TFM or another synchronous motor with permanent magnet it is possible to improve the quality of the forming technology.

Keywords: *synchronous motor with permanent magnets, transverse flux machine, cogging torque, the phase delay and the amplitude ratio factor*

Мера. Розробка простого модифікованого закону компенсації зубцевого моменту для елек-

тричної машини з поперечним полем (TFM), що є різновидом синхронної машини з постійними магнітами у складі безредукторного електропривода промислового сервопреса, виконаного за технологією Servo-Direkt.

Методика. Була розглянута можливість компенсації зубцевого моменту шляхом завдання струму необхідної форми.

Результати. Розроблено простий модифікований закон компенсації зубцевого моменту для TFM та для синхронних машин з постійними магнітами, що дозволяє мінімізувати коливання моменту у всьому діапазоні робочих швидкостей електропривода.

Наукова новизна. Встановлено, що компенсація зубцевого моменту повинна залежати від швидкості обертання двигуна. Тому повинні враховуватися модуль та фаза частотної характеристики ланки між вхідним компенсаційним сигналом та моментом.

Практична значимість. Застосування даного закону в електроприводі сервопреса на базі TFM або іншої синхронної машини з постійними магнітами приведе до підвищення якості роботи процесів пресування/кування.

Ключові слова: синхронні машини з постійними магнітами, електрична машина з поперечним полем, зубцевий момент, коливання моменту, модуль та фаза частотної характеристики

Цель. Разработка простого модифицированного закона компенсации зубцевого момента для электрической машины с поперечным полем

(TFM), которая является разновидностью синхронной машины с постоянными магнитами в составе безредукторного электропривода промышленного сервопреса, выполненного по технологии Servo-Direkt.

Методика. Была рассмотрена возможность компенсации зубцевого момента путем задания тока необходимой формы.

Результаты. Разработан простой модифицированный закон компенсации зубцевого момента для TFM и для синхронных машин с постоянными магнитами, который позволяет минимизировать колебания момента во всем диапазоне рабочих скоростей электропривода.

Научная новизна. Установлено, что компенсация зубцевого момента должна зависеть от частоты вращения двигателя. Поэтому должны учитываться модуль и фаза частотної характеристики звена между входным компенсационным сигналом и моментом.

Практическая значимость. Применение данного закона в электроприводе сервопреса на базе TFM или другого синхронного двигателя с постоянными магнитами приведет к повышению качества процессов пресования/ковки.

Ключевые слова: синхронные машины с постоянными магнитами, электрическая машина с поперечным полем, зубцевой момент, колебания момента, модуль и фаза частотної характеристики

Рекомендовано до публікації докт. техн. наук В. І. Корсунем. Дата надходження рукопису 27.01.16.

UDC 621.313

M. Zagirnyak¹, Dr. Sc. (Tech.), Prof.,
 V. Prus¹, Cand. Sc. (Tech.), Assoc. Prof.,
 I. Kushch¹,
 D. Miljavec², Dr. Sc. (Tech.), Prof.

1 – Kremenchuk Mykhailo Ostrohradskyi National University, Kremenchuk, Ukraine, e-mail: mzagirn@kdu.edu.ua
 2 – University of Ljubljana, Ljubljana, Slovenia

FEATURES OF MODELING OF ELECTROMAGNETIC FIELD OF ELECTRIC MACHINES WHEN MAGNETIC SYSTEM PROPERTIES CHANGE

М. В. Загірняк¹, д-р техн. наук, проф.,
 В. В. Прус¹, канд. техн. наук, доц.,
 І. А. Куш¹,
 Д. Мілявець², д-р техн. наук, проф.

1 – Кременчуцький національний університет імені Михайла Остроградського, м. Кременчук, Україна, e-mail: mzagirn@kdu.edu.ua
 2 – Університет Любляни, м. Любляна, Словенія

ОСОБЛИВОСТІ МОДЕЛЮВАННЯ ЕЛЕКТРОМАГНІТНОГО ПОЛЯ ЕЛЕКТРИЧНИХ МАШИН ПРИ ЗМІНІ ВЛАСТИВОСТЕЙ МАГНІТНОЇ СИСТЕМИ

Purpose. Determination of particular features of electric machines electromagnetic field modeling when the change of magnetic system properties is caused by the presence of damages of the main types occurring during electric machines long-term operation and repairs.

Methodology. The comparative experimental analysis of changes of the properties of electric machine magnetic systems during their repair and long-term operation is substantiated. Mathematical grounds for influence of magnetic system main faults on electromagnetic field described by Maxwell's equations. Numerical modeling of magnetic field in electric machines with damaged magnetic systems with the finite-element method.

Findings. The principles of modeling electromagnetic field in electric machines with magnetic system damages characterized by considerable error-free running time and subjected to a number of overhauls have been grounded. As a result, the necessity of the use of models of various types for calculation of electromagnetic field, depending on the presence and localization of the main types of magnetic system damages, has been proved. The adequacy of the proposed approach to modeling core defects of DC motors has been confirmed.

Originality. The peculiarities of different types of damages in laminated cores and the ways to take them into account while simulating electric machine electromagnetic field are studied. The ways of solving the mentioned task using the finite element method by the example of computation of the change of vibroexcitation forces caused by the electromagnetic nature in direct current machines are developed.

Practical value. The obtained results make it possible to predict the change of an electromagnetic component of vibration and irregularity of torque distribution of DC motor, caused by laminated core defects. There is also a possibility of estimating the rate of laminated core damage influence on the main IM operating characteristics.

Keywords: *DC motor, defects, laminated core, electromagnetic field*

Introduction. The properties of electric machine (EM) magnetic system change in the process of their repair and long-term operation [1]. It results in increase in losses, deterioration of EM performance characteristics, variation of thermal and vibration operating conditions [2]. A similar problem occurs when improper magnetic materials are used in EM designs, which has been typical of the electric machine industry in the recent years. The analysis of processes in EM as a rule is based on the electric circuit theory and implies the use of equivalent circuits. Equivalent circuit parameters contain implicit information about the design and the connecting circuit of the machine windings, configuration of magnetic system, etc. However, these methods are based on a number of simplifications, which considerably affects the calculation accu-

racy. The calculation of EM parameters using electromagnetic field analysis is an alternative for such methods [3].

Magnetic field research is the most informative approach to taking magnetic system properties variation into consideration. However, estimation of influence of EM magnetic system condition on electromagnetic field is a complicated scientific and practical problem. Taking into account the nonlinearity of magnetic parameters dependences and nonuniformity of their distribution, as well as magnetic material saturation rate for existing geometry of magnetic systems is only possible when numerical methods are used. The performed analysis resulted in the substantiation of the possibility of determining EM main parameters and characteristics in the process of their modeling by creating models based on the finite element method (FEM).

The purpose of the paper consists in determining particular features of EM electromagnetic field modeling when the change of magnetic system properties is caused by the presence of damages of the main types occurring during EM long-term operation and repairs.

Presentation of the main research and explanation of the results. Laminated cores of stator, rotor, armature, poles, etc. are magnetic system components of most EMs. The earlier research revealed the necessity of taking into account the variation of their properties both for the whole cores and locally for their different sections.

Variations of core properties on the whole can be explained by their heating and reversal magnetization influence on the main electric and magnetic parameters during operation. As a rule, these parameters deteriorate when the operation time increases, which can be explained by electrical steel ageing. Admissible parameter variations are usually normalized by corresponding standards. Ageing processes are considerably intensified during repairs of electric machines. This is mainly explained by the repair technology itself. So, when windings are removed during an overhaul, the cores are annealed in a furnace at the temperature of 400 °C for 4 hours.

Fig. 1 shows technical magnetization curves $B_m = f(H)$ for electrical steel of 1211 type before and after a number of annealings, Fig. 2 contains curves of steel losses $P_{st} = f(B_m)$ (the curve before annealing is designated by number 1, the curves after the 1st – 3d annealings – by numbers 2–4 correspondingly). The results were obtained for rectangular laminated samples with the use of Epstein’s device.

It can be seen in Figs. 1–2 that steel thermal annealing results in: first, the magnetic induction value at which steel saturation takes place reduces; second, steel losses increase.

Steel properties deteriorate uniformly after the first and the second annealing. So, if the initial magnetization curve for unannealed steel (curve 1, Fig. 1) is considered to be the reference, for the saturation point, when intensity is $H = 741.861$ A/m, magnetic induc-

tion decreases by 2.57 and 5.21 %, respectively. After the third annealing there occurs a sudden change in properties deterioration (induction decreases by 9.35 % in relation to the initial curve). In this case steel losses growth occurs in the following way. After the first and the second annealing normal condition steel losses (magnetization curve operating point $H = 741.861$ A/m, $B_m = 0.824$ T) increase by 4.14 and 7.81 %, respectively, and after the third annealing – only by 5.94 % in relation to the initial value, which is difficult to provide a logical explanation for.

If supply voltage is constant, in case of annealed steel, increased current consumption is observed, which results in the shift of operating point at the magnetization curve into the saturation zone. So, for rated voltage, at which the operating point for unannealed steel is located on the bend of the magnetization curve (point A, Fig. 1), due to current growth and, consequently, magnetic intensity, by 4.01, 8.41 and 21.59 %, respectively, the values of induction, less than the initial rated one by 1.59, 3.35 and 4.7 %, respectively, (points B, C and D in Fig. 1) correspond to operating points for annealed steel. When the values of losses were corrected in relation to new operating points, their values exceeding the value of losses in point A by 7.29, 14.72 and 24.86 %, respectively, were obtained (Fig. 2).

These results can be explained by comparing them with variation of properties of sheet electrical steel, which is known from literature. On this ground the mentioned variations can be accounted for by the growth of eddy currents in the cores steel due to deterioration of the properties of intersheet insulation covering under thermal action. Besides, the variation of magnetic circuit saturation rate is evident, which is to be properly taken into account in calculation models.

Alongside with this, in particular cases, there can be observed general slackening of core pressing caused by both destruction of intersheet insulation and worsening of the core fit on the body or on the shaft. The mentioned variations result in the growth of the core

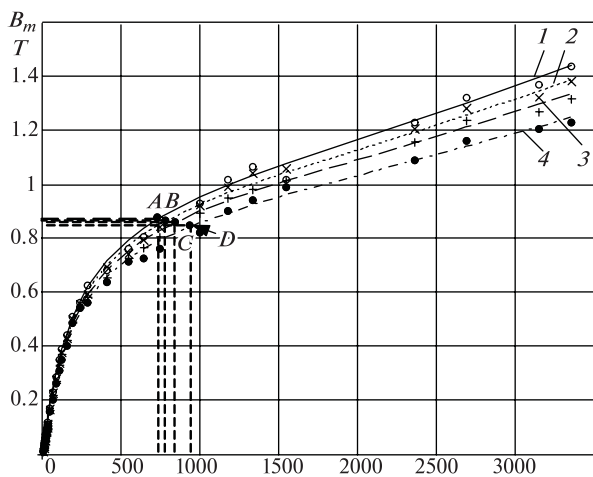


Fig. 1. Technical magnetization curves $B_m = f(H)$ of 1211 type steel

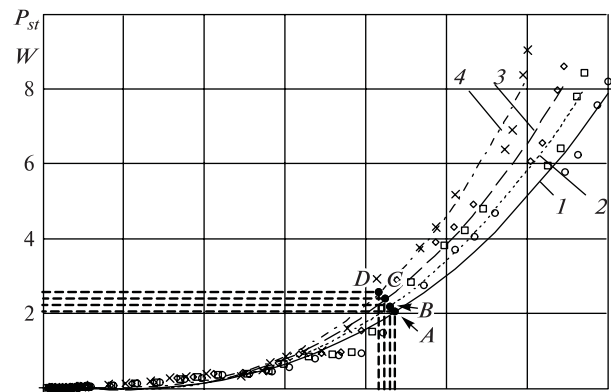


Fig. 2. Curves of losses $P_{st} = f(B_m)$ in 1211 type steel at successive annealings at the temperature of 400 °C

magnetic reluctance, thereby reducing the main flux. It causes decrease in the moment on IM shaft.

The considered local core damages include crushing of top part of the teeth zone and shorting of electrical steel sheets [4]. All these damages mainly influence the variation of magnetic and electric parameters of magnetic system sections in the axial and radial directions.

Decrease in magnetic induction at such sections may reach 7–10 %, increase in magnetic intensity – 60–70 %, growth of steel losses – up to 50 %.

The results of EM research by field methods confirm the efficiency of the use of application packages based on the finite element method [5, 6] for solution of such problems.

To choose the type of the created field model rationally it is necessary to analyze the kind and location of core damages. For the case of uniform variation of magnetic parameters along the EM core, sufficient accuracy of the analysis results is provided by a 2D model of calculation of the electromagnetic field in the cross section of the active zone. Variation of parameters in the axial direction is caused by damages along the core (pressing slackening, lengthwise teeth shortening).

To determine integral values of a torque moment, research of the influence of axial redistribution of vibroexciting forces, when vibroparameters are calculated, as well as winding temperature ununiform distribution caused by local exceed of steel losses, it is necessary to use 3D models.

Modeling was performed on the basis of Maxwell equations supplemented with material properties coupling equations describing its behavior in electromagnetic field [7]. Simplified coupling equations are of the form

$$\vec{\delta}_{con} = \gamma \vec{E};$$

$$\vec{H} = \vec{v}_a (\vec{B} - \vec{B}_r) + q_1 \frac{\partial}{\partial t} (\vec{B} - \vec{B}_r) - q_2 \frac{\partial^2}{\partial t^2} (\vec{B} - \vec{B}_r),$$

where $\vec{\delta}_{con}$ is conduction current density; γ is material electric conductivity; \vec{E} is a vector of electric field strength; \vec{H} is a vector of magnetic intensity; \vec{v}_a is velocity vector field; \vec{B} is a vector of magnetic induction; \vec{B}_r is a vector of residual magnetic induction; q_1, q_2 are dynamic indices of laminated material electrophysical parameters, that are determined from equations

$$q_1 = (1/12)\Delta^2 \gamma_{el}; \quad (1)$$

$$q_2 = (1/720)\Delta^4 \mu_{max} \gamma_{el}^2. \quad (2)$$

In (1–2) Δ is steel sheet thickness in cores; μ_{max} is absolute magnetic permeability; γ_{el} is sheet material conductivity.

The features of modeling include, first of all, the necessity of taking into consideration all the above considered phenomena: decrease in magnetic induction B , growth of magnetic intensity H , increase in

steel losses P_{st} , rise of magnetic system saturation rate.

As a first approximation, it is rather simple to solve this problem. With this purpose in view, it is necessary to take into account the fact that the considered variations of magnetic system properties will cause the decrease in active resistance r_μ and reactance x_μ of magnetization circuit. It will result in the increase in IM consumed current. Thus, current cannot be the main invariable parameter in calculations, the value of IM supply voltage is to be used instead, which is easily done in [6].

Then it is necessary to single out the damaged sections in the volume of laminated cores and determine their geometry in the form of closed figures. Variations of magnetic properties are assigned for these sections through real magnetization curves corresponding to the form and rate of damage.

When electric steel sheets of EM laminated cores are short-circuited, the calculation of eddy currents circuits was made on the basis of the analysis of vector magnetic potential distribution

$$\sigma \frac{\partial \vec{A}}{\partial t} + \nabla \times (\mu_0^{-1} \mu_r^{-1} \times \vec{A}) = \vec{J}.$$

Here σ is electric conductivity of the analyzed area; μ_0 – permeability of free space; μ_r is core steel relative permeability; \vec{A} is vector magnetic potential; \vec{J} is external source current density.

Variation of cores electric properties due to eddy currents growth was taken into consideration by steel electric conduction reduction equivalent to eddy EMF growth. Steel losses P_{st} at magnetic circuit sections were determined according to modified Steinmetz equations [6]

$$P_{st} = P_h + P_c + P_e = K_1 B_m^2 + K_2 B_m^{1.5};$$

$$K_1 = k_h f + k_c f^2; \quad K_2 = k_e f^{1.5},$$

where P_h, P_c, P_e are hysteresis, eddy currents and additional losses components, respectively; B_m is amplitude value of magnetic induction component at the alternating current; f is frequency; k_h is coefficient of hysteresis losses; k_c is coefficient of eddy currents losses; k_e is coefficient of additional losses in the core.

Coefficients K_1 and K_2 were calculated according to the losses curve $P_{st} = f(B_m)$ using quadratic minimization function

$$err(K_1, K_2) = \sum_i [P_{sti} - (K_1 B_{mi}^2 + K_2 B_{mi}^{1.5})]^2 = \min,$$

where P_{sti} stands for losses in the i -th point of the curve; B_{mi} – magnetic induction in this point.

With the aim of experimental verification of the above stated provisions, a P–31U4 type direct current motor (DCM) with nominal power of $P_n = 700$ W and nominal rotation frequency of $n_n = 1000$ rpm was taken as the object of modeling.

The influence of four contiguous partially shortened armature teeth was investigated. The teeth were shortened in their upper part along the height of the top from the external end of the core along its full length. The area of shortening across the external surface of the teeth was changed from 25 to 100 % of their total area with 25 % pitch (Fig. 3).

Variation of steel properties was assigned in accordance with the results obtained during local testing of laminated cores in the course of repairs [4] with the help of corrected material magnetization curves and for the whole core – in accordance with the data in Figs. 1–2.

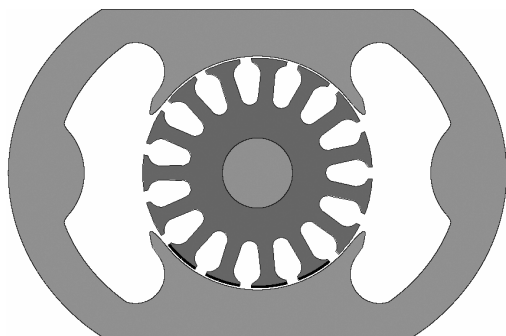


Fig. 3. Model of direct current motor with damaged armature tooth steel

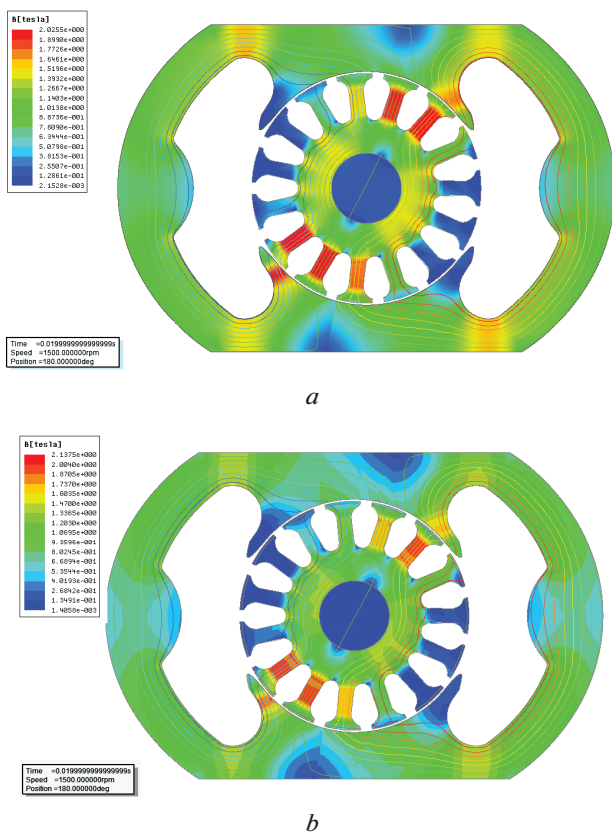


Fig. 4. Distribution of magnetic induction vector \vec{B}, T in DCM with an armature core in normal condition (a) and when 25 % of the upper part of a four armature tooth area is shortened (b)

Modeling results shown in Fig. 4, a, b demonstrated that even insignificant (as to its depth and area) shortening of the armature tooth zone causes reduction of magnetic induction value in the area of damaged teeth by 17–23 %.

This range of magnetic induction variation practically corresponds to the one obtained experimentally for a stalled armature of the investigated DCM (Fig. 5).

The value of magnetic induction was calculated according to the EMF level of the magnetic-test coils put on the investigated armature teeth. The teeth were shortened artificially by grinding. Difference between experimental and calculated data was from 5 to 8 % depending on the area of teeth shortening across the external surface, which confirms the adequacy of the proposed approach to modeling EM core defects.

In addition, the considered armature defects, mainly due to eddy currents from rotary magnetization, cause decrease in torque mean value and its fluctuation at the level of 5–12 % depending on the armature tooth damage rate. Such irregularity of torque distribution may result in deterioration of loaded DCM operation stability, especially in transient conditions.

Distribution of normal component of electromagnetic force (Fig. 6) and variation of torque instantaneous value (Fig. 7), obtained in a different position of the defect area in relation to the main poles of DCM, were investigated on the basis of the developed DCM model with damaged armature core steel.

The obtained results point out a considerable variation (from 20 to 45 %) of the value of electromagnetic force normal component in the area of laminated core defects, which will result in nonuniformity of efforts distribution and growth of vibration electromagnetic component.

Taking into account the calculation features according to [6], similar results can be obtained for the main parameters of any type IM in static and dynamic conditions. There is also a possibility to estimate the

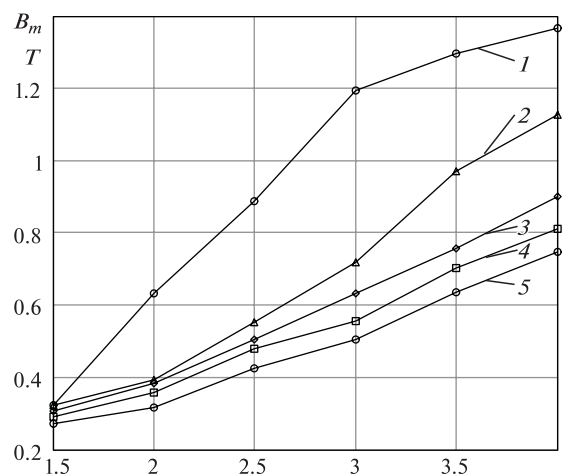


Fig. 5. Magnetic induction B_m, T experimental dependences on the armature current I_a, A :
1 – normal condition of the core; 2–5 – shortening of 25, 50, 75 and 100 % of the tooth surface

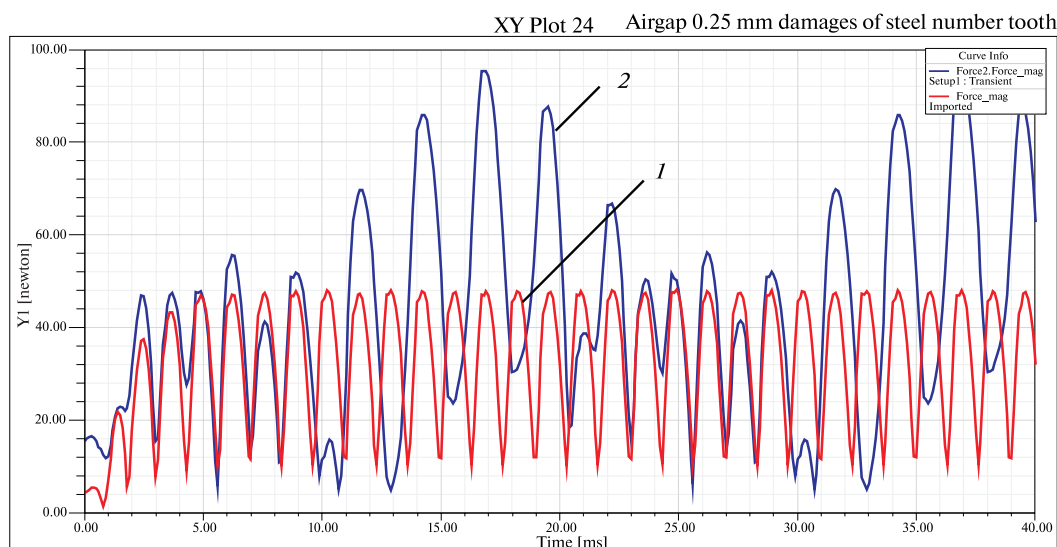


Fig. 6. Distribution of the normal component F_n , N of electromagnetic force in DCM in the function of time t , ms:
 1 – with normal condition of the core; 2 – when the upper part of four teeth is shortened

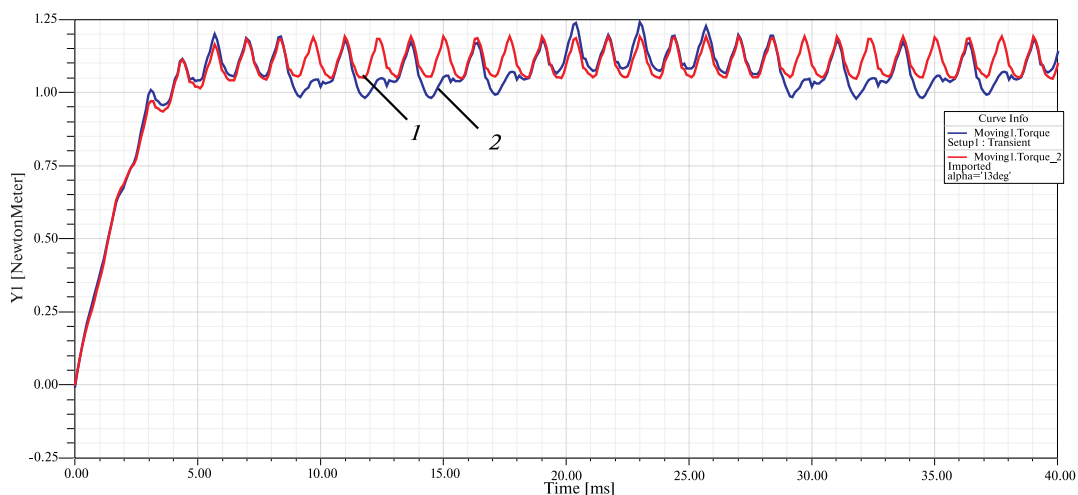


Fig. 7. Variation of the instantaneous value M , Nm of the torque in the function of time t , ms when the armature turns:
 1 – with normal condition of the core; 2 – when the upper part of four teeth is shortened

rate of laminated core damage influence on the main IM operating characteristics.

Conclusions. The particular features of modeling electromagnetic field in EMs with magnetic system damages characterized by considerable error-free running time and subjected to a number of overhauls have been determined. As a result, the necessity of the use of models of various types for calculating electromagnetic field, depending on the presence and localization of the main types of magnetic system damages, has been substantiated. The adequacy of the proposed approach to modeling EM cores defects has been confirmed.

References / Список літератури

1. Zagirnyak, M., Prus, V., Kolotilo, I. and Miljavec, D., 2012. Determination of power indices for a three-phase induction motor with a phase-wound rotor through par-

ticular losses components. *Przegląd Elektrotechniczny (Electrical Review)*, No. 12b, pp. 80–82.

2. Hadziselimovec, M., Marcic, T., Stumberger, B. and Zagradicnik, I., 2011. Winding type influence on efficiency of an induction motor. *Przegląd Elektrotechniczny (Electrical Review)*, Vol. 87, Iss. 3, pp. 61–64.

3. Vaskovskii, Yu. M., 2007. *Poliiovyi analiz elektrychnykh mashyn* [Electric machines field analysis]. Kyiv: NTU “KPI”.

Васьковський Ю. М. Польовий аналіз електричних машин / Васьковський Ю. М. – К.: НТУ „КПІ“, 2007. – 190 с.

4. Prus, V.V., Zagirnyak, M.V. and Nikitina, A.V., 2006. Grounds for Efficiency and Prospect of the Use of Instantaneous Power Components in Electric Systems Diagnostics. *Przegląd Elektrotechniczny (Electrical Review)*, No. 12, pp. 123–125.

5. COMSOL, 2008. *Multiphysics Reference Guide*, Version 3.5a. COMSOL AB.

6. Ansoft Corporation, 2011. *Ansoft Maxwell 3D User's Guide*, Rev 3.0. Pittsburgh: Ansoft Corporation

7. Shmelev, V. E., 2010. *Prostranstvenno-fazovoiye modelirovaniie elektromekhanicheskoho preobrazovaniia energii v apparatahk i mashynakh vraschchatelnogo dvixheniia* [Space-phase modeling of energy electromechanical transformation in rotational motion units and machines] Vladimir: Publishing house of Vladimir State University.

Шмелев В. Е. Пространственно-фазовое моделирование электромеханического преобразования энергии в аппаратах и машинах вращательного движения / Шмелев В. Е. // Владим. гос. ун-т. — Владимир: Изд-во Владим. гос. ун-та, 2010. — 172 с.

Мета. Визначення особливостей моделювання електромагнітного поля електричних машин при зміні властивостей магнітної системи, обумовленому наявністю основних видів пошкоджень, що виникають при тривалій експлуатації та ремонтах електричних машин.

Методика. Порівняльний експериментальний аналіз змін властивостей магнітних систем електричних машин, що виникають у процесі їх ремонту й тривалої експлуатації. Математичне обґрунтування впливу основних видів дефектів магнітної системи на електромагнітне поле, що описується рівняннями Максвелла. Чисельне моделювання електромагнітного поля в електричних машинах із пошкодженнями магнітних систем методом скінчених елементів.

Результати. Обґрунтовані принципи моделювання електромагнітного поля в електричних машинах з пошкодженнями магнітних систем, що характеризуються значним часом наробітку на відмову та рядом проведених капітальних ремонтів. У результаті доведена необхідність використання різних типів моделей для розрахунків електромагнітного поля залежно від наявності й локалізації основних видів пошкоджень магнітної системи. Підтверджена адекватність запропонованого підходу до моделювання дефектів осердь двигунів постійного струму.

Наукова новизна. Розглянуті особливості й запропоновані способи урахування різних видів пошкоджень шихтованих осердь при моделюванні електромагнітного поля електричних машин. Розкриті підходи до розв'язку такого завдання методом скінчених елементів на прикладі розрахунків зміни віброзбуджуючих сил електромагнітного характеру в електричних машинах постійного струму.

Практична значимість. Отримані результати дозволяють прогнозувати зміну електромагнітної складової вібрації та нерівномірність розподілу обертового моменту двигуна постійного струму, викликані ушкодженнями шихтованих осердь. Також існує можливість оцінки ступеня впливу пошкоджень шихтованих осердь на основні робочі характеристики електричних машин.

Ключові слова: *двигун постійного струму, пошкодження, шихтоване осердя, електромагнітне поле*

Цель. Определение особенностей моделирования электромагнитного поля электрических машин при изменении свойств магнитной системы, обусловленном наличием основных видов повреждений, возникающих при продолжительной эксплуатации и ремонтах электрических машин.

Методика. Сравнительный экспериментальный анализ изменений свойств магнитных систем электрических машин, возникающих в процессе их ремонта и продолжительной эксплуатации. Математическое обоснование влияния основных видов дефектов магнитной системы на электромагнитное поле, описываемое уравнениями Максвелла. Численное моделирование электромагнитного поля в электрических машинах с повреждениями магнитных систем методом конечных элементов.

Результаты. Обоснованы принципы моделирования электромагнитного поля в электрических машинах с повреждениями магнитных систем, характеризующихся значительным временем наработки на отказ и прошедших ряд капитальных ремонтов. В результате доказана необходимость использования различных типов моделей для расчета электромагнитного поля в зависимости от наличия и локализации основных видов повреждений магнитной системы. Подтверждена адекватность предложенного подхода к моделированию дефектов сердечников двигателей постоянного тока.

Научная новизна. Рассмотрены особенности и предложены способы учета различных видов повреждений шихтованных сердечников при моделировании электромагнитного поля электрических машин. Раскрыты подходы к решению такой задачи методом конечных элементов на примере расчета изменения вибровозбуждающих сил электромагнитного характера в электрических машинах постоянного тока.

Практическая значимость. Полученные результаты позволяют прогнозировать изменение электромагнитной составляющей вибрации и неравномерность распределения вращающего момента двигателя постоянного тока, вызванные повреждениями шихтованных сердечников. Также существует возможность оценки степени влияния повреждений шихтованных сердечников на основные рабочие характеристики электрических машин.

Ключевые слова: *двигатель постоянного тока, повреждения, шихтованный сердечник, электромагнитное поле*

Рекомендовано до публікації докт. техн. наук В. П. Ляшенком. Дата надходження рукопису 03.07.15.

UDC 621.313.823.2

O. V. Makarchuk, Cand. Sc. (Tech.), Assoc. Prof.

Lviv Polytechnic National University, Lviv, Ukraine, e-mail: oleksandr.v.makarchuk@lpnu.ua

ADDITIONAL LOSSES IN THE STATOR WINDINGS OF THE HIGH-SPEED BRUSHLESS ELECTRICAL MACHINE WITH PERMANENT MAGNETS

О. В. Макаrchук, канд. техн. наук, доц.

Національний університет „Львівська політехніка”, м. Львів, Україна, e-mail: oleksandr.v.makarchuk@lpnu.ua

ДОДАТКОВІ ВТРАТИ У СТАТОРНИХ ОБМОТКАХ ВИСОКОШВИДКІСНИХ БЕЗКОНТАКТНИХ ЕЛЕКТРИЧНИХ МАШИН З ПОСТІЙНИМИ МАГНІТАМИ

Purpose. To propose a method for determining the additional losses in the stator windings of electrical machines, in which the current frequency is significantly higher than the mains frequency.

Methodology. The numerical methods for solving differential equations of mathematical physics are applied for the study. The Finite Element Method is used for algebraization of partial derivatives; an implicit method of backward differentiation formula is used for algebraization of time derivatives while the Newton-Raphson method is applied for solving nonlinear algebraic equations.

Findings. A mathematical model, which allows counting the total losses caused by skin effect in the slot of the stator winding of a high-speed electrical machine, was created. The model takes into account: its own slot leakage flux, the main magnetic flux, a saturation of the magnetic core, various slot forms and the method of electrical connection of conductor strands in the slot. The mathematical formulation and the boundary condition of this problem are offered.

The results of mathematical experiments of defining additional and total losses in the windings located in the half-closed and open slots for high-speed generator with permanent magnet excitation of 200 kW, 50000 rpm, are presented. The cause-and-effect relationships are analyzed. Findings can help while designing such machines.

Originality. The problem of calculating losses is formulated as a 2-dimensional boundary problem of electro-dynamics, which allows us to take into account an interference of the above factors.

Practical value. The necessity for accurate determination of the losses in the phase windings of high-speed machines occurs not only when designing the windings, but also while assessing the thermal condition of such machines.

Keywords: *additional losses, current displacement, skin effect, FEM-analysis, boundary condition, high-speed electrical machine*

If high-speed electrical machines are considered as machines of ultimate power, they may be a sort of production indicators. Therefore, they have been the focus of attention for many researchers, and tasks, associated with their development, are still relevant.

Objectives of the article. The slot effect in stator windings of high-speed permanent magnet electrical machines (HSPMEM) is considerably stronger than that in machines, operating at industrial frequency. Fac-

tors, ignored by classical analytical theory for determination of this phenomenon that was developed by Edme in 1922, have become more critical and change entire picture of nonuniform distribution of current density in the cross section of embedded coil side not only quantitatively but also qualitatively. Increasing losses in the stator winding appear to be a negative consequence of this phenomenon that can challenge the implementation of the project for developing HSPMEM.

Analysis of the recent research. The review of available recent research studies in this field gives evi-

dence of a small number of publications devoted to research of losses in machine stator windings that operate at frequencies that are considerably higher than industrial frequency [1]. Most research studies focus on improvement of the methods for calculation of additional losses in convenient machines of BLDC or PMSM types [2, 3] and asynchronous machines [4, 5]. Some interesting approaches were proposed for calculation of slot effect in transformers and choke coils [6, 7].

Analysis of literature sources allowed distinguishing study methods that are used most frequently for solution of similar tasks on calculation of additional losses in transformers and asynchronous machines. Non-linearity of this task and the need to consider additional critical factors suggests the usefulness of applying numerical methods. The most suitable method for this purpose is the finite element method, used in combination with numerical time integration methods.

Unsolved aspects of the problem. Local saturation of tooth area is caused by the current of the conductor and magnetic field of dissipation as a prime cause of slot effect and the first harmonic field. The higher saturation level is, the larger share of magnetic flow penetrates from the tooth into the slot changing current density redistribution and increasing slot losses.

Considering this fact, we can speak of availability of additional influencing factors such as saturation of the magnetic core and the form of the slot, namely its “opening”. The factor of increasing armature resistance (Field’s factor) is conventionally determined by Edme’s functions obtained due to absence of saturation of tooth area and for open rectangular slots. Moreover, the influence of the first harmonic field is not taken into account.

It should be mentioned that classical approach provides for tandem coupling of coils, but phase coils of HSPMEM are similar as a rule. Therefore, one (for one-layer coils) or two (for two-layer coils) effective conductors, which consist of multiple strands connected in parallel, are located in the slot.

We state that additional losses in armature coils of HSPMEM exceed the main losses. Therefore, a special attention should be paid to their calculation while designing such machines.

Purpose of the study. The aim of this study is to develop methods for calculating additional losses that would consider the main factors influencing slot effect process in their interrelation.

Study object is phase coil, located in the slots of non-salient pole laminated stator of HSPMEM.

Presentation of the main research. We have developed a mathematical model for calculation of additional losses in HSPMEM coil that considers actual distribution of current density vector field in coil conductors, located in ferromagnetic slot of free form and penetrated by external magnetic field of set amplitude. The mode provides for the actual method for coupling of effective conductors and strands in a slot and saturation of the magnetic core. The task is defined in two planes.

The need in determination of the actual current density vector field, induced by this or that method, results in necessity for solving the dynamical problem in terms of field theory.

Poisson’s invariant equation in coulomb calibration for magnetic vector potential is ($\nabla \cdot \bar{A} = 0$)

$$\nabla^2 \bar{A} = \sigma \nabla U + \sigma \frac{\partial \bar{A}}{\partial t} - \bar{v} \times \sigma \nabla \times \bar{A}, \quad (1)$$

where ∇ is a differential Hamiltonian operator; σ is a matrix of electrical conductivity of the medium; \bar{v} is medium velocity vector; U is electrostatic scalar potential of external field.

Current density field will be determined by the following formula

$$\bar{J} = \sigma \left(-\nabla U - \frac{\partial \bar{A}}{\partial t} + [\bar{v} \times \bar{B}] \right), \quad (2)$$

on the basis of which it is possible to state that total current density vector specified in formula (2), consists of three components: the 1st component is conditioned by the external electrical field, the 2nd component is conditioned by the magnetic field that changes in time and the 3d element is conditioned by movement of the conductor at \bar{v} speed in the magnetic field with \bar{B} amplitude.

The equation (1) itself is used for further conversion. Together with boundary conditions, it forms the basis of mathematical formulation of the problem of calculating the dynamic magnetic field, considering electromagnetic and mechanic loads.

It is clear that solution of equation (1) requires integration on the basis of spatial and time coordinates.

The computational domain of this model is represented by tooth separation of the stator core (Fig. 1).

You can see symbols and dimensions of the figure, Boundary conditions are represented by expressions that allow configuring the external magnetic field (the inductor field) so that it corresponds to the vision of possible routes of the field passing through the stator core. The excitation field is determined by linear distribution of vector potential along the upper horizontal line

$$A_z[x, t] \Big|_{y=h_{sc}+\delta} = \frac{B_\delta}{\beta} \sin(\omega t + \beta x + \nu), \quad (3)$$

where $\beta = \pi/\tau$ is a factor of proportionality between coordinates of the point, expressed in angular and linear measurement units; ν is phase shift between the current of the effective conductor and radial component of the vector \bar{B}_δ .

Lines that limit the left and the right edges of computational domain are determined by Dirichlet condition

$$\begin{aligned} A_z[t] \Big|_{x=-0,5\tau_z} &= \frac{B_\delta}{\beta} \sin(\omega t - 0,5\tau_z \beta + \nu); \\ A_z[t] \Big|_{x=0,5\tau_z} &= \frac{B_\delta}{\beta} \sin(\omega t + 0,5\tau_z \beta + \nu). \end{aligned} \quad (4)$$

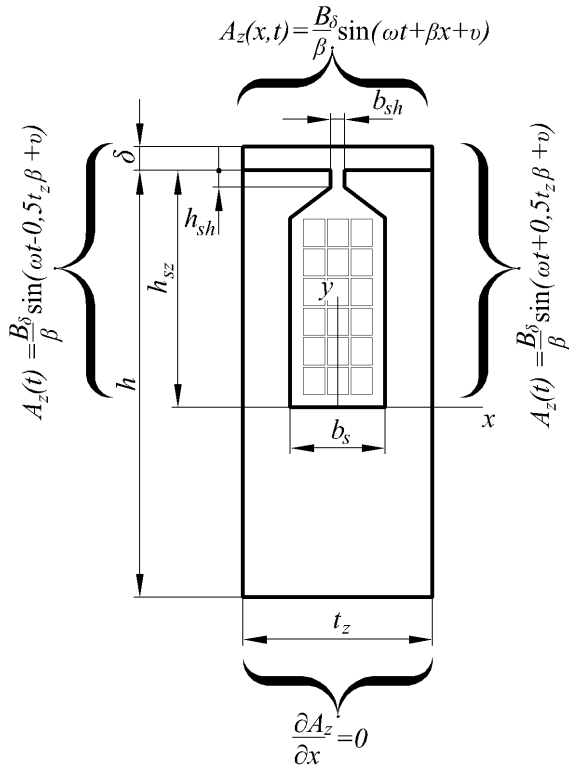


Fig. 1. Computational domain of the model and boundary condition

Lines and outer generating lines of the stator are determined by Neumann condition

$$\left. \frac{\partial A_z}{\partial x} \right|_{y=h_z-h} = 0. \quad (5)$$

Driving forces in this formulation are represented by current of the conductors that are located in the slot and the inductance amplitude is in the air gap.

The equation is written in accordance with the 1st Kirchhoff's law (Fig. 2) in order to determine a method for coupling of strands and effective conductors in the slot before formulating the problem (1)

$$i_\Sigma = \sum_{n=1}^{n_{el}} i_{jn}, \quad (6)$$

where $n = \overline{1, n_{el}}$ is a current number of the strand (n_{el} is a number of strands in effective conductor); i_Σ, i_{jn} are current of effective conductor (set) and strand (initial) that relate to j effective conductor. Thus

$$i_{jn} = \int_S \bar{J} dS = \iint_S J_z[x,y] dx dy = \sum_{e=1}^E \frac{S^{[e]}}{K} \sum_{k=1}^K J_{zk}^{[e]}, \quad (7)$$

where $e = \overline{1, E}$ is a consecutive number of the finite element (FE); $k = \overline{1, K}$ is a consecutive number of the FE node; $S^{[e]}$ is FE area with number $[e]$; $J_{zk}^{[e]}$ is a nodal value of z projection of the current density vector.

Expression (1) along with the circular equation (6) and boundary condition (3–5) expresses the nature of

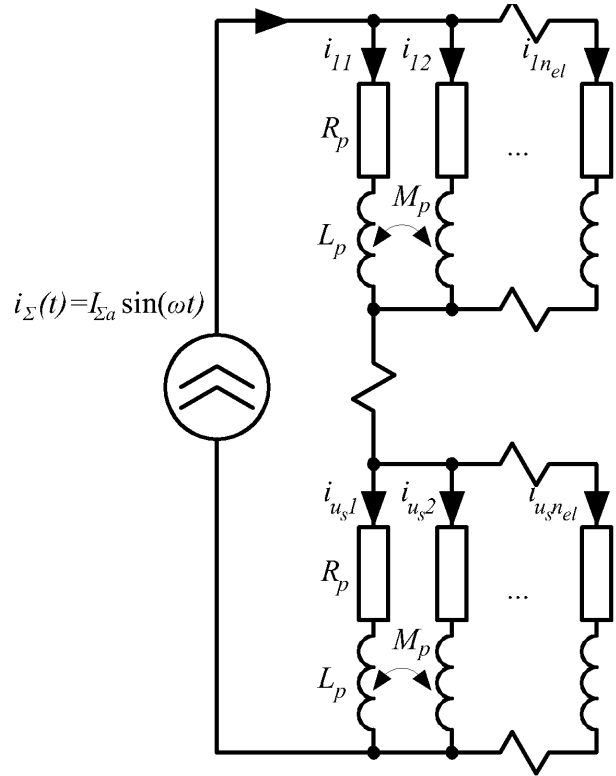


Fig. 2. Electrical diagram of connection of strands in a slot

mathematical formulation of the problem of calculating the current density field in computational area.

We have carried out a series of topic experiments with use of this model. The purpose of these experiments was to study the effect of its own dispersion flux, the main magnetic flux, saturation of the magnetic core and slot shape on distribution of the current density vector in slot area of the coil considering the interrelation of all these factors.

Program-based realization of the algorithm of this model is made with package ANSYS Multiphysics by means of APDL programming.

Fragments of the grid of finite element models for slot elements of different shape are shown in Fig. 3. Total number of CE is 3010. Total number of nodes is 8670.

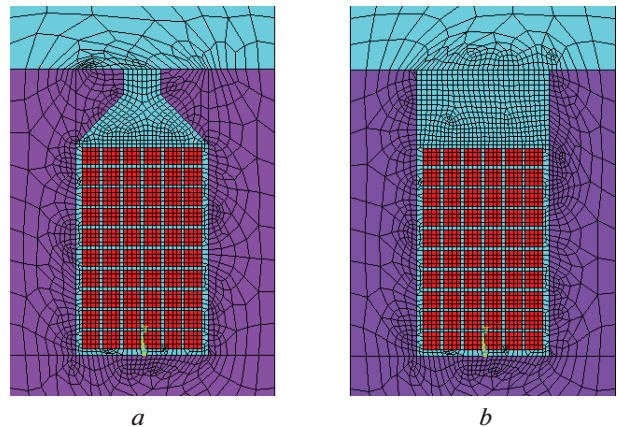


Fig. 3. Fragment of FE grids:

a – for semiclosed slot; b – for opened slot

The output data for modeling were presented by dimensions, coil data and characteristics of magnetizing of the core of high-speed generator of 200 kW, operating at the speed of 50000 rpm ($2p = 2$).

The dimensions of computational domain are as follows:

- slot width $b_s = 7.8$ mm;
- full height of slot $h_{sz} = 16.8$ mm;
- area height $h = 63.8$;
- spline width $b_{sh} = 2.2$ mm;
- spline height $h_{sh} = 1.5$ mm;
- air gap $\delta = 6$ mm;
- area width (tooth separation) $t_z = 15.6$ mm;
- area length in z direction $l_p = 240.0$ mm;
- width of strand $b_p = 1.0$ mm;
- height of strand $h_p = 1.0$ mm;
- thickness of frame insulation $t_{kt} = 0.4$ mm;
- thickness of insulation between conductors $\Delta_{iz} = 0.2$ mm.

Winding data:

- the number of effective conductors in a slot $u_s = 2$;
- the number of strands in effective $n_{el} = 30$;
- the number of strands along the slot width $m_c = 6$;
- the number of strands along the slot height $m_r = 5$.

Driving forces of the problem:

- RMS current of the effective conductor $I_s = 175.4$ A;
- current frequency $f_n = 833.3$ Hz;
- amplitude of radial component of induction of the main field $B_\delta = 0.72$ T;
- phase shift between current and the radial element of induction $\nu = \pi/2$ rad;
- proportionality factor between angular and metrical coordinates $\beta = 14.54$ rad/m.

Specific resistance of the conductor material was $\rho_{Cu} = 1.75 \cdot 10^{-8}$ Oh \cdot m. This value corresponds to specific resistance of copper at temperature of 20 °C. Magnetization characteristics of the magnetic core correspond to properties of electric steel of 2411 type (GOST21427.2-83).

The calculation is performed within 6 periods of feed current, time increment was 1/80 of the period.

Fig. 4 shows the results of calculations of vector magnetic potential fields, magnetic field induction and current density at the time $t = 7.05$ ms.

Fig. 5 shows dependence of the voltage on the time, calculated by (7) at the last computational period.

The diagrams, shown in Figure 5 *a, c*, correspond to the currents of strands in the 3*d* left column of the effective conductor, located near the spline.

Valid values of these currents, losses and Field's factors K_R for two conducted studies are recorded in Table.

It should be mentioned that Field's factor, calculated by classical method for opened rectangular slot of specified dimensions is equal to $K_R = 3.8$, and its value, calculated upon the absence of external field and in linear arrangement, is $K_R = 6.3$.

Conclusions. Mathematical model for calculation of additional losses in slot area of the stator winding of a permanent magnet electrical machine is developed on the basis of Poisson's numerical solution for quasi-

Table

The influence of the slot shape on the skin effect

Index name	Semiclosed slot	Opened slot
Effective conductor at the bottom of the slot		
$I_{1,3}, A$	4.001	3.948
$I_{1,9}, A$	4.306	4.212
$I_{1,15}, A$	5.327	5.322
$I_{1,21}, A$	7.602	7.878
$I_{1,27}, A$	11.602	12.259
Main losses (DC), W	4.318	4.318
Full losses (AC), W	9.417	9.695
Effective conductor near the spline		
$I_{2,3}, A$	14.948	16.666
$I_{2,9}, A$	7.471	8.960
$I_{2,15}, A$	5.434	5.656
$I_{2,21}, A$	14.141	10.830
$I_{2,27}, A$	26.889	19.815
Main losses (DC), W	4.318	4.318
Full losses (AC), W	37.367	64.346
For all conductors in the slot		
Main losses (DC), W	8.636	8.636
Full losses (AC), W	46.785	74.041
Field's factor	5.418	8.574

steady approximation of electromagnetic field within 2-dimensional formulations. The model considers the actual shape of stator slot, the influence of the excitation field and saturation of the magnetic core.

Analysis of the obtained results suggests the following conclusions that can help in developing high-speed permanent magnet electrical machines:

Classical method for calculation of additional losses in the slot area of machine stators, operating at frequencies that are considerably higher than industrial frequency, on the basis of Edme's functions is in significant error.

The first harmonic field induces eddy currents in upper layers of the stator winding while saturating tooth area. This results in increasing losses in it.

Opening of the slot considerably increases penetration of the excitation field into the slot and the value of additional losses in the stator winding.

The excitation filed in semiclosed slots does not affect redistribution of the current density vector field and currents in electromagnetic conductors of the coil.

Saturation of the magnetic core reduces the value of additional losses in the stator winding and makes current distribution more even due to reduction of magnetic conductivity of the slot dissipation flux path. It is necessary to remember that excessive saturation of tooth area increases the main losses in the magnetic core of the stator core.

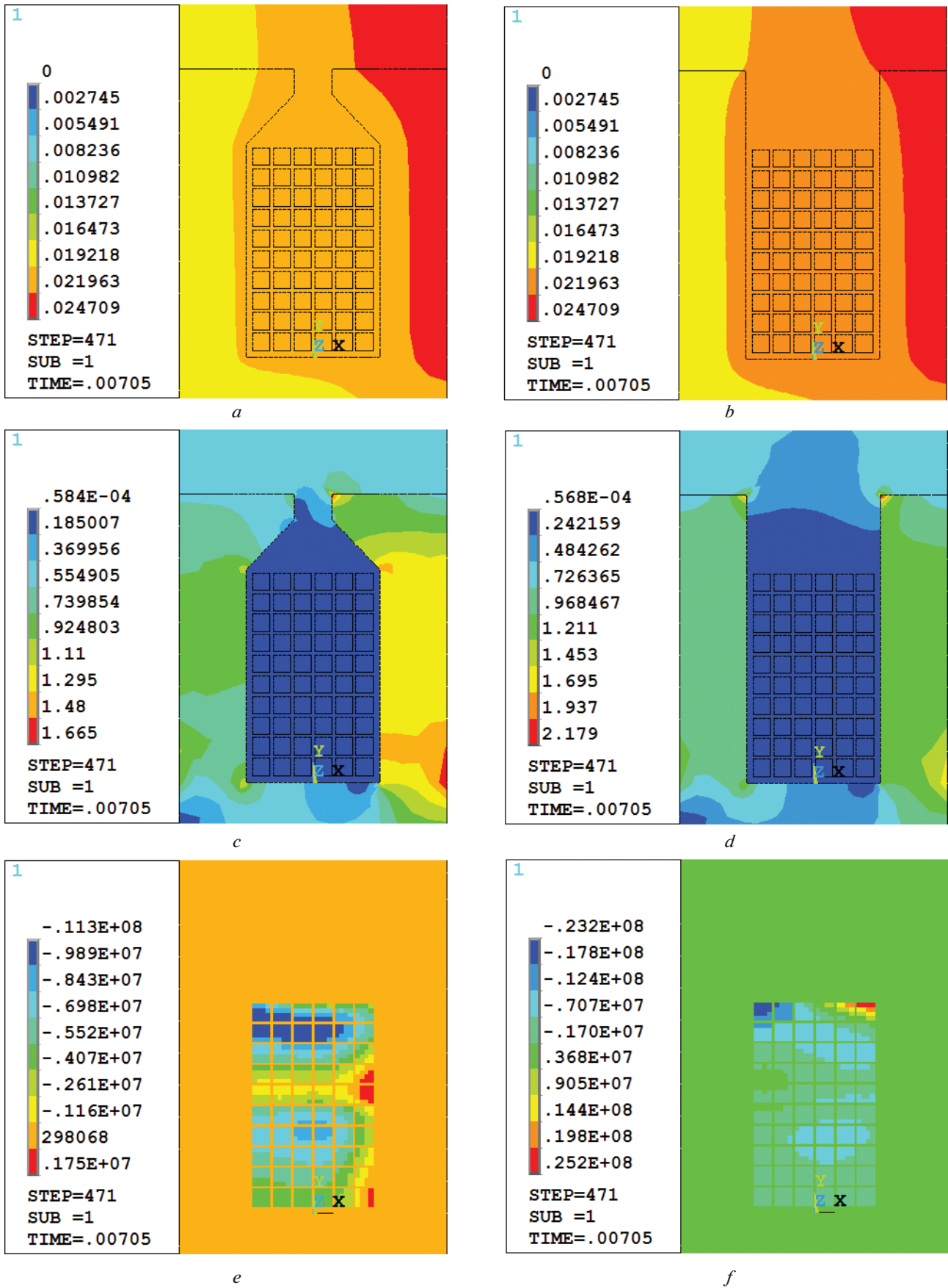


Fig. 4. Results of calculation:

a, b and c – for semiclosed slot; d, e, f – for opened slot; a, d – field of vector magnetic potential, Vs/m; b, e – magnetic induction vector field, T; c, d – current density vector field, A/m²

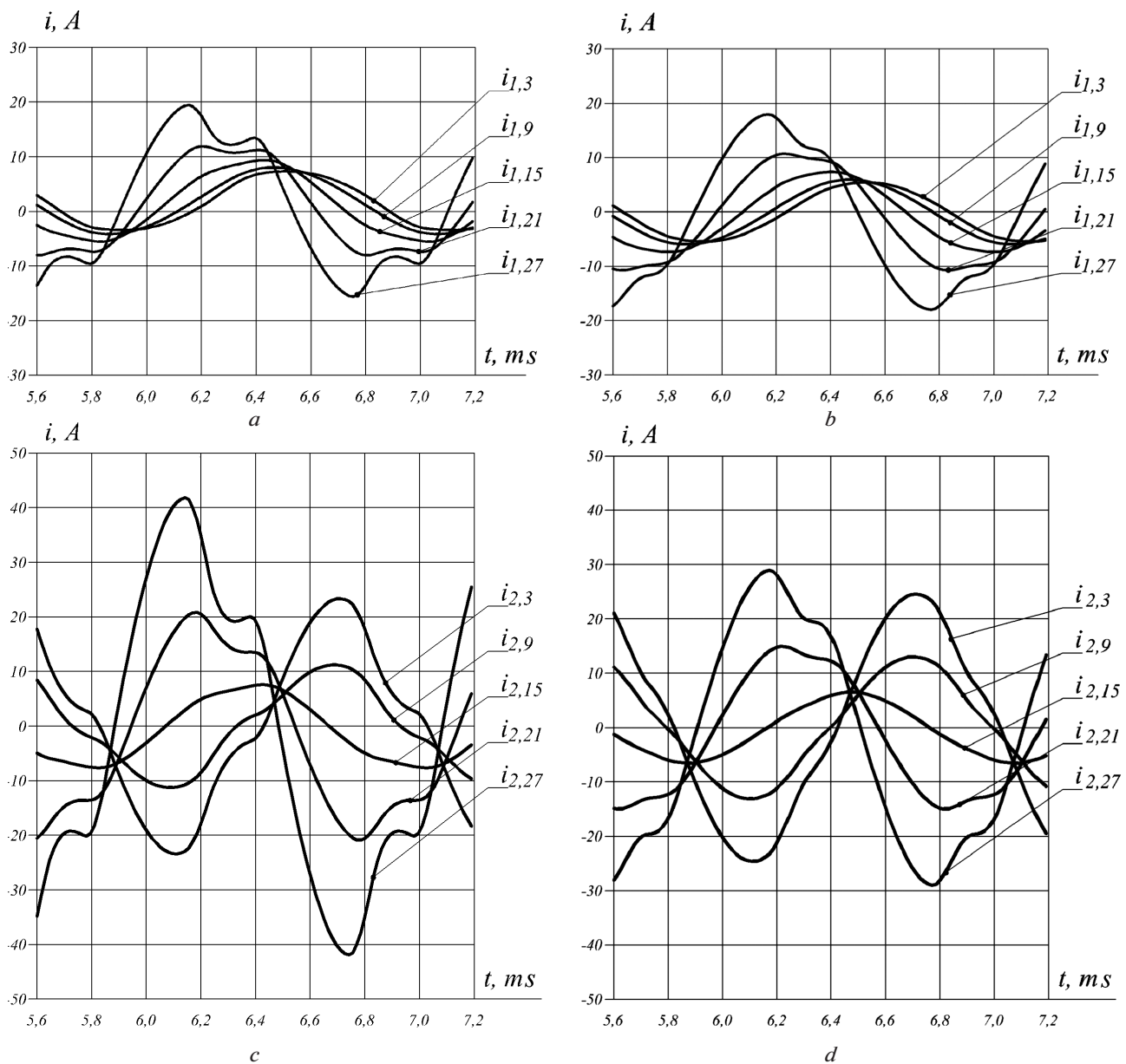


Fig. 5. Dependency of currents of electromagnetic conductors on time, A:

a, b – for semiclosed slot; c, d – for opened slot; a, c – effective conductor at the bottom of the slot; c, d – effective conductor near the spline

References / Список літератури

1. Thomas, A. S., Zhu, Z. Q. and Jewell, G. W., 2009. Proximity Loss Study In High Speed Flux-Switching Magnet Machine. *IEEE Transactions on Magnetics*, Vol. 45(10), pp. 4748–4751.
 2. Amara, Y., Reghem, P. and Barakat, G., 2010. Analytical prediction of eddy-current loss in armature windings of permanent magnet brushless AC machines. *IEEE Transactions on Magnetics*, Vol. 46(8), pp. 3481–3484.
 3. Yamazaki, K., Fukushima, Y. and Sato, M., 2008. Loss analysis of permanent magnet motors with concentrated windings-variation of magnet eddy current loss due to stator and rotor shapes. In: *IEEE, Industry Applications Society Annual Meeting*.

Edmonton, Alberta, Canada, 5 9 October, 2008. IEEE.
 4. Islam, M. J., Khang, H. V., Repo, A. K. and Arkio, A., 2010. Eddy-current loss and temperature rise in the form-wound stator winding of an inverter-fed cage induction motor. *IEEE Transactions on Magnetics*, Vol. 46(8), pp. 3413–3416.
 5. Bottauscio, O., Oriano, M., Manzin, A. and Zucca, M., 2004. Additional losses in induction machines under synchronous no-load conditions. *IEEE Transactions on Magnetics*, Vol. 40(5), pp. 3254–3261.
 6. Ouyang, Z., Thomsen, O. C. and Andersen, M. A., 2009. The analysis and comparison of leakage inductance in different winding arrangements for planar

transformer. In: IEEE, *International Conference on Power Electronics and Drive Systems*. Taipei, Taiwan, 2–5 November, 2009, Taipei.

7. Frelin, W., Berthet, M., Petit, M. and Vannier, J. C., 2009. Transformer winding losses evaluation when supplying nonlinear load. In: the 44th International IEEE *Universities Power Engineering Conference (UPEC 09)*, Glasgow, United Kingdom, 1–4 September, 2009, IEEE.

Мета. Запропонувати спосіб визначення додаткових втрат в обмотках статорів електричних машин, частота струму в яких значно перевищує промислову.

Методика. Для дослідження використовуються чисельні методи розв'язування рівнянь математичної фізики, а саме: для алгебраїзації частинних похідних – метод скінченних елементів, для алгебраїзації похідних за часом – метод формул диференціювання назад, для розв'язування нелінійних систем алгебраїчних рівнянь – метод Ньютона-Рафсона.

Результати. Створена математична модель, що дозволяє розраховувати повні втрати в пазовій частині обмотки статора високошвидкісної електричної машини, обумовлені ефектом витіснення струму, та з урахуванням чинників, що здійснюють визначальний вплив на перебіг цього явища: власного потоку пазового розсіювання, основного магнітного потоку, насичення магнітопроводу, форми паза та способу електричного сполучення елементарних провідників котушки. Подане математичне формулювання та краєва умова даної задачі.

Для високошвидкісного генератора зі збудженням від постійних магнітів 200 кВт, 50 000 об/хв, наведені результати математичних експериментів із визначення додаткових та повних втрат в обмотках, що лежать у напівзакритих та відкритих пазах. Аналізуються причинно-наслідкові зв'язки, наведені висновки, що можуть допомогти у створенні таких машин.

Наукова новизна. Проблема розрахунку втрат формулюється як 2-вимірною краєвою задачею електродинаміки, що дозволяє врахувати вплив усіх вищезгаданих чинників у взаємозв'язку.

Практична значимість. Потреба в точному визначенні втрат у фазних обмотках високошвидкісних машин виникає не лише під час проектування обмоток, але й за оцінки теплового стану таких машин.

Ключові слова: додаткові втрати, витіснення струму, скін-ефект, FEM-аналіз, краєва умова, високошвидкісна електрична машина

йова умова, високошвидкісна електрична машина

Цель. Предложить способ определения добавочных потерь в обмотках статоров электрических машин, частота тока в которых существенно выше промышленной частоты.

Методика. Для исследования применяются численные методы решения дифференциальных уравнений математической физики, а именно: для алгебраизации частных производных – метод конечных элементов, для алгебраизации производных по времени – неявный метод формул дифференцирования назад, для решения нелинейных систем алгебраических уравнений – метод Ньютона-Рафсона.

Результаты. Создана математическая модель, позволяющая рассчитывать полные потери в пазовой части обмотки статора высокоскоростной электрической машины, вызванные эффектом вытеснения тока и с учетом причин, оказывающих определяющее влияние: собственного потока пазового рассеивания, основного магнитного потока, насыщения магнітопровода, формы паза и способа электрического соединения элементарных проводников в пазу. Приведены математическая формулировка и краевое условие данной задачи.

Для высокоскоростного генератора с возбуждением от постоянных магнитов 200 кВт, 50 000 об/мин, приводятся результаты математических экспериментов по определению дополнительных и полных потерь в обмотках, расположенных в полужакрытых и открытых пазах. Анализируются причинно-следственные связи. Сделанные выводы могут помочь при создании таких машин.

Научная новизна. Проблема расчета потерь формулируется как 2-мерная краевая задача электродинамики, что и позволяет учесть все вышеупомянутые факторы в их взаимосвязи.

Практическая значимость. Необходимость в точном определении потерь в фазных обмотках высокоскоростных машин возникает не только во время проектирования обмоток, но и при оценке теплового состояния таких машин.

Ключевые слова: добавочные потери, вытеснение тока, скін-ефект, FEM-аналіз, краєвое условие, высокоскоростная электрическая машина

Рекомендовано до публікації докт. техн. наук І. З. Щуром. Дата надходження рукопису 18.12.15.

UDC 622.232:72.007.2:622.86

V. G. Shevchenko, Dr. Sc. (Tech.), Senior
Research Fellow

M. S. Polyakov Institute of Geotechnical Mechanics of National Academy of Sciences of Ukraine, Dnipro, Ukraine

DEVELOPING METHODS FOR INCREASING READINESS OF THE MANAGERS OF COAL MINE DIVISIONS TO ACCIDENT-FREE OPERATION ACCORDING TO QUANTITATIVE ESTIMATIONS OF THEIR PERSONALITY CHARACTERISTICS

В. Г. Шевченко, д-р техн. наук, старш. наук.
співроб.

Інститут геотехнічної механіки ім. М. С. Полякова НАН
України, м. Дніпро, Україна

РОЗРОБКА МЕТОДИКИ ПІДВИЩЕННЯ ГОТОВНОСТІ КЕРІВНИКІВ ДІЛЬНИЦЬ ВУГІЛЬНОЇ ШАХТИ ДО БЕЗАВАРІЙНОЇ РОБОТИ ЗА КІЛЬКІСНИМИ ОЦІНКАМИ ЇХ ОСОБИСТІСНИХ ХАРАКТЕРИСТИК

Purpose. To perform a quantitative estimation of the personal characteristics of managers of coal mine divisions and to develop a methods for increasing their readiness for trouble-free work.

Methodology. A complex method of research with methods of mathematical modeling, system, factor, mathematical, and information analysis, mathematical statistics, probability theory, reliability theory, psychophysiology methods, engineering psychology with the use of statistical data on injuries and accidents.

Findings. The dependence of the deviations on the regulatory decisions in a series of professional training on the specific number of experienced managers was established; an exponential dependence of the growth of professional knowledge of managers on the amount of information that received in the course of professional training was found; conditions under which managers' emergency actions approach to being automatic were defined. The criterion of professional readiness of a team of managers to control work in areas in an accident-free mode was proposed and substantiated. The criterion is directly proportional to their self-discipline when issuing directives to subordinates and in monitoring performance, vigilance in the analysis of situations and inversely proportional to blenching safety work breaches. A direct correlation between the frequency of accidents and the criteria of professional readiness of the team of managers to work without accidents was established.

Originality. For the first time, the relationship between personal psychophysiological characteristics of managers, their work experience, age and incidence of injuries at the mine as a result of emergency situations was defined.

Practical value. Methods for increasing the readiness of managers of coal mine sections for accident-free work according to the quantitative estimation of their personal characteristics were developed.

Keywords: *managers of a coal mine divisions, accident-free work, methods for increasing the readiness, quantitative estimation of personal characteristics*

Introduction. Working in high hazard environment in coal mines, miners often work overextending themselves physiologically. This leads to difficulties in predicting their behavior and in many cases is the

cause of accidents. To avoid them, it is necessary to increase their personal readiness to work without accidents. The professional training of managers of the main mine divisions is an effective measure in this context. Scientific substantiation and application of such training in production activities is an urgent so-

cial task aimed at saving people who are the most precious national resource.

Currently, there are only general statements of the possible directions of solving emergent problems. Theoretical basis which is suitable for analysis and quantitative estimation of miner personal characteristics is still under development. Regarding investigations of accidents, analyzing their circumstances and causes, it has been established that human actions are determined, above all, by their mental temperament, then by the level of their professionalism and physical capabilities.

Analysis of recent research and publications.

Significant contribution to the development of research studies on the specific aspects and solution of the problem as a whole has been made by foreign and Ukrainian scholars and experts and mine associations workers. Thus, University of Wyoming scientists (USA) has been analyzing the influence of production organization level on accidents at coal mines, estimating the mine safety with different infrastructure [1]. Scientists of the National Institute of Health and Safety (USA) perform a statistical evaluation of data on disability to develop methods for the hazard assessment of technological operations carried out in the mines [2]. Scholars' papers [3] analyze accidents in underground coal mines in Turkey, give the statistical relationship between the post, age and probability of accident occurrence as well as formulas to determine the total probability of an accident at a mine taking into account the number of miners; also the statistical model of analyzing risk factors, accidents and injuries at coal mines are given. In [4] the issues of participation and role of the employee and supervisor are reflected, behavioral negatives, a person's attitude to safety and the importance of workers' training are analyzed, causes and factors of injuries are given, the features and effectiveness of state supervision of safety and its influence on the industrial injuries are considered.

As a result of studying the problem, the modern approaches and investigation methods for studying miners' labor by certain sciences and disciplines are identified. They consist in determining the physiological, sanitary, psychological, sociological, economic, organizational and other characteristics and requirements to ensure labor regulatory conditions as well as miners' personal characteristics [5].

Unsolved aspects of the problem. However, in scientific aspect the methodology of quantitative estimation of personal physiological characteristics of managers and workers has not been developed yet. The scientific and methodological support of professional training for safety is also lacking. The system of professional training of division managers should be developed in such a way that their actions at work in an accident-free mode and in emergency cases are brought to a certain level of automaticity. Moreover, managers' actions are to satisfy all requirements of normative and legislative acts which allows eliminating the original cause and conditions of emergencies.

Thus, quantitative estimation of personal characteristics of division managers and their relation to the ability to prevent emergency situations, which is used as methods, allows increasing the readiness of personnel to work without accidents is an urgent scientific task that is essential in ensuring safety in coal mines.

Objectives of the article. The purpose of the article is to perform a quantitative estimation of personal characteristics of coal mine division managers and to develop a method to increase their readiness for accident-free work.

Presentation of the main research. Based on the conceptual foundations of accident-free coalmining, the periodic assessment of readiness of the main division managers is proposed. The basis of their professional training involves the following scientific and methodological principles.

1. The action estimation principle

$$i(t)^* = \begin{cases} +i_{in}k_1, i = i_n \\ -i_{i_0}k_2, i = i_0 \end{cases}$$

where $i(t)^*$ is value of knowledge obtaining function in the implementation of a game situation with the answers to questions; $i_{in}k_1$, $i_{i_0}k_2$ are the amount of new knowledge obtained during training and the number of errors removed in, correspondingly; k_1 , k_2 are the ability to assimilate knowledge or eliminate errors in the game situation.

2. The consolidation of collective desire principle (the group unity principle)

$$\sum_{i=1}^n (m+x+d) + W = (mx)N + dN + TC,$$

where N is the number of employees in the group who: m – can escape; x – want to do it and know that it is their duty (d); W is a manager's will – a special combination of their m , x and d ; $(mx)N$ is a qualitatively new collective desire to escape, based on the realization that everybody can and wants to do it; dN is a collective support and assistance; TC is the concern of one for all and all for one (total concern).

3. The principle of necessity to bring the actions of managers in an emergency situation to the reflex level

$$R = R_0 e^n,$$

where R_0 is the basic level of reflexive action according to hesitation time and doubts before making a decision; n is the number of trainings.

4. The system assessment hierarchy principle.

As a result of the training, the growth of knowledge is

$$I_T = I_N + I_E + I_G,$$

where I_N is the knowledge that comes from a facilitator; I_E the a knowledge that comes from an expert; I_G is the knowledge generated in the process of making independent and collective decisions.

Probability (according to the level of deviations from regulatory decisions) is

$$D = 1 - (1 - D_M)(1 - D_C)(1 - D_E) = 1 - \prod_{i=1}^n (1 - D_i),$$

where D_M is the probability of a manager's knowledge; D_C is the probability of collective knowledge; D_E is the probability of an expert's knowledge; n is the rank of organizational structure of the training ($n = 3$).

5. The principle of developing innovative solutions

$$I_T = f(C, SO, T, D, Det),$$

where C is the completeness of information; SO is the subject orientation of information; T is the timeliness of information; D is the probability of information; Det is the level of the information details.

The growth of intensity of synthesis of ideas is

$$I(n, m) = I_B + I_N m + (i k_y)(m + n),$$

where I_B is basic knowledge on education and life experience; I_N is new knowledge of the work practice at a mine; m is the number of descendings into the mine (work experience); n is the number of repetitions of information (the number of trainings).

Conditions for innovative solutions occurrence are

$$P = \lim I(n, m) \rightarrow I(n, m) + \Delta i.$$

Mathematical modeling of prevention of emergency situations allowing for the psychophysiology futures of miners and their leader was as follows.

Relation of miners' characteristics to the final result of their work

$$A = \sum_{i=1}^n q_{A_i} k_{g_i} \approx 3(n - m) q_A k_g,$$

where A is output per face, t/day; q_A is a productivity per employee, t/person; $\sum_{i=1}^n q_i$ is a collective productivity of mining, t/day; 3 is the number of shifts of coal mining per day; k_g is integrated face readiness for coal mining in quantity A_i t/day.

Relation of psychophysiological characteristics of an employee to the labor parameters:

- the pursuit of material wealth

$$x = \frac{ZP + \Delta ZPS_x}{ZP_{\max}};$$

- sense of responsibility

$$\begin{cases} d_1 = \left(1 + \frac{\Delta q S_d}{q}\right) \frac{T_s - t_p}{T_s}; \\ d_2 = TR - \Delta T_p S_{ir} \end{cases};$$

- psychophysiological capabilities and experience

$$m = \frac{T_e}{T} = \frac{N + \Delta NS_m}{H_w (1 - US_w)},$$

where x is the aspiration expressed in relative currency to earn more, to get other benefits which can be measured with money, UAH; ZP is payment, such as wage

rate UAH; ΔZP is a desirable premium, UAH; S_x is an indicator that characterizes the "self-adjustment" for ΔZP , d_i is a call of duty of an employee to themselves and to the team expressed in terms of relative productivity units; TR is the number of accidents at while realizing q ; S_{ir} is the commitment to safe work; $\Delta q S_d$ is the implementation of an employee's desire to contribute to a common cause more efforts when necessary (q); S_d is "self-adjustment" for additional help (advice, labor) to those who need it on the analogy of S_{ZP} ; m stands for an employee's professional opportunities expressed in terms of relative power units N ; ΔNS_m is implementation of additional capacity; S_m is "self-adjustment" for implementation ΔN ; T_e is effective time during the shift T_s ; U is the ability to spend less effort than others while performing activities; t_p is duration of breaks.

The scientific methods of training has been developed and for the first time dependence of a manager's readiness for successful actions in an emergency situation on the total new knowledge obtained during the training. Moreover, scientific foundation to create conditions for generating innovative solutions has been elaborated.

The results of professional training of the main mine division managers of one of the mining enterprises are presented. During the training, certain emergency situations such as "Fire within the division", "Sudden eboulement" in the workspace tunneling, cleaning excavation and their conjugation were simulated. In these situations, leaders of the divisions were operating characters on the posts of a "manager", an "underground miner", a "division mechanic", a "machinist of the underground facilities" and others on the staff. Four of the leaders in the training period formed a small integral group of professionals with different levels of experience, knowledge, skills, aspirations and other qualities typical of each individual. However, under conditions of training every leader had to make specific decisions to save each group member's life as well as their own lives. The solution was to be made quickly, but professionally, taking into account the situation, which conventionally prevented any error. Professional, civil and personal qualities were revealed individually for each manager. However, common features of group leaders were revealed that differed according to the mine where they work, their age and experience.

During the professional training, the leaders' action process in an emergency situation was considered as consisting of elementary operating acts: identification of an emergency situation, guidance by standards when making decisions as the situation progresses, informing other officials and miners about the situation, determining the order of leaving the workings, sequence of following the route, sorting miners into groups according to their age, experience, physical condition, etc.

The trends of changing personal characteristics of managers depending on their work experience were obtained for a mine of one of the production coalmin-

ing enterprises. It was established that the readiness of the team for each of the main mine divisions for the high-performance and safe work is determined by the amount of positive work experience, the features of the structure and dynamics of relationships in the “managers-workers” system. While preventing emergencies, the coefficient of readiness is estimated by positive dynamic of criteria of authoritarian-collaborating qualities of the chief, which is directly proportional to the level of their qualifications and varies polynomially with increasing work experience, and reaches extreme values at the stages of formation and stable tenure, equal, respectively, to 1/3 and 2/3 of the total experience.

The dependence of the decreasing frequency of accidents on increasing criterion of professional readiness of a team of managers to control the work at divisions in an accident-free mode was established.

The criterion is determined by the following equation

$$K = \frac{TP+V}{B},$$

where *TP* is the demand for making personal decisions and monitoring the implementation of directives, %; *V* is the vigilance to reports on threat to subordinates’ health or loss of the division asset; *B* is blenching safety rule violations and other standards requirements.

The values of the criteria are listed in the Table.

The method for increasing the readiness of managers coal mine divisions for accident-free work includes: developing and approving a plan of professional training; determining general rules for professional training; formulating the open monologue thesis (conversations, dialogues); determining the questions of the facilitator during the game situation; determining the order of group organization, testing and professional training; developing the game situation scenarios for professional training; assessing the readiness of the main division managers of a coal mine for actions to prevent accidents; giving recommendations for improving the management of teams; calculating the economic efficiency of testing and professional training.

Based on the experience of professional training on labor safety of division managers, their deputies, as-

sistants and mining masters, it follows: all trainees without any exception consider that the idea and its implementation are appropriate and such training should be definitely organized and conducted in Centers for Professional Advancement and mines; moreover, it is advisable to discuss, legitimize, refine or reject the technical proposals made by participants of professional training during meetings on safety issues.

Decreasing occupational injuries confirm the feasibility of professional training for safety.

Working methods for ranking mines according to the state of their mining economy, technical equipment and the staff’s professional level were developed. Probability of trouble-free performance in a given time interval *P(t)* is adopted as an indicator of reliability and the readiness coefficient *k_g* at a given time is adopted for integrated assessment of reliability. To determine the performances of the systems with branched structure, formulas for systems of zero and first order were obtained.

Blocking unprofessional actions of an individual has to be ensured by special technical means of control, security, alarm and warning communication, systems of environment monitoring and equipment diagnostic with elements of forecasting and organizational measures. However, first and foremost the measurements to improve the technical and professional level by performers of all ranks should be introduced in the industry.

The calculations confirm quantitatively that economic losses from adopting incorrect decisions on appointing the management of mining or tunneling divisions can be hundreds of thousand UAH per day. A hour of face downtime due to a manager’s error makes 16,111.00 USD for the mine with an average productivity of 2,000 tons, a price of raw coal of 700 UAH/t and production cost of 555 UAH/t; this is equal to the sum of the manager and his deputy salaries. The price of the same risk, but for a day face downtime is almost 20 times as much, i.e. 290 thousand UAH. To compare, up to 1000 m³ of wood materials or 30–35 tons of fuel for vehicles can be purchased for the requirements of the mine using these finances. To produce 1 million tons of coal per year, it is necessary to pass 7–8 km of opening and tunneling workings of the mine. Delays in tunneling work are failures of the strategic level that are not corrected quickly. The rate of tunneling work is the main factor of stabilizing coalmining for a long time. The manager of a tunneling division must comply with the planned values of this indicator. Shortfall in tunneling volumes, for example, 100 m per year, will result in losses of the whole enterprise in the range of 1.8 to 2.1 million UAH. The planned rate of preparing reserves to slot considering raising production, for example, by 10 %, is 128–144 days. If there are 20 brigades of tunneling workers, each of them is to ensure the average rate of 6.4–7.2 m/day. The brigade should tunnel 100 m for 13.8–15.6 days. Losses due to poor performance versus plan will be 128–165 thousand UAH. With an average duration of downtime in the industry due to the

Table

The values of criteria of professional readiness of division managers

Coalmines	Changing criteria of professional readiness of division managers		
	minimum	average	maximum
Mine 1	1.113	1.14	1.2
Mine 2	1.26	1.42	1.68
Mine 3	1.34	1.45	1.49

elimination of accidents of 1,500 hours or 62.5 days per year, the annual economic effect will be of 8006.25 to 10333.125 thousand UAH, i. e. an average of 9156.25 thousand UAH per year for a mine.

Conclusions.

1. Readiness to work in an accident-free mode of each team of divisions of high production mine is determined by the volume of production experience, features of the structure and dynamics of relationships in the “managers-workers” system. The increase of readiness to work in an accident-free mode is determined by the positive dynamics of criteria of professional readiness of the team leaders that increases with their work experience.

2. According to the professional training results, it was found that the efficiency of collective action of each working division, which is necessary for work without accidents, depends on the level of automaticity of managers’ professional activities. As a result of production and regular training, this level is based on the uniqueness of their directives and correctness of solutions. Correctness of decisions and directives is determined by insistence on personal decisions and implementation of directives by subordinates, diligence while analyzing situations and rigidity to violations of safety rules that reach rational values in the last third of the working experience. In other words, it is necessary to speed up the improvement of professional readiness of young division managers, including their training.

3. Division managers’ readiness to control works in an accident-free mode is determined by personal characteristics apart from knowledge and professional experience that is measured by length of service on duty. The most significant of these are: demand (*TP*) for completeness and quality performance of the work by themselves and subordinates, vigilance (*V*) to messages about the threat of loss of health and division asset and blenching (*B*) violations of safety rules.

For each team of medium-level managers in a coal mine, there are specific and generalized trends of change *TP*, *V*, *B* and other characteristics over time.

The ratio $\frac{TP+V}{B}$ may be characterized as a vector of professional commitment and availability or as a criterion of readiness of team leaders to work without accidents, that is $K = \frac{TP+V}{B}$.

4. The relationship between frequency of injuries for several years of the mine work $\frac{N}{1000}$ and the criterion of professional readiness of the team leaders to work in an accident-free mode, which is inversely proportional, is determined. Comparing $\frac{N}{1000}$ to $\frac{TP+V}{B}$ it was established that with increasing levels of professional readiness of leaders to work in an accident-free mode from 1.113 to 1.68, the relative number of injuries decreased accordingly from 14–16 to 4–11.

5. Increase in knowledge depends on the amount of new data which comes from the facilitator, experts or is generated by those who are trained to make independent and collective decisions. Their compliance with standards depends on the objective evaluation system, based on its collective and expert components which are embedded in the organizational structure of the training.

6. On the basis of new scientific results, the methods for increasing the readiness of coal mine managers for accident-free work according to quantitative estimation of their personal characteristics, scenarios and methods of professional training managers of the main divisions of coal mines were obtained. Methods have been approved at the industrial level, implemented in a number of coal mines with the expected economic effect of 9,156.25 thousand UAH per year for a mine.

References / Список літератури

1. Page, K., 2009. Blood on the coal: The effect of organizational size and differentiation on coal mine accidents. *Journal of Safety Research*, Vol. 40, Issue 2, pp. 85–95.
2. Coleman, P.J. and Kerkering, J. C., 2007. Measuring mining safety with injury statistics: lost workdays as indicators of risk. *Journal of Safety Research*, Vol. 38, Issue 5, pp. 523–533.
3. Sari, M., Selcuk, A. S., Karpuz, C. and Duzgun, H. S. B., 2009. Stochastic modeling of accident risks associated with an underground coal mine in Turkey. *Safety Science*, Vol. 47, Issue 1, pp. 78–87.
4. Pashin, N. P. and Lysiuk, N. A. eds., 2008. Labor safety: the human factor and Government control. Kyiv: NNIPBOT.

Охрана труда: человеческий фактор и государственный контроль / Под редакцией Н. П. Пашина, Н. А. Лысюка. — К.: ННИИПБОТ, 2008. — 116 с.

5. Shevchenko, V. G., 2013. *Nauchno-metodicheskiye osnovy otsenki psikhofiziologicheskikh kharakteristik rukovoditelei uchastkov ugolnoi shakhty* [Scientifically-methodological basis of estimation of psycho-physiological characteristics of coal mine division managers]. Kyiv: Naukova Dumka.

Шевченко В. Г. Научно-методические основы оценки психофизиологических характеристик руководителей участков угольной шахты: монография / Шевченко В. Г. — К.: Наукова думка, 2013. — 280 с.

Мета. Виконати кількісну оцінку особистісних характеристик керівників дільниць вугільної шахти та розробити методику підвищення їхньої готовності до безаварійної роботи.

Методика. Використано комплексний метод дослідження із застосуванням методів математичного моделювання, системного, факторного, математичного, інформаційного аналізу, математичної статистики, теорії ймовірностей, теорії надійності, методів психофізіології, інженерної психології з використанням статистичних даних про травматизм і аварії.

Результати. Встановлена залежність відхилення прийнятих рішень від нормативних у циклі професійних тренінгів від питомої кількості досвідчених керівників; знайдена експоненціальна залежність росту професійних знань керівників від кількості інформації, отриманої ними у процесі професійного тренінгу; визначені умови, за яких дії керівників в аварійній ситуації наближаються до автоматичних. Запропонований і обґрунтований критерій професійної готовності колективу керівників до управління роботами на дільницях у безаварійному режимі, що прямо пропорційний їхній вимогливості до себе при розробці директив і до підлеглих при контролі виконання, пильності при аналізі ситуацій та обернено пропорційний лояльності до порушень безпечного режиму роботи; встановлена пряма залежність між частотою травматизму працюючих і критерієм професійної готовності колективу керівників до праці без аварій.

Наукова новизна. Уперше визначені залежності між особистісними психофізіологічними характеристиками керівників, стажем їх роботи, віком і частотою випадків травмування на шахті внаслідок аварійних ситуацій.

Практична значимість. Розроблена методика підвищення готовності керівників дільниць вугільної шахти до безаварійної роботи за кількісними оцінками їх особистісних характеристик.

Ключові слова: *керівники дільниць вугільної шахти, безаварійна робота, методика підвищення готовності, кількісні оцінки особистісних характеристик*

Цель. Выполнить количественную оценку личностных характеристик руководителей участков угольной шахты и разработать методику повышения их готовности к безаварийной работе.

Методика. Использован комплексный метод исследований с применением методов математического моделирования, системного, факторного, математического, информационного анализа, математической статистики, теории вероятностей, теории надежности, методов психофизио-

логии, инженерной психологии с использованием статистических данных о травматизме и авариях.

Результаты. Установлена зависимость отклонения принятых решений от нормативных в цикле профессиональных тренингов от удельного количества опытных руководителей; найдена экспоненциальная зависимость роста профессиональных знаний руководителей от количества информации, полученной ими в процессе профессионального тренинга; определены условия, при которых действия руководителей в аварийной ситуации приближаются к автоматическим. Предложен и обоснован критерий профессиональной готовности коллектива руководителей к управлению работами на участках в безаварийном режиме, который прямо пропорционален их требовательности к себе при выдаче директив и к подчиненным при контроле выполнения, внимательности при анализе ситуаций и обратно пропорционален лояльности к нарушениям безопасного режима работы; установлена прямая зависимость между частотой травматизма работающих и критерием профессиональной готовности коллектива руководителей к работе без аварий.

Научная новизна. Впервые определены зависимости между личностными психофизиологическими характеристиками руководителей, стажем их работы, возрастом и частотой случаев травмирования на шахте вследствие аварийных ситуаций.

Практическая значимость. Разработана методика повышения готовности руководителей участков угольной шахты к безаварийной работе по количественным оценкам их личностных характеристик.

Ключевые слова: *руководители участков угольной шахты, безаварийная работа, методика повышения готовности, количественные оценки личностных характеристик*

Рекомендовано до публікації докт. техн. наук В. І. Дирдою. Дата надходження рукопису 13.11.15.

UDC 622.5 : 504.4.054 : 628.316

V. Ye. Kolesnyk, Dr. Sc. (Tech.), Prof.,
D. V. Kulikova, Cand. Sc. (Tech.),
A. V. Pavlychenko, Cand. Sc. (Biol.), Assoc. Prof.

State Higher Educational Institution "National Mining University", Dnipro, Ukraine, e-mail: kafedra_ecology@ukr.net

SUBSTANTIATION OF RATIONAL PARAMETERS OF PERFORATED AREA OF PARTITIONS IN AN IMPROVED MINE WATER SETTLING BASIN

В. Є. Колесник, д-р техн. наук, проф.,
Д. В. Кулікова, канд. техн. наук,
А. В. Павличенко, канд. біол. наук, доц.

Державний вищий навчальний заклад „Національний гірничий університет“, м. Дніпро, Україна, e-mail: kafedra_ecology@ukr.net

ОБҐРУНТУВАННЯ РАЦІОНАЛЬНИХ ПАРАМЕТРІВ ПЕРФОРОВАНОЇ ОБЛАСТІ ПЕРЕГОРОДОК В УДОСКОНАЛЕНОМУ ВІДСТІЙНИКУ ШАХТНОЇ ВОДИ

Purpose. Scientific substantiation of the most rational geometrical parameters of the perforated area (shape and configuration of holes relative to each other) of vertical cross partitions placed in an improved mine water settling basin in order to increase their flow factor and, consequently, the efficiency of treatment (clearing) of water through removal of suspended particles.

Methodology. Selection of a partition perforation pattern is carried out on the basis of study and comparison of perforated area geometrical parameters, namely shape, size of holes and their configuration relative to each other; a correction factor that allows determining a distance between hole centers (perforation pitch); partition perforated area flow factor.

Findings. The partition perforated area flow factors have been determined for various perforation patterns. Analytical dependences of a partition perforated area flow factor change on the distance between hole centers have been obtained.

Originality. Revealed regularities of the partition perforated area flow factor change with a correction factor value allow determining a distance between hole centers for various perforation patterns. The dependencies (in the form of graphs and regression equations) between suspended particles settling depth in the improved settling basin and mine water treatment efficiency have been first identified for various perforation patterns.

Practical value. The research findings allowed justifying rational geometrical parameters of the perforated area of vertical cross partitions placed in an improved mine water settling basin. Implementation of findings will allow increasing efficiency of mine waters cleaning from suspended particles, as well as decreasing the level of surface waters contamination in coal mining regions.

Keywords: *mine waters, suspended particles, water body pollution, horizontal settling basin, perforated partitions, treatment efficiency*

The problem substantiation. Mine waters are distinguished by a wide variety of chemical composition and exhibit properties, which exclude their usage for engineering purposes or their discharge into the neighboring bodies of water without pretreatment [1]. Opening of coal deposits under complicated geological and hydrological conditions, as well as carrying out of mining operations at deeper levels result in increased volume of mine waters pumped away to the surface and increased level of their pollution by various chemical substances [2]. Subsequently, the discharge of contaminated mine waters poses an environmental hazard to the components of the environment, particularly for the neighboring surface bodies of water, in which the quality of water changes for the worse in respect of pollution content level [3].

The quality of water in surface bodies of water located in coal mining regions does not comply with the environmental safety standards in respect of the level of maximum permissible concentration of pollutants as a consequence of mine water discharge. The worsening of ecological condition of surface bodies of water is observed after the discharge of mine waters from operational storage ponds [4]. Mine waters also have a significant negative impact on underground waters, in this case deterioration of conditions of providing population with qualitative drinking-water is observed [5].

Mine waters pumped away to the surface in the course of coal mining contain a significant amount of pollutants including heavy metal compounds with toxic properties [6]. The distinctive feature of their behavior in the hydrologic system is absorbability on the surface of water-suspended particles of coal and rock with different particle-size distribution, which contribute to

accumulation of toxic substances in the settling gravitating to the bottom of a body of water. The abovementioned issues become front most during coal mine abandonment [7].

Horizontal settling basins are widely used by collieries of Ukraine for increase of the environmental safety level of mine water discharge into the surface bodies of water by removing suspended particles from it (clearing). Their operating efficiency on the disperse phase removal is around 30 %. It should be noted that only coarse fractions are mainly removed, and almost all fine particles are discharged with water into the neighboring bodies of water, the level of contamination of which exceeds the level of maximum permissible concentration. In view of this, the existing settling basins do not comply with the requirements of the current *Regulations on Surface Water Protection against Recirculated Water Pollution* providing for the discharge of pollutants into the bodies of water in quantities that should not exceed their MPC value. It is evident that the further increase of the efficiency of treatment of contaminated mine waters and thus the increase of the environmental safety level of their discharge should be associated with the efficient removal of fine particles. This is precisely why the existing horizontal settling basin constructions are required to be improved in respect of enhancement of the process of settlement of the finest suspended particles and, as a consequence, increase of the environmental safety level due to the discharge of highly clarified mine waters into the surface bodies of water.

The mine water treatment process improvement will allow ensuring coal comprehensive use [8], as well as sustainable development and further reorganisation of mining industry [9].

Review of the related researches. Papers by A. I. Bereza, K. V. Gnedin, V. A. Gorshkov, M. V. Demura, L. F. Dolina, A. A. Kroik, I. I. Levi, D. M. Mints, I. L. Mongayt, G. I. Nikoladze, P. I. Piskunov, D. G. Sukhorukov, K. D. Tekinidi, A. A. Kharionovskiy, S. M. Shyphrin, S. M. Epoyan, etc. are focused on solution of the issue of enhancement of mine water treatment efficiency at mining enterprises.

The analysis of published findings of research of the existing industrial horizontal settling basins allows coming sufficiently to improvement of their constructions. It was found that a necessary condition for effective operation of settling structures, as well as consistency of the clarified water is the existence of its laminar flow regime. With regard to the above mentioned, it is important to maintain its stability as turbulence increases the transporting capacity of suspended matter in the flow, and water clarification efficiency is lowered. Consequently, a settling basin design should ensure the maximum uniform flow rate distribution over its cross-section and possibly more complete utilization of its volume by removal of stagnation areas [10].

It is believed that the best condition for settling industrial waste waters is a horizontal movement of the main water flow, which is perpendicular to the motion

of settling suspended particles. In such event, settling rate is not increased, but only the reduction of disturbance of flow motion of liquid is achieved during the process of its clarification.

The improvement of conditions of the suspended matter settling process in the presence of a free surface in the flow can be achieved by creating a stable hydrodynamic flow pattern, i.e. by means of reducing the intensity of highly turbid bottom flows and the elimination of large-scale vortexes in the upper part of the flow. This may be achieved by placing along the length of a settling basin some intermediate perforated vertical partitions covering almost the whole vertical cross-section of the settling basin body. Meanwhile, the partition holes divide the flow of the liquid to be treated into a great number of individual layers (streams) of small height (size).

The effect of partitions consists in a change of a longitudinal velocity diagram, at which flow velocity vertical components directed to the settling basin bottom occur under the effect of viscosity forces. The value of these velocities exceeds significantly the settling rate (median fall diameter) of suspended particles retained in the settling basin. Meanwhile, the direction of transport force effecting a particle is the same as the direction of gravity force, that leads to the enhancement of the efficiency of suspended particles settling upstream of each partition.

The intermediate perforated partitions covering the settling basin cross-section contribute to dissipation of energy of bottom and surface flows, adjustment of horizontal velocity profile in all cross-sections of the structure, as well as make for increase in the factor of its volume utilization and enhancement of settling intensity of particles in the water to be clarified.

Experimental research of the functional mock-up of the settling basin with intermediate perforated partitions [10] showed that its structural volume is used completely enough (about 70 %) and, thus, the actual time of waste water settling and the flow rate approximate to the calculated values. Furthermore, the settling capacity of the settling basin having partitions increases significantly (by 30–50 %) compared to typical horizontal settling basins at the same degree of clarification (treatment) of water.

The allocation of unsolved issues. A horizontal settling basin of a unique design for waste water treatment from mechanical impurities (suspended particles) with polydisperse composition by means of gravity settling in a flow has been proposed for the purpose of ensuring environmental safety conditions where mine water discharge into surface bodies of water takes place [10]. This treatment plant can be used in various industrial sectors, including coal mining, for waste water treatment from undissolved solids with mainly homogeneous chemical composition and specific density exceeding water density.

The main difference between the proposed settling basin design and the traditional structures for mechanical treatment of waste waters from suspended particles (matters) is that the body of the first is made

in the shape of a trough, which tapers towards the drain with increase of its depth.

The perforated vertical cross partitions with cross-sections conforming to the settling basin body variable cross-section have been sequentially installed inside the settling basin (Fig. 1). The perforation shall mean punching of holes in various shapes and sizes in the partition material, generally, in a metal plate. The primary purpose of partitions is an adjustment of profile of horizontal velocity of movement of water to be treated along the depth when its level is gradually decreased along the length of the settling basin rather than solids retention. This significantly improves the hydraulic operation of the settling structure, and, therefore, increases the efficiency of treatment (clearing) of contaminated water.

Available perforated partitions, installed in different settling areas having variable shapes, allow a change of liquid flow trajectory and make an unidirectional laminar behavior of the flow, that in turn, contributes to more efficient precipitation of mechanical

impurities (suspended particles) at the bottom of the settling structure. Laminar water flow regime in improved horizontal settling basin accelerates the settlement and precipitation process of fine particles. In addition, it eliminates the destruction of sludge bed, sliding down the inclined bottom, i. e. essentially eliminates the “effect of repeated sludge breaking” in the bottom water.

The flow structure is also significantly affected by hole shapes in partitions. Most commonly the two types of distributive partitions such as perforated and slotted ones are installed in settling basins, where the slits may be horizontal or vertical. In paper [10] it is noted that coefficient of efficiency of horizontal settling basins having cross partitions with vertical slits is somewhat higher, than those with horizontal ones, and is only slightly different from the efficiency coefficient of settling basin having perforated partitions. However, the scientific literature gives no unambiguous answer to the question on what shape the holes shall have and on their configuration relative to each other.

The purpose formulation. The objective of the paper is scientific justification of the most rational geometrical parameters of a perforated area (shape and configuration of holes relative to each other) of vertical cross partitions placed in an improved settling basin in order to increase efficiency of cleaning mine waters of suspended particles (substances).

The main part. For practical perforation of a settling basin partition it is important to calculate parameters of the perforated area, namely, to determine the partition flow factor (k) and select the required distance between the centers of holes (p). In addition, the main geometric parameters of the perforated area to be considered in the calculation are shape and configuration of the holes relative to each other, their size and the correction factor (K_p) which allows the distance between the centers of holes (perforation pitch) to be determined.

The choice of a partition perforation pattern depends on the flow factor of the perforated area, which is determined from the formula

$$k = \frac{f}{S_{total}}$$

where f is area with perforated holes, cm^2 ; S_{total} is total area on which the holes are placed, cm^2 .

For the purpose of justification of rational geometric parameters for a perforated area of partitions placed in an improved mine water settling basin, the most common shape of holes in settling basin partitions and their configuration relative to each other were analyzed. The obtained values of factor k were compared to each other. When choosing the perforation pattern, the preference was given to that one with which factor k would be maximum and the efficiency of suspended particles removal from mine waters should also increase.

To calculate the factor k the following parameters of a perforated area were taken:

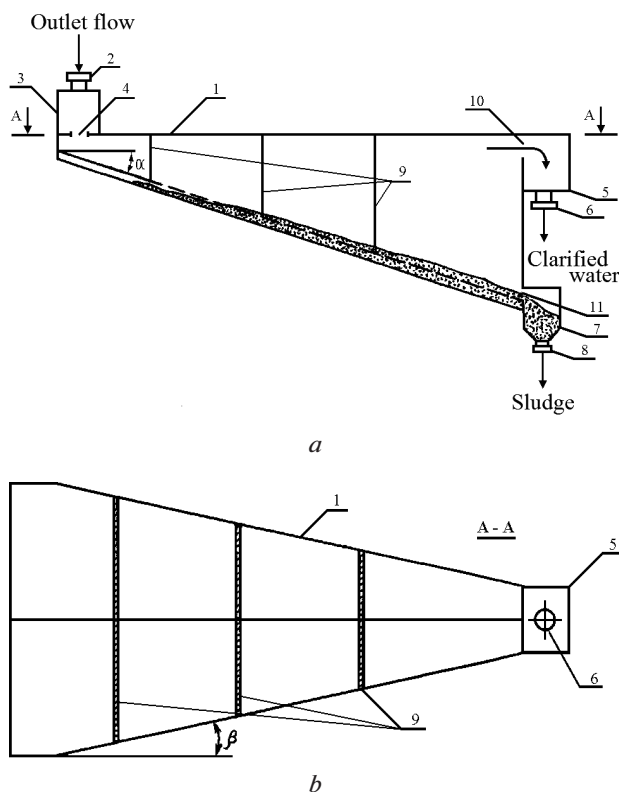


Fig. 1. The improved settling basin structural diagram:

a – side view; *b* – A-A sectional view of settling basin: 1 – settling basin body; 2 – pipeline for supply of polluted water; 3 – tank for distribution of streams; 4 – perforated holes at the tank bottom; 5 – water-collecting tank; 6 – pipeline for clarified water drain away; 7 – receiving hopper for collection and compaction of sludge; 8 – pipeline for compacted sludge drain away; 9 – perforated partitions; 10 – clarified water drain; 11 – sludge drain; α – slope of settling basin bottom towards horizontal area; β – settling basin contraction angles

- hole shape: round, square, rectangular, hexagonal;
- configuration of holes relative to each other: square pattern, rectangular pattern, hexagon pattern, with offset;
- hole size (w , cm): diameter and side length for square and hexagonal holes or width (a) and length (b) for rectangular holes. In calculation the values w and width a ranged from 1 to 10 cm, and value b from 0.1 to ($a-0.1$) cm;
- correction factor, which allows the distance between the centers of holes (K_p) determination.

Since the perforation pitch (p) should not be less than the size of a hole itself, in calculation the factor K_p ranged from 1.1 to 1.3.

Table 1 gives a systematized description for the type of perforation holes of different shape showing the key formulas for factor k calculation.

Using design ratio given in Table 1 (columns 1–4), the coefficient k values were determined for various holes patterns and their types in partitions with varying the preset geometric parameters of perforated area.

The obtained calculation data showed that with the same area of different types of the holes (like circle,

Table 1

Determination of partition flow coefficient (k) with various hole shapes and their configurations relative to each other

Pos.	Configuration of rows of holes in the partitions	Design ratio to calculate coefficient k	Description and permissible variations of design ratio parameters	Formula for calculation of coefficient k
1. For round holes				
1.1	straight rows as square pattern	$f = 4 \cdot S_s = 4 \cdot \frac{1}{4} \cdot S_w = \frac{\pi \cdot w^2}{4}$; $S_{square} = p^2$; $k = \frac{\pi \cdot w^2}{4 \cdot p^2}$	S_s is area of the hole part (sector), cm ² ; S_w is hole area, cm ² ; w is hole diameter, cm ($w = 1-10$ cm);	$k = 0.785 \cdot \frac{1}{(K_p)^2}$
1.2	offset rows as hexagon pattern	$f = 3 \cdot S_s = 3 \cdot \frac{1}{6} \cdot S_w = \frac{\pi \cdot w^2}{8}$; $S_{triangle} = \frac{1}{2} \cdot p \cdot \left(\frac{p}{2}\right) \cdot \text{tg}60^\circ = \frac{p^2 \cdot \sqrt{3}}{4}$; $k = \frac{\pi \cdot w^2}{2 \cdot p^2 \cdot \sqrt{3}}$	p is distance between centers of the holes, cm; ($p = K_p \cdot w$, with $K_p = 1.1-1.3$)	$k = 0.9064 \cdot \frac{1}{(K_p)^2}$
1.3	straight rows as rectangular pattern	$f = 4 \cdot S_s = 4 \cdot \frac{1}{4} \cdot S_w = \frac{\pi \cdot w^2}{4}$; $S_{rectang} = p_1 \cdot p_2$; $k = \frac{\pi \cdot w^2}{4 \cdot p_1 \cdot p_2}$	p_1 is vertical distance between centers of the holes, cm; ($p_1 = K_p \cdot w$, with $K_p = 1.1-1.3$); p_2 is horizontal distance between centers of the holes, cm ($p_2 = p_1 + 0.1 \dots p_2 = p_1 + 0.4$)	$k = 0.7144 \cdot \frac{1}{(K_p)^{1.9228}}$, at $p_2 = K_p + 0.1$
1.4	diagonally-offset rows as square pattern, rotated by 45°	$f = S_w + 4 \cdot S_s = S_w + 4 \cdot \frac{1}{4} \cdot S_w = \frac{\pi \cdot w^2}{2}$; $S_{square} = p^2$; $k = \frac{\pi \cdot w^2}{2 \cdot p^2}$	$P = 0.7071 \cdot p_d$, at $R^2 = 1$; p_d is diagonal distance between centers of the holes, cm; ($p_d = K_p \cdot 2w$, at $K_p = 1.1-1.3$)	$k = 0.785 \cdot \frac{1}{(K_p)^2}$
2. For square-shaped holes				
2.1	straight rows as square pattern	$f = 4 \cdot S_s = 4 \cdot \frac{1}{4} \cdot S_w = w^2$; $S_{square} = p^2$; $k = \frac{w^2}{p^2}$	w is square side, cm ($w = 1-10$ cm); p is distance between centers of the holes, cm; ($p = K_p \cdot w$, at $K_p = 1.1-1.3$)	$k = \frac{1}{(K_p)^2}$
2.2	straight rows as rectangular pattern	$f = 4 \cdot S_s = 4 \cdot \frac{1}{4} \cdot S_w = w^2$; $S_{rectang} = p_1 \cdot p_2$; $k = \frac{w^2}{p_1 \cdot p_2}$	see description to point 1.3	$k = 0.9101 \cdot \frac{1}{(K_p)^{1.9228}}$, at $p_2 = K_p + 0.1$
2.3	diagonally-offset rows as square pattern, rotated by 45°	$f = S_w + 4 \cdot S_s = S_w + 4 \cdot \frac{1}{4} \cdot S_w = 2 \cdot w^2$; $S_{square} = p^2$; $k = \frac{2 \cdot w^2}{p^2}$	see description to point 1.4	$k = \frac{1}{(K_p)^2}$

Pos.	Configuration of rows of holes in the partitions	Design ratio to calculate coefficient k	Description and permissible variations of design ratio parameters	Formula for calculation of coefficient k
2.4	offset rows as hexagon pattern	$f = S_w + 4 \cdot S_s = S_w + 4 \cdot \frac{1}{4} \cdot S_w = 2 \cdot w^2$; $S_{\text{rectang}} = p_1 \cdot p_2$; $k = \frac{2 \cdot w^2}{p_1 \cdot p_2}$	see description to point 1.1 and 1.3	$k = \frac{1}{(K_p)^2}$
3. For rectangular-shaped holes				
3.1	straight rows as rectangular pattern	$f = 4 \cdot S_s = 4 \cdot \frac{1}{4} \cdot S_w = a \cdot b$; $S_{\text{rectang}} = p_1 \cdot p_2$; $k = \frac{a \cdot b}{p_1 \cdot p_2}$	a is hole width, cm ($a = 1 - 10$ cm); b is hole length, cm ($b = 0,1 \dots a - 0,1$ cm); p_1 is horizontal distance between centers of the holes, cm; ($p_1 = K_p \cdot a$, at $K_p = 1.1 - 1.3$); p_2 is vertical distance between centers of the holes, cm ($p_2 = K_p \cdot b$, at $K_p = 1.1 - 1.3$)	$k = \frac{1}{(K_p)^2}$
3.2	offset rows	$f = S_w + 4 \cdot S_s = S_w + 4 \cdot \frac{1}{4} \cdot S_w = 2 \cdot a \cdot b$; $S_{\text{rectang}} = p_1 \cdot p_2$; $k = \frac{2 \cdot a \cdot b}{p_1 \cdot p_2}$	the range of selected values a, b , p_1 is given in description to p. 3.1; $p_2 = K_p \cdot 2b$, at $K_p = 1.1 - 1.3$)	$k = \frac{1}{(K_p)^2}$
4. For hexagon-shaped holes				
4.1	offset rows as hexagon pattern	$f = \frac{1}{2} \cdot S_w = \frac{1}{2} \cdot \frac{1}{2} \cdot w^2 \cdot n \cdot \sin \frac{360^\circ}{n} =$ $= \frac{3 \cdot \sqrt{3} \cdot w^2}{4}$; $S_{\text{triangle}} = \frac{1}{2} \cdot p \cdot \left(\frac{p}{2}\right) \cdot \text{tg} 60^\circ =$ $= \frac{p^2 \cdot \sqrt{3}}{4}$; $k = \frac{3 \cdot w^2}{p^2}$	w is hexagon side, cm ($w = 1 - 10$ cm); n is number of regular polygon sides ($n = 6$); p is distance between centers of the holes, cm; $p = 1.7321 \cdot K_p \cdot w$, at $K_p = 1.1 - 1.3$)	$k = 0.9999 \cdot \frac{1}{(K_p)^2}$
4.2	straight rows as square pattern	$f = 4 \cdot S_s = 4 \cdot \frac{1}{4} \cdot S_w =$ $\frac{1}{2} \cdot w^2 \cdot n \cdot \sin \frac{360^\circ}{n} = \frac{3 \cdot \sqrt{3} \cdot w^2}{2}$; $S_{\text{square}} = p^2$; $k = \frac{3 \cdot \sqrt{3} \cdot w^2}{2 \cdot p^2}$	$P = K_p \cdot 2w$, at $K_p = 1.1 - 1.3$	$k = 0.25 \cdot \frac{1}{(K_p)^2}$

square, hexagon and rectangle) the coefficient k depends only on the perforation pitch, i. e. the correction factor K_p . Therefore, the coefficient k value can be determined by the formulas shown in column 5 of Table 1.

At the end of the analysis we determine the settling depth of suspended particles of different settling velocity for various types of partition perforated areas and for their related flow coefficient (k), calculated from the formulas obtained. The calculations are performed with assigning the specific values of effect of suspended particles removal from mine waters ($P, \%$), by the method described in [10].

For the calculation of initial data we select the following geometric parameters of the settling basin: initial width $B_0 = 10$ m, slope of bottom $\alpha \approx 30^\circ$, plan view of the contraction angles $\beta \approx 84^\circ$ and the length of the settling basin $L = 20$ m, finite width $B_k = 6$ m and maximum depth $H_k = 11.5$ m.

The calculation data for six hole types and their configuration in partitions are given in Fig. 2 with related curve fitting equations provided below:

- first perforation pattern – offset, diagonally-offset and straight rows of square and rectangular holes as square pattern; offset rows of hexagon holes: $h_{os} = -0.0017 \cdot P^2 + 0.0396 \cdot P + 10.728$, at $R^2 = 0.992$;

- second perforation pattern – offset rows of round holes: $h_{os} = -0.0022 \cdot P^2 + 0.058 \cdot P + 10.55$, at $R^2 = 0.989$;

- third perforation pattern – diagonally-offset and straight rows of round holes as square pattern: $h_{os} = -0.0032 \cdot P^2 + 0.0961 \cdot P + 10.178$, at $R^2 = 0.984$;

- fourth perforation pattern – straight rows of hexagon holes: $h_{os} = -0.00146 \cdot P^2 + 0.03566 \cdot P + 8.2592$, at $R^2 = 1$;

- fifth perforation pattern – straight rows of square holes as rectangular pattern: $h_{os} = -0.002 \cdot P^2 + 0.0508 \cdot P + 10.624$, at $R^2 = 0.992$;

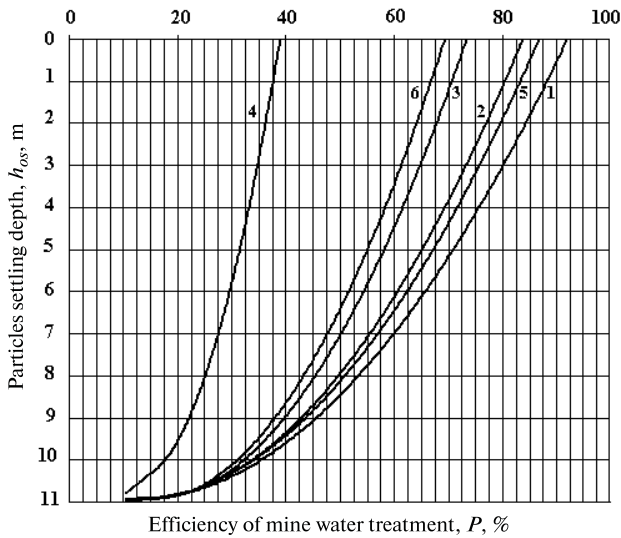


Fig. 2. Settling depth of suspended particles versus efficiency level of mine waters treatment for various perforation patterns:

1 – offset, diagonally-offset and straight rows of square and rectangular holes as square pattern; offset rows of hexagon holes; 2 – offset rows of round holes; 3 – diagonally-offset and straight rows of round holes as square pattern; 4 – straight rows of hexagon holes; 5 – straight rows of square holes as rectangular pattern; 6 – straight rows of round holes as rectangular pattern

- sixth perforation pattern – straight rows of round holes as rectangular pattern: $h_{os} = -0.0037 \cdot P^2 + 0.1108 \cdot P + 10.09$, at $R^2 = 0.988$.

Some of the expected process parameters of horizontal settling basin as per partition perforation patterns are shown in the Table 2.

Presented relationships and values illustrate obviously the effect of removal of particles of different settling velocity from mine waters. As we can see, the maximum effect of mine water treatment is provided by the perforation pattern 1.

Table 2

Values of the expected process parameters of a horizontal settling basin as per patterns

Perforation pattern	Expected effect of mine water treatment, P, %	Approximate settling depth of particles, h _{os} , m	Settling velocity of particles, mm/s
1	91.0	0.25	0.073
2	83.0	0.21	0.120
3	73.0	0.14	0.228
4	38.0	0.73	2.070
5	86.0	0.20	0.100
6	69.0	0.12	0.292

Therefore, the vertical cross partitions with square, rectangular or hexagonal holes are recommended to set in an improved horizontal settling basin. In this case their configuration related to each other may be as follows:

- in case of square perforation pattern – with straight rows as square pattern, with offset or diagonally-offset rows;
- in case of rectangular perforation pattern - with straight or offset rows;
- in case of hexagon perforation pattern – with offset rows.

The conclusions and further development perspectives. Based on the investigations performed, the following results and parameters have been obtained and determined:

- flow coefficient of the partition perforated area for various perforation patterns;
- analytical dependences of variation of flow coefficient of the partition perforated area - on pitch of holes that allows determining a distance between holes centers for various perforation patterns;
- characteristic curves and analytical dependences of suspended particles settling depth on the effect of mine water treatment for various perforation patterns;
- the most rational geometric parameters of perforated areas of partitions installed in the improved settling basin to enable obtaining the maximum efficiency of mine waters cleaning of suspended particles with regard to their settling velocity.

As the future research activity prospective, it is planned to implement the results obtained and to assess operational efficiency of improved horizontal settling basins in mines of major coal mining regions of Ukraine.

References / Список літератури

1. Zvereva, V. and Krupskaya, L., 2015. Rare earth elements in mine, slime, and river waters in the Kavalerovsky and Dalnegorsky districts of the Russian Far East. *Russian Journal of General Chemistry*, Vol. 85, No. 12, pp. 2867–2873.
2. Perkova, T.I. and Rudakov, D.V., 2014. Study of leaching in fractured rocks affected by mineralized mine water, *Naukovyi Visnyk Natsionalnoho Hirnychoho Universytetu*, No. 5, pp. 5–10.
3. Перкова Т.И. Исследование выщелачивания трещиноватых пород под влиянием минерализованных шахтных вод / Т.И. Перкова, Д.В. Рудakov // *Науковий вісник НГУ*. – 2014. – № 5. – С. 5–10.
4. Biliaiev, M.M., Kirichenko, P.S. and Kharytonov, M.M., 2013. Numerical Simulation of the Sea Pollution for the Case of Mine Waters Discharge. *Black Sea Energy Resource Development and Hydrogen Energy Problems Part of the series NATO Science for Peace and Security Series C: Environmental Security*, pp. 315–324.
4. Gorova, A., Pavlychenko, A., Kulyna, S. and Shkremetko, O., 2013. *The investigation of coal mines influence on ecological state of surface water*

bodies. In: Annual Scientific-Technical Collection Mining of Mineral Deposits. Leiden, The Netherlands: CRC Press / Balkema, pp. 303–305.

5. Kroik, A.A., 2014. Ecological safety of subterranean water on the territory of mining enterprises, *Journal of Water Chemistry and Technology*, Vol. 36, No. 4, pp. 198–202.

6. Wei, X., Wolfe, F.A. and Han, Y., 2014. Mine Drainage: Characterization, Treatment, Modeling, and Environmental Aspect. *Water Environment Research*, No. 86(10), pp. 1515–1534.

7. Wolkersdorfer, Christian, 2008. *Water Management at Abandoned Flooded Underground Mines: Fundamentals, Tracer Tests, Modelling, Water Treatment*. Springer-Verlag Berlin Heidelberg.

8. Savchuk, V., Prykhodchenko, V., Buzylko, V., Prykhodchenko, D. and Tykhonenko, V., 2013. *Complex use of coal of Northern part of Donbass*. In: Annual Scientific-Technical Collection Mining of Mineral Deposits. Leiden, The Netherlands: CRC Press / Balkema, pp. 185–191.

9. Vagonova, O.G. and Volosheniuk, V.V., 2012. Mining enterprises' economic strategies as derivatives of nature management in the system of social relations, *Naukovyi Visnyk Natsionalnoho Hirnychoho Universytetu*, No. 2, pp. 127–134.

Вагонова О.Г. Економічні стратегії гірничих підприємств як похідна раціональності природокористування в системі суспільних відносин / О.Г. Вагонова, В.В. Волошенко // Науковий вісник НГУ. – 2012. – № 2. – С. 127–134.

10. Kolesnyk, V. Ye. and Kulikova, D. V., 2013. Justification of quantity perforated partitions and intervals their placement in improved sedimentation tank of mine water. *Naukovyi Visnyk Natsionalnoho Hirnychoho Universytetu*, No. 4, pp. 92–98.

Колесник В.Е. Обоснование количества перфорированных перегородок и области их размещения в усовершенствованном отстойнике шахтной воды / В.Е. Колесник, Д.В. Куликова // Науковий вісник НГУ. – 2013. – № 4. – С. 92–98.

Мета. Наукове обґрунтування найбільш раціональних геометричних параметрів перфорованої області (форми й розташування отворів один щодо одного) вертикальних поперечних перегородок, що розміщуються в удосконаленому відстійнику шахтної води, для підвищення коефіцієнта їх пропускної здатності та, як наслідок, ефективності очищення (освітлення) води від завислих часток.

Методика. Вибір варіанту перфорації перегородок здійснювався на основі вивчення та зіставлення геометричних параметрів перфорованої області, а саме: форми, розміру отворів і їх розташування один щодо одного; поправочного коефіцієнта, що дозволяє визначити відстань між центрами отворів (крок перфорації); коефіцієнта пропускної здатності перфорованої області перегородки.

Результати. Визначені коефіцієнти пропускної здатності перфорованої області перегородки

за різних варіантів перфорації. Отримані аналітичні залежності зміни пропускної здатності перфорованої області перегородки від відстані між центрами отворів.

Наукова новизна. Виявлені закономірності зміни коефіцієнтів пропускної здатності перфорованої області перегородки, у залежності від величини поправочного коефіцієнта, дозволяють визначити відстань між центрами отворів за різних варіантів перфорації. Уперше встановлені залежності (у вигляді графіків і рівнянь регресії) між глибиною осідання завислих часток в удосконаленому відстійнику та ефективністю очищення шахтної води для різних варіантів перфорації перегородок.

Практична значимість. Результати дослідження дозволили обґрунтувати раціональні геометричні параметри перфорованої області поперечних вертикальних перегородок, що розміщуються в удосконаленому відстійнику шахтної води. Впровадження отриманих результатів дозволить підвищити ефективність очищення шахтних вод від завислих речовин і знизити рівень забруднення поверхневих вод у вугледобувних регіонах.

Ключові слова: шахтні води, завислі речовини, забруднення водою, горизонтальний відстійник, перфоровані перегородки, ефективність очищення

Цель. Научное обоснование наиболее рациональных геометрических параметров перфорированной области (формы и расположения отверстий друг относительно друга) вертикальных поперечных перегородок, размещаемых в усовершенствованном отстойнике шахтной воды, для повышения коэффициента их пропускной способности и, как следствие, эффективности очистки (осветления) воды от взвешенных частиц.

Методика. Выбор варианта перфорации перегородок осуществлялся на основании изучения и сопоставления геометрических параметров перфорированной области, а именно: формы, размера отверстий и их расположения друг относительно друга; поправочного коэффициента, позволяющего определить расстояние между центрами отверстий (шаг перфорации); коэффициента пропускной способности перфорированной области перегородки.

Результаты. Определены коэффициенты пропускной способности перфорированной области перегородки при различных вариантах перфорации. Получены аналитические зависимости изменения пропускной способности перфорированной области перегородки от расстояния между центрами отверстий.

Научная новизна. Выявленные закономерности изменения коэффициентов пропускной способности перфорированной области перегородки, в зависимости от величины поправочного коэффициента, позволяют определить расстояние между центрами отверстий, при разных вари-

антах перфорации. Впервые установлены зависимости (в виде графиков и уравнений регрессии) между глубиной оседания взвешенных частиц в усовершенствованном отстойнике и эффективностью очистки шахтной воды для различных вариантов перфорации перегородок.

Практическая значимость. Результаты исследования позволили обосновать рациональные геометрические параметры перфорированной области поперечных вертикальных перегородок, размещаемых в усовершенствованном отстойнике шахтной воды. Внедрение полученных резуль-

татов позволит повысить эффективность очистки шахтных вод от взвешенных веществ и снизить уровень загрязнения поверхностных вод в угледобывающих регионах.

Ключевые слова: шахтные воды, взвешенные вещества, загрязнение водоемов, горизонтальный отстойник, перфорированные перегородки, эффективность очистки

Рекомендовано до публікації докт. техн. наук В. І. Голінком. Дата надходження рукопису 08.12.15.

ІНФОРМАЦІЙНІ ТЕХНОЛОГІЇ, СИСТЕМНИЙ АНАЛІЗ ТА КЕРУВАННЯ

UDC 681.3

T. O. Ruzova¹, Cand. Sc. (Tech.),
O. P. Tolstopyat¹, Cand. Sc. (Tech.), Senior
Research Fellow,
V. I. Yeliseyev², Cand. Sc. (Phys.-Math.) Senior
Research Fellow,
L. O. Fleer¹

1 – Oles Honchar Dnipropetrovsk National University
Dnipro, Ukraine, e-mail: ruzov1973@bk.ru

2 – M. S. Polyakov Institute of Geotechnical Mechanics the
NAS of Ukraine, Dnipro, Ukraine

EVALUATING GEOMETRIC PARAMETERS OF DISPERSED PARTICLE AGGREGATES

Т. О. Рузова¹, канд. техн. наук,
О. П. Толстопят¹, канд. техн. наук, старш.
наук. співроб.,
В. І. Єлісеєв², канд. фіз.-мат. наук, старш.
наук. співроб.,
Л. О. Флеєр¹

1 – Дніпропетровський національний університет,
імені Олесь Гончара, м. Дніпро, Україна, e-mail:
ruzov1973@bk.ru

2 – Інститут геотехнічної механіки ім. М. С. Полякова
НАН України, м. Дніпро, Україна

ВИЗНАЧЕННЯ ГЕОМЕТРИЧНИХ ХАРАКТЕРИСТИК АГРЕГОВАНИХ УТВОРЕНЬ ДИСПЕРСНИХ ЧАСТИНОК

The particle size largely determines the properties of dispersed materials. It is a key parameter for equipment performance evaluation. The measurement process is substantially complicated by the presence of aggregated structures.

Purpose. To develop complex method for evaluating geometrics of emulsion drops and other dispersed formations of spherical particles considering their aggregation. The method is based on aggregate structure and contours, using marking of analyzed objects.

Methodology. The method includes several steps: image filtering, converting it to a monochrome mode, evaluating the aggregate contour, correcting the contour, setting particle markers according to glares on particle surfaces, making the skeleton, determining connecting points. To decompose aggregate fragments containing several markers, aggregate's area is distributed between the particles according to the Voronoi diagram. Parameters of circles corresponding to particles are evaluated from geometrics of corresponding aggregate fragments. The method is illustrated by the images of real emulsion fragments (type II emulsions – water in oil).

Findings. The developed method allows realizing segmentation of complex structured aggregates, consisting of many spherical particles, containing internal objects whose contour is located entirely inside the aggregate. The number of incoming particles is not limited.

Originality. The developed method of aggregate segmentation (emulsion drops) is noise-resistant and allows segmenting the aggregates of a complex structure by evaluation of connecting points of its particles, according to the aggregate structure and by marking the particles when evaluation of connecting points with the necessary precision is impossible (in case of a small convexity defect or presence of internal particles). The glares on particle surfaces may serve as markers.

Practical value. The method may be used to evaluate dispersity of emulsions and other finely divided materials at various industries.

Keywords: *aggregate, dispersive structures, segmentation, Voronoi diagram, markers, particle connecting points*

Introduction. The finely divided materials are used in different branches of activity: in the energy sector, metallurgy, chemical industry, and food industry. The particle size of used disperse mediums – emulsions, powders, aerosols and gas-liquid systems largely determines their physical and chemical properties and is often a key parameter for evaluating the effectiveness of the equipment such as dust removal devices, emulsifiers, sprays, centrifuges [1–3]. It should be noted that the particle size (dust, aerosols, drug ingredients and dietary supplements) is the most important factor in determining their impact on the human body [4].

The technology progress has led to development of a fundamentally new approach to dispersed composition determination. It is based on measuring sizes of microparticles by their images. The progress of computer technology has greatly accelerated image analysis process and made it much less labor-intensive. This method, unfortunately, is not free of problems associated with noisy images, the heterogeneity of their illumination, the presence of shades on the measured object, etc.

Problem statement. A separate problem is the presence of agglomerated, aggregated particles, which significantly complicates the process of measurement and leads to a significant distortion of the results; so much attention is paid to the solution of this problem [5–8]. Known approaches to solving the problem of aggregate formation decomposition are based on the analysis of object geometry using morphological approaches, the shades as a source of information about the study group of overlapping objects, intensity fluctuations in contact area and other approaches. Excessive refinement of objects, sensitivity to noise and significant computational cost, as well as the impossibility to separate units consisting of a large number of particles with sufficient accuracy – these and other drawbacks complicate practical application of these methods. A separate problem is segmentation of units with low convexity defect consisting of a large number of particles, and segmentation formations consisting of objects with a high degree of overlap.

The objective of this study is to provide a research-based comprehensive method for determining the geometric characteristics of aggregated elements of dispersed formations (emulsion drops) which is resistant to image noises and is able to segment aggregates of complex configuration, both by determining points of particle contact, analyzing the aggregate structure and by marking particles when it is impossible to find contact points with the necessary precision (in the case of a small convexity defect or presence of internal particles). Light spots on the drops surfaces can serve as such markers.

Methodology. At the first stage the image is filtered. It is cleared from high-frequency noises and transferred to a monochrome mode. The process is based on threshold segmentation algorithm with a sliding window involving calculation of adaptive brightness threshold T for each pixel with coordinates (x_0, y_0)

$$T(x_0, y_0) = \frac{1}{W * H} \sum_{y=y_0-H/2}^{y=y_0+H/2} \sum_{x=x_0-W/2}^{x=x_0+W/2} g(x, y),$$

where W is width; H is height of a sliding window.

The next step is to determine coordinates of the aggregate contour points. For correct identification of objects whose contour is crossed by the image frame (Fig. 1, *a*) in order to avoid errors due to the addition of excess space, the authors propose to consider each of these figures twice, taking into account the additional image area between the object contour and frame – type “B” aggregate (Fig. 1, *c, d*) and without it – type “A” aggregate (Fig. 1, *b*) and then select the image which is the most adequate to the real object.

The main feature of the images of dispersed structures is uneven lighting, noisiness and low contrast. Therefore, the method of adaptive threshold selection is not always useful as well. Sometimes it leads to gaps in objects’ contours in an obtained monochrome picture. That is why it is advisable to correct selected contours [9] by clarifying the threshold based on brightness analysis.

The conclusion about the success of correction may be made by comparing the geometric parameters of the unit, calculated from the contour on the basis of previous and new thresholds.

$$P_1 < P_0; \quad (1)$$

$$\left| \frac{P_1 - P_0}{P_0} \right| < 0,1, \quad \left| \frac{S_1 - S_0}{S_0} \right| < 0,1, \quad (2)$$

where P_0, S_0 are the perimeter and area of the figure measured by the results of adaptive threshold segmentation; P_1, S_1 are the perimeter and area measured by the adjusted threshold value.

A common defect of contour segmentation is “transformation” of the circle (drop contour) (Fig. 2, *a*) in the crescent (Fig. 2, *b*), whose perimeter is much greater than the perimeter of the respective circle. Therefore, a decrease in perimeter (1) indicates a successful solution of this problem (Fig. 2, *c*). A large increase in the area, on the contrary, indicates overvalued

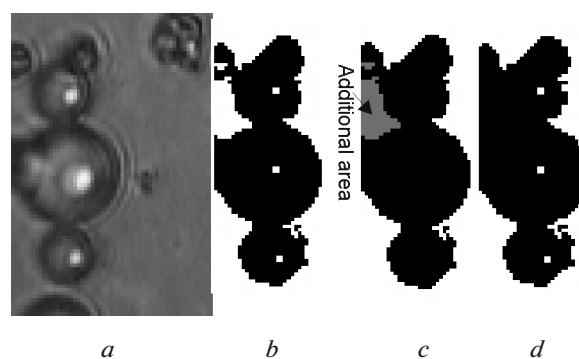


Fig. 1. Analysis of the aggregates touching the image border:

a – source object; *b* – type “A” aggregate; *c, d* – type “B” aggregate. Aggregates markers are indicated by the dots

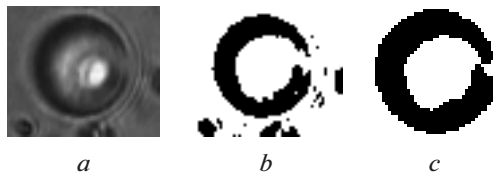


Fig. 2. Closing the gaps by correcting the contour of water drop in the oil:

a – the original image; *b* – monochrome image before contour correction; *c* – resulting image of a drop contour

threshold, resulting in a connection of the noises to the object – unrelated areas. Criteria (2) limit the growth of the area and perimeter.

The next step is to mark aggregate particles. Light flares on the surfaces of water-oil emulsion drops can act as such markers. This marking allows decomposing aggregates with low defect of convexity if structure analysis [10] is not effective and/or in the presence of internal particles.

Heterogeneity of substance of a drop and the inclusion of foreign objects can lead to various optical effects on the drop surface, leading to fanciful flares (Fig. 3).

To use the flare as a marker, it is necessary to prevent its decomposition. So we must filter the object in order to clean flare image from the noise and make it more uniform. Then we can take flare centers as markers.

The information about the markers can be used not only for aggregate decomposition, but also for the correct identification of objects, whose contour is crossed by an image frame.

Thus, if the contour of “B” aggregate has more glares than the corresponding “A” aggregate, this fact indicates that one or more drops within the aggregate are cut by frame (Fig. 4). In this case, the “A” unit is removed and, instead, “B” unit is used for further analysis. If the connection of an additional field has not led to an increase in the number of markers, we

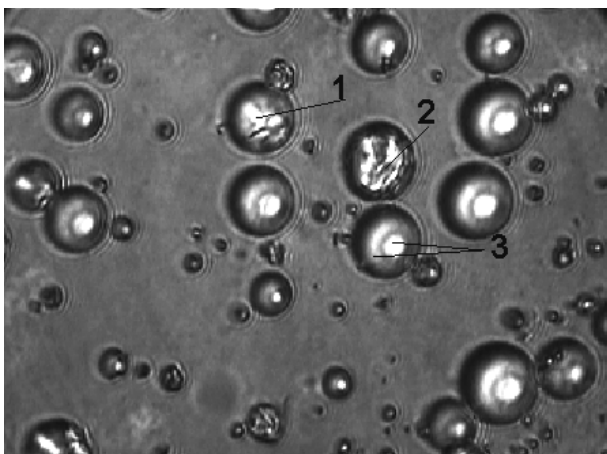


Fig. 3. The image of a water-oil emulsion:

1–3 – optical effects when light passes through a drop

can say that the added area in “B” unit corresponds to the background (Fig. 1). In this case, “A” unit is kept for further analysis.

The skeleton of the aggregate is constructed from the points of the refined contour. It allows obtaining general information about the aggregate structure. The proposed method for skeleton construction includes the following steps: building a pilot skeleton based on Zhang-Suen algorithm, removing redundant connectivity, finding reference points and presenting the skeleton as a set of branches between reference points, refining the skeleton structure to represent the branch by line segments, ordering branches according to advancing from the periphery to the center of the aggregate.

Drop attachment points are defined as the “narrowest” places of the considered aggregate – the isthmuses $Q_1^{(1)}Q_2^{(1)}$, $Q_1^{(2)}Q_2^{(2)}$, $Q_1^{(3)}Q_2^{(3)}$ – Fig. 5.

To do this, we build perpendicular AB at each point P of the considered skeleton branch, and find the point of its intersection P_1 , P_2 with the aggregate contour. We call P_1P_2 the inner part of the perpendicular. Since the isthmuses are the narrowest parts of the aggregate, perpendiculars corresponding to them have the shortest internal parts.

However, unit nonconvexity complicates the problem, because in general the line can cross a non-convex object in more than two points. In this case, the search of isthmus requires a special method. A detailed description of this method is presented in [10].

For efficient segmentation of internal elements and aggregate fragments formed by several drops with high overlapping, when the search of connection points is not effective, it is advisable to supplement this method

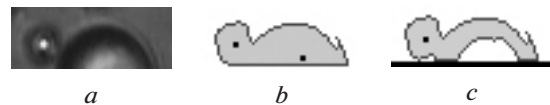


Fig. 4. Analysis of the aggregates, cut with an image frame:

a – the image of the original object; *b* – the image without taking an additional area (“A” type unit); *c* – the image with an additional area (“B” type unit). The points indicate markers

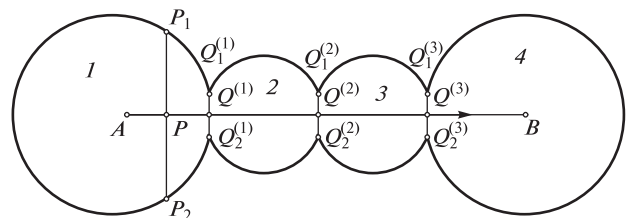


Fig. 5. The general scheme of aggregate decomposition:

AB – skeleton branch; P – an arbitrary point of AB branch; P_1 , P_2 – the points of intersection of the contour and perpendicular to AB at point P ; $Q^{(1)}$, $Q^{(2)}$, $Q^{(3)}$ – the points where aggregate width function is minimal; $Q_1^{(1)}Q_2^{(1)}$, $Q_1^{(2)}Q_2^{(2)}$, $Q_1^{(3)}Q_2^{(3)}$ – the point of drop connection; *1–4* – the number of drops

with markers [9]. In this case the number of markers corresponds to the number of drops in the unit. For example, if the unit or a fragment contains only one marker, we can say that it contains a single drop, several glares indicate the presence of several drops and aggregate area may be distributed between them according to Voronoi diagram. Each particle corresponds to a certain diagram cell. The particle radii can be calculated from the area and the perimeter of the corresponding diagram cell. The method of constructing Voronoi diagram on the base of marker points in non-convex area was considered in [9].

Some drops may have no glares, so it is advisable to combine these two methods. Thus, application of marking technique to the object in Fig. 6 without analyzing its structure leads to errors in segmentation of the fragments 1 and 2, which contain no glare, while a combination of these methods can eliminate this disadvantage.

Analysis of the aggregate structure allows selecting the point of particle attachment (Fig. 7, b). Decompo-

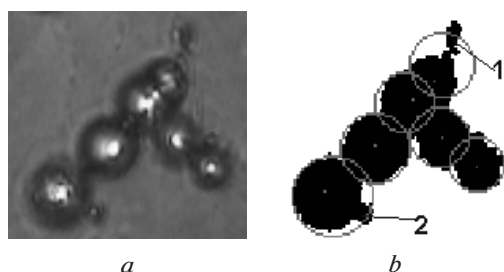


Fig. 6. Decomposition of the unit by marking drops without analyzing the structure:
a – the original image; *b* – the resulting image; points represent the particles markers; 1, 2 – fragments with segmentation inaccuracy

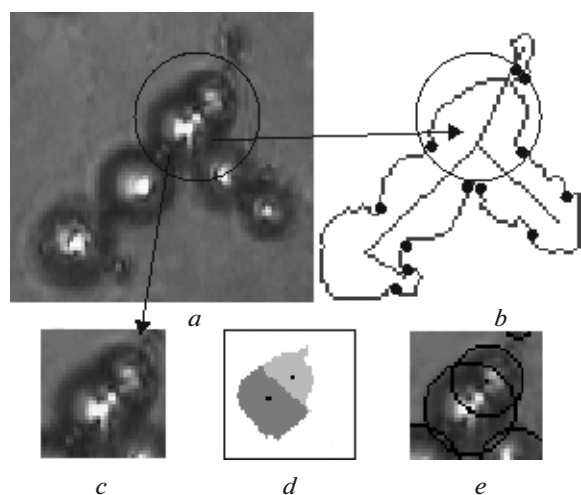


Fig. 7. Decomposition of type II emulsion (water in oil) image:
a – the original image; *b* – the image with attachment points; *c* – segment with low defect of convexity; *d* – separation of Fig. 7, *c* by means of Voronoi diagram; *e* – segmentation of Fig. 7, *c*; square points represent the particle markers, round points – drop connections

sition of the aggregate according to these points provides adequate segmentation of the drops, including non-glaring drops. Analysis of this unit is difficult because of the section with low convexity defect (Fig. 7, *c*). The use of the marker method followed by distribution of the area according to Voronoi diagram (Fig. 7, *d*) provides adequate segmentation of this object (Fig. 7, *e*). The segmentation of the whole unit made by the complex method combining the analysis of the structure with markers placement is shown in Fig. 8.

The described method of aggregate separation is illustrated by the image of type II emulsion – Fig. 9.

Conclusions. The problems of image processing are heterogeneity of lighting, noisy background and low contrast. While measuring microobjects, the presence of aggregated structures often leads to significant errors in dispersed composition evaluation.

The authors developed a complex method for evaluating geometrics of emulsion drops and other dispersed formations of spherical particles considering their aggregation. The method is based on the aggregate structure and contours, using marking of analyzed objects.

The method includes several steps: image filtering, converting it to a monochrome mode, evaluating the aggregate contour, correcting the contour, setting particle markers according to glares on particle surfaces, making the skeleton, introducing the function for each skeleton branch, which characterizes the width of cor-

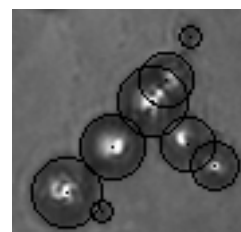


Fig. 8. Segmentation of the aggregate shown in Fig. 7, *a* by analyzing its structure and marking particles

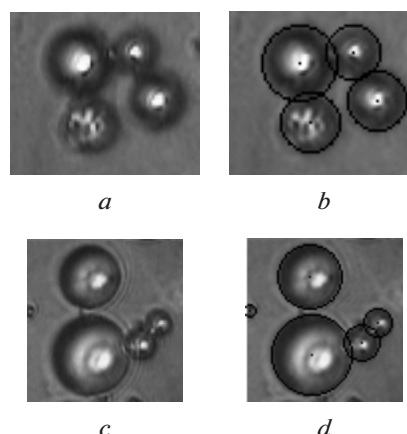


Fig. 9. Decomposition of type II emulsion (water in oil) images:
a, c – original images; *b, d* – results of segmentation

responding aggregate portion, determining connecting points as local minimums of this function. To decompose aggregate fragments containing several markers, the aggregate's area is distributed between the particles according to the Voronoi diagram. Parameters of circles corresponding to particles are evaluated from geometrics of corresponding aggregate fragments.

The method is illustrated by the images of real emulsion fragments (type II emulsions – water in oil)

The developed method allows realizing segmentation of complex structured aggregates consisting of many spherical particles, containing internal objects whose contour is located entirely inside the aggregate. The number of incoming particles is not limited.

The method may be used to evaluate dispersity of emulsions and other finely divided materials at various industries.

References / Список літератури

1. Vasylevskiy, M. V., Nekrasova, K. V., Razva, A. S. and Zykov, Ye. G., 2009. Cohesion estimation of dispersed material of aggregated particles. *Zavodskaya Laboratoriya. Diagnostika materialov*, Vol. 75, No. 5, pp. 32–36.

Оценка связности дисперсного материала из агрегированных частиц / М. В. Василевский, К. В. Некрасова, А. С. Разва, Е. Г. Зыков // Заводская лаборатория. Диагностика материалов. – 2009. – Т. 75. – № 5. – С. 32–36.

2. Dubrovskiy, V. V., Podvysotskiy, A. M. and Bashtovoy, A. I., 2004. Drops dispersity evaluation when liquid spraying out of centrifugal nozzle. *Tekhnologiya i tekhnika drukarstva*, No. 2–3(4–5), pp. 94–99.

Дубровский В. В. Определение дисперсного состава капель при распыливании жидкости из центробежной форсунки / В. В. Дубровский, А. М. Подвысоцкий, А. И. Баштовой // Технологія і техніка друкарства. – 2004. – № 2–3(4–5). – С. 94–99.

3. Nakobian, M. G., 2013. Determination of the dispersity level of working emulsion liquids by the optical method. *Proceedings of state engineering university of Armenia. Mechanics, machine-building, machine science*, Issue 16, No. 1, pp. 1–4.

Акопян М. Г. О методе экспресс-анализа степени дисперсности эмульсионных рабочих жидкостей оптическим методом / М. Г. Акопян // Вестник государственного инженерного университета Армении. Серия „Механика, машиноведение, машиностроение“. – 2013 – Вып. 16. – № 1. – С. 1–4.

4. Uriash, V. F., Stepanova, E. A., Grishatova, N. V., Gruzdeva, A. E., Demarin, V. T. and Tumanova, A. N., 2009. The influence of dispersity degree of food additives on joint sorption of lead and cadmium. *Vestnik of Lobachevsky University of Nizhni Novgorod*, No. 5, pp. 113–117.

Влияние степени дисперсности пищевых добавок на совместную сорбцию свинца и кадмия / В. Ф. Урьяш, Е. А. Степанова, Н. В. Гриша-

това [и др.] // Вестник Нижегородского университета им. Н. И. Лобачевского. – 2009. – № 5. – С. 113–117.

5. Charters, G. and Graham, J., 2002. Disentangling chromosome overlaps by combining trainable shape models with classification evidence. *IEEE Transactions on Signal Processing*, Vol. 50, pp. 2080–2086.

6. Honkanen, M., 2007. Analysis of the overlapping images of irregularly-shaped particles, bubbles and droplets. In: *Papers of International Conference on Multiphase Flow, ICMF 2007*, Leipzig, Germany, pp. 370–382.

7. Adiga, P. S. U., Malladi, R., Baxter, W. and Glaeser, R. M., 2004. A binary segmentation approach for boxing ribosome particles in cryo EM micrographs. *Journal of Structural Biology*, Vol. 145, Issue 1–2, pp. 142–151.

8. Korath, J. M., Abbas, A. and Romagnoli, J. A., 2007. Separating touching and overlapping objects in particle images – a combined approach. *Chemical Engineering Transactions*, No. 11, pp. 167–172.

9. Ruzova, T. A., Tolstopyat, A. P., Yeliseyev, V. I. and Fler, L. A., 2014. Segmentation of aggregated elements in dispersive formations using Voronoi diagram. *Naukovyi Visnyk Natsionalnoho Hirnychoho Universytetu*, No. 2, pp. 112–118.

Сегментация агрегированных элементов дисперсных образований с помощью диаграммы Вороного / Т. А. Рузова, А. П. Толстопят, В. И. Елисеєв, Л. А. Флеєр // Науковий вісник Національного гірничого університету. – 2014. – № 2. – С. 112–118.

10. Ruzova, T. A., Tolstopyat, A. P., Yeliseyev, V. I. and Fler, L. A., 2013. Images decomposition of aggregated elements in dispersive formations by their structure. *Naukovyi Visnyk Natsionalnoho Hirnychoho Universytetu*, No. 6, pp. 117–123.

Декомпозиція зображень агрегированих елементів дисперсних образований по їх структурі / Т. А. Рузова, А. П. Толстопят, В. И. Елисеєв, Л. А. Флеєр // Науковий вісник Національного гірничого університету. – 2013. – № 6. – С. 117–123.

Розмір частинок, у значній мірі, визначає властивості дисперсних матеріалів і є вирішальним параметром при оцінюванні ефективності обладнання. Наявність агрегованих частинок істотно ускладнює процес вимірювань.

Мета. Створення комплексного методу визначення геометричних характеристик крапель емульсій та інших дисперсних частинок сферичної форми з урахуванням їх агрегування, заснований на інформації про структуру та контур агрегату, із застосуванням маркування аналізованих об'єктів.

Методика. Метод включає кілька етапів: фільтрація зображення та переведення його до монохромного режиму, визначення контуру агрегату, корекція виділеного контуру, розстановка маркерів частинок за відблесками на їхній по-

верхні, побудова скелету, визначення точок приєднання частинок. Для декомпозиції фрагментів агрегату, що містять декілька маркерів, розподіл площі фрагмента агрегату між частинками, що входять до його складу, здійснюється шляхом побудови діаграми Вороного. Параметри окружностей, відповідних зображень частинок, визначаються за геометричними характеристиками відповідних їм фрагментів агрегату. Метод проілюстрований на фрагментах зображень реальних емульсій другого роду (вода в маслі).

Результати. Розроблений метод дозволяє здійснювати сегментацію агрегатів складної конфігурації, що складаються з частинок сферичної форми та містять внутрішні об'єкти, контур яких розташовується цілком усередині агрегату, без обмежень на число частинок.

Наукова новизна. Розроблено метод сегментації агрегованих елементів дисперсних утворень (крапель емульсій), що є стійким до шумів зображення та дозволяє здійснювати сегментацію агрегатів складної конфігурації як шляхом визначення точок контакту частинок агрегату за даними про його структуру, так і шляхом маркування частинок у випадках, коли знаходження точок приєднання з необхідною точністю неможливе (у разі малого дефекту опуклості або наявності внутрішніх частинок). Такими маркерами можуть виступати світлові відблиски на поверхні крапель.

Практична значимість. Метод може бути застосований для визначення ступеня дисперсності емульсій та інших тонкоподрібнених матеріалів у різних галузях промисловості.

Ключові слова: агрегат, дисперсні утворення, сегментація, діаграма Вороного, маркери, точки приєднання частинок

Размер частиц, в значительной степени, определяет свойства дисперсных материалов и является решающим параметром при оценке эффективности оборудования. Наличие агрегированных частиц существенно затрудняет процесс измерений.

Цель. Создание комплексного метода определения геометрических характеристик капель эмульсий и других дисперсных частиц сферической формы с учетом их агрегирования, основанного на информации о структуре и контурах агрегата, с использованием маркирования анализируемых объектов.

Методика. Метод включает следующие этапы: фильтрация изображения и перевод его в монохромный режим, определение контура агрегата, коррекция выделенного контура, расстановка маркеров частиц по бликам на их поверхности, построение скелета, определение точек присоединения частиц. Для декомпозиции фрагментов агрегата, содержащих несколько маркеров, распределение площади фрагмента агрегата между входящими в него частицами осуществляется путем построения диаграммы Вороного. Параметры окружностей, соответствующих изображениям частиц, определяются по геометрическим характеристикам соответствующих им фрагментов агрегата. Метод проиллюстрирован на фрагментах изображений эмульсий второго рода (вода в масле).

Результаты. Разработанный метод позволяет осуществлять сегментацию агрегатов сложной конфигурации, состоящих из частиц сферической формы, содержащих внутренние объекты, контур которых располагается целиком внутри агрегата, без ограничений на число входящих частиц.

Научная новизна. Разработан метод сегментации агрегированных элементов дисперсных образований (капель эмульсий), устойчивый к шумам изображения и позволяющий осуществлять сегментацию агрегатов сложной конфигурации как путем определения точек контакта частиц агрегата по данным о его структуре, так и путем маркирования частиц в случаях, когда нахождение точек соприкосновения с необходимой точностью невозможно (в случае малого дефекта выпуклости или наличия внутренних частиц). Такими маркерами могут выступать световые блики на поверхности капель.

Практическая значимость. Метод может быть применен для определения степени дисперсности эмульсий и других тонкоизмельченных материалов в различных отраслях промышленности.

Ключевые слова: агрегат, дисперсные образования, сегментация, диаграмма Вороного, маркеры, точки присоединения частиц

Рекомендовано до публікації докт. техн. наук В. І. Корсуном. Дата надходження рукопису 16.11.15.

Hongyi Cao,
Junhui Yang,
Li Wang

Xi'an Medical University, Xi'an 710021, Shaanxi, China

FAST TIME SEQUENCE DATA MINING ALGORITHM BASED ON GREY SYSTEM THEORY

Хуні Цао,
Цзюньхой Ян,
Лі Ван

Сіаньський медичний університет, м. Сіань, Шеньсі,
Китай

ШВИДКИЙ АЛГОРИТМ ІНТЕЛЕКТУАЛЬНОГО АНАЛІЗУ ЧАСОВИХ РЯДІВ НА ОСНОВІ ТЕОРІЇ СІРИХ СИСТЕМ

Purpose. With the development of the big data technology, the time sequence data mining has become a hot spot that attracts the attention of the public. Based on the correlation and cooperativity of the time sequence data, we propose the fast time sequence data mining model based on the grey system theory.

Methodology. The correlation determination method that is based on the features of the relevant coefficient of the time shift sequence is obtained. As a result, a kind of fast time sequence data mining model based on the grey system theory is proposed.

Findings. The correlation determination methodology proposed in this paper is more effective than the Pearson linear correlation coefficient, Spearman rank correlation coefficient, Kendall rank correlation coefficient and Granger causality test.

Originality. In this paper, the double sequence fast correlation determination method and curve alignment method are provided. So far, we have not found other literature on the related research.

Practical value. The research results can provide theoretical basis for the determination of the correlation of regression analysis and the time alignment.

Keywords: *grey system theory, time warping, correlation, time sequence data, data mining, curve alignment, causality test*

Introduction. Time series data is one of the most commonly seen types of data in the data mining, which is applied in many fields such as the monthly volume of runoff of a certain river, the local mean monthly temperature and precipitation, our country's consumer price index (CPI) and the gross domestic product (GDP), the earthquake wave sequence acquired at multiple observation points at the time of the occurrence of the earthquake, etc. [1]. Through the analysis on the time sequence data, some useful conclusions can be drawn, for example: Through studying the history of flow volume of the river, the temperature, precipitation and other characteristics, the forecast level for flood can be effectively improved; through the application of CPI and GDP, the degree of inflation and the momentum of economic development of the country or region can be analysed; according to the multiple seismic wave sequence, the seismic source and seismic magnitude, etc. can be accurately located [2]. Some of the non-time sequence data can also be handled through the conversion and application of the time sequence data mining method for processing, for example: Through the application of the distance from the edge of leaf to the center of the mass to describe its characteristics from different angles, a column of data can be acquired, which then can further distinguish the type of the leaf [3].

In the process of time sequence data mining, if the time difference of the data is not taken into consideration, it is easy to be influenced by intuition or prejudice, and thus cause wrong determination on the correlation; however, it does not make sense if the time difference of the related time sequence is not taken into account [4]. That is to say, in the assessment of the correlation of the sequence, it does not only require considering the time difference, but also requires that the data is correlated, therefore, the correlation and time difference between the sequences are mutually restrained [5]. At present, the correlation analysis on the time sequence data is faced with some problems, for example, the data relationship is relatively complex, the data contains noise, there is missing data or abnormal data, etc. [6]. Homogeneous data (data from the same source or with the same attributes, such as the earthquake seismic data of the same earthquake acquired in multiple locations) has natural similarity, which does not require determining the correlation, and there is no correlation or time difference constraint problem either, hence mostly applied for the classification or clustering. For the heterogeneous data (data from different sources or with different attributes, such as the amount of precipitation and river runoff volume, CPI and GDP), its correlation shall be determined, and its relevance and regression analysis etc. shall be conducted [7–9]. Therefore, the main object of the time sequence data correlation analysis is the heterogeneous data.

Similar to the binary classification problems or the two types of errors in hypothesis testing, in correlation with heterogeneous data mining or data regression to two types of errors: 1) it is believed that the related data does not have correlation; 2) it is believed that the irrelevant data has correlation and regression analysis is conducted [10]. The former often appears in actual application, such as the elevation of the sun and the ground temperature, precipitation and river runoff, if in accordance with the time control study the correlation of two groups of data may not be able to get relevant conclusions, but in fact, if both will be in time for translation, there will be close correlation. The above two types of errors can occur, for example, in the past 20 years China's GDP and the height of a person can grow before the age of 20 certainly has significant positive correlation, and this is meaningless, illogical regression, which is called nonsense regression or spurious regression. So, prior to the analysis of the data, if not considering the correlation of data, class 1 correlation error will cause the waste of potential information, data category 2 correlation errors may cause misleading for subsequent analysis. The correlation of multiple sets of data can be provided through the correlation of two groups of data.

Homogeneous data has natural similarity and a curve line can be developed. Constrained for heterogeneous time sequence data correlation and the time difference problem, based on the theory of grey system, fixed time determine the move sequence correlation, on the basis of serial correlation, and then through the curve line refining time function. When making correlation judgment on heterogeneous data, on the one hand, there is a deviation due to the sample correlation coefficient and the overall correlation coefficient; it studies the upper and lower bounds of the overall correlation coefficient. On the other hand, in order to prevent the two kinds of correlation mistakes, starting from the main causes, the study of the characteristics of two kinds of correlation error and corresponding correlation judgment method is put forward. Applicable to the curve of the heterogeneous data, line method is also applicable to homogeneous data, but what applies to homogeneous data (such as AISE) does not apply to heterogeneous data (dimension is not unified, and negative correlation, etc.). Therefore, the maximum correlation coefficient (absolute value) curve standard mainly based on the characteristics of heterogeneous data is put forward, and the GQS algorithm is applied for the solution.

Basic concept. Grey Theory Class Set. Customer confidence in businesses depends on many factors, "complete trust", "somewhat trust", "general trust" and "distrust" and other information can exactly describe the state. Therefore, we introduce a grey element, the concept of grey number, ash content and ash. Ash element refers to the incomplete information elements, grey number refers to the volume of incomplete information, grey variables refer to incomplete information, and grey variables of a specific value constitute a grey class. For example, users who evaluate the quality of products constitute a grey element; product quality assessment values, such as about 0.40

points, constitutes a grey number. All the sets of gray classes are called grey class set, noted as $G = \{g_k | k = 1, 2, \dots, r\}$, in which g_k is the k -th grey class.

For example, assume that the product quality is the grey variable, which can be "good", "general" and "poor", etc. Let the grey class set $G = \{g_1, g_2, g_3\}$, which, respectively, represents the first, second, third class, in turn, showing good, general, poor product quality in turn.

Grey class whitening function, weight matrix.

Let us set clustering entity set $D = \{d_i | i = 1, 2, \dots, m\}$, the key attributes $A = \{a_h | h = 1, 2, \dots, e\}$, grey class set $G = \{g_k | k = 1, 2, \dots, r\}$, $T_i(a_h)$ represents the entity d_i 's key attribute a_h 's score value, the monotonic function f_{hk} is defined as the grey class whitening function, as shown in Fig. 1, $E(\lambda_{hk}, 1)$ is the turning point, $f_{hk}(T_i(a_h)) = 0.81$ represents the rating value. $T_i(a_h)$ belongs to grey class with the possibility of 0.81.

Weight matrix is defined as W , as shown in Fig. 2, the matrix elements

$$W_{jk} = \lambda_{hk} / (\lambda_{1k} + \lambda_{2k} + \dots + \lambda_{hk} + \dots + \lambda_{ek});$$

$$1 \leq i \leq m, \quad 1 \leq h \leq e, \quad 1 \leq k \leq r;$$

$$W = \begin{pmatrix} w_{11} & w_{12} & \dots & w_{1k} & \dots & w_{1r} \\ w_{21} & w_{22} & \dots & w_{2k} & \dots & w_{2r} \\ \vdots & \vdots & & \vdots & & \vdots \\ w_{h1} & w_{h2} & \dots & w_{hk} & \dots & w_{hr} \\ \vdots & \vdots & & \vdots & & \vdots \\ w_{e1} & w_{e2} & \dots & w_{ek} & \dots & w_{er} \end{pmatrix}.$$

Clustering vector. W represents the weight matrix, the whitening matrix of the entity d_i is F_i , F_i and W are noted as column matrix respectively

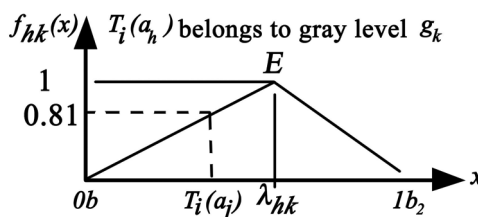


Fig. 1. Grey class whitening function

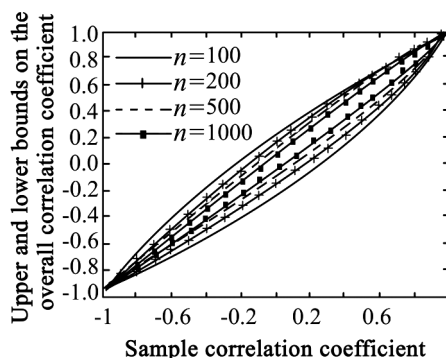


Fig. 2. Overall Correlation Coefficient Bounds (significance level $\alpha = 0.05$)

$$F_i = (\alpha_1, \alpha_2, \dots, \alpha_k, \dots, \alpha_r),$$

in which

$$a_k = (f_{1k}(T_i(a_1)), f_{2k}(T_i(a_2)), \dots, f_{hk}(T_i(a_h)), \dots; f_{ek}(T_i(a_e))); \quad W_i = (\beta_1, \beta_2, \dots, \beta_k, \dots, \beta_r),$$

in which

$$\beta_k = (W_{1k}, W_{2k}, \dots, W_{hk}, \dots, W_{ek}).$$

The clustering vector of the entity d_i is defined as σ_i ,

$$\begin{aligned} \sigma_i &= (\sigma_{i1}, \sigma_{i2}, \dots, \sigma_{ik}, \dots, \sigma_{ir}) = \\ &= (\alpha_1 \times \beta_1, \alpha_2 \times \beta_2, \dots, \alpha_k \times \beta_k, \dots, \alpha_r \times \beta_r), \end{aligned}$$

in which

$$\begin{aligned} \sigma_{ik} &= \alpha_k \times \beta_k = (f_{1k}(T_i(a_1)), f_{2k}(T_i(a_2)), \dots, f_{hk}(T_i(a_h)), \dots; \\ &f_{ek}(T_i(a_e))) \times (w_{1k}, w_{2k}, \dots, w_{hk}, \dots, w_{ek}), \quad k = 1, 2, \dots, r. \end{aligned}$$

Curve alignment relevant mining method. As in the solution for the actual problem, only sample data can be obtained. When using the sample, the overall estimation may be biased, as a result, this paper uses the sample correlation coefficient to infer the overall correlation coefficient with certain level of significance on the boundary. At the same time, in order to prevent the two types of error, this paper studies the correlation coefficient of two kinds of error under the move sequence characteristics to rule out two types of error correlation accordingly. From the above two aspects, the correlation determination method of the two sets of time sequence data can be obtained.

Correlation determination to the related sequence with the time warping. In order to determine the serial correlation, it is necessary to obtain the upper and lower bounds of the general correlation coefficient. In this paper, through the two asymptotic distributions of the sample correlation coefficients, the upper and lower bounds of the overall correlation coefficient at a certain significance level are obtained, and combined with the characteristics of the correlation errors of the first type, the method of the correlation determination of the correlated sequence with the time warping is achieved.

Bounds of the correlation coefficient. Pearson correlation coefficient is the most commonly used when measuring serial correlation measure. If there are two sets of corresponding data $\{(x_i, y_i), i = 1, 2, \dots, n\}$ (n is the quantity of the samples) which is from the bivariate normal overall sample $(x, y) \sim N(\mu_x, \mu_y, \sigma_x^2, \sigma_y^2, \rho)$, the sample correlation coefficient is as follows

$$\begin{aligned} \hat{\rho}(X, Y) &= \frac{\sum_{i=1}^n (x_i - \bar{x})(y_i - \bar{y})}{\sqrt{\sum_{i=1}^n (x_i - \bar{x})^2 \cdot \sum_{i=1}^n (y_i - \bar{y})^2}} = \\ &= \frac{n \sum_{i=1}^n x_i y_i - \sum_{i=1}^n x_i \sum_{i=1}^n y_i}{\sqrt{n \sum_{i=1}^n x_i^2 - \left(\sum_{i=1}^n x_i\right)^2} \cdot \sqrt{n \sum_{i=1}^n y_i^2 - \left(\sum_{i=1}^n y_i\right)^2}}. \end{aligned} \quad (1)$$

In which, \bar{x} , \bar{y} are the sample mean of X , Y respectively.

Sample correlation coefficient $\hat{\rho}(X, Y)$ can be used as the correlation coefficient ρ of two normal population (X, Y) of unbiased estimator and consistent, but the correlation coefficient has an obvious shortcoming, namely the degree that it is close to 1 is related to the number of n sets of data, it is easy to send a kind of illusion. When n is small, the absolute value of the correlation coefficient of some samples is close to 1, and when $n = 2$, the absolute value of correlation coefficient is 1. When n is bigger, the absolute value of correlation coefficient is smaller. There are many scholars who have obtained the distribution results about the sample correlation coefficient, sample size and bivariate normal of overall correlation coefficient.

For binary normal population (X, Y) and under the assumption $\rho = 0$, the following distribution is obtained

$$T = \frac{\sqrt{n-2}\hat{\rho}}{\sqrt{n-\hat{\rho}^2}} \sim t(n-2). \quad (2)$$

When $\rho = \rho_0$, Fisher gives a relatively complex $\hat{\rho}$ probability density function, after proper transform, the asymptotic distribution can be obtained

$$z = \frac{\varphi(\hat{\rho}) - \varphi(\rho)^{n \rightarrow \infty}}{2\sqrt{n-3}} \sim N(0,1), \quad (3)$$

where $\varphi(x) = \ln \frac{1+x}{1-x}$. When the sample size is large, the overall correlation coefficient can be estimated from the sample correlation coefficient.

The literature proves that in binary normal population, the extraction of n samples and the asymptotic distribution can be obtained.

$$\begin{aligned} \sqrt{n}(\hat{\rho} - \rho)^{n \rightarrow \infty} &\sim N(0, (1-\rho^2)^2), \\ \text{that is } \frac{\sqrt{n}(\hat{\rho} - \rho)^{n \rightarrow \infty}}{(1-\rho^2)} &\sim N(0,1). \end{aligned} \quad (4)$$

This paper has estimated the overall correlation coefficient based on the above two asymptotic distributions.

As the $\varphi(x)$ in Formula (3) is monotonically increasing, it can be known that:

- When $\rho \geq \hat{\rho}$

$$P\left\{\rho \leq \varphi^{-1}\left[\varphi(\hat{\rho}) + 2z_{1-\frac{a}{2}} \cdot \sqrt{n-3}\right]\right\} = 1-a. \quad (5)$$

- When $\rho \leq \hat{\rho}$

$$P\left\{\rho \geq \varphi^{-1}\left[\varphi(\hat{\rho}) - 2z_{1-\frac{a}{2}} \cdot \sqrt{n-3}\right]\right\} = 1-a, \quad (6)$$

in which, $\varphi^{-1}(x) = \ln \frac{e^x - 1}{e^x + 1}$; Z_α is the α quantile of standard normal distribution, namely, $P(x \leq Z_\alpha) = \alpha$; Random variable $x \sim N(0, 1)$.

In this paper, on the basis of Formula (4) further inference of the bounds of the overall correlation coefficient can be obtained, namely:

- When $\rho \geq \hat{\rho}$

$$P \left\{ \frac{-\sqrt{n} - \sqrt{n+4\sqrt{n}z_{1-\frac{\alpha}{2}} \cdot \hat{\rho} + 4z_{1-\frac{\alpha}{2}}^2}}{2z_{1-\frac{\alpha}{2}}} \leq \rho \leq \frac{-\sqrt{n} + \sqrt{n+4\sqrt{n}z_{1-\frac{\alpha}{2}} \cdot \hat{\rho} + 4z_{1-\frac{\alpha}{2}}^2}}{2z_{1-\frac{\alpha}{2}}} \right\} = 1 - \alpha. \quad (7)$$

- When $\rho \leq \hat{\rho}$

$$P \left\{ \frac{\sqrt{n} - \sqrt{n-4\sqrt{n}z_{1-\frac{\alpha}{2}} \cdot \hat{\rho} + 4z_{1-\frac{\alpha}{2}}^2}}{2z_{1-\frac{\alpha}{2}}} \leq \rho \leq \frac{\sqrt{n} + \sqrt{n-4\sqrt{n}z_{1-\frac{\alpha}{2}} \cdot \hat{\rho} + 4z_{1-\frac{\alpha}{2}}^2}}{2z_{1-\frac{\alpha}{2}}} \right\} = 1 - \alpha. \quad (8)$$

Integrate Formulas (5–8), when $\alpha = 0.05$, the approximation can be obtained:

- When $\rho \geq \hat{\rho}$

$$\inf_{\alpha=0.05} \rho = \max \left\{ \frac{-\sqrt{n} - \sqrt{n+8\sqrt{n} \cdot \hat{\rho} + 16}}{4}, \hat{\rho}, -1 \right\}; \quad (9)$$

$$\sup_{\alpha=0.05} \rho = \min \left\{ \frac{-\sqrt{n} - \sqrt{n+8\sqrt{n} \cdot \hat{\rho} + 16}}{4}, \varphi^{-1} \left[\varphi(\hat{\rho}) + 4\sqrt{n-3} \right], 1 \right\}. \quad (10)$$

- When $\rho \leq \hat{\rho}$

$$\inf_{\alpha=0.05} \rho = \max \left\{ \frac{\sqrt{n} - \sqrt{n-8\sqrt{n} \cdot \hat{\rho} + 16}}{4}, \varphi^{-1} \left[\varphi(\hat{\rho}) - 4\sqrt{n-3} \right], -1 \right\}; \quad (11)$$

$$\sup_{\alpha=0.05} \rho = \min \left\{ \frac{\sqrt{n} + \sqrt{n-8\sqrt{n} \cdot \hat{\rho} + 16}}{4}, \hat{\rho}, 1 \right\}. \quad (12)$$

Fig. 2 provides the upper and lower bounds of the general correlation coefficient under different sample size and sample correlation coefficient. As can be seen from the figure, in this paper, the upper and lower

bounds of the curve provided are of the following features:

1. The larger the sample size is, the more compact the upper and lower bounds are.

2. With the same sample size, the upper and lower curve centres are in symmetry.

3. The larger the absolute value of the correlation coefficient is, the more compact the upper and lower bounds are.

The above features can easily be proved by formulas (9–12).

Correlation determination method. For the convenience of the description of the relevant characteristics of the sequence, the definition of the time shift sequence (time-lag series) is first given.

Assume two sequences $(X, Y) = \{(x_i, y_i), i = 1, 2, \dots, n\}$, the following time shift sequences are defined

$$\begin{aligned} (X_t, Y_{t+m}) &= \{(x_i, y_{i+m}), i = 1, 2, \dots, n-m\}, \\ &1 \leq m < n, m \in N^+; \\ (X_t, Y_{t-m}) &= \{(x_i, y_{i-m}), i = m+1, 2, \dots, n\}, \\ &1 \leq m < n, m \in N^+. \end{aligned} \quad (13)$$

On the first type of regression errors, start the consideration of the initial sequence directly, and their relevance must be relatively small. If considering the moving time sequence correlation, there must be $m_0 (1 \leq |m_0| \ll n, |m_0| \in N^+)$, which makes the correlation coefficient relatively large.

The resulting time sequence correlation methods are: the sequence correlation coefficient changes with m , and achieves the maximum at m_0 , namely, the graph $\rho = \hat{\rho}(m)$ presents obvious convex phenomenon, according to the formulas (9–12) it can estimate the range of overall correlation coefficient. If $|\rho(m_0)| > \rho_0$ (i.e., more than the given threshold value, such as 0.6), it is believed that the time shift sequence (X_t, Y_{t+m_0}) has correlation, and the curve alignment and regression analysis, etc. can be conducted.

Curve alignment method based on grey theory. According to the correlation coefficient analysis of the time-lag series, we can determine whether there is correlation existing between the series. In the presence of correlation between two series but with the time bias, through the curve alignment method, they can be aligned so as to eliminate the difference on the phase time axis. For heterogeneous data, when AISE criterion is used, the result will change with the dimensional change and, therefore, it is necessary to propose a dimensionless criterion to align the heterogeneous data.

Curve alignment method based on grey theory. Pearson correlation coefficient is actually a dimensionless measure, with the inner product to represent the connectivity of the continuity function, at the same time, to achieve the inner product value in line with the norm; it is then divided by two functions of the norm. The alignment criteria of curves composed of heterogeneous data, in fact, can be constructed through the function correlation coefficient

$$\max_{h(t)} \left| \rho(x_1^*, x_2) \right| = \max_{h(t)} \left| \frac{\int_T x_1^*(s) x_2(s) ds}{\sqrt{\int_T [x_1^*(s)]^2 ds} \sqrt{\int_T [x_2(s)]^2 ds}} \right|, \quad (14)$$

where $x_1^*(t) = x_1[h(t)]$ represents the function after alignment. As the representation is too complicated, this paper gives the corresponding discretization state.

Let us assume that the two functional data $x_1(t)$ and $x_2(t)$ at the sampling time point $T = (t_1, t_2, \dots, t_n)$ have the sample sequence

$$x_1(T) = [x_1(t_1), x_1(t_2), \dots, x_1(t_n)],$$

and

$$x_2(T) = [x_2(t_1), x_2(t_2), \dots, x_2(t_n)],$$

the alignment of function $x_1(t)$ in contrast to curve $x_2(t)$ is to be performed.

Let $\Delta = (\delta_1, \delta_2, \dots, \delta_n)$ be the offset of $x_1(t)$ at the time point T relative to $x_2(t)$, namely, the time curve function shall meet $h(T) = T + \Delta$, then the temporal samples are transformed into $x_1(T + \Delta) = [x_1(t_1 + \delta_1), \dots, x_1(t_n + \delta_n)]$ after alignment, the two groups of functional data sequence of samples will have high correlation. The curve alignment problem can be converted into solving the following

$$\max_{\Delta} \left| \rho[x_1(T + \Delta) x_2(T)] \right|. \quad (15)$$

General time warping function features the consistent monotonicity, namely, to meet $t_{i-1} + \delta_{i-1} < t_i + \delta_i < t_{i+1} + \delta_{i+1}$. However, the offset vector which is chaotic at bending function does not meet the same time and will make $bndl_i = t_{i-1} + \delta_{i-1}^k - t_i$, $bndr_i = t_{i+1} + \delta_{i+1}^k - t_i$, δ_i^k represents the value of δ_i at the k -th iteration. In specific implementation, the search interval of δ_i^{k+1} can be narrowed down as the closed interval $[bndl_i + p \cdot (bndr_i - bndl_i), bndr_i - p \cdot (bndr_i - bndl_i)]$, in which, p is the constant within (0.05).

Finally, the problem of curve alignment is transformed into solving the following constrained optimization problem

$$\begin{cases} \Delta^* = \arg \max_{\Delta} \left| \rho[x_1(T + \Delta), x_2(T)] \right| \\ s.t. \delta_i \in [bndl_i + p \cdot (bndr_i - bndl_i), bndr_i - p \cdot (bndr_i - bndl_i)] \end{cases}. \quad (16)$$

At last, the time offset vector Δ^* is transformed into functional form, and the time offset function $d(t)$ is obtained, the corresponding time for bending function is $h(t) = d(t) + t$.

Model solution – gqs algorithm. When Parameter has high dimension, it is hard to solve the maximization problem of function Q . In order to overcome this problem, in this paper, the problem of the objective function is taken as function Q (i.e., the expectation of the logarithm likelihood function in the EM

algorithm), the extended EM algorithm (generalized maximum expectation maximization algorithm (GEM)) is applied to solve the problem. Due to the good time-smoothness of the time warping function, every time the update on Δ^* is performed, spline smoothing is performed on P for one time, thus the smoothness of the time difference vector can be increased, but the spline has regular term, which can prevent the problem of time difference function instability caused by overoptimization. Therefore, the smooth generalized expectation maximization method (S-GEM) for solving the model is obtained. The solving steps are as follows:

Input: Two sets of correlated time sequence data TS_1 and TS_2 with the time warping on time $T_0 = (t_{01}, t_{02}, \dots, t_{0m})$;

Step 1: Initialization time vector $\Delta_0 = \text{zeros}(1, n)$, error tolerance for iteration is eps .

Step 2: Time sequence data functions TS_1, TS_2 can be converted into function type data $x_1(t)$ and $x_2(t)$, take n points $T = (t_1, t_2, \dots, t_n)$ in T_0 uniformly, the smooth sequence $\{x_1(t_i)\}$ and $\{x_2(t_i)\}$ ($i = 1, 2, \dots, n$) can be obtained, in which $t_1 = t_{01}, t_n = t_{0m}$.

Step 3: Using generalized expectation maximization for the time difference vector. Record the k -th iteration time difference vector as $\Delta^k = (\delta_1^k, \delta_2^k, \dots, \delta_n^k)$, perform $n - 2$ times of conditional maximization (assuming starting point without time difference, namely $\delta_1^k = \delta_n^k = 0$), $\Delta^{k+1} = (\delta_1^{k+1}, \delta_2^{k+1}, \dots, \delta_n^{k+1})$ can be obtained.

Step 4: Smooth processing of the time difference vector: Using P spline function fitting on sequences Δ^{k+1} of function $d^{k+1}(t)$, and use the fitting value to replace the original value, namely: $\Delta^{k+1} = d^{k+1}(t_i) i = 1, 2, \dots, n$.

Step 5: Repeat Step 3 and Step 4 until convergence ($|\Delta^{k+1} - \Delta_k| < \text{eps}$).

Output: Time difference function $d(t) = d^k(t)$ or time warping function ($|\Delta^{k+1} - \Delta_k| < \text{eps}$).

Similar to many functional data mining methods, the proposed algorithm can deal with large volume of data line problems, even if there is missing data or abnormal data, the current information can still be fully used; in addition, through smooth processing, the algorithm can quickly converge to the extreme. It is important that the running time or time complexity of the algorithm mainly depends on the number of sampling, and has nothing to do with the number of the original sample. GQS algorithm complexity analysis is shown in Table 1, where m is the initial sample size, n is the uniform sampling volume, d is functional order (highest number minus 1), fm is the condition of maximizing the average time complexity in Step 3, k is the total number of iterations. As fm and k is related to the accuracy, parameters, and the problem itself, it is set out separately. P spline is applied when the data is functional or smooth, and the most complicated part in the coefficient vector estimation of the spline function obtains the inversion in the spline basis function matrix, and the time complexity and space complexity are 3 and 2 times of the number of the base function,

Table 1

GQS Algorithm Complexity Analysis

Steps	Time complexity	Space complexity
Step 1	$O(n)$	$O(n)$
Step 2	Function: $O[(m + d - 2)^3]$ Value: $O(nd^2)$	Function: $O[(m + d - 2)^2]$ Value: $O(n)$
Step 3	$O[n \times fm]$	$O(n)$
Step 4	Smooth: $O[(m + d - 2)^3]$ Value: $O(nd^2)$	Smooth: $O[(m + d - 2)^2]$ Value: $O(n)$
Overall	$O[(m + d - 2)^3 + k((n + d - 2)^3 + n \times fm)]$	$O[(m + d - 2)^2 + (n + d - 2)^2]$

respectively. In general, m^3 is a limited amount of calculation, relative to the iterative process it can be left out; when d takes smaller values, in the experiment of this paper, $d = 4$, at this point the time complexity and space complexity of the algorithm is $O[k(n^3 + n \times fm)]$ and $O[m^2 + n^2]$ respectively.

Experimental result and analysis. This paper has validated the proposed correlation determination method and the curve alignment method based on the simulated data. And the sensitivity of the parameters is compared with the existing methods for the time warping data collected by the curve alignment method and analytical method as well.

Time warping sequence correlation determination experiment. Select the Sinc function $\text{Sinc}(x) = \sin \pi x / \pi x$, $\xi \in [-6, 6]$ with volatility as the research object for the correlation of simulation data, and make the following two time functions: $d_1(t) = 0.01t^2 - 0.36$, $d_2(t) = 0.005t(t - 6)(t + 6)$. In both cases, the trend of variation with the standard Sinc function and the time shift sequence correlation coefficient are shown in Fig. 4.

As it can be seen from Fig. 3, *b*: when two sequence correlation coefficient curve is on the convex, and the bounds of the two correlation coefficients are [0.991, 0.996] and [0.914, 0.962] respectively. Thus, it can be determined that based on the sequence correlation between the two groups $d_1(t)$ and $d_2(t)$, with the standard Sinc function sequence, the average amount of lag is 0 and 3, respectively.

Curve alignment experiment. This section mainly tests on the GQS algorithm performance, and makes comparison with the classical CMRM algorithm, maximum likelihood registration (hereinafter referred to as MLR) and the self-modelling registration (referred to as SMR) are compared. To be fair, the results of CMRM algorithm and MLR are 5 times the average results of operation. The experimental machine is configured as the following: Intel quad-core CPU (frequency of 2.83 GHz), 3G memory.

Align the Sinc function containing noise with the time difference functions $d_1(t) = 0.01t^2 - 0.36$ and $d_2(t) = 0.005t(t - 6)(t + 6)$ with the standard Sinc function curve. And the trend of variation with the standard Sinc function and the time-lag series correlation coefficient is shown in Fig. 4.

As shown in Fig. 4: For the time difference function, MLR alignment effect is poorer, the other three kinds are close to the actual value; for the time difference function, the MLR and CMRM alignment effect is poorer, SMR and S-GEM are very close to the time difference function.

Tables 2–5 are the alignment results of the Sinc function, respectively, using CMRM, MLR, SMR, S-GEM under two kinds of time functions.

As can be seen from Table 5, GQS algorithm accuracy is closely related to the sampling points, and for more complicated time function, it requires more sampling points; the run time of GQS algorithm changes mainly with the increase of the sampling points.

It can be seen from the results of the comparison of Tables 2–5: when time difference function is $d_1(t)$,

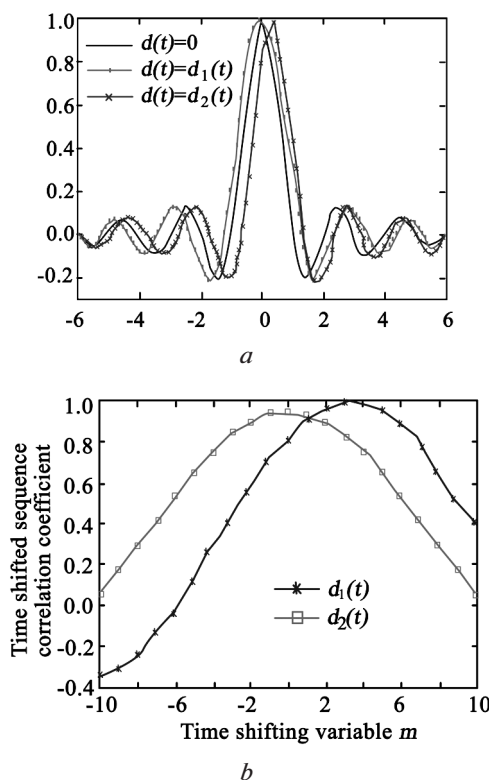


Fig. 3. Sinc Function and Time Shift Sequence Correlation Coefficient Variation Diagram

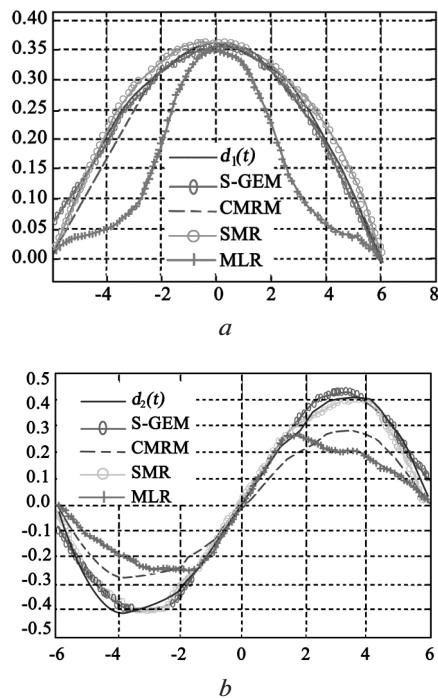


Fig. 4. Results of 4 Methods of Alignment

CMRM has the highest precision, but also the lowest efficiency; SMR and S-GEM's accuracy and efficiency are about the same, but the SMR results are not as stable as S-GEM; the precision of MLR is the worst, and the efficiency is not high; when time difference function takes $d_2(t)$, the precision of SMR and S-GEM is relatively high, but the SMR efficiency is far worse than S-GEM, but not as stable as S-GEM.

The above experiments show that, when the time difference function is simple, the precision of CMRM,

Table 2

Sinc Function CMRM Alignment Results (mean of 5 Times)

Time difference function	Run duration (s)	RMSE
$d_1(t)$	20.32	0.0038
$d_2(t)$	30.74	0.0891

Table 3

Sinc Function MLR Alignment Results (mean of 5 times)

Time difference function	Parameter		Run duration (s)	RMSE
	Scale parameter	Maximum number of iterations		
$d_1(t)$	0.1	50	14.60	0.1086
	0.1	100	22.24	0.1462
$d_2(t)$	0.1	50	14.51	0.1504
	0.1	100	21.83	0.1337

Table 4

Sinc Function SMR Alignment Results

Time difference function	Experiment serial number	Parameter		Run duration (s)	RMSE
		Number of components	Number of primary functions		
$d_1(t)$	1	4	7	5.49	0.0606
	2	3	8	6.87	0.0118
	3	3	8	6.05	0.0133
	4	4	7	5.65	0.0632
	5	3	7	6.27	0.0512
	Mean	3.4	7.4	6.06	0.0400
$d_2(t)$	1	4	12	21.99	0.0208
	2	4	11	25.10	0.0474
	3	5	13	24.56	0.0674
	4	4	12	23.82	0.0611
	5	4	15	23.00	0.0888
	Mean	4.2	12.6	23.69	0.0571

Table 5

Sinc Function GQS Algorithm Alignment Results

Time difference function	Iteration error eps	Sampling points n	Run duration (s)	RMSE
$d_1(t)$	0.01	10	0.15	0.2618
		30	4.29	0.0293
		50	7.76	0.0119
		80	16.52	0.0135
		100	25.47	0.0169
	0.05	10	1.13	0.0835
		30	3.2	0.0180
		50	7.96	0.0120
		80	17.15	0.0239
		100	24.87	0.0245
	0.1	10	0.15	0.2618
		30	3.13	0.0301
		50	7.33	0.0191
		80	15.19	0.0232
		100	19.72	0.0298
$d_2(t)$	0.01	10	0.15	0.2969
		30	4.74	0.0356
		50	8.04	0.0297
		80	16.61	0.0269
		100	27.82	0.0340
	0.05	10	0.15	0.2969
		30	4.09	0.0337
		50	8.15	0.0224
		80	16.78	0.0261
		100	22.75	0.0288
	0.1	10	0.15	0.2969
		30	3.31	0.0379
		50	7.09	0.0324
		80	14.73	0.0265
		100	20.60	0.0374

SMR and S-GEM is all relatively higher, but the effect of CMRM is relatively poor; when the time difference function is relatively complicated, the alignment results of SMR and S-GEM are good, but S-GEM is better in the efficiency and stability.

In conclusion, it is noteworthy that in the alignment of the leading index contrast consistent process, compared with CMRM, SMR and MLR, GQS algorithm is superior in alignment effect (the correlation coefficient and intuitive graphics) to the other methods, and the computation efficiency is higher than CMRM and SMR.

Summary and outlook. At a certain significance level, this paper has proposed that the upper and lower bounds of the overall correlation coefficient shall be applied to determine the correlation; there are multiple causes of spurious regression problem, at present a strict and accurate identification method has not yet been identified. For the correlation error, this paper can determine its correlation from the characteristics of the relevant coefficient of the grey theory time shift sequence. For the relevant sequences with time warping, the maximum model based on the grey theory correlation coefficient and the improved algorithm is established, with the applicable scope wider than the AISE standards. The experimental results show that the correlation determination method proposed in this paper is more effective than Pearson linear correlation coefficient, Spearman rank correlation coefficient, Kendall rank correlation coefficient and the Granger causality test. In most cases the proposed GQS algorithm is superior to CMRM, SMR and MLR. This paper has taken the double sequence linear correlation issue and function type curve alignment method into consideration, and the results can be used to provide the theoretical basis for the correlation determination of the regression analysis and the time alignment, and can also offer the reference direction for the multiple sequential correlation mining and curve alignment.

References / Список літератури

1. Yin, M. S., 2013. Fifteen years of grey system theory research: a historical review and bibliometric analysis. *Expert systems with Applications*, Vol. 40, No. 7, pp. 2767–2775.
2. Low, Y., Bickson, D., Gonzalez, J., Guestrin, C., Kyrola, A. and Joseph M. Hellerstein, 2012. Distributed GraphLab: a framework for machine learning and data mining in the cloud' *Proceedings of the VLDB Endowment*, Vol. 5, No. 8, pp. 716–727.
3. Demšar, J., Curk, T., Erjavec, A., Gorup, Č., Hočevar, T., Milutinovič, M., Možina, M., Polajnar, M., Toplak, M., Starič, A., Štajdohar, M., Umek, L., Žagar, L., Žbontar, J., Žitnik, M. and Zupan, B., 2013. Orange: data mining toolbox in Python. *The Journal of Machine Learning Research*, Vol. 14, No. 1, pp. 2349–2353.
4. Nguyen, P. H., Sheu, T. W., Nguyen, P. T., et al., 2014. Taylor Approximation Method in Grey System Theory and Its Application to Predict the Number of Foreign Students Studying in Taiwan, *International Journal of Innovation and Scientific Research*, Vol. 10, No. 2, pp. 409–420.
5. Romero, C. and Ventura, S., 2013. Data mining in education, *Wiley Interdisciplinary Reviews: Data Mining and Knowledge Discovery*, Vol. 3, No. 1, pp. 12–27.
6. Tserng, H. P., Ngo, T. L. and Chen, P. C., 2015. A Grey System Theory Based Default Prediction Model for Construction Firms. *Computer Aided Civil and Infrastructure Engineering*, Vol. 30, No. 2, pp. 120–134.
7. Wei, M. C., 2014. The Influence Factor Analysis for Sexual Harassment on Campus in Taiwan via Grey System Theory. *Journal of Grey System*, Vol. 17, No. 4, pp. 207–213.
8. Ghodrati Amiri, G., Zare Hosseinzadeh, A. and Jafarian Abyaneh, M., 2016. A new two-stage method for damage identification in linear-shaped structures via Grey System Theory and optimization algorithm, *Journal of Rehabilitation in Civil Engineering*, Vol. 3, No. 2, pp. 36–50.
9. Raju, P. S., Bai, D. V. R. and Chaitanya, G. K., 2014. Data mining: Techniques for enhancing customer relationship management in banking and retail industries. *International Journal of Innovative Research in Computer and Communication Engineering*, Vol. 2, No. 1, pp. 2650–2657.
10. Liao, S. H., Chu, P. H. and Hsiao, P. Y., 2012. Data mining techniques and applications—A decade review from 2000 to 2011. *Expert Systems with Applications*, Vol. 39, No. 12, pp. 11303–11311.

Мета. Із розвитком передачі великих об'ємів даних, інтелектуальний аналіз часових рядів став важливою темою, що привертає до себе увагу суспільства. На основі кореляції та спільності часових рядів, розглянута швидка модель інтелектуального аналізу часових послідовностей.

Методика. Запропоновано метод визначення кореляції, заснований на особливостях відповідного коефіцієнта зсунутої часової послідовності. У кінцевому рахунку, запропонована швидка модель інтелектуального аналізу часових послідовностей, заснована на теорії сірих систем.

Результати. Методологія визначення кореляції, запропонована в даній роботі, є більш ефективною, ніж коефіцієнт лінійної кореляції Пірсона, коефіцієнт рангової кореляції Спірмена, коефіцієнт рангової кореляції Кендалла та тест Гренджера на причинність.

Наукова новизна. У роботі запропоноване об'єднання швидкого метода визначення кореляції послідовностей і метода вирівнювання по кривій.

Практична значимість. Результати можуть забезпечити теоретичну базу для визначення кореляції регресійного аналізу та часового вирівнювання.

Ключові слова: теорія сірих систем, часове вирівнювання, кореляція, часова послідовність даних, інтелектуальний аналіз даних, вирівнювання по кривій, тест на причинність

Цель. С развитием технологии передачи больших объемов, интеллектуальный анализ временных рядов стал важной темой, которая привлекает к себе внимание общественности. На основании корреляции и общности временных рядов, рассмотрена быстрая модель интеллектуального анализа временных последовательностей.

Методика. Предложен метод определения корреляции, основанный на особенностях соответствующего коэффициента сдвинутой временной последовательности. В конечном счете, предложена быстрая модель интеллектуального анализа временных последовательностей, основанная на теории серых систем.

Результаты. Методология определения корреляции, предложенная в данной работе, является более эффективной, чем коэффициент линейной корреляции Пирсона, коэффициент ранговой корреляции Спирмена, коэффициент ранго-

вой корреляции Кендалла и тест Гренджера на причинность.

Научная новизна. В работе предложено объединение быстрого метода определения корреляции последовательностей и метода выравнивания по кривой.

Практическая значимость. Результаты могут обеспечить теоретическую базу для определения корреляции регрессионного анализа и временно-го выравнивания.

Ключевые слова: теория серых систем, временное выравнивание, корреляция, временная последовательность данных, интеллектуальный анализ данных, выравнивание по кривой, тест на причинность

Рекомендовано до публікації докт. техн. наук В. В. Гнатушенком. Дата надходження рукопису 20.10.15.

Fei Hu^{1,2},
Changjiu Pu²,
Haowei Gao³,
Mengzi Tang¹,
Li Li¹

1 – School of Computer and Information Science, Southwest University, Chongqing, China
2 – Network Centre, Chongqing University of Education, Chongqing, China
3 – The Webb Schools, 1175 West Baseline Road Claremont, CA 91711, USA

IMAGE COMPRESSION AND ENCRYPTION SCHEME BASED ON DEEP LEARNING

Фей Ху^{1,2},
Чанцзю Пу²,
Хаовей Гао³,
Менци Тан¹,
Ли Ли¹

1 – Школа комп'ютерних та інформаційних наук, Південно-Західний університет, Чунцін, Китай
2 – Мережевий центр, Чунцінський університет освіти, Чунцін, Китай
3 – Школа Уебб, Клермонт, США

СХЕМА СТИСНЕННЯ ТА ШИФРУВАННЯ ЗОБРАЖЕНЬ НА ОСНОВІ ГЛИБИННОГО НАВЧАННЯ

Purpose. With the growing demands of image processing on the Internet, image compression and encryption have been playing an important role in image protection and transferring. In this paper we will investigate deep learning technology in image compression, and chaotic logistic map in image encryption, to obtain a scheme in image compression and encryption. We have evaluated this scheme with some performance measures and results show it is effective.

Methodology. We formulate the scheme using deep learning and chaos. With the deep learning technology, levels of features are extracted from an image and a certain level of features can be used as a compressed representation of the image. Chaos is used to encrypt the compressed image.

Findings. We first introduced a five-layer Stacked Auto-Encoder model, which is trained by the Back Propagation method, and then we obtained the compressed representation of an image. By using the logistic map method, a pseudo-stochastic sequence is generated to encrypt the compressed image.

Originality. We conducted a study of image compression and encryption. Image characteristics are extracted from an arbitrary level of our deep learning model, and they are used as the compressed representation of the image. The research on this aspect has not been found at present.

Practical value. We have evaluated this scheme on several randomly selected images. And results show it is robust and can be widely used for most images.

Keywords: stacked auto-encode, deep learning, image protection, image feature, image compression, image encryption

Introduction. With the development of multimedia technology and communication technology, multimedia entertainment has played an important role in people's daily lives. Pictures and videos take up the main part of multimedia entertainment. It brings austere challenge to store and transmit those data, and puts forward higher requirement on the limited-bandwidth Internet, especially for large and high-quality digital images. The limited bandwidth of the Internet greatly restricts the development of image communication, and thus the image compression technology has been attracting more and more people's attention [1]. The purpose of image compression is to represent and transmit the original large image with minimal bytes, and to restore the image with not-so-bad quality. Image compression reduced the burden of image storage and transmission on the network, and achieved rapid real-time processing on line. The information of an image is fixed, but the different representations of the image lead to different changes in the amount of data stored in the image. So in the representation with larger amount of data, some data is useless or represent the information that is represented by other data, they are irrelevant or redundant. The main purpose of image compression is to compress the image by removing redundant or irrelevant information, and to store and transmit digital compressed data on a low bandwidth network.

Image compression techniques can be traced back to the digital television signals proposed in the year of 1948. There is almost 70 years of history. During this period there have been a variety of image compression coding methods. Especially in the late 1980s, due to the wavelet transform theory, the fractal theory, the artificial neural network theory and the visual simulation method, image compression technology was well developed. Image compression methods can be classified into two kinds: one may lose information during compression, and the other one can keep full information, that is, lossless coding methods and limited-distortion coding methods. Lossless coding methods will not suffer loss of information after compressing images, yet without a good compression ratio. The basic principle of this kind of methods is as follows: an image consists of features, using the statistical features of the image, if a feature appears many times in the image, it will be encoded in shorter bits, and if a feature appears only once or limited times, it will be encoded in longer bits. And a complete image is always composed of a large number of repeated features. According to that, the image will be represented by many short-bits coding features and few long-bits coding features. On the basis of guaranteeing the image quality after compression, limited-distortion coding methods maximize the compression ratio. The original image and the compressed image look very similar though some information has changed. The normally used limited-distortion coding methods are: the predictive coding method, the transform coding method and the statistical coding method. The limited-distortion coding method is more frequently used than the lossless

coding method because the former has a larger compression ratio. Its premises guarantee visual effects, which remove the information that the human eyes are not sensitive to.

The features of images can be learned automatically using deep learning models, rather than proposed manually. Suitable features can improve the performance of image recognition. Over the past years, features of images were always specified manually that depended on the designers' prior knowledge, and the number of features were very limited. Deep learning models can learn unlimited number of features automatically. A good feature-extraction method is a prerequisite for optimization of image processing. Using deep learning models, unpredictable features of images can be learned, and these unpredictable features can also be used for image protection. In this study, we proposed a model to compress and encrypt images. Based on SAE, a multi-layer model is constructed. An image is put into the first layer and the output data from a different level of layers reconstruct the original image at a different level of comprehension. If the size of the output data from an arbitrary layer is smaller than the size of the original image, the representation at this layer is a compression representation. Because the model has more than one hidden layer whose neurons are smaller than the input layer's, the model can achieve multiple levels of features, and each level of features represents a compressed image. So, multiple compression ratio can be obtained using this model. The compressed image is further encrypted using chaotic logistic map. This model can be used in tasks that have certain requirements for image transmission speed and security.

Analysis of the recent research and publications. Stacked Auto-Encoder. Auto-Encoder (AE) is a single hidden layer model, and is an unsupervised learning neural network, Fig. 1, *b*. It is actually generated by two identical Restricted Boltzmann Machine models (RBMs) [2], Fig. 1, *a*. A RBM and a reversed RBM generate an AE model. Stacked Auto-Encoder (SAE) is a multilayer AE, it is composed of several AEs. The previous AE's output is the later AE's input, i.e. several AEs' encoding sections are put together one by one and their decoding sections are put together in reverse order. This is a more complex AE model, having several hidden layers rather than one. Using greedy training methods, monolayer AE can be trained to learn weights directly, however, it is hard for SAE because several more hidden layers would consume too much computation time. In order to cut down the training time, the training process of SAE is divided into two steps: pre-training and fine-training. At first, each hidden layer is trained one by one, then the entire model is trained using the Contrastive Divergence (CD-k) [3].

In Fig. 2, the left three layers (X, h_1, h_2) constitute the encoding part of the SAE model. In the pre-training phase, the input data X is encoded and yield h_1 , and then h_1 is decoded and yield X' , the error $e = X' - X$, e is used to adjust the weights between the layer X and

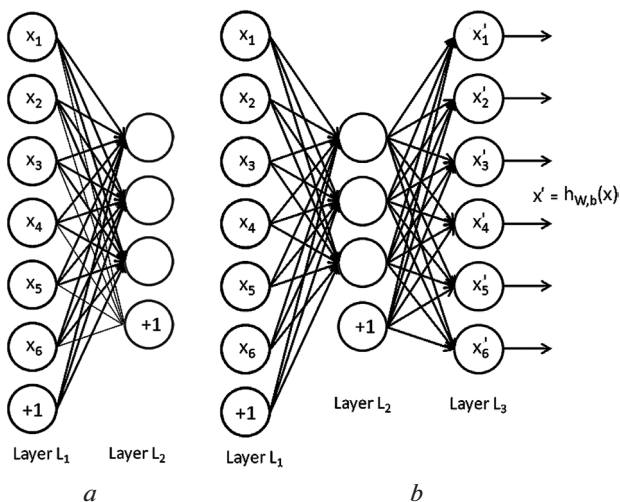


Fig. 1. RBM & Auto-encoder:
 a – Restricted Boltzmann Machine (RBM); b – Auto-Encoder

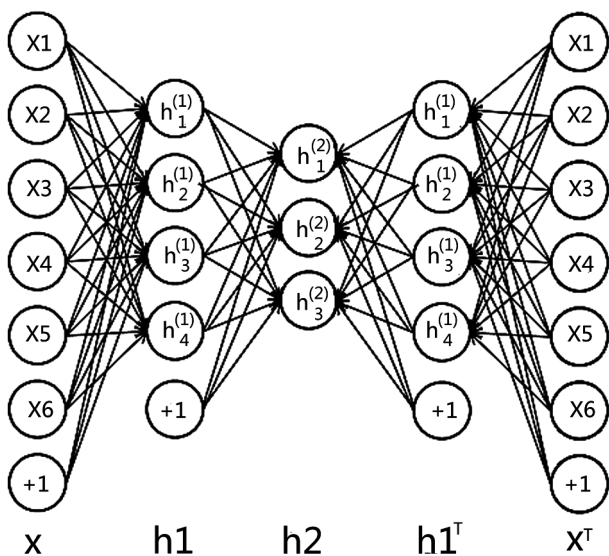


Fig. 2. Stacked Auto-encoder

the layer h_1 ; then the output value of previous AE is set as the input data of layer h_1 , it is encoded and yield h_2 , h_2 is decoded and yield h'_1 , the weights between the layer h_1 and the layer h_2 are adjusted using $e = h'_1 - h_1$; after multiple encoding and decoding operations, pre-optimal parameters (W, b) are obtained, and they make the model easy to train in the fine-training phase.

The encoding part (X, h_1, h_2) of the SAE model is flipped to get a decoding part: (h_2, h_1^T, X^T). The two parts are combined to form a model that has the functions of encoding and decoding, Fig. 2. In the fine-training phase, the weights are finely adjusted so that the optimal solution is closer little by little. Using the CD-k algorithm and the gradient descent algorithm, the fine-tuning process gradually approximates the optimal solution of the model. The detailed fine-training process is described as the following steps [4]:

1. Feedforward processing is performed by computing the activation for each middle layer.

2. The grade error for the output layer is

$$\delta^{(ni)} = -(y - a^{(ni)}) \cdot f'(z^{(ni)}). \quad (1)$$

3. The grade error for every middle layer is

$$\delta^{(l)} = ((W^{(l)})^T \delta^{(l+1)}) \cdot f'(z^{(l)}). \quad (2)$$

4. The partial derivatives

$$\nabla_{w^{(l)}} J(W, b; x, y) = \delta^{(l+1)} (a^{(l)})^T; \quad (3)$$

$$\nabla_{b^{(l)}} J(W, b; x, y) = \delta^{(l+1)}. \quad (4)$$

5. The overall cost function is set as the following

$$J(W, b) = \left[\frac{1}{m} \sum_{i=1}^m J(W, b; x^{(i)}, y^{(i)}) \right]. \quad (5)$$

SAE has strong representation expression ability and advantages of deep neural networks. AE can learn the characteristics of input data, then SAE can learn multi-level characteristics. In the first hidden layer, SAE can learn first-order features of the input data; in the second hidden layer, SAE can learn second-order features of the input data. E.g. the input data is a set of images, the first hidden layer may learn a collection of edges, and the second hidden layers may learn how to combine a number of edges together to form an outline, a higher hidden layer may learn much more vivid, special and meaningful features. Features of each level can help us better operate image processing, such as image classification, information retrieval of images, and so on. These features can also be used to compress images. For example, an image with 100 pixels is put into the input layer, the input layer has 100 neurons, each pixel is put into a corresponding neuron, then a hidden layer with only 10 neurons yields a 10-dimensional vector, which owns features of the input data and can be considered as a reconstruction of the input image, so this image is compressed and the compression ratio is 10.

Image encryption schema using chaotic logistic map.

Chaos-based cryptographic algorithms have suggested efficient ways to develop secure image encryption. These algorithms are sensitive to their initial conditions. Any tiny change can cause greatly different responses that guarantees the efficiency of encryption schemas. The logistic map is one of them. It is an iterated logistic map that has proved great importance in many fields of information processing. Such fields include but are not limited in the following: population of biology, chemistry, encryption, communication and ecology. It also works in modelling the dynamics of a single species. The stability and bifurcation of the logistic map has been studied a lot, such as Cohen-Grossberg neural networks with delays [5] and the Neimark-Sacker bifurcation with delay [6].

The logistic map is of a non-linear recursive relation. It can suggest deterministic chaos. Its mathematical equation is written as

$$x_{n+1} = rx_n(1 - x_n), \quad (6)$$

where x_0 is an initial condition which is a float number between 0 and 1 (exclude 0 or 1), r is a positive constant which is also a float number between 3.5699 and 4 (include 4, and 3.5699 is an approximation). After N iterations, a sequence will be obtained. The sequence is like the form of $\{x_1, x_2, x_3, \dots, x_N\}$. It is a stochastic sequence which can further be used for encryption tasks. In this study, the initialized number x_0 is generated from the SAE model, and then is used for image encryption.

Image compression encryption model. The image is compressed using the SAE, and then the compressed image is encrypted using the sequence generated by the chaotic logistic map.

The diagram in Fig. 3 shows the algorithm of this model. See the following for detail:

1. Initialization. A five-layer SAE model is constructed (Fig. 2). In the model, the second layer has a smaller number of neurons than the input layer in order to realize the primary image compression, and the third layer has a smaller number of neurons than the second layer in order to realize the second-stage image compression. The rest fourth and fifth layers are separately the mirrors for the second and first layers. In the study of image processing using Convolutional Neural Networks (CNN), it was supposed and has been proved by a large number of experiments [7] that an image could be divided into a number of regions and the characteristics learned by CNN from different regions are similar or even the same. We use this supposition in our study. The image is divided into pieces which have the same size. Every piece is a sample. A training set consists of all pieces from one single image. For the convenience of handling images in SAE, values in this data set will be normalized as float numbers in the range of 0 to 1 before they are put into the model. Our model is trained using this normalized data set. Levels of learned features will be anti-normalized to get the final output, which are values of pixels for a compressed image. According to the dense representation, the image is compressed. The constant r is initialized.

2. Learning compression representation using the SAE model. The activation function $f(\cdot)$ is a nonlinear function, and the sigmoid function is used in the experiment. By training the SAE model, we get a compression representation from an arbitrary hidden layer. This representation then forms a compressed image. Because the sigmoid function output is a float number between 0 and 1, which meets the requirements for ini-

tializing x_0 , a certain one from the output values is chosen as x_0 . In the experiment, the first one is chosen.

3. Generating a chaotic sequence. Using chaotic logistic map with x_0 and r , a sequence S is generated, $S = \{x_1, x_2, x_3, \dots, x_N\}$, where N is the size of the compressed image, e.g., a compressed image has $100 * 100$ pixels, $N = 100 * 100 = 10000$.

4. Image encryption and image decryption. The encryption and decryption functions are described following, where E is the encrypted image, C is the plain image (the compressed image), S is the sequence generated in step 3), $\text{bitxor}(-)$ is a bit XOR function

$$E = \text{bitxor}(C, S); \quad (7)$$

$$C = \text{bitxor}(E, S). \quad (8)$$

5. Image reconstruction. The compressed image is recovered through the SAE model. Fig. 2, if the compressed image came from the layer of h_2 , a new model is reconstructed with only the layers of $\{X, h_1, h_2\}$ which shares the parameters learned in step 2). The compressed image is normalized and is put into the layer of h_2 , then the output from the layer of X represent the recovered image.

The practicability of the algorithm will be verified in the next section.

Experiments. This new model was evaluated on several images taken from the standard set of images. They are house, airplane, lake and pepper. They have the same size as 512 by 512. Images split into pieces with the same size of 8 by 8. The number of neurons in the input layer was 64, and the number of neurons in the hidden layers was adjusted to achieve different compression ratios (CRs), that is, 4 : 1 and 16 : 1 for 16 and 4 neurons. In the back part of this section, the compressed images were encrypted. Correlation Analysis was performed to evaluate the effect of the encryption schema.

Compression effects are shown in Fig. 4. In order to quantitatively verify the effects, Mean Square Error (MSE) and Peak Signal-to-Noise Ratio (PSNR) are introduced. MSE [8] is the average of the square of the difference between the expected response and the actual output. It is also called squared error loss. PSNR [9] is the ratio of maximum power of the signal and the power of noise. It is commonly used to measure the quality of reconstruction in image compression. Their mathematical definitions are following equations

$$MSE = \frac{1}{m \times n} \sum_{i=0}^{m-1} \sum_{j=0}^{n-1} [I_0(i, j) - I_R(i, j)]^2; \quad (9)$$

$$PSNR = 10 \log_{10} \left(\frac{MAX_I^2}{MSE} \right), \quad (10)$$

where MAX_I is the maximum possible pixel value of the image, that is 255 in this experiment, $m * n$ is the image size, I_0 is the original image and I_R is the reconstructed image.

MSE and PSNR were computed for three primary colour channels (Red, Green and Blue, also called RGB), respectively. And the results at the CRs of 4 : 1

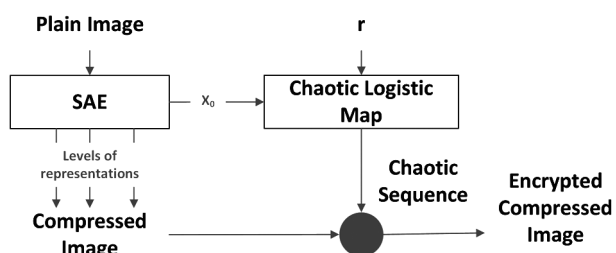


Fig. 3. The compression encryption model

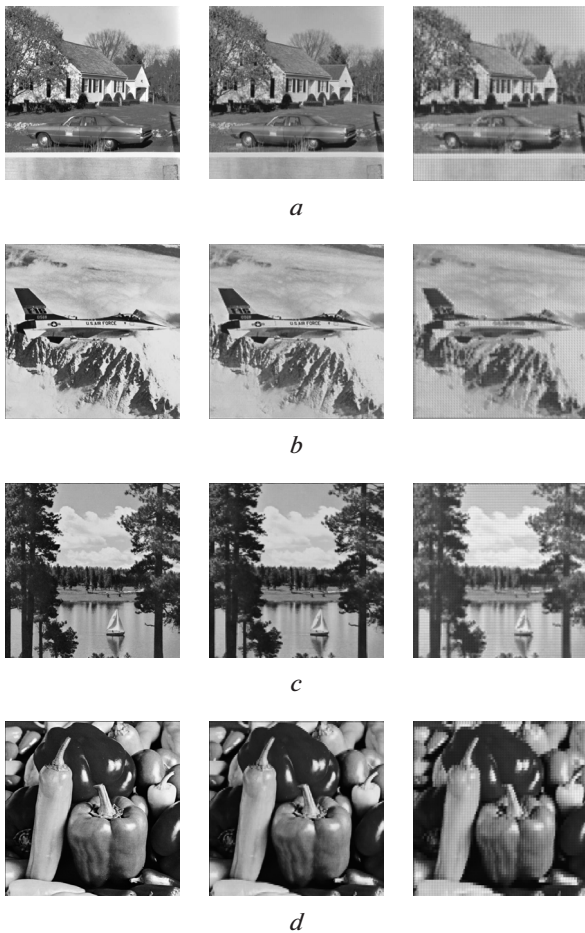


Fig. 4. Compression effects:

a – original image of house, image reconstructed at a CR of 4 : 1, image reconstructed at a CR of 16 : 1; *b* – original image of airplane, image reconstructed at a CR of 4 : 1, image reconstructed at a CR of 16 : 1; *c* – original image of lake, image reconstructed at a CR of 4 : 1, image reconstructed at a CR of 16 : 1; *d* – original image of pepper, image reconstructed at a CR of 4 : 1, image reconstructed at a CR of 16 : 1

Table 1

MSE and PSNR of the reconstructed images at a CR of 4 : 1

Images		R	G	B
House	MSE	37.7696	51.1280	37.0831
	PSNR	32.3594	31.0442	32.4390
Air-plane	MSE	21.4800	32.9829	15.8055
	PSNR	34.8105	32.9479	36.1427
Lake	MSE	32.2390	101.1015	56.4297
	PSNR	33.0470	28.0832	30.6157
Pepper	MSE	48.8470	60.6932	39.5987
	PSNR	31.2424	30.2994	32.1540

Table 2

MSE and PSNR of the reconstructed images at a CR of 16 : 1

Images		R	G	B
House	MSE	110.9180	136.8415	118.2971
	PSNR	27.6808	26.7686	27.4011
Air-plane	MSE	119.2817	114.3715	71.0135
	PSNR	27.3651	27.5476	29.6174
Lake	MSE	62.2023	174.2972	144.9320
	PSNR	30.1927	25.7179	26.5192
Pepper	MSE	71.5491	149.3480	74.9371
	PSNR	29.5848	26.3888	29.3838

and 16 : 1 are listed in Table 1 and Table 2, respectively.

The encrypted images of the compressed ones at CRs of 4 : 1 and 16 : 1 are shown in Fig. 5 and Fig. 6, respectively. Correlation Analysis was performed to quantitatively evaluate the effect of the encryption schema. The correlation coefficient is used to evaluate the correlation of a pair of adjacent pixels, and it is defined below [10]

$$r_{xy} = (E(xy) - E(x)E(y)) / (\sqrt{D(x)}\sqrt{D(y)}), \quad (11)$$

where r_{xy} is the correlation coefficient of the variables x and y , $E(\cdot)$ is the mean function, $D(\cdot)$ is the variance function, x and y are adjacent pixels.

To simplify the processing, colour images were converted to grayscale before use. Experiments were repeated ten times, correlation coefficients of each image were averaged. Results for reconstructed images and encrypted compression images at the CRs of 4 : 1 and 16 : 1 are listed in Table 3.

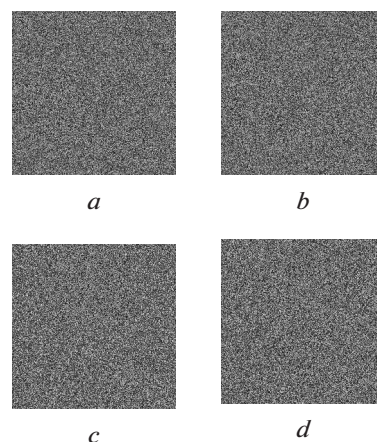


Fig. 5. Encrypted images of the compressed ones at a CR of 4 : 1:

a – encrypted house; *b* – encrypted airplane; *c* – encrypted lake; *d* – encrypted pepper

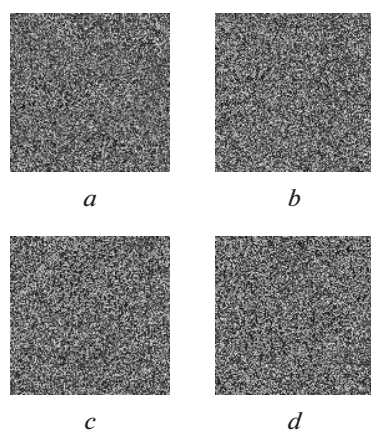


Fig. 6. Encrypted images of the compressed at a CR of 16 : 1:

a – encrypted house; *b* – encrypted airplane; *c* – encrypted lake; *d* – encrypted pepper

The experimental results show that this new model is effective and it can be used for image transmission and image protection on the Internet simultaneously.

Conclusions. A scheme of deep learning in image compression and encryption was proposed. Based on SAE neural networks, images are compressed. And then the compressed ones are encrypted using chaotic logistic map. This scheme can be used for image transmission and image protection on the Internet simultaneously.

Acknowledgements. This work was supported by Scientific and Technological Research Program of Chongqing Municipal Education Commission (No. KJ1501405, No. KJ1501409); Scientific and Technological Research Program of Chongqing University of Education (No. KY201522B, No. KY201520B); Fundamental Research Funds for the Central Universities (No. XDJK2016E068); Natural Science Foundation of China (No. 61170192) and National High-tech R&D Program (No. 2013AA013801).

Table 3

Correlation Analysis for reconstructed images and encrypted compressed images at the CRs of 4 : 1

Images	CR of 4 : 1		CR of 16 : 1	
	Com-pressed	Encrypted	Com-pressed	Encrypted
House	0.9532	-0.0391	0.9369	0.0079
Air-plane	0.9632	0.0038	0.9745	0.0361
Lake	0.9820	-0.0087	0.9855	0.0267
Pepper	0.9796	0.0488	0.9902	0.0261

References / Список літератури

- Zhang, Chunhong, 2016. Application of Multi-Wavelet Analysis in Image Compression. *Revista Tecnica De La Facultad De Ingenieria Universidad Del Zulia*, No. 39(3), pp. 760–82.
- Fischer, A., and Igel, C., 2014. Training restricted Boltzmann machines: An introduction. *Pattern Recognition*, No. 47(1), pp. 25–39.
- Ma, X., and Wang, X., 2016. Average Contrastive Divergence for Training Restricted Boltzmann Machines. *Entropy*, No. 18(1), pp. 35–49.
- Sarangi, P. P., Sahu, A., and Panda, M., 2013. A hybrid differential evolution and back-propagation algorithm for feedforward neural network training. *International Journal of Computer Applications*, No. 84(14), pp. 1–9.
- Liu, Q., and Yang, S., 2014. Stability and bifurcation of a class of discrete-time Cohen–Grossberg neural networks with discrete delays. *Neural Processing Letters*, No. 40(3), pp. 289–300.
- Sarmah, H. K. R., Das, M. C., and Baishya, T. K. R., 2014. Neimark-Sacker bifurcation in delayed logistic map. *International Journal of Applied Mathematics & Statistical Sciences*, No. 3(1), pp.19–34.
- LeCun, Y., Bengio, Y., and Hinton, G., 2015. Deep learning. *Nature*, No. 521(7553), pp. 436–444.
- Tiwari, M., and Gupta, B., 2015. Image Denoising Using Spatial Gradient Based Bilateral Filter and Minimum Mean Square Error Filtering. *Procedia Computer Science*, No. 54, pp. 638–645.
- Karamchandani, S.H., Gandhi, K.J., Gosalia, S.R., Madan, V.K., Merchant, S.N., and Desai, U.B., 2015. PCA encrypted short acoustic data inculcated in Digital Color Images. *International Journal of Computers Communications & Control*, No. 10(5), pp. 678–685.
- Zhang, Y. Q., and Wang, X. Y., 2015. A new image encryption algorithm based on non-adjacent coupled map lattices. *Applied Soft Computing*, No. 26, pp. 10–20.

Мета. З посиленням вимог до обробки зображень в Інтернеті, стиснення зображень та шифрування грають важливу роль у захисті зображень при передачі. Задля отримання нової схеми стиснення та шифрування зображень у цій роботі досліджується технологія глибокого навчання при стисненні зображень і хаотичне логістичне відображення в шифруванні зображень. Нами проведена оцінка цієї схеми за декількома критеріями ефективності, і результати підтвердили її ефективність.

Методика. Нами запропонована схема з використанням глибокого навчання та хаосу. За допомогою технології глибокого навчання із зображення вилучають рівні характеристик, і певний рівень характеристик далі може бути використаний в якості стиснутого представлення зображення. Хаос використовується для шифрування стиснутого зображення.

Результати. Спочатку нами введена п'ятирівнева (п'ятишарова) модель каскадного автокоду-

вальника, що навчається за методом оберненого розповсюдження помилки, а потім ми отримали стиснене представлення зображення. За допомогою методу логістичного відображення генерується псевдостохастична послідовність для шифрування стиснутого образу.

Наукова новизна. Нами проведено дослідження стиснення та шифрування зображень. Із довільного рівня запропонованої моделі глибокого навчання вилучаються характеристики зображення, що використовуються в якості стиснутого представлення зображення. Дослідження за цим аспектом не були знайдені на сьогодні.

Практична значимість. Ми оцінили цю схему на декількох випадково обраних зображеннях. Результати показують, що схема стиснення та шифрування є робастною та може широко використовуватися для більшості зображень.

Ключові слова: каскадний автокодувальник, глибоке навчання, захист зображення, ознака зображення, стиснення зображень, шифрування зображення

Цель. С ростом требований к обработке изображений в Интернете, сжатие изображений и шифрование играют важную роль в защите изображения при передаче. Для получения новой схемы сжатия и шифрования изображений в этой работе исследуется технология глубокого обучения при сжатии изображений и хаотическое логистическое отображение в шифровании изображений. Нами проведена оценка этой схемы по нескольким критериям эффективности, и результаты подтвердили её эффективность.

Методика. Нами предложена схема с использованием глубокого обучения и хаоса. С помо-

щью технологии глубокого обучения из изображения извлекаются уровни характеристик, и определенный уровень характеристик далее может быть использован в качестве сжатого представления изображения. Хаос используется для шифрования сжатого изображения.

Результаты. Сначала нами введена пятиуровневая (пятислойная) модель каскадного автокодировщика, которая обучается по методу обратного распространения ошибки, а затем мы получили сжатое представление изображения. С помощью метода логистического отображения генерируется псевдостохастическая последовательность для шифрования сжатого образа.

Научная новизна. Нами проведено исследование сжатия и шифрования изображений. Из произвольного уровня предложенной модели глубокого обучения извлекаются характеристики изображения, которые используются в качестве сжатого представления изображения. Исследования по этому аспекту не были найдены в настоящее время.

Практическая значимость. Мы оценили эту схему на нескольких случайно выбранных изображениях. Результаты показывают, что схема сжатия и шифрования является робастной и может широко использоваться для большинства изображений.

Ключевые слова: каскадный автокодировщик, глубокое обучение, защита изображения, признак изображения, сжатие изображений, шифрование изображения

Рекомендовано до публікації докт. техн. наук В. В. Гнатушенком. Дата надходження рукопису 09.01.16.

Lili Chen¹,
Hongjun Guo²

1 – Laboratory of Intelligent Information Processing, Suzhou University, Suzhou, China
2 – The Key Laboratory of Intelligent Computing & Signal Processing of MOE, Anhui University, Hefei, China

A SIMPLE AND EFFICIENT FUSION FRAMEWORK FOR SURVEILLANCE IMAGES

Лілі Чен¹,
Хунцзюнь Го²

1 – Лабораторія інтелектуальної обробки інформації, Сучжоу університет, Сучжоу, Китай
2 – Лабораторія інтелектуальних обчислень і обробки сигналів Міністерства освіти, Аньхой університет, Хефей, Китай

ПРОСТІЙ ТА ЕФЕКТИВНИЙ ФРЕЙМВОРК ЗЛИТТЯ ДЛЯ ЗОБРАЖЕНЬ З КАМЕР СПОСТЕРЕЖЕННЯ

Purpose. Aiming at solving the fusion issue of surveillance images, a simple and efficient fusion framework using block compressed sensing sampling (BCSS) is proposed in this paper, which consists of two fusion methods using basic-BCSS and sliding-BCSS respectively.

Methodology. With the superiority of low sampling ratio and low computational complexity, compressed sensing (CS) theory is widely used in signal processing. The basic-BCSS is a basic version of block based CS, in which the source image is divided into distinct blocks, and the sliding-BCSS is a modified version of basic-BCSS proposed for the first time, in which the image is divided into small sliding blocks for each pixel with appropriate padding. The basic idea of the fusion framework is to select the blocks or pixels with greater L₂-norm of the BCSS measurement outputs of the divided blocks in spatial domain.

Findings. The fusion framework is tested on three pairs of grayscale surveillance images, including infrared and visible images, and millimeter-wave and visible images, and compared with several traditional fusion methods. Experimental results demonstrate that the proposed fusion framework can significantly improve the fusion quality and speed simultaneously.

Originality. A simple and efficient fusion framework using BCSS in spatial domain is proposed for the first time.

Practical value. It has a certain practical meaning for real-time surveillance applications.

Keywords: *image fusion, spatial domain, surveillance, infrared, block compressed sensing sampling, real-time*

Introduction. In surveillance applications, the design of sensors with better quality or some specific characteristics may be limited by technical constraints [1], and image fusion can fuse the information across the electromagnetic spectrum, such as infrared, near-infrared, millimeter-wave (MMW) and visible bands [1].

The widely used visible image reflects the characteristics of the targets in the visible band, and it is sensitive to the change of the brightness in the scene and accord with human visual perception [2, 3]. The infrared image is sensitive to the objects which have higher temperature than the background, which make it able to see at night without illumination, and the disadvantage is its poor spatial resolution [1]. The MMW image is widely used to detect objects concealed underneath a person's clothing using a form of electromagnetic radiation, and it usually have low contrast and higher noise. Image fusion can take full advantages of the different and complementary information from those images to make up for the limitation of one single sensor. The fusion of infrared and visible images also has been investigated for other surveillance problems in recent

years, such as image dehazing, face recognition and many military reconnaissance [1].

In response to the requirements in real-time surveillance applications, the experts and scholars pay much attention in proposing more effective fusion methods. The methods are usually categorized into two basic groups: the spatial domain methods and the frequency domain based methods.

In spatial domain, the fusion methods are generally directly functioned on the pixels. The simplest method is to take the average of the source images pixel by pixel, which is known as spatial average (SA) method. An often mentioned principal component analysis (PCA) based fusion method mainly adopts the idea of the so-called 'component substitution', which is not suitable for fusion of two grayscale images and is usually used in remote sensing image fusion. The Matlab code of PCA based fusion method provided by Oliver Rockinger [4] is actually a simple spatial weighted average method, where the weights are determined by the normalized eigenvalues of the corresponding covariance matrix of the stacked images. However, along with simplicity there come several undesired side effects including contrast reduction.

In frequency domain, the experts and scholars developed the multiscale decomposition (MSD) based fusion methods and achieved better fusion performance. The classical MSD methods include the discrete wavelet transform (DWT), the shift-invariant DWT (SIDWT), the nonsubsampled contourlet transform (NSCT) and the nonsubsampled shearlet transform (NSST) etc. Generally, there are three basic steps for MSD to fuse: 1) the source images are decomposed into multiscale representations in different scales and directions; 2) the multiscale representations are composited according to certain fusion rules; 3) the fused image is reconstructed using the corresponding inverse MSD transform [5]. However, no matter which one of the MSD is used, fusion cannot be achieved perfectly since MSD requires downsampling and upsampling during the decomposition and reconstruction process, and the original and reliable information of the source images may be changed to a certain degree. Besides, each MSD has its own drawbacks. For example, a common limitation of the DWT and SIDWT is that they cannot well represent the curves and edges of images since they lack directionality; the curvelet and contourlet transforms are shift-invariant, which are the same as the DWT [1]; the excellent performance of the NSCT and NSST is achieved at the cost of increasing computational complexity and memory, which is not suitable for surveillance image fusion due to their time-consuming property.

Surveillance applications usually involve continuous real-time monitoring, and the major challenge is to reduce computational complexity while preserving the fusion quality. Therefore, the important question in surveillance applications is how to improve the fusion speed [1].

Nowadays, compressed sensing (CS) is widely used for simultaneous data sampling and compression [6]. The CS principle provides the potential of dramatic reduction of sampling rates, power consumption and computational complexity in signal processing [6]. Inspired by this superiority, a novel surveillance image fusion method based on CS in spatial domain is proposed.

The rest of this paper is organized as follows. Section 2 presents the basic sampling theory of the CS,

and then introduces the block-based sampling method; at last it proposes a modified version of the block-based sampling for fusion. In Section 3, a simple spatial domain fusion framework based on the two form of block-based sampling is proposed. Experimental results and conclusion are demonstrated in Section 4 and Section 5 respectively.

Block-based CS sampling and a modified version. Most existing works of CS are not suitable for real-time applications since the sampling process requires accessing the entire image at once.

Gan [6] proposed a block-based CS sampling (BCSS) technique for fast CS, where the original image is divided into small distinct blocks and each block is sampled independently using the same measurement matrix in a low sampling rate. For simplicity, we term this divided block scheme the basic-BCSS or distinct-BCSS, and its schematic diagram is shown in Fig. 1. The main advantages of the basic-BCSS include: 1) measurement operator can be easily stored and implemented through a random undersampled filter bank; 2) block-based measurement is more advantageous for real-time applications since the encoder does not need to send the sampled data until the whole image is measured; 3) each block is processed independently.

Let us consider an $I_r \times I_c$ image X with $N = I_r \times I_c$ pixels in total and suppose we want to take n CS measurements. In the basic-BCSS, the image is divided into small distinct blocks with size of $B \times B$ each and sampled with the same operator. Let x_i represent the vectorized signal of the i -th block through raster scanning, the corresponding output CS vector y_i can be written as

$$y_i = \Phi_B x_i,$$

where Φ_B is an $n_B \times B^2$ orthonormalized i. i. d matrix with $n_B = \left\lfloor \frac{nB^2}{N} \right\rfloor$.

On the basis of the basic-BCSS, a modified BCSS is proposed in this paper, which is termed sliding-BCSS and shown in Fig. 1. In the sliding-BCSS, the image X is divided into small sliding blocks instead, where X is appropriately padded by repeating border elements

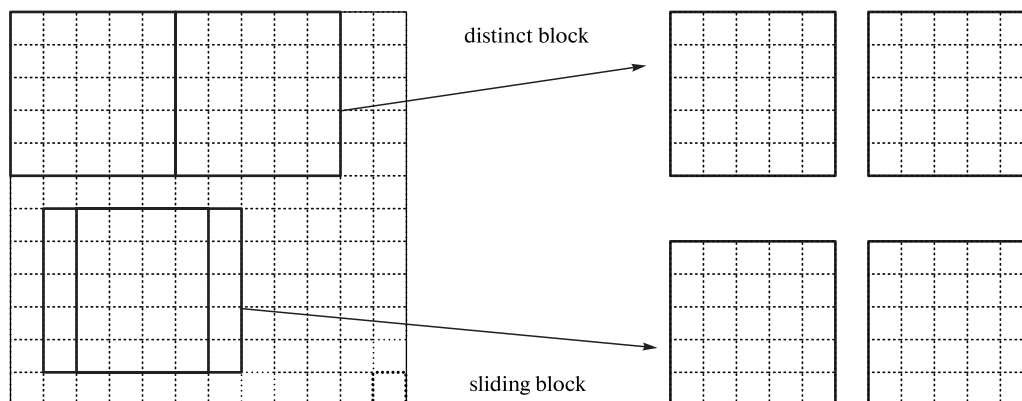


Fig. 1. The schematic diagram of distinct block and sliding block

in advance. Let us suppose that $x_{i,j}$ is a vector representing the sliding block centered on the location (x, y) , then the measurement result can be written as

$$y_{i,j} = \Phi_B x_{i,j}.$$

The other parameters are the same as before.

The advantages are: 1) the measurement result of each sliding block can be utilized to describe the feature of the specific pixel quantitatively since each pixel is correlative to its surrounding; 2) the measurement matrix is conveniently stored and employed because of its compact size [7].

Fusion framework. In this section, a simple and efficient spatial domain fusion framework is proposed for surveillance images. A fused image F is assumed to be composed of a pair of the original source images A and B that have already been registered perfectly. The fusion framework consists of the following essential stages.

1. Obtaining the measurements of A and B using the basic-BCSS or sliding-BCSS.

2. Calculating the L_2 -norm of the measurement for each block or pixel as the significance.

3. Generating a decision map through comparing the significances with the same location to form the fused image F in spatial domain.

This fusion framework is essentially presented by two proposed fusion methods.

Experimental results. In this section, three pairs of grayscale surveillance images shown in Fig. 2, a, b , Fig. 4, a, b and Fig. 5, a, b are provided to demonstrate the validity and effectiveness of the two proposed fusion methods. All the images to be fused have been geometrically registered, which can be downloaded on the websites <http://imagefusion.org> and <http://www.ece.lehigh.edu/SPCRL/IF/cwd.htm>. These images have 256 grayscales and have different sizes. All the experiments are conducted in Matlab 8.5 on a PC with Intel Core 2.4GHz i3-4000M CPU and 4.00GB RAM.

Apart from the proposed fusion methods, several different traditional methods are also used in this paper. All the fusion methods are listed as follows.

(M1) SA fusion method [4].

(M2) PCA based fusion method [4].

(M3) DWT based fusion method [4].

(M4) SIDWT based fusion method [4].

(M5) NSCT based fusion method.

(M6) NSST based fusion method.

(M7) The proposed fusion method based on basic-BCSS.

(M8) The proposed fusion method based on sliding-BCSS.

In the above DWT, SIDWT, NSCT and NSST based fusion methods, all the decomposition levels are 3, and all the fusion rules are the average scheme for lowpass subbands and the maximum choosing scheme for highpass subbands. The wavelets used in DWT, SIDWT and NSST are DBSS(2, 2), Haar and 'maxflat', respectively, and the wavelets in NSCT are '9-7' for the pyramid filter and 'pkva' for the directional filter.

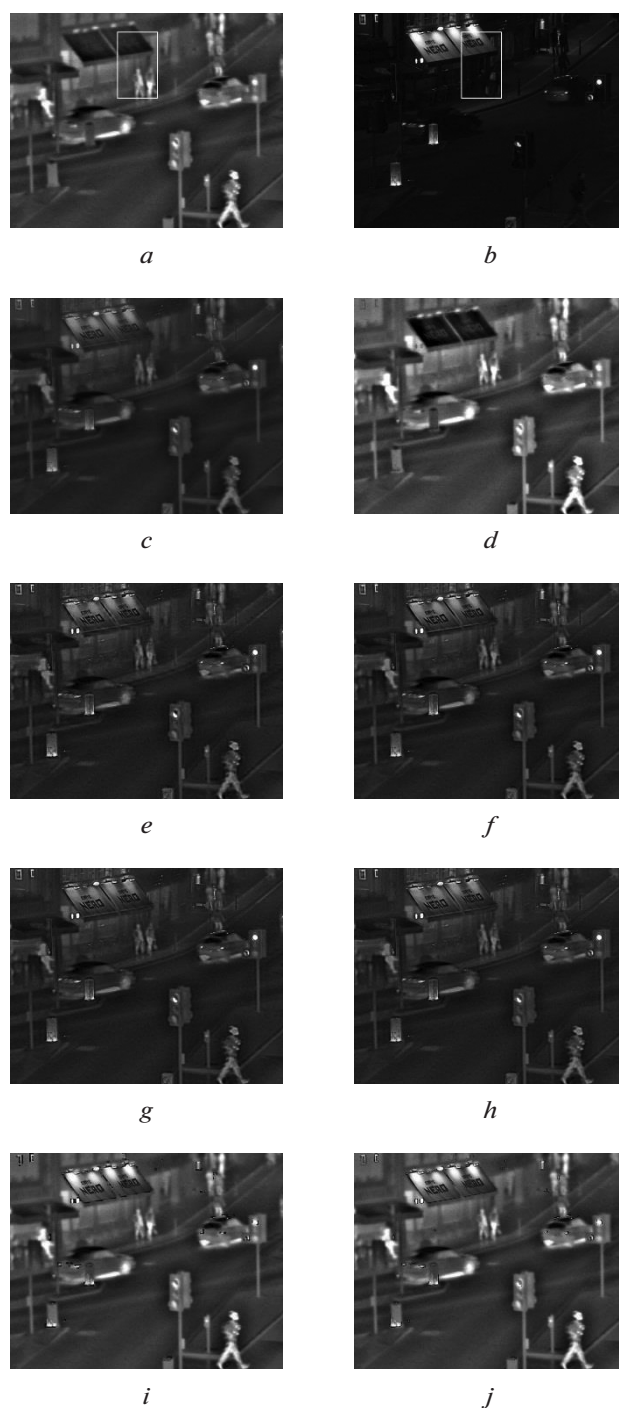


Fig. 2. 'Quad' infrared and visible images and the fused images:

a – infrared image; b – visible image; c – j – the fused images using M1–M8, respectively

For evaluating the performance of the proposed fusion methods, several experiments are designed and the computed fusion results are compared by visual effect subjectively and quantitative image criteria objectively.

The visual effect analysis mainly focuses on the quality of the preservations and improvements of important image features and the overall image contrast, brightness and saturation.

The first experiment is performed on ‘quad’ infrared and visible images with a size of 496×632 shown in Fig. 2, *a, b*. From the source images, one can see that the images contain much complementary information. The visible image is only sensitive to the light, and almost all objects are invisible in the image. The entire image looks dark so that the image lacks brightness and contrast. The infrared image is sensitive to the difference of temperature, the pedestrians, the cars and the traffic lights have great contrast in the images. The resultant fused images based on M1–M8 are shown in Fig. 2, *c–j*. From the fused images, we can easily find that: 1) Fig. 2, *c* obtained by M1 has the lowest contrast without suspense; 2) Fig. 2, *d* obtained by M2 has pretty much the same appearance as the source infrared image, and the information of the source visible image is not transferred to the fused image at all, which indicates that M2 is with the worst fusion performance in this experiment; 3) Fig. 2, *e–h* obtain almost the same fusion effect, which are obviously better than Fig. 2, *c, d*. However, the images have low brightness and saturation, and the contrast is reduced to a certain extent, which are not suitable for human to perceive; 4) Fig. 2, *i, j* have approximately the equivalent results, where the most image features are conducted, and the images have the same brightness and saturation as the source infrared image.

For a clearer comparison, Fig. 3 depicts the details of the enlarged areas extracted from the images of Fig. 2, where the extracted area is shown in Fig. 2, *a, b*. It can be seen that the fused image obtained by M8 is with the best visual quality since almost all the useful information of the source images has been transferred to it, and it preserves the high contrast and brightness, which makes the objects very prominent for human observation. The fused image obtained by M7 is with the second best quality because it has certain block effects. Obviously, the block effects will become more serious as the block size increases. The block size used in M7 is 5×5 . The performances of the other fused images are relatively poor, which is consistent with the previous discussion.

The second experiment is also performed on infrared and visible images. The source images ‘kayak’ are shown in Fig. 4, *a, b* with size of 510×505 . Fig. 4, *a* is an AMB image captured by a Radiance HS infrared camera (Raytheon), and Fig. 4, *b* is a CCD image captured by Philips LTC500 CCD camera. Fig. 4, *c–j* show the fused images. Through visual observation, similar conclusion can be obtained, that is, the proposed two fusion methods provide the higher fusion performances.

The third experiment is performed on ‘gun’ MMW and visible images with size of 200×256 shown in Fig. 5, *a, b*. The MMW image is captured under 94 GHz millimeter-wave. As seen from the images, a concealed gun underneath the right person’s clothing. The fused images are shown in Fig. 5, *c–j*, and Fig. 5, *i, j* provide the relative better performances with high contrast and brightness, which make it easy to identify the gun. The other images still have the sim-

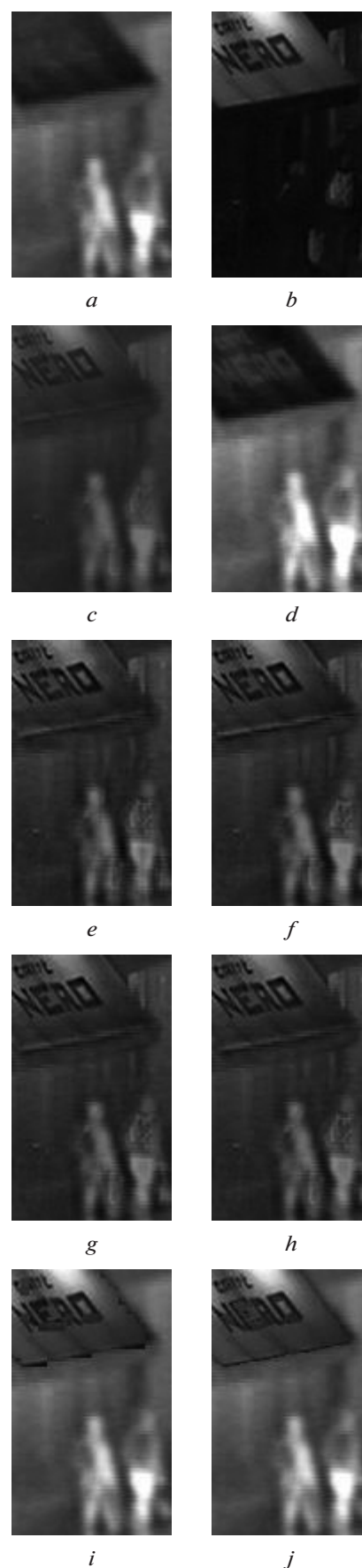


Fig. 3. Detail of the enlarged areas:
a–j – the enlarged areas extracted from Fig. 2, *a–j*, respectively

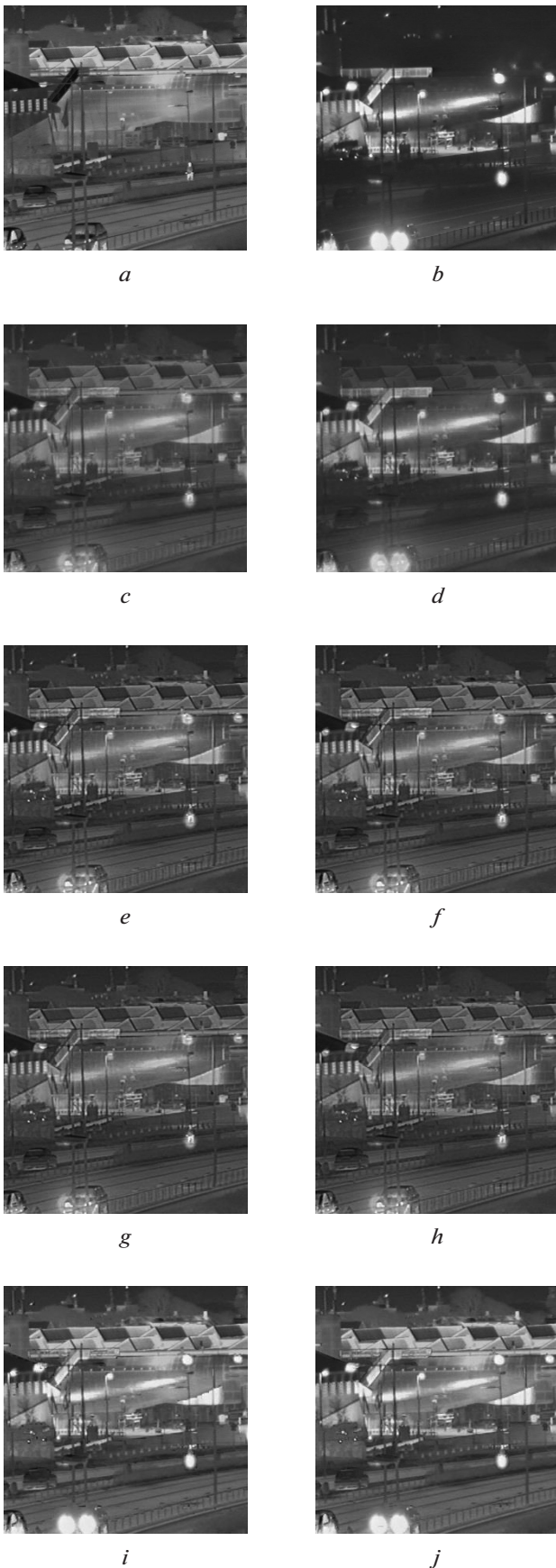


Fig. 4. 'Kayak' AMB and CCD images and the fused images:

a – AMB image; *b* – CCD image; *c*–*j* the fused images using *M1*–*M8*, respectively



Fig. 5. 'Gun' MMW and visible images and the fused images:

a – MMW image; *b* – visible image; *c*–*j* the fused images using *M1*–*M8*, respectively

ilar poor characteristics as in the first and second experiments.

To provide quantitative comparison of different fusion methods, the following image quality metrics are used in this paper: 1) standard deviation (SD), average gradient (AG), spatial frequency (SF) and information entropy (IE) are used to evaluate the spatial quality of the fused image; 2) correlation coefficient (CC), average error (AE) and mutual information (MI) are used to evaluate the relativity or difference between the fused image and one informative source image; 3) fea-

tured mutual information (FMI) [8], structural similarity image metric (SSIM) [9] and quality metric based on gradient (QAB/F) [10] are used to measure the degree of information transferred from the source images to the fused image. In addition, to measure the computational complexity of the fusion methods, the runtime (in seconds) of the corresponding Matlab fusion procedures is adopted as one fusion criterion, which is acquired by averaging the results of 10 times fusion procedure. Generally speaking, the larger the metrics values are, the better the fusion performance is, except for AE and the runtime.

The performance results of the three experiments are listed in Tables 1, 2, 3, respectively, where the best values are indicated in bold. As seen from the tables, there are two values shown in bold for each criterion because this paper refers to two proposed fusion methods. And according to the previous discussion of visual effect, M1 and M2 provide the poor fusion performance, so the corresponding data are not displayed in

the tables. In the aspects of SD, CC, AE, AG, MI, SSIM and QAB/F metrics, the comparative performance of all the fusion methods is stable, and the two proposed fusion methods provide the best quality (the two methods have roughly the same performance). On the other hand, in the aspects of SF, IE and FMI metrics, despite the poor values occasionally, the two proposed methods still provide the best quality with larger probability. In the aspect of runtime metric, the DWT based fusion method is with the best values, and M7, one of the proposed methods, is with the second best values. The runtimes of M8 procedure are approximately the two times of that of M7, which results from the more blocks divided from the images and more computations to cost.

Overall, the fusion framework can provide the relatively perfect performance.

Conclusion. In this paper, a simple, effective and fast fusion framework using the basic-BCSS and the sliding-BCSS in spatial domain is proposed. Motivat-

Table 1

Quantitative results of fusion performance of the first ‘quad’ experiment

Method	SD	AG	SF	IE	CC	AE	MI	FMI	SSIM	QAB/F	runtime
M3	0.0919	0.0296	0.0490	6.0317	0.7033	0.1282	1.0211	0.9190	0.7682	0.5290	0.0891
M4	0.0952	0.0307	0.0488	6.0780	0.7193	0.1284	1.1198	0.9210	0.7867	0.6062	0.3013
M5	0.0908	0.0292	0.0482	6.0054	0.7057	0.1281	1.0833	0.9211	0.7778	0.5588	147.4756
M6	0.0903	0.0291	0.0482	6.0018	0.7063	0.1280	1.0915	0.9209	0.7778	0.5525	6.9346
M7	0.1411	0.0479	0.0508	6.7898	0.8425	0.0138	4.3262	0.9163	0.9428	0.7002	0.2023
M8	0.1409	0.0479	0.0533	6.7835	0.8455	0.0135	4.3263	0.9157	0.9429	0.7002	0.4375

Table 2

Quantitative results of fusion performance of the second ‘kayak’ experiment

Method	SD	AG	SF	IE	CC	AE	MI	FMI	SSIM	QAB/F	runtime
M3	0.1317	0.0474	0.0501	6.9531	0.6906	0.0898	0.7922	0.8797	0.8050	0.5816	0.0739
M4	0.1335	0.0481	0.0498	6.9620	0.6928	0.0905	0.8601	0.8843	0.8168	0.6389	0.2494
M5	0.1297	0.0466	0.0484	6.9281	0.6943	0.0890	0.8289	0.8826	0.8197	0.6080	121.5679
M6	0.1293	0.0465	0.0484	6.9241	0.6940	0.0889	0.8285	0.8818	0.8183	0.6015	5.9640
M7	0.1692	0.0617	0.0516	7.2599	0.7212	0.0452	3.4752	0.8820	0.8209	0.6704	0.1785
M8	0.1687	0.0615	0.0509	7.2501	0.7208	0.0453	3.4798	0.8867	0.8253	0.6730	0.3624

Table 3

Quantitative results of fusion performance of the third ‘gun’ experiment

Method	SD	AG	SF	IE	CC	AE	MI	FMI	SSIM	QAB/F	runtime
M3	0.1113	0.0433	0.1374	5.8432	0.6999	0.0835	0.4082	0.7990	0.3262	0.5906	0.0160
M4	0.1115	0.0435	0.1349	5.7846	0.7234	0.0809	0.4635	0.8063	0.3395	0.6471	0.0305
M5	0.1076	0.0421	0.1323	5.8564	0.7133	0.0814	0.4419	0.8058	0.3489	0.6302	24.2515
M6	0.1072	0.0419	0.1329	5.8626	0.7121	0.0815	0.4399	0.8064	0.3499	0.6252	0.8689
M7	0.1461	0.0557	0.1315	4.3700	0.7485	0.0806	1.1523	0.8152	0.3845	0.7408	0.0862
M8	0.1458	0.0556	0.1322	4.3734	0.7488	0.0807	1.1580	0.8203	0.3800	0.7297	0.1221

ed by the real-time requirement of surveillance applications and the superiority of low sampling basic-BCSS technique is firstly investigated, and then a modified version, namely sliding-BCSS, is put forward. The fusion framework mainly adopts the idea of selection scheme which is widely used in a fusion process. The experiments are performed on three pairs of surveillance images. Compared with traditional SA, PCA, DWT, SIDWT, NSCT and NSSCT based fusion methods; the fusion framework provides the relatively perfect performance with high contrast and brightness in visual effect and better values in quantitative criteria. Moreover, the fusion framework has low computational complexity, and it has a certain practical meaning for real-time surveillance applications.

Acknowledgements. This work was supported by Open Project of Intelligent Information Processing Lab at Suzhou University of China (No. 2013YKF17), Horizontal Project at Suzhou University of China (No. 2015h x 025) and Quality project of Anhui Province: Software engineering teaching team (2015jxt041).

References / Список літератури

1. Li, S., Kang, X., Fang, L., Hu, J. and Yin, H., 2016. Pixel-level image fusion: A survey of the state of the art. *Information Fusion*, Vol. 33, pp. 100–112.
2. Adu, J., Gan, J., Wang, Y. and Huang, J., 2013. Image fusion based on nonsubsampling contourlet transform for infrared and visible light image. *Infrared Physics & Technology*, Vol. 61, pp. 94–100.
3. Hu, D., Shi, H., and Jiang, W., 2016. Infrared and visible image fusion using multiscale top-Hat transform and modified adaptive dual-channel pcnn. *Revista Tecnica De La Facultad De Ingenieria Universidad Del Zulia*, Vol. 39, No. 3, pp. 173–180.
4. Oliver Rockinger image fusion toolbox. [online] Available at: <<http://www.metapix.de/toolbox.htm>>.
5. Li, C., Ye, H., and Ye, J., 2016. Image fusion based on curvelet transform and principal component analysis. *Revista Tecnica De La Facultad De Ingenieria Universidad Del Zulia*, Vol. 39, No. 1, pp. 392–396.
6. Gan, L., 2007. Block compressed sensing of natural images. In: *Proc. 15th International conference on digital signal processing*, pp. 403–406.
7. Mun, S. and Fowler, J. E., 2009. Block compressed sensing of images using directional transforms. In: *Proc. 16th IEEE international conference on image processing*, pp. 3021–3024.
8. Haghghat, M. B. A., Aghagolzadeh, A. and Seyedarabi, H., 2011. A non-reference image fusion metric based on mutual information of image features. *Computers & Electrical Engineering*, Vol. 37, No. 5, pp. 744–756.
9. Wang, Z., Bovik, A. C., Sheikh, H. R. and Simoncelli, E. P., 2004. Image quality assessment: from error visibility to structural similarity. *IEEE transactions on image processing*, Vol. 13, No. 4, pp. 600–612.
10. Petrovic, V. and Xydeas, C., 2005. Objective image fusion performance characterization. In: *Proc. 10th IEEE International Conference on Computer Vision*, Vol. 2, pp. 1866–1871.

Мета. З метою вирішення проблеми злиття зображень спостереження в даній роботі пропонується простий та ефективний фреймворк злиття з використанням блочного стиснення вимірювань (BCSS), що складається з двох методів синтезу з використанням базового BCSS і ковзаючого BCSS відповідно.

Методика. За переваги низької частоти дискретизації та низької вимірювальної складності, в обробці сигналів широко використовується теорія стискування вимірів (CS). Основний алгоритм BCSS представляє собою базовий варіант блочного CS, в якому вихідне зображення розділяється на окремі блоки, а ковзаючий BCSS є модифікованою версією базового BCSS, запропонованого раніше, в якому зображення ділиться на невеликі ковзаючі блоки для кожного пікселя з відповідним відступом. Основна ідея фреймворка злиття полягає у виборі блоків чи пікселів з великою L2-нормою BCSS результатів вимірювань розділених блоків у просторовій області.

Результати. Фреймворк злиття протестовано на трьох парах зображень у відтінках сірого, у тому числі інфрачервоному та видимому зображеннях, міліметровому та видимому зображеннях, і проведено порівняння з декількома традиційними методами синтезу. Експериментальні результати показують, що запропонований фреймворк злиття може одночасно значно покращити якість злиття та швидкість.

Наукова новизна. Уперше запропоновано простий та ефективний фреймворк злиття з використанням BCSS у просторовій області.

Практична значимість. Результат має практичне значення для відеоспостереження в режимі реального часу.

Ключові слова: злиття зображень, просторова область, спостереження, інфрачервоний, блочне стискування вимірювань, режим реального часу

Цель. С целью решения проблемы слияния изображений наблюдения в данной работе предлагается простой и эффективный фреймворк слияния с использованием блочного сжатия измерений (BCSS), который состоит из двух методов синтеза с использованием базового BCSS и скользящего BCSS соответственно.

Методика. При перевесе низкой частоты дискретизации и низкой вычислительной сложности, в обработке сигналов широко используется теория сжатия измерений (CS). Основной алгоритм BCSS представляет собой базовый вариант блочного CS, в котором исходное изображение разделяется на отдельные блоки, а скользящий BCSS является модифицированной версией базового BCSS, предложенного ранее, в котором изображение делится на небольшие скользящие блоки для каждого пикселя с соответствующим отступом. Основная идея фреймворка слияния заключается в выборе блоков или пикселов с боль-

шой L2-нормой BCSS результатов измерений разделенных блоков в пространственной области.

Результаты. Фреймворк слияния протестирован на трех парах изображений в оттенках серого, в том числе инфракрасном и видимом изображениях, миллиметровом и видимом изображениях, и проведено сравнение с несколькими традиционными методами синтеза. Экспериментальные результаты показывают, что предлагаемый фреймворк слияния может одновременно значительно улучшить качество слияния и скорость.

Научная новизна. Впервые предложен простой и эффективный фреймворк слияния с ис-

пользованием BCSS в пространственной области.

Практическая значимость. Результат имеет практическое значение для видеонаблюдения в режиме реального времени.

Ключевые слова: слияние изображений, пространственная область, наблюдение, инфракрасный, блочное сжатие измерений, режим реального времени

Рекомендовано до публікації докт. техн. наук В. В. Гнатушенком. Дата надходження рукопису 25.12.15.

ЕКОНОМІКА ТА УПРАВЛІННЯ

UDC 330:658.5

**О. Н. Vagonova¹, Dr. Sc. (Econ.), Prof.,
О. М. Vakulchik², Dr. Sc. (Econ.), Prof.,
Ye. V. Protasova³, Cand. Sc. (Econ.)**

1 – State Higher Educational Institution “National Mining University”, Dnipro, Ukraine, e-mail: vagonova@nmu.org.ua
2 – University of Customs and Finance, Dnipro, Ukraine
3 – Prydniprov'ska State Academy of Civil Engineering and Architecture, Dnipro, Ukraine

ANALYTICAL DECOMPOSITION MODEL OF THE INDICATOR OF CORPORATE MANAGEMENT QUALITY AND EFFECTIVENESS

**А. Г. Вагонова¹, д-р екон. наук, проф.,
О. М. Вакульчик², д-р екон. наук, проф.,
Є. В. Протасова³, канд. екон. наук**

1 – „Національний гірничий університет“, м. Дніпро, Україна, e-mail: vagonova@nmu.org.ua
2 – Університет митної справи та фінансів, м. Дніпро, Україна
3 – Придніпровська державна академія будівництва та архітектури, м. Дніпро, Україна

АНАЛІТИЧНА МОДЕЛЬ ДЕКОМПОЗИЦІЇ ПОКАЗНИКА ЯКОСТІ ТА ЕФЕКТИВНОСТІ КОРПОРАТИВНОГО

Purpose. The purpose of the article is the grounding and choice of generalizing index which describes the corporate management quality and effectiveness, as well as the development of the analytical model of index decomposition in accordance with stages of capital transformation.

Methodology. The results were obtained by applying the method of scientific generalization to formulate of scientific problems and general conclusions; statistical method to calculate dynamic indexes of basic indicators of mining enterprises' activities; method of simulation to develop an indicator of corporate management quality and effectiveness; analysis and synthesis were used to construct the analytical decomposition of generalizing index and determine the influence factors.

Findings. Index of quality and efficiency of corporate management was grounded and selected. An analytical model of decomposition of this index considering certain basic economic factors of company operations and dependencies of their dynamics was developed.

The proposed expanded (compared with the “golden rule of economics”) model of the dynamics of basic indicators of activity of the company describes stages of transformation processes taking place at the company – the conversion of an enterprise's investment (physical) capital into the market capital.

The dynamics of the market value of PJSC “Pivnichnyi GZK”, and the basic economic indicators of its activities during the period from 2007 to 2015 was analyzed. It was determined that only in 2010 the dynamics of indicators corresponded to the model offered for companies with corporate management.

Indicators of the analytical decomposition index of the corporate management quality and efficiency of the PJSC “Pivnichnyi GZK” were analyzed, the dynamics tendencies and influence on the ratio of the market value of the enterprise and the value of assets were determined.

Originality. For the first time, an analytical decomposition model of the quality and the effectiveness of corporate management indicator was proposed, management was calculated as the ratio of the market value of the enterprise to the value of its assets and can be represented as the product of four factors, which consistently describe stages of capital transformation: asset turnover, the share of value added in the income, part of the profit in the value added, ratio of the market value to the enterprise profit.

The “golden rule of economics” has been further developed by additional indicators: the market value of the company which characterizes the enterprise management efficiency, and added value, which is created at the enterprise and is distributed among all the participants of corporate management.

Practical value. The presented methodical developments allow the management of joint stock companies to apply the mechanism of managing change of the value of enterprise capital based on the generalizing index which displays the ratio of the enterprise’s market value and the value of its assets and can be decomposed on separate financing ratios, forming information and analytical support of the management process to determine the trends of effectiveness development, searching for opportunities for growth and influence factors.

Keywords: *corporate management, analytical model, the market value, value added*

Introduction. The peculiarity of the joint-stock company performance is the isolation of capital owners from the possibility of direct participation in the daily management of the enterprise economic activity. It requires the special control over the process of attracting resources, their transformation into the final product, sales and distribution of created value added among all participants of corporate management.

Corporate management requires the development of appropriate evaluation criteria which would allow not only determining the results and financial state of the company, but also performing the strategic analysis of related economic factors of the enterprise by using the model of analytical decomposition of index which describes the quality and efficiency of enterprise management.

Analysis of recent research and publications.

Theoretical and methodological principles of corporate management are constantly in sight of both domestic and foreign scientists. The necessity of protecting the interests of capital owners and coordination of the rights of all stakeholders resulted in the research on finding relevant economic indicators of the quality and effectiveness of corporate management which reflect achieving the main financial purpose of Joint Stock Company’s activity – the increase of shareholders’ capital. Thus, the most well-known foreign experts in analyzing the effectiveness of corporate management are Richard A. Brealey, Eugene Brigham, James C. Van Horne, Randolph Westerfield, Bradford D. Jordan, Steven D. Levitt, William Stanley Jevons, Stewart C. Myers, and Stephen Ross. Considering the current state of corporate management in Ukraine, the implementation of developments of foreign authors without any changes and additional research is problematic, as they relate to established corporate and financial relations when the effectiveness of the corporate management is measured by traditional market indicators such as earnings per share (EPS), Market-to-Book Ratio (MV / BV), share rendit (R), total shareholder return ratio (TSR) and others.

A classic representative of the integrated model of measuring and evaluation activity of the companies is the multiplicative DuPont model of financial decomposition that analyzes the rate of return on equity, ROE.

In recent years, other conceptions of valuation and the effectiveness of the company have appeared, among which the most popular are balanced scorecard – BSC and economic value added – EVA. Most analysts do not doubt about necessity of using certain

financial indicators, but proposals for the use of a non-financial factors and dynamic indicators are also quite topical. Developers of the Balanced Scorecard Robert Caplan and D. Norton proposed the system of indicators, which alongside with traditional financial indicators, uses a number of new ones which take into account four important aspects of the company: finance, customers, internal business processes, training and development of personnel. Many experts in economics tend to believe that one of the most correct indicators of dynamics of the company’s development is the ratio of the rate of changes of some of its characteristics. In particular, one of the leading analysis and financial management researchers V. Kovalev argues that the effectiveness of the company and its development are characterized by the ratio of pace of changes of the capital, sales and profits. V. Kovalev stresses the fundamental importance of the proposed ratio and called it “the golden rule of economics”. The truth of this rule is recognized by many Russian experts: P. Alekseev, V. Bykadorov, A. Grishchenko, A. Tarushkin, L. Romanov, S. Chornohorskyi et al., as well as Ukrainian scientists: A. Bandurka, P. Buriak, N. Ry-mar, V. Mets, N. Prytuliak, N. Nevmerzhytska. At the same time, S. Chornohorskyi, A. Tarushkin, V. Bykadorov. and P. Alekseev propose consider the dynamics of sales proceeds instead the dynamics of sales index, while Professor V. Belolypetskyi claims that each of the three parameters of the general model of the “golden rule of economics” reflects the value of the company. A. Chernova offers her own interpretation of the “golden rule of economics”, and adapts it for joint stock companies by adding the following indicators to the dynamic range: the growth rate of the market value of stocks and the growth rate of the staff number [1], which, in her opinion, will allow analyzing the productivity.

Issues of corporate management have been considered in the works of national experts, such as: D. Baiura, L. Ptashchenko, N. Rekova, A. Manoilenko, N. Suprun and others. Works of these researchers have been devoted mainly to the research and improvement of corporate management, namely, features of crisis management, the balance of economic interests of participants, institutional and evolutionary analysis. At the same time, researchers have not proposed specific indicators that, unlike the existing traditional economic factors, would allow evaluating the effectiveness and efficiency of corporate management.

Particular attention to the value indicators of the enterprise management efficiency is given in the works

of O. Vakulchyk, T. Momot, T. Hovorushko, N. Klimash, Y. Kamarytskyi, A. Kovalenko and others. However, most researchers propose to use the market value of the company [2–6] that is not always possible in terms of underdeveloped stock market in Ukraine [7]; there are proposals to use the indicator of value added as a criterion of effectiveness of corporate management and to integrate it into the system of balanced scorecard of the company; the scientists have also developed the rate of dividend potential of the joint stock company, which evaluates the effectiveness of corporate management [8].

Undoubtedly, the proposed specific factors provide additional information that can be useful in decision-making in the system of corporate management, but the issue of searching indicators that reflect the processes of transformation of capital value and, at the same time, can be integrated into the synthesis factor which is to reflect the quality and effectiveness of corporate management and create the information and analytical support of the management process, still remains relevant.

Presentation of the main research. The effectiveness of business management is determined by increasing business value rather than by its liquidity or profitability, profit margins; thus, this is the value of the share capital which should be the subject of strategic management. The growth of the value is an important integrated feature of the joint stock company's effective activity which reflects the quality of corporate management. So it is traditionally considered that the summary criterion for the quality of enterprise management is its value and the positive dynamics of efficiency is determined by increasing business value, while well-known analytical indicators such as income, liquidity or profitability, describe only the individual properties of the company. In this regard, enterprise value becomes the object of strategic management, and, therefore, the subject of analysis, planning and control. The volume and proportions of distribution of created value added that is distributed among all stakeholders in the form of net income and fee on borrowed capital, wages and taxes is of particular importance for the successful operation of the company and making informed management decisions. If management focuses on increasing value added, enterprises create more value for all stakeholders – owners of capital, customers, employees as well as for the government and the society in general (through taxes paid and distributed). Thus, the owners of capital, worrying about maximizing their profits at the same time help to increase the welfare of other subjects of economic relations.

It should be mentioned that evaluation criteria only fix the level of effectiveness or efficiency of the business over a particular period of time. Dynamic factors that describe development trends of the company are more informative and convenient in terms of management

The so-called “golden rule of economy” is based precisely on the comparison of dynamic characteris-

tics – indexes (I) of indicators such as profit (P), income (INC) and the assets (A) and points out the necessity to observe the following relation that provides effective and promising development of the business

$$I_P > I_{INC} > I_A. \quad (1)$$

As noted above, particular role for achieving the goals of joint stock company is played by the volume of value-added (VA) that is distributed among all participants of corporate management. On the other hand, the market value of business (MV) is traditionally considered to be the summary criterion of business management effectiveness and positive trend of efficiency is determined by the increase in business value.

Thus, the further development of the “golden rule economy” can be presented as the following model

$$I_{MV} > I_P > I_{VA} > I_{INC} > I_A. \quad (2)$$

Let us analyze the correspondence of basic economic indicators of the company to the proposed model. Fig. 1 shows the chain indexes of the key financial indicators of Northern Iron Ore Enrichment Works (or Pivnichnyi GZK,) for 9 years.

Thus, in 2009, 2011–2012 and 2015, almost all indicators decrease, except insignificant assets increasing in 2012. In 2010, certain economic growth occurs, indexes of all indicators are greater than one and the market value growth is the fastest, while asset growth was the slowest. It means that the investment attractiveness of the company significantly increased in this period that marked on market quotations of its shares immediately in subsequent periods.

The actual model of business development was close to the desired type $I_{MV} > I_P > I_{VA} > I_{INC} > I_A$ only in 2010 that, of course, was a positive factor. In 2012 and 2014 within the analyzed period, assets increased, but this did not lead to the expected increasing of their return – the income and the net profit reduced (in 2012 by 39 and 38 %, respectively and in 2014 by 6 and 65 %). This indicates decrease in efficiency of assets – the asset turnover and the asset profitability decreased. Such a model of the main economic indicators describes the inefficient management of the process of the capital transformation at the company.

In terms of market relations, the center of the economic activity is the enterprise that is created on the basis of capital investment, and together with other enterprises multiplies the total capital of the economic complex. At the enterprise level, the main task of the economy is solved, that is the consumer satisfaction, namely, products needed by the society are created, works are done, necessary services are provided. At the same time, these processes are accompanied by the transformation of the investment capital into its monetary, productive and commodity form that leads to permanent changes in the capital structure, its quality characteristics and volume.

Basically, the developed model of the main indicators of the company (2), that was presented, describes step by step the sequence of transformation processes happening to the capital of the company (Fig. 2).

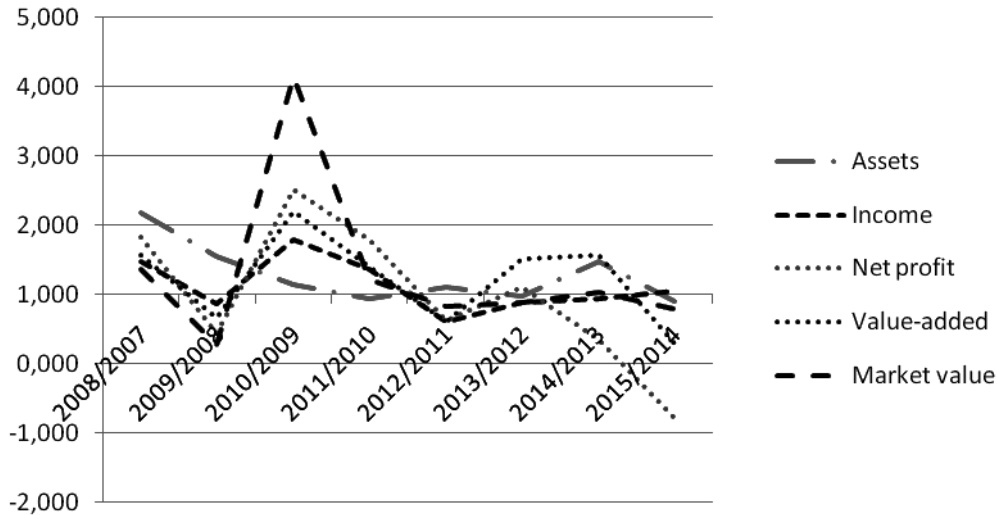


Fig. 1. Dynamic parameters (indexes) of key indicators of PJSC “Pivnichnyi GZK” effectiveness

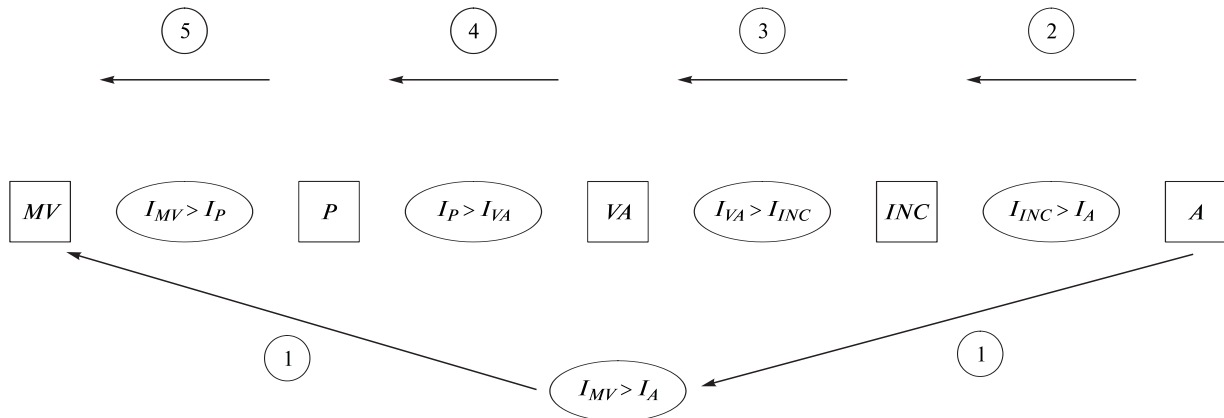


Fig. 2. The process of the transformation of the investment capital of the company in the market capital, taking into account the dynamics of the main economic indicators

Step 1: (A → MV) – the objective function that is actually carried out through the consistent implementation of stages 2–5. The transformation process of investment capital (of assets) in the market value of the company is a key economic function of the company.

Step 2: (A → INC) – there occurs “the return” of assets during the creation of products and the transfer of the share of their value to the cost of outcomes that form the income.

Step 3: (INC → VA) – the value added is formed due to effective use of the value of the materialized past labor – material costs and the depreciation.

Step 4: (VA → P) the profit is formed by reducing the expenditure share in the value added – namely, wages, interest on loans and etc.

Step 5: (P → MV) – the capitalization of profits in the market value of the company occurs. In this case, the market value is also influenced by market factors that contribute to accelerating the growth rate of the market value compared to the growth rate of profit.

The proposed developed model for the relation of financial indexes of joint stock company presupposes the following:

- firstly, higher rates of growth of the total value of the company compared with the increase in the profit achieved by the formation of the intellectual capital (goodwill);

- secondly, there are certain requirements regarding changes in the value structure of sales, namely, the share of the created value added in the volume of income must increase and the share of the profit in the value added should increase as well;

- thirdly, increasing intensity of using assets due to their turnover which can be achieved both by improving qualitative composition of the assets, optimizing their volume and structure, and by using quantitative or price factors of production revenue and sales.

Thus, the specified structure of the key economic factors of the company with corporate management and grounded laws of dynamics give an opportunity to present the model as the decomposition of the quality and the effectiveness of corporate management indicator.

As for the selection of such a generalizing index, the analysis of profitability indicators of market shares showed that foreign corporate management traditionally refers to the following indexes:

- earnings per share (*EPS*), which are calculated as the ratio of net income to the weighted average number of shares and display the potential profitability of a share;

- the ratio of the market value of shares (*P/E*), which is defined as the ratio of the market share price (*P* – price) to the value of annual income per share (*E* – earning per share) and describes the payback period of the capital;

- share rendit (*R*), which reflects the possibility of dividend payments to shareholders, is calculated as the ratio of the annual amount of dividends paid per share (*D*) to its market value (*R*);

- market-to-Book Ratio (*MV/BV*), which is determined as a ratio of the market (Market price per share) and the accounting price of shares (Book value per share), the indicator allows estimating the quality of shares on the stock market – it shows how much the company is protected from shares buying up and what is the degree of the shareholder’s wealth.

In our opinion, this is the Market-to-Book Ratio built on comparing the market value of the company and the book value of the investment capital, which is the best to reflect the level of achieving the goal of corporate management – the welfare of shareholders.

In its turn, the effectiveness of Phase 1 in Fig. 2, that describes the target process of transformation of physical (investment) capital (assets) in the market value of the company, which is the basic economic function of the enterprise, is characterized by a ratio of similar indicators – the market value of the company and its assets value (*MV/A*).

Thus, the decomposition model of the indicator of the quality and the effectiveness of corporate management considering the key economic factors of the company with corporate management and grounded laws of dynamics can be presented as follows

$$MV/A = INC/A * VA/INC * P/VA * MV/P,$$

where *INC/A* is assets turnover ratio; *VA/INC* is the share of value added in revenues from sales of products; *P/VA* is the share of profit in the value added; *MV/P* is the payback period for shares.

Table shows the decomposition results of the indicator of the management quality and effectiveness of PJSC “Pivnichnyi GZK”. In the analyzed period, the target indicator got its maximum in 2007, 2008 and 2011 that was caused by substantial increase in the market value compared to the value of assets. The highest excess of the market value of the company over its assets was observed in 2007 (2.45), but the decrease in asset turnover (from 1.45 to 0.56), the share of profit in the value added (from 0.44 to 0.26) in 2009 led to a sharp decrease in the market value and its relation with assets of the company (from 2.45 to 0.28). *MV/A* Index in 2010 was almost 1.00, this means the equality of accounting and the market value of assets; however, the positive dynamics of all indicators in the developed model of “the golden rule of economy” and the approaching of the actual model of business development in 2010 to a desired form ((2); Fig. 1) yielded the following results – in 2011, the market value exceeded value of assets by 1.28 times (Table). The gradual decrease in *MV/A* parameter since 2012 occurred due to reducing of all coefficients of the model of analytical decomposition, asset turnover ratio decreased from 1.24 to 0.55; the share of profit in the value added – from 0.45 to 0.10 in 2014, and in 2015 – because of a loss-making activity – even to negative value; while the share of the value added in the income was quite stable for almost all years of the analyzed period and ranged from 0.53–0.64, but last year’s sharp decline in income led to losses and to reduction down to 0.31. Regarding the *MV/P*, even with its significant growth to 17.74 in 2014, there was a decrease in the generalizing parameter of quality and effectiveness of corporate management – from 0.60 to 0.52. Although formally the *RV/A* indicator is positive, unprofitable activities can significantly affect the further dynamic of the market value of the company and all factors of analytical decomposition.

Conclusions.

1. The effective management of corporations requires not only the appropriate level of managers’ skills, but also the application of specific analytical methods and evaluation criteria. The market value of

Table

Decomposition factors of the quality and management effectiveness indicator for PJSC “Pivnichnyi GZK”

Year	<i>INC/A</i>	<i>VA/INC</i>	<i>P/VA</i>	<i>MV/P</i>	<i>MV/A</i>
2007	1.45	0.53	0.44	7.25	2.45
2008	0.99	0.64	0.45	5.40	1.54
2009	0.56	0.54	0.26	3.49	0.28
2010	0.86	0.59	0.34	5.77	0.99
2011	1.24	0.60	0.43	3.95	1.28
2012	0.68	0.58	0.45	5.29	0.96
2013	0.79	0.63	0.39	4.40	0.86
2014	0.51	0.64	0.10	17.74	0.60
2015	0.55	0.31	-0.24	-12.67	0.52

an enterprise has traditionally been considered as synthesis criterion of management effectiveness, whereas the volume of created value added that is distributed among all participants of corporate management in the form of salaries, interest on loans, dividends, taxes, etc., is of particular importance for achieving the goals of the company as well.

Evaluation criteria that were selected only fix a level of effectiveness or efficiency of the business over a time period, and dynamic factors that characterize the development trends of the company are more informative and convenient in terms of the management. The proposed further development of the “the golden rule of economy” for conditions of corporate management uses not three but five indicators and includes: a higher rate of growth of the market value compared with the increase in income; excess of profit growth rate over the growth of the value added; excess of the growth of value added over the growth of income; a more rapid income growth compared to the growth of assets.

The model of the dynamics of basic indicators of the joint stock company describes the sequence of stages of transformation processes that happen to the capital at the company – the transformation of investment capital of the company into the market capital, taking into account the dynamics of basic economic indicators.

As a summary measure that describes the quality and effectiveness of corporate governance, it is appropriate to use the factor, which is calculated as the ratio of the market value of the company to the value of its assets and can be represented as an analytical decomposition of four factors: assets turnover ratio, the share of the value added in the income, the share of the profit in value added, the ratio of market value to company profits. The value of factors that were proposed should be formed in the process of the strategic corporate management and should be based on planning values under the proposed model.

References / Список літератури

1. Chernova, A. N., 2011. *Analyses of the company activities in accordance with «golden rule of the enterprise's economy»*. [online] Available at: <http://science-bsea.narod.ru/2011/ekonom_2011_1/chernova_analiz.htm>.

Чернова А. Г. Анализ деятельности фирмы в соответствии „золотому правилу экономики предприятия“ [Электронный режим] – Режим доступа: http://sciencebsea.narod.ru/2011/ekonom_2011_1/chernova_analiz.htm.

2. Momot, T. V., 2006. *Vartisno-orientovane korporatyvne upravlinnia: vid teorii do praktychnoho uprovadzhenia* [Value-based corporate management: from theory to practical implementation: Monograph]. Kharkiv: HNAMG.

Момот Т. В. Вартісно-орієнтоване корпоративне управління: від теорії до практичного впровадження: монографія / Момот Т. В. – Харків: ХНАМГ, 2006. – 380 с.

3. Govorushko, T. A. and Klimash, N. I., 2013. *Upravlinnia efektyvnistiu diialnosti pidpriemstv na osnovi vartisno-orientovanoho pidkhodu* [The management of enterprise's effectiveness on the basis of value-based approach]. Kyiv: Logos.

Говорушко Т. А. Управління ефективністю діяльності підприємств на основі вартісно-орієнтованого підходу: монографія / Говорушко Т. А., Климаш Н. І. – К.: Логос, 2013. – 204 с.

4. Kamaritskiy, Yu. S., 2012. *Management of the market value of companies*. PhD. Private Higher Educational Institution European University.

Камарицький Ю. С. Управління ринковою вартістю підприємств: автореф. дис. на здобуття наук. ступеня канд. екон. наук: 08.00.04 / Камарицький Ю. С. // ПВНЗ „Європ. ун-т“. – К., 2012. – 20 с.

5. Kovalenko, A. D., 2011. *Value-based management of enterprise development (based on leasing companies of Ukraine)*. Abstract of dissertation on the competition of rank of Cand. Econ. Sciences. Kyiv National Economic University named after Vadim Hetman.

Коваленко А. Д. Вартісно-орієнтоване управління розвитком підприємства (за матеріалами лізингових компаній України): автореф. дис. на здобуття наук. ступеня канд. екон. наук: 08.00.04 / Коваленко А. Д. // ДВНЗ „КНЕУ ім. Вадима Гетьмана“. – К., 2011. – 20 с.

6. Protasova, E. V., 2013. Model of assessing the impact of management decisions on the enterprise value. *Economical bulletin of National mining university*. No. 3(43), pp. 161–170.

Протасова Є. В. Модель оцінювання впливу управлінських рішень на вартість підприємства / Є. В. Протасова // Економічний вісник Національного гірничого університету. – 2013. – № 3(43). – С. 161–170.

7. Dychkovskiy, R. O., Avdiushchenko, A. S., Falshynskiy, V. S. and Saik, P. B., 2013. On the issue of estimation of the coal mine extraction area economic efficiency. *Naukovyi Visnyk Natsionalnoho Hirnychoho Universytetu*, No. 4, pp. 107–114.

До питання оцінки економічної ефективності роботи виймальної ділянки вугільної шахти / [Р. О. Дичковський, А. С. Авдющенко, В. С. Фальшинський та ін.] // Науковий вісник НГУ. – 2013. – № 4. – С. 107–114.

8. Vakulchuk, O. M. and Kozlova, O. V., 2006. The model of estimation of joint stock company dividend capacity based on the integral index. *Economist*, No. 10, pp. 32–35.

Вакульчик О. М. Модель оцінки дивідендного потенціалу акціонерного товариства на основі інтегрального показника / О. М. Вакульчик, О. В. Козлова // Економіст. – 2006. – № 10. – С. 32–35.

Мета. Обґрунтування та вибір узагальнюючого показника, що характеризує якість і результативність корпоративного управління, та розробка аналітичної моделі його декомпозиції у відповід-

ності до етапів трансформації капіталу підприємства.

Методика. Результати отримані за рахунок застосування методів: наукового узагальнення — для формулювання наукових завдань і загальних висновків; статистичний — при розрахунку динамічних індексів основних показників діяльності гірничо-збагачувального комбінату; моделювання — при розробці показника якості й результативності корпоративного управління; аналізу й синтезу — при побудові аналітичного розкладання узагальнюючого показника та визначенні факторів впливу на нього.

Результати. Обґрунтовано та обрано показник якості й ефективності корпоративного управління, розроблена аналітична модель його декомпозиції з урахуванням визначених основних економічних чинників діяльності акціонерного товариства та залежностей їх динаміки.

Запропонована розширена (у порівнянні із „золотим правилом економіки“) модель динаміки основних показників діяльності акціонерного товариства, яка поетапно описує послідовність трансформаційних процесів, що відбуваються з капіталом на підприємстві — перетворення інвестиційного (фізичного) капіталу підприємства в ринковий капітал.

Проаналізована динаміка ринкової вартості ПАТ „Північний ГЗК“ і основних економічних показників його діяльності за період з 2007 по 2015 рр. Визначено, що тільки у 2010 році динаміка показників відповідала моделі, що пропонується для підприємств з корпоративним управлінням.

Проаналізовані чинники декомпозиції показника якості та ефективності корпоративного управління ПАТ „Північний ГЗК“, визначені тенденції їх динаміки та вплив на співвідношення ринкової вартості підприємства й вартості його активів.

Наукова новизна. Уперше запропонована аналітична модель декомпозиції показника якості та ефективності корпоративного управління, що розраховується як відношення ринкової вартості підприємства до вартості його активів і може бути представлений як добуток чотирьох коефіцієнтів, які послідовно відображають етапи трансформації капіталу підприємства: оборотності активів, питомої ваги доданої вартості в доході, частки прибутку в доданій вартості, відношення ринкової вартості до прибутку підприємства.

Подальший розвиток отримало „золоте правило економіки“ за рахунок включення до нерівності індексів додаткових показників: ринкової вартості підприємства, що узагальнюючим чином характеризує результативність управління підприємством, та доданої вартості, яка створюється на підприємстві та розподіляється між усіма учасниками корпоративного управління.

Практична значимість. Здійснені методичні розробки дозволяють менеджменту акціонерних

товариств застосувати механізм управління процесом перетворення вартості капіталу підприємства на основі узагальнюючого показника, що відображає співвідношення ринкової вартості підприємства й вартості його активів та розкладається на окремі фінансові коефіцієнти, які формують інформаційно-аналітичне забезпечення управлінського процесу для визначення тенденцій розвитку ефективності, пошуку можливостей її росту та факторів впливу.

Ключові слова: корпоративне управління, аналітична модель, ринкова вартість, додана вартість

Цель. Обоснование и выбор обобщающего показателя, который характеризует качество и результативность корпоративного управления, и разработка аналитической модели его декомпозиции в соответствии с этапами трансформации капитала предприятия.

Методика. Результаты получены за счет применения методов: научного обобщения — для формулирования научных задач и общих выводов; статистический — при расчете динамических индексов основных показателей деятельности горно-обогатительного комбината; моделирования — при разработке показателя качества и результативности корпоративного управления; анализа и синтеза — при построении аналитического разложения обобщающего показателя и определении факторов влияния на него.

Результаты. Обоснован и выбран показатель качества и эффективности корпоративного управления, разработана аналитическая модель его декомпозиции с учетом определенных основных экономических факторов деятельности акционерного общества и зависимостей их динамики.

Предложена расширенная (по сравнению с „золотым правилом экономики“) модель динамики основных показателей деятельности акционерного общества, что поэтапно описывает последовательность трансформационных процессов, которые происходят с капиталом на предприятии — преобразование инвестиционного (физического) капитала предприятия в рыночный капитал.

Проанализирована динамика рыночной стоимости ЧАО „Северный ГОК“ и основных экономических показателей его деятельности за период с 2007 по 2015 гг. Определено, что только в 2010 году динамика показателей отвечала модели, которая предлагается для предприятий с корпоративным управлением.

Проанализированы показатели аналитического разложения показателя качества и эффективности корпоративного управления ЧАО „Северный ГОК“, определены тенденции их динамики и влияние на соотношение рыночной стоимости предприятия и стоимости его активов.

Научная новизна. Впервые предложена аналитическая модель декомпозиции показателя ка-

чества и эффективности корпоративного управления, который рассчитывается как отношение рыночной стоимости предприятия к стоимости его активов и может быть представлен как произведение четырех коэффициентов, которые последовательно отображают этапы трансформации капитала предприятия: оборачиваемости активов, удельного веса добавленной стоимости в доходе, части прибыли в добавленной стоимости, отношения рыночной стоимости к прибыли предприятия.

Дальнейшее развитие получило „золотое правило экономики“ за счет включения в неравенство индексов дополнительных показателей: рыночной стоимости предприятия, которая обобщающим образом характеризует результативность управления предприятием, и добавленной стоимости, которая создается на предприятии и распределяется между всеми участниками корпоративного управления.

Практическая значимость. Представленные методические разработки позволят менеджменту акционерных обществ применить механизм управления процессом преобразования стоимости капитала предприятия на основе обобщающего показателя, который отображает соотношение рыночной стоимости предприятия и стоимости его активов, и раскладывается на отдельные финансовые коэффициенты, формирующие информационно-аналитическое обеспечение управленческого процесса для определения тенденций развития эффективности, поиска возможностей ее роста и факторов влияния.

Ключевые слова: *корпоративное управление, аналитическая модель, рыночная стоимость, добавленная стоимость*

Рекомендовано до публікації докт. екон. наук Ю. Є. Петрунею. Дата надходження рукопису 19.12.15.

CONTENTS

Geology	5
T. P. Volkova, O. V. Nikitenko, O. G. Chernysh. Tectonophysical aspects of the development of geological structure of the western closure of the Horlivka anticline of the Donbas	5
I. S. Paranko, O. A. Matishchuk. The interrelation between the Novokryvorizka and Skeliuvatska suites of the Kryvyi Rih series	14
H. A. Kalashnyk, Yu. I. Fedoryshyn, A. V. Kuzmin, M. M. Kirianov. Preconditions of formation and criteria for prediction of diamondiferous structures on the ukrainian shield	22
Mining	41
B. Yu. Sobko, O. V. Lozhnikov, A. M. Haidin, O. M. Laznikov. Substantiation of rational mining method at the Motronivskiy titanium-zirconium ore deposit exploration	41
V. P. Kurinnyi, I. P. Garkusha, V. O. Nikiforova. Processes of initial stage of expansions of explosive cavity in blasthole charge	49
O. M. Shashenko, O. S. Kovrov. Comparative analysis of two failure criteria for rocks and massifs.	54
P. B. Saik, R. O. Dychkovskiy, V. H. Lozynskiy, Z. R. Malanchuk, Ye. Z. Malanchuk. Revisiting the underground gasification of coal reserves from contiguous seams.	60
Solid-State Physics, Mineral Processing	67
A. Chaib, M. Bounouala, S. Bouabdallah, A. Benselhou. New condition for separation of orthoclase from quartz by flotation; case of Ain Barbar quarry (Algeria)	67
V. V. Sobolev, O. S. Baskevych, L. M. Shyman, S. M. Usherenko. Mechanism of thick metal walls penetration by high-speed microparticles	75
Geotechnical and mining mechanical engineering, machine building	84
J. A. Nechytailo, T. O. Bazhynova, M. A. Vesela. The energy estimation of transportation vehicles.	84
V. P. Shpachuk. Effect of mutually amplifying action of two coordinate shock loading in problems of dynamics of knots of machines	89
Electrical complexes and system	95
O. Beshta, E. Nolle, M. Kuvaiev. The development of the simple modified control law for the compensation of the cogging torque in the synchronous motor with permanent magnets (O. Beschta, E. Nolle, M. Kuvaiev. Entwurf einer einfachen und modifizierten rastmomentkompensation für die permanenterregte synchronmaschine).	95
M. Zagirnyak, V. Prus, I. Kushch, D. Miljavec. Features of modeling of electromagnetic field of electric machines when magnetic system properties change	101

Power supply technologies	107
O. V. Makarchuk. Additional losses in the stator windings of the high-speed brushless electrical machine with permanent magnets.	107
Environmental safety, labour protection	114
V. G. Shevchenko. Developing methods for increasing readiness of the managers of coal mine divisions to accident-free operation according to quantitative estimations of their personality characteristics	114
V. Ye. Kolesnyk, D. V. Kulikova, A. V. Pavlychenko. Substantiation of rational parameters of perforated area of partitions in an improved mine water settling basin	120
Information technologies, systems analysis and administration	128
T. O. Ruzova, O. P. Tolstopyat, V. I. Yeliseyev, L. O. Fler. Evaluating geometric parameters of dispersed particle aggregates	128
Hongyi Cao, Junhui Yang, Li Wang. Fast time sequence data mining algorithm based on grey system theory	134
Fei Hu, Changjiu Pu, Haowei Gao, Mengzi Tang, Li Li. Image compression and encryption scheme based on deep learning	142
Lili Chen, Hongjun Guo. A simple and efficient fusion framework for surveillance images	149
Economy and management	157
O. H. Vagonova, O. M. Vakulchyk, Ye. V. Protasova. Analytical decomposition model of the indicator of corporate management quality and effectiveness	157

ЗМІСТ

Геологія	5
Т. П. Волкова, О. В. Нікітенко, О. Г. Черниш. Тектонофізичні аспекти розвитку геологічної структури західного змикання Горлівської антикліналі Донбасу	5
І. С. Паранько, О. А. Матіщук. До питання про взаємовідношення новокриворізької та скелюватської світ Криворізької серії	14
Г. А. Калашник, Ю. І. Федоришин, А. В. Кузьмін, М. М. Кір'янов. Передумови формування та критерії прогнозування алмазоносних структур на Українському щиті	22
Розробка родовищ корисних копалин	41
Б. Ю. Собко, О. В. Ложніков, А. М. Гайдін, О. М. Лазніков. Обґрунтування раціонального способу розробки Мотронівського розсипу титано-цирконієвих руд	41
В. П. Курінний, І. П. Гаркуша, В. О. Нікіфорова. Процеси початкової стадії розширення порожнини вибуху свердловинного заряду	49
О. М. Шашенко, О. С. Ковров. Порівняльний аналіз двох критеріїв руйнування гірських порід і масивів	54
П. Б. Саїк, Р. О. Дичковський, В. Г. Лозинський, З. Р. Маланчук, Є. З. Маланчук. Характеристика підземної газифікації запасів вугілля зближених пластів	60
Фізика твердого тіла, збагачення корисних копалин	67
А. Шаїб, М. Бунуала, С. Буабделла, А. Бенселгуб. Нові умови сепарації ортоклазу із кварцу методом флотації на прикладі кар'єру Айн-Барбар (Алжир)	67
В. В. Соболев, О. С. Баскевич, Л. М. Шиман, С. М. Ушеренко. Про механізм пробивання металевих товстих стінок високошвидкісними мікрочастинками	75
Геотехнічна і гірнична механіка, машинобудування	84
Ю. А. Нечитайло, Т. О. Бажинова, М. А. Весела. Енергетична оцінка транспортних машин	84
В. П. Шпачук. Ефект взаємопідсилюючої дії двокоординатного ударного навантаження в задачах динаміки вузлів машин	89
Електротехнічні комплекси та системи	95
О. С. Бешта, О. Нолле, М. В. Куваєв. Розробка простого модифікованого закону компенсації зубцевого моменту синхронної машини з постійними магнітами	95
М. В. Загірняк, В. В. Прус, І. А. Куц, Д. Мілявець. Особливості моделювання електромагнітного поля електричних машин при зміні властивостей магнітної системи	101

Технології енергозабезпечення	107
О. В. Макарчук. Додаткові втрати у статорних обмотках високошвидкісних безконтактних електричних машин з постійними магнітами.	107
Екологічна безпека, охорона праці	114
В. Г. Шевченко. Розробка методики підвищення готовності керівників дільниць вугільної шахти до безаварійної роботи за кількісними оцінками їх особистісних характеристик.	114
В. Є. Колесник, Д. В. Кулікова, А. В. Павличенко. Обґрунтування раціональних параметрів перфорованої області перегородок в удосконаленому відстійнику шахтної води	120
Інформаційні технології, системний аналіз та керування	128
Т. О. Рузова, О. П. Толстопят, В. І. Єлісєєв, Л. О. Флеєр. Визначення геометричних характеристик агрегованих утворень дисперсних частинок	128
Хуні Цао, Цзюньхой Ян, Лі Ван. Швидкий алгоритм інтелектуального аналізу часових рядів на основі теорії сірих систем	134
Фей Ху, Чанцзю Пу, Хаовей Гао, Менцзи Тан, Лі Лі. Схема стиснення та шифрування зображень на основі глибинного навчання.	142
Лілі Чен, Хунцзюнь Го. Простий та ефективний фреймворк злиття для зображень з камер спостереження	149
Економіка та управління	157
О. Г. Вагонова, О. М. Вакульчик, Є. В. Протасова. Аналітична модель декомпозиції показника якості та ефективності корпоративного	157

СОДЕРЖАНИЕ

Геология	5
Т. П. Волкова, А. В. Никитенко, О. Г. Черныш. Тектонофизические аспекты развития геологической структуры западного смыкания Горловской антиклинали Донбасса	5
И. С. Паранько, А. А. Матищук. К вопросу о взаимоотношении новокриворожской и скелеватской свит Криворожской серии	14
А. А. Калашник, Ю. И. Федоришин, А. В. Кузьмин, Н. Н. Кирьянов. Предпосылки формирования и критерии прогнозирования алмазоносных структур на Украинском щите	22
Разработка месторождений полезных ископаемых	41
Б. Е. Собко, А. В. Ложников, А. М. Гайдин, А. М. Лазников. Обоснование рационального способа разработки Мотроновской россыпи титано-циркониевых руд	41
В. П. Куринной, И. П. Гаркуша, В. А. Никифорова. Процессы начальной стадии расширения полости взрыва скважинного заряда	49
А. Н. Шашенко, А. С. Ковров. Сравнительный анализ двух критериев разрушения горных пород и массивов	54
П. Б. Саик, Р. Е. Дычковский, В. Г. Лозинский, З. Р. Маланчук, Е. З. Маланчук. Характеристика подземной газификации углей сближенных пластов	60
Физика твердого тела, обогащение полезных ископаемых	67
А. Шаиб, М. Бунуала, С. Буабделла, А. Бенселгуб. Новые условия сепарации ортоклаза из кварца методом флотации на примере карьера Айн-Барбар (Алжир)	67
В. В. Соболев, А. С. Баскевич, Л. Н. Шиман, С. М. Ушеренко. О механизме пробивания металлических толстых стенок высокоскоростными микрочастицами	75
Геотехническая и горная механика, машиностроение	84
Ю. А. Нечитайло, Т. А. Бажинова, М. А. Веселая. Энергетическая оценка транспортных машин	84
В. П. Шпачук. Эффект взаимоусиливающегося действия двухкоординатного ударного нагружения в задачах динамики узлов машин	89
Электротехнические комплексы и системы	95
А. С. Бешта, О. Нолле, Н. В. Куваев. Разработка простого модифицированного закона компенсации зубцового момента синхронной машины с постоянными магнитами	95
М. В. Загирняк, В. В. Прус, И. А. Куш, Д. Милявец. Особенности моделирования электромагнитного поля электрических машин при изменении свойств магнитной системы	101

Технологии энергообеспечения	107
А. В. Макарчук. Добавочные потери в статорных обмотках высокоскоростных бесконтактных электрических машин с постоянными магнитами	107
Экологическая безопасность, охрана труда	114
В. Г. Шевченко. Разработка методики повышения готовности руководителей участков угольной шахты к безаварийной работе по количественным оценкам их личностных характеристик	114
В. Е. Колесник, Д. В. Куликова, А. В. Павличенко. Обоснование рациональных параметров перфорированной области перегородок в усовершенствованном отстойнике шахтной воды	120
Информационные технологии, системный анализ и управление	128
Т. А. Рузова, А. П. Толстопят, В. И. Елисеев, Л. А. Флеер. Определение геометрических характеристик агрегированных образований дисперсных частиц	128
Хуни Цао, Цзюньхой Ян, Ли Ван. Быстрый алгоритм интеллектуального анализа временных рядов на основе теории серых систем	134
Фэй Ху, Чанцзю Пу, Хаовэй Гао, Мэнцзы Тан, Ли Ли. Схема сжатия и шифрования изображений на основе глубинного обучения	142
Лили Чэн, Хунцзюнь Го. Простой и эффективный фреймворк слияния для изображений с камер наблюдения	149
Экономика и управление	157
А. Г. Вагонова, Е. М. Вакульчик, Е. В. Протасова. Аналитическая модель декомпозиции показателя качества и эффективности корпоративного управления	157

**НАУКОВИЙ ВІСНИК
НГУ**

ФАХОВЕ ВИДАННЯ

„Науковий вісник НГУ“ включений до
„Переліку наукових фахових видань України“
з геологічних і технічних наук (Наказ МОН
України від 21.12.2015 р. № 1328).

**НАУЧНЫЙ ВЕСТНИК
НГУ**

**СПЕЦИАЛИЗИРОВАННОЕ
ИЗДАНИЕ**

„Научный вестник НГУ“ включен в „Перечень
научных специализированных изданий
Украины“ по геологическим и техническим
наукам (Приказ МОН Украины от
21.12.2015 г. № 1328).

**SCIENTIFIC BULLETIN
OF NMU**

**AN OCCUPATIONAL
EDITION**

“Scientific Bulletin of National Mining
University” was included in the “List of
Scientific occupational editions of Ukraine”
on geological and technical sciences (Order
of Ministry of Education and Science of
Ukraine No.1328 dated December 21, 2015).

Вимоги до оформлення статей

До розгляду приймаються статті, надруковані в одному примірнику, на стандартних аркушах паперу А4, що супроводжуються електронною версією (Microsoft Word 2007, 2010) на CD чи надіслані електронною поштою (друкований примірник надсилається поштою).

Параметри сторінки: поля верхні та нижні — 2,5 см, ліві і праві — 2,0 см. Форматування статті — у дві колонки з проміжком 0,7 см. Перші рядки всіх абзаців з відступом 0,5 см, шрифт Times New Roman, кегль 10, інтервал 1. Назва статті — кегль 14. Заголовки елементів основного тексту виділяються напівжирним шрифтом.

Структура статті:

- індекс УДК (у верхньому лівому кутку сторінки);
- ініціали, прізвища всіх авторів (не більше, ніж 4 особи) та назва статті трьома мовами — українською, російською, англійською (форматуванням на всю сторінку);
- реферат (200–300 слів виключно загальноприйнятої термінології) повинен бути структурованим і містити наступні елементи: мета; методика; результати; наукова новизна; практична значимість; ключові слова (6–8 слів) мовою статті (форматуванням на всю сторінку); реферат не повинен повторювати назву статті;
- основний текст статті;
- бібліографія;
- реферат та ключові слова двома іншими мовами (у дві колонки);
- ким рекомендовано статтю до публікації;
- розділ журналу для розміщення статті.

Відповідно до вимог постанови Президії ВАК України від 15.01.03 № 7-05/1, основний текст статті повинен містити такі необхідні елементи:

- постановка проблеми в загальному вигляді та її зв'язок із важливими науковими або практичними завданнями;
- аналіз останніх досліджень і публікацій, в яких започатковано розв'язання даної проблеми, на які спирається автор;
- виділення невирішених раніше частин загальної проблеми, яким присвячується означена стаття;
- формулювання цілей статті (постановка завдання);
- виклад основного матеріалу дослідження з повним обґрунтуванням отриманих наукових результатів;
- висновки з даного дослідження та перспективи подальшого розвитку в цьому напрямі.

Обсяг статті, включаючи текст, таблиці, рисунки, повинен складати від 6 до 9 сторінок. Рекомендується, щоб площа, зайнята рисунками, становила не більше 25% загального обсягу. Матеріал має бути викладений стисло, без повторюваних даних таблиць і рисунків у тексті. Не припустимо використовувати такі елементи форматування як „розрив розділу з нової сторінки“ і колонтитули.

Рисунки (діаграми, фото та ін.) подаються у кольоровому та чорно-білому зображенні разом із текстом у місцях посилок на них та обов'язково в окремих файлах (*.TIFF, *.jpg та ін.) з роздільністю 300 dpi. Бажана ширина рисунків — 8,15 см або не більше 17 см для карт, схем та інших об'ємних матеріалів. Рисунок має бути розташований по центру, без обтікання текстом. Рисунки розміщують „у тексті“ (не в таблицях). Символи, підписи, лінії рисунків слід виконувати таким чином, щоб вони сприймалися після приведення розміру рисунка до ширини 1 колонки. Підписи до рисунків повинні містити нумерацію в порядку розміщення в тексті та пояснювальний підпис, що виділяється курсивом. Не припустимо включати підписи до самого рисунка.

Формули в статтях мають бути набрані за допомогою редактора формул (внутрішній редактор формул в редакторі Microsoft Word for Windows). Прості формули та символи, що їх складають, набираються за допомогою редактора формул, стиль — математичний (курсив), розмір формул — 10 pt. Складні формули набирають у редакторі Microsoft Equation. Формули завдовжки понад 8 см розбивають на окремі блоки до 8 см (за окремими винятками — 17 см). Формули відокремлюють від тексту зверху та знизу одним інтервалом. Нумерація формул, на які є посилання в тексті, — справа в дужках. Усі фізичні величини подаються в системі СІ. Цілі частини від десяткових відокремлюються комою.

Таблиці подаються у книжній орієнтації, вони повинні мати тематичні заголовки і номери, фон таблиці іншим кольором не виділяють. Бажана довжина таблиці — не більше однієї сторінки, ширина — 8,15 або 17 см. Рекомендований розмір символів у таблицях — 8–9 pt (для емких не менше, ніж 6 pt).

Список літератури (не більше 10 джерел з датою їх видання не раніше, ніж за 10 років та кількістю самопосилань до 15%) наводиться у порядку згадування у тексті згідно з ДСТУ ГОСТ 7.1:2006 „Система стандартів з інформації, бібліотечної та видавничої справи. Бібліографічний запис. Бібліографічний опис. Загальні вимоги та правила складання“. Посилання на літературні джерела в тексті подають у квадратних дужках. У списку літератури кожне україномовне чи російськомовне джерело слід подавати спочатку мовою оригіналу, а потім у перекладі, англійською мовою. Транслітерація прізвищ авторів, залежно від мови оригіналу джерела, виконується відповідно до Постанови Кабінету Міністрів України від 27 січня 2010 року №55 „Про впорядкування транслітерації українського алфавіту латиницею“ (для української мови) або вимогам системи ВGN/HCN (для російської мови). Деталі — на веб-сторінці журналу.

Стаття має бути ретельно перевірена, підписана всіма авторами і супроводжуватися: письмовою рекомендацією, підписаною доктором наук відповідного профілю; експертним висновком про можливість відкритої публікації поданої статті. При здаванні статті автори вказують розділ журналу для її розміщення та підписують ліцензійний договір на використання твору.

Відомості про авторів у надрукованому та електронному вигляді: прізвище, ім'я та по батькові повністю, науковий ступінь, вчене звання, місце роботи (повна та скорочена назва організації), посада, місто, країна, контактні телефони та електронна пошта (форматуванням на всю сторінку, запис даних у ряд через коми) подаються в окремому файлі українською, російською та англійською мовами. При наданні відомостей про авторів англійською мовою слід використовувати загальноприйнятну лексику для перекладу наукових ступенів, вчених звань та посад.

Відповідальність за зміст статті несе автор. Надіслані матеріали не повертаються.

Статті, що не відповідають указаним вимогам, не розглядаються.

Контакти: тел.: (0562) 47 45 24, www.nvngu.in.ua, nv.ngu@ukr.net.